REACTIONS OF SMALL MOLECULES WITH RHODIUM PORPHYRIN COMPLEXES

by

David C. Thackray

B.Sc., Concordia University, 1978

M.Sc., The University of British Columbia, 1983

A THESIS SUBMITTED IN PARTIAL FULFILLMENT OF

THE REQUIREMENTS FOR THE DEGREE OF

DOCTOR OF PHILOSOPHY

in

THE FACULTY OF GRADUATE STUDIES

THE DEPARTMENT OF CHEMISTRY

We accept this thesis as conforming

to the required standard

THE UNIVERSITY OF BRITISH COLUMBIA

May, 1990

In presenting this thesis in partial fulfilment of the requirements for an advanced degree at the University of British Columbia, I agree that the Library shall make it freely available for reference and study. I further agree that permission for extensive copying of this thesis for scholarly purposes may be granted by the head of my department or by his or her representatives. It is understood that copying or publication of this thesis for financial gain shall not be allowed without my written permission.

Department of Chemistry

The University of British Columbia
Vancouver, Canada

Date 5 Sept 1990

Abstract

The reaction of Rh(OEP)(H) (OEP = 2,3,7,8,12,13,17,18-octaethylporphyrin) with O_2 in organic solvents was examined by visible, proton and phosphorus nuclear magnetic resonance spectroscopy (nmr) as a candidate system for the net insertion of O_2 into the metal-hydride bond. The nmr data for a thermally unstable $Rh^{III}(OEP)(OOH)(H_2O)$ intermediate were obtained at -40 °C in CD_2Cl_2. Addition of O_2 to CH_2Cl_2 solutions of Rh(OEP)(H) with triphenylphosphine resulted in reaction with solvent forming Rh(OEP)(Cl)(PPh_3) and Rh(OEP)(CH_2Cl)(PPh_3) as the major species (in equimolar amounts), without concomitant formation of $OPPh_3$. The sensitivity of the reaction of Rh(OEP)(H) with O_2 to initial conditions, and the observation of products containing Rh(II) and Rh-CH_2Cl, suggest a radical mechanism.

Initiation/termination:

$$2Rh(OEP)(H) \rightleftharpoons [Rh(OEP)]_2 + H_2$$

$$[Rh(OEP)]_2 \rightleftharpoons 2Rh(OEP)\cdot$$

and in the presence of PPh_3

$$[Rh(OEP)]_2 + PPh_3 \rightleftharpoons \cdot Rh(OEP)(PPh_3) + Rh(OEP)\cdot$$

Propagation:

$$Rh(OEP)\cdot + O_2 \rightleftharpoons Rh(OEP)(O_2)$$

$$Rh(OEP)(O_2) + Rh(OEP)(H) \longrightarrow Rh(OEP)(OOH) + Rh(OEP)\cdot$$

Termination:

$$Rh(OEP)(OOH) + Rh(OEP)(H) \longrightarrow [Rh(OEP)]_2 + H_2O + \tfrac{1}{2}O_2$$

and in the presence of PPh_3

$$\cdot Rh(OEP)(PPh_3) + CH_2Cl_2 \rightleftharpoons Rh(OEP)(Cl)(PPh_3) + \cdot CH_2Cl$$

$$Rh(OEP)\cdot + \cdot CH_2Cl \rightleftharpoons Rh(OEP)(CH_2Cl)$$

The reaction of Et_3N with Rh(por)(Cl)(L) (por = OEP or 5,10,15,20-tetramesitylporphyrin(TMP), L = H_2O, $(CH_3)_2CHOH$, CH_3CN) gave products, identified by visible (scanning and stopped-flow) and proton nmr spectroscopy to be Rh(por)(CH(Me)NEt_2),

Et_2NH as Rh(por)(Cl)(Et_2NH), and Rh(por)(CH_2CHO). This indicated amine C-H and C-N cleavage and net one-electron reduction of Rh(III) to Rh(II) species ($[Rh(OEP)]_2$). Of other amines examined, aniline, N-methyl-diphenylamine and N-ethyl piperidine all formed complexes of the type Rh(OEP)(Cl)(amine). Proton Sponge and tributylamine with Rh(OEP)(Cl)(H_2O) give $[Rh(OEP)]_2$ as a major product under anærobic conditions. Only the mechanism of the Et_3N system was examined in detail.

Stopped-flow data indicated that Et_3N initially replaced L in the Rh^{III}(por)(Cl)(L) species to form a Rh^{III}(por)(Cl)(Et_3N) complex. An equilibrium involving reduction of Rh^{III} to Rh^{II} resulted and, in aromatic solvents under anærobic conditions, slow reaction of Rh^{II}(por) with Et_3N occurred to give Rh(por)(CH(Me)NEt_3). In CH_2Cl_2, reaction of Et_3N with Rh(por)(Cl)(L) was fast, giving a mixture principally of Rh(por)(CH_2Cl)(amine) and the η^1-ylidic enamine complex, Rh(por)(Cl)($CH_2CH{=}NEt_2$) with minor mounts of Rh(por)(CH(Me)NEt_3). The Rh(por)(Cl)($CH_2CH{=}NEt_2$) and Rh(por)(CH(Me)NEt_3) species were unstable, both ultimately giving Rh^{III}(por)(Cl)(Et_2NH).

The synthesis, along with characterization by visible, proton and phosphorus nmr spectroscopy, of the previously structurally characterised, mono-phosphine complex Rh(OEP)(Cl)(PPh_3) are presented. Additionally, spectroscopic evidence is presented for solution equilibria of Rh(OEP)(Cl)(PPh_3) involving formation of Rh(OEP)$(L)_2^+$ (L = PPh_3, P^nBu_3) via thermal reactions, and Rh(OEP)(Cl)(L') (L' = CO, THF, CH_3CN) via photochemical processes. Thermodynamic data ($\Delta H^o = -33 \pm 2$ kJ mol^{-1} and $\Delta S^o = -146 \pm 8$ J $K^{-1}mol^{-1}$) have been estimated for formation of the bis(triphenylphosphine) species in CH_2Cl_2:

$$Rh(OEP)(Cl)(PPh_3) + PPh_3 \overset{K}{\rightleftharpoons} [Rh(OEP)(PPh_3)_2]+ + Cl^-$$

Some complexes of Rh^{III}(OEP) containing 1,4-bis(diphenylphosphino)butane (dppb), 1,2-bis(diphenylphosphino)ethane (dppe), bis(diphenylphosphino)methane (dppm) and 1,3-bis(diphenylphosphino)propane (dppp) have been characterized in situ using visible, proton and phosphorus nmr spectroscopy. The diphosphines (PP) are bound to Rh(III) porphyrins in a monodentate dangling fashion (Rh^{III}(OEP)(Cl)(PP) and $[Rh^{III}(OEP)(PP)_2]^+$), or a bridging mode between two metal centers ($[Rh^{III}(OEP)(Cl)]$-μPP-$[Rh^{III}(OEP)(Cl)]$).

Table of contents

Abstract ii

Table of Contents iv

List of figures vii

List of tables xii

Abbreviations xiv

Acknowledgements xvii

Chapter 1. Introduction and literature review 1

1.1. Introduction 1

1.2. Metallation 3

1.3. Non-Organometallic Complexes 6
1.3.1. Homo- and hetero-bimetallic complexes 7
1.3.2. Lewis-Base donor complexes 9
1.3.2.1. Halides/pseudo-Halides 9
1.3.2.2. O- and S-donors 10
1.3.2.3. N- and P-donors 11
1.3.3. Hydride complexes 13
1.3.4. Carbonyl complexes 14
1.3.5. Nitric oxide complexes 15
1.3.6. Isocyanide complexes 15
1.3.7. Dioxygen complexes 16

1.4. Organometallic Complexes 17
1.4.1. σ-Bonded complexes (mono-hapto) 17
1.4.2. Carbene complexes 21
1.4.3. π-Bonded complexes (dihapto) 21

1.5. Stoichiometric Reactions 21
1.5.1. Ligand Substitution and Exchange 22
1.5.2. Oxidative-Addition and Reductive-Elimination 25
1.5.3. Insertion 30
1.5.4. Electrophilic Aromatic Metallation 35
1.5.5. Reactions at an axial ligand 35
1.5.6. Migrations between metal and porphyrin 37
1.5.7. Photochemistry 38

1.6. Catalytic Reactions 39
1.6.1. Reactions of dihydrogen 39
1.6.2. Reactions of dioxygen 40
1.6.3. Dehydrogenation/Hydride transfer 41
1.6.4. Borane transfer reactions 42
1.6.5. Carbon-carbon bond formation 43

1.7. Summary 44

1.8. Goals of the present work 44

Chapter 2. Experimental methods 45

2.1. General techniques used 45
2.1.1. Infrared spectra 45
2.1.2. Electronic spectra 45
2.1.3. NMR spectra 47
2.1.4. Mass spectroscopy 49
2.1.5. Micro-analysis 49
2.1.6. Chromatography 49
2.1.7. Electrochemistry 50
2.1.8. Stopped-flow measurements 50

2.2. Materials 52
2.2.1. Solvents 52
2.2.2. Gases 52
2.23. Other materials 52
2.2.3.1. Amines 52
2.2.3.2. Phosphines 52
2.2.4. Porphyrins 53
2.2.5. Rhodium porphyrin complexes 53
2.2.5.1. Rh(OEP)(Cl)(L) 53
2.2.5.1.1. L = H_2O, Rh(OEP)(Cl)(H_2O)·H_2O 53
2.2.5.1.2. L = CH_3CN, Rh(OEP)(Cl)(CH_3CN) 56
2.2.5.1.3. L = PPh_3, Rh(OEP)(Cl)(PPh_3) 57
2.2.5.2. Rh(OEP)(H) 58
2.2.5.3. Rh(TMP)(Cl)(L) 60
2.2.5.3.1. L = iPrOH, Rh(TMP)(Cl)(iPrOH) 61
2.2.5.3.2. L = CH_3CN, Rh(TMP)(Cl)(CH_3CN) 63
2.2.5.3.3. L = none, Rh(TMP)(Cl) 64
2.2.5.4. Rh(TMP)(H) 65

Chapter 3. Reactions involving Rh(OEP)(H) 67

3.1. Introduction 67

3.2. Results and Discussion 69
3.2.1. Reaction of Rh(OEP)(H) with O_2 69
3.2.1.1. In benzene and toluene 69
3.2.1.2. In CH_2Cl_2 77
3.2.2. Reaction of Rh(OEP)(H) with O_2 in presence of PPh_3 86
3.2.2.1. Reaction of Rh(OEP)(H) with PPh_3 87
3.2.2.1.1. In CH_2Cl_2 solvent 87
3.2.2.1.2. In benzene and toluene 93
3.2.2.2. Reaction with O_2 in CH_2Cl_2 95
3.2.2.3. Reaction with O_2 in benzene and toluene 100
3.2.3. Reaction of Rh(OEP)(H) with CO and O_2 /air 104

3.3. General Discussion 107

Chapter 4. The reaction of Rh^{III}(por)(Cl)(L) complexes with tertiary amines 110

4.1. Introduction 110

4.2. Results and Discussion of Product Analysis 111
4.2.1. Amine reaction with Rh(OEP)(Cl)(L) in benzene or toluene 111
4.2.2. Amine reaction with Rh(TMP)(Cl)(L) in benzene or toluene 123
4.2.3. Amine reaction with Rh(OEP)(Cl)(H_2O) in CH_2Cl_2 132

4.2.4. Amine reaction with Rh(TMP)(Cl)(L) in CH_2Cl_2 136
4.3. Results and discussion of kinetic studies 145
4.4. General Discussion 151

Chapter 5. Characterisation and chemistry of Rh^{III}(por) phosphine complexes 154
5.1. Introduction 154
5.2. Results and Discussion 155
5.2.1. Reaction of Rh(OEP)(Cl)(PPh_3) with monophosphines 155
5.2.2. Solution equilibrium measurements 158
5.2.3. Reactions of Rh(OEP)(Cl)(PPh_3) with CO 163
5.2.4. Reactions of Rh(OEP)(Cl)(H_2O) with diphosphines 164
5.3. General Discussion 174

Chapter 6. General conclusions and suggestions for further work 177

References 182

Appendix A. Literature data summary for rhodium porphyrin organometallics 192

Appendix B. Spectral data for Rh(TMP)(Cl)(phosphine) complexes 198

Appendix C. The derivation of equation 5.3 199

Appendix D. Tables of K_{obs} for reaction 5.1 at various ionic strengths and temperatures 200

Appendix E. Assignment of the ligand ^1H nmr resonances of Rh(OEP)(CH(Me)NEt_2) 205

List of figures

Figure 1.1.	The structures of un-metallated tetraphenyl- and octaethyl-porphyrins showing the numbering scheme for the porphine core.	2
Figure 1.2.	The structure of 5,15-bis(2-pyridyl)octaethylporphyrin and of its Rh(III) chloride dimer.	7
Figure 1.3.	The binding of the amino acid esters to chloro- and acetylmethyl-trans-5,15-bis(2-hydroxy-1-naphthyl)octaethylporphyrinrhodium(III).	12
Figure 1.4.	The isoshielding lines of the OEP porphyrin ring current of $Rh^{III}(OEP)(R)$ complexes, based on data from a modified Johnson-Bovey equation.	18
Figure 1.5.	Cis- and trans-isomers of $Rh^{III}(por)(CH_2C(O)CH_3)$ (por = 5,15-bis(2-hydroxy-1-naphthyl)-octaethylporphyrin).	23
Figure 1.6.	Cationic π- and σ-complex intermediates in the reaction of $Rh^{III}(OEP)(Cl)$ and vinylethers.	34
Figure 2.1.	Tonometer for anærobic sample handling.	46
Figure 2.2.	Example of temperature variation of the ^1H nmr shifts of C_7D_8.	48
Figure 2.3.	A small scale bulb-to-bulb distillation apparatus.	50
Figure 2.4.	The arrangement of reagent reservoirs for handling air-sensitive solutions during stopped-flow experiments using the Durrum Stopped-flow.	51
Figure 2.5.	The ^1H nmr spectrum of $Rh(OEP)(Cl)(H_2O)\cdot H_2O$in $CDCl_3$.	55
Figure 2.6.	The IR spectrum (in Nujol) of $Rh(OEP)(Cl)(H_2O)\cdot H_2O$.	56
Figure 2.7.	The IR spectrum of Rh(OEP)(H).	60
Figure 2.8.	The ^1H nmr spectrum of Rh(TMP)(Cl)(iPrOH)·iPrOH in C_6D_6, at 20°C.	63
Figure 2.9.	The IR spectrum of $Rh(TMP)(Cl)(CH_3CN)$.	64
Figure 2.10.	Vacuum pyrolysis tube.	65
Figure 3.1.	The 300 MHz ^1H nmr spectra of (a) Rh(OEP)(H) in C_6D_6 and (b) 30 min after addition of O_2 at 20°C.	70
Figure 3.2.	The visible spectrum of the nmr sample illustrated in Fig. 3.1b.	72
Figure 3.3.	The visible spectrum of the products of the reaction of Rh(OEP)(H) and O_2 in C_6D_6 30 min after addition of O_2.	72
Figure 3.4.	Change in apparent extinction coefficient at 542 nm during the reaction of Rh(OEP)(H) with O_2 in benzene from various sources.	73
Figure 3.5.	The visible spectra of Rh(OEP)(H) in C_6D_6 (in vacuo) dried only over ketyl and 30 min after addition of O_2.	74
Figure 3.6.	The IR spectrum of a purple precipitate isolated from the reaction of Rh(OEP)(H) and O_2 in benzene.	75

Figure 3.7. Change in apparent extinction coefficient at 542 nm during the reaction of Rh(OEP)(H) with O_2 in toluene from various sources. 77

Figure 3.8. The 300 MHz ^1H nmr spectra of (a) Rh(OEP)(H) in CD_2Cl_2 and (b) 15 min after addition of O_2 at 20°C. 78

Figure 3.9. The visible spectra of Rh(OEP)(H) in CD_2Cl_2 and 30 min after addition of O_2. 79

Figure 3.10. Change in apparent extinction coefficient at 542 nm during the reaction of Rh(OEP)(H) with O_2 in freshly dried CD_2Cl_2 for various $[Rh]_o$. 80

Figure 3.11. Changes in the 80 MHz ^1H nmr spectra during the reaction of Rh(OEP)(H) with O_2 at -40 °C in CD_2Cl_2. 81

Figure 3.12. The IR spectrum of the residue from the reaction of Rh(OEP)(H) and O_2 in CD_2Cl_2. 83

Figure 3.13. Expansion of an upfield region of a 400 MHz ^1H nmr spectrum during the reaction of Rh(OEP)(H) with O_2 in CD_2Cl_2 at -40 °C. 83

Figure 3.14. Changes in the methine region of the 80 MHz ^1H nmr spectra during (a) cooling a solution of Rh(OEP)(H) in CD_2Cl_2 to -40 °C and (b) addition of O_2 at -40 °C. 85

Figure 3.15. The 32.3 MHz $^{31}P\{^1H\}$ nmr spectrum of Rh(OEP)(H) with excess PPh_3 in CD_2Cl_2 at -60 °C. 87

Figure 3.16. The 300 MHz ^1H nmr spectra of Rh(OEP)(H) with PPh_3 in CD_2Cl_2 at -60 °C. 88

Figure 3.17. The 121.42 MHz $^{31}P\{^1H\}$ nmr spectra of Rh(OEP)(H) with PPh_3 in CD_2Cl_2 at -60 °C. 88

Figure 3.18. The 300 MHz ^1H VT nmr spectra of Rh(OEP)(H) with PPh_3 in CD_2Cl_2 over the temperature range 20 to -60 °C. 90

Figure 3.19. The 121.42 MHz $^{31}P\{^1H\}$ VT nmr spectra of Rh(OEP)(H) with PPh_3 in CD_2Cl_2 over the temperature range 20 to -60 °C. 90

Figure 3.20. The visible spectrum of the nmr sample illustrated in Fig. 3.18/19 for Rh(OEP)(H) with PPh_3 in CD_2Cl_2. 91

Figure 3.21. The 300 MHz ^1H nmr spectrum of Rh(OEP)(H) with PPh_3 in CH_2Cl_2 at 20 °C. 92

Figure 3.22. The 300 MHz ^1H nmr spectra of Rh(OEP)(H) with PPh_3 in C_7D_8 over the temperature range 20 to -60 °C. 94

Figure 3.23. The 121.42 MHz $^{31}P\{^1H\}$ nmr spectra of Rh(OEP)(H) with PPh_3 in C_7D_8 over the temperature range 20 to -60 °C. 94

Figure 3.24. Selected regions of the 300 MHz ^1H nmr spectra of (a) Rh(OEP)(H) with PPh_3 in CH_2Cl_2 and (b) 20 min after addition of O_2 at 20°C. 96

Figure 3.25. The 121.42 MHz $^{31}P\{^1H\}$ nmr spectra of (a) Rh(OEP)(H) with PPh_3 in CH_2Cl_2 and (b) ~ 30 min after addition of O_2 at 20°C. 96

Figure 3.26. The visible spectrum of the nmr sample illustrated in Figs. 3.24/25, after the reaction of Rh(OEP)(H) with PPh_3 and O_2 in CH_2Cl_2. 97

Figure 3.27. A selected region of the 300 MHz ^1H nmr spectra of (a) Rh(OEP)(H) with PPh_3 in CD_2Cl_2 and (b) 20 min after addition of O_2 at 20°C. 97

Figure 3.28. The 121.42 MHz $^{31}P\{^1H\}$ nmr spectra of (a) Rh(OEP)(H) with PPh_3 in CD_2Cl_2 and (b) ~ 30 min after addition of O_2 at 20°C. 98

Figure 3.29. The visible spectrum of the nmr sample illustrated in Figs. 3.27/28 for the reaction of Rh(OEP)(H) with PPh_3 and O_2 in CD_2Cl_2 with the spectrum of Rh(OEP)(Cl)(PPh_3) overlaid. 98

Figure 3.30. The visible spectrum of the products of the reaction of Rh(OEP)(H) with PPh_3 and O_2 in CH_2Cl_2. 99

Figure 3.31. The 300 MHz ^1H nmr spectra at 19°C of (a) Rh(OEP)(H) with PPh_3 in C_7D_8, (b) 30 min after addition of O_2 at 19°C and (c) 5 days later. 101

Figure 3.32. The 121.42 MHz $^{31}P\{^1H\}$ nmr spectrum at 19°C of Rh(OEP)(H) with PPh_3 in C_7D_8 5 days after addition of O_2. 102

Figure 3.33. The visible spectrum of the nmr sample illustrated in Fig. 3.30b, for the reaction of Rh(OEP)(H) with PPh_3 and O_2 in C_7D_8. 103

Figure 3.34. The visible spectrum of Rh(OEP)(H) with PPh_3 in C_6H_6 and 30 min after addition of O_2. 104

Figure 3.35. The IR spectrum of the residue from the reaction of Rh(OEP)(H) and air-contaminated CO in benzene. 105

Figure 3.36. The changes in ^1H nmr spectra during the reaction in C_6D_6 of Rh(OEP)(H) with CO contaminated with O_2. 106

Figure 4.1. The ^1H nmr spectrum of Rh(OEP)(Cl)(Et_2NH) in C_6D_6 at 20 °C. 112

Figure 4.2. The ^1H nmr spectrum of a C_6D_6 solution of Rh(OEP)(Cl)(H_2O), 4 h after addition of Et_3N. 112

Figure 4.3. The visible spectrum in C_6H_6 at 25 °C of Rh(OEP)(Cl)(Et_2NH) a few minutes after preparation in situ, and a solution of Rh(OEP)(Cl)(H_2O) ~6 h after addition of Et_3N. 113

Figure 4.4. The ^1H nmr spectrum of a C_6D_6 solution of Rh(OEP)(Cl)(H_2O) (a) 15 min after addition of Et_3N and (b) 7 days later. 116

Figure 4.5. The visible spectrum of a C_6H_6 solution of Rh(OEP)(Cl)(H_2O) wth Et_3N, 30 min after the addition of Et_3N. 119

Figure 4.6. The ^1H nmr spectrum of the C_6D_6 solution sample illustrated in Figure 4.4, immediately after exposing to air. 120

Figure 4.7. The visible spectrum of a C_6H_6 solution of Rh(OEP)(Cl)(H_2O) wth Et_3N 100 min after the addition of Et_3N and then 90 min after addition of O_2. 122

Figure 4.8. The ^1H nmr spectrum of a C_6D_6 solution of Rh(TMP)(Cl)(iPrOH) (a) 10 min after addition of Et_3N and (b) 3.5 days later. 124

Figure 4.9. The ^1H nmr spectrum of a C_7D_8 solution of Rh(TMP)(Cl)(iPrOH) 1 day after addition of Et_3N. 127

Figure 4.10. Plot of the ^1H nmr shifts of the ortho-methyls of the unknown complex vs. temperature. 128

Figure 4.11. The ^1H nmr spectrum of a C_7D_8 solution of Rh(TMP)(Cl)(iPrOH) with Et_3N, after addition of O_2. 130

Figure 4.12. The ^1H nmr spectrum of a CD_2Cl_2 solution of Rh(OEP)(Cl)(H_2O) and Et_3N, 2 h after addition of Et_3N. 133

Figure 4.13. The ^1H nmr spectrum of a CD_2Cl_2 solution of Rh(OEP)(Cl)(H_2O) and Et_3N, 3 days after addition of Et_3N. 135

Figure 4.14. Plot of the ^1H nmr shifts of selected amine resonances. 136

Figure 4.15. The ^1H nmr spectrum of a CD_2Cl_2 solution of Rh(TMP)(Cl)(iPrOH) and Et_3N, 10 min after thawing a liquid nitrogen frozen sample. 137

Figure 4.16. The ^1H nmr spectrum of a CH_2Cl_2 solution of Rh(TMP)(Cl)(iPrOH) and Et_3N, at various times after thawing a liquid nitrogen frozen sample. 140

Figure 4.17. The ^1H nmr spectrum of a CD_2Cl_2 solution of Rh(TMP)(Cl)(iPrOH) and Et_3N, at various times after thawing a liquid nitrogen frozen sample. 142

Figure 4.18. The ^1H nmr spectrum of a CD_2Cl_2 solution of Rh(TMP)(Cl)(iPrOH) and Et_3N, 14 days after thawing a liquid nitrogen frozen sample, at various temperatures. 143

Figure 4.19. The comparison of ^1H nmr spectra of solutions of Rh(TMP)(Cl)(iPrOH) with added Et_3N in (a) CH_2Cl_2 at -53 °C and (b) CD_2Cl_2. 144

Figure 4.20. A typical stopped-flow trace of the change of absorbance at 540 nm of Rh(OEP)(Cl)(CH_3CN) during the reaction with Et_3N in CH_2Cl_2 . 146

Figure 4.21. Changes of the visible spectrum during the first 2 seconds of the reaction of Et_3N with Rh(OEP)(Cl)(CH_3CN) in CH_2Cl_2. 147

Figure 4.22. Changes of the visible spectrum during the first 10 seconds of the reaction of Et_3N with Rh(TMP)(Cl)(CH_3CN) in CH_2Cl_2. 147

Figure 5.1. Spectroscopic titration of Rh(OEP)(Cl)(PPh_3) with added PPh_3 in CH_2Cl_2 at 25 °C. 159

Figure 5.2. Plot of $\log_{10} K_{obs}$ vs. $\mu^{0.5}$ for data in Table 5.3. 161

Figure 5.3. Variation of $^{31}P\{^1H\}$ nmr δ–δ_{free} shifts for the PP ligand of Rh(OEP)(Cl)(PP) with the chain length of the diphosphine backbone. 167

Figure 5.4. The $^{31}P\{^1H\}$ nmr spectrum of $[Rh(OEP)(dppm)_2]^+$ in $CDCl_3$ at 20 °C. 168

Figure 5.5. The $^{31}P\{^1H\}$ nmr spectrum of a C_6D_6 solution of Rh(OEP)(Cl) in the presence of ~2.4 equivalents of dppm at 20 °C. 168

Figure 5.6. The COSY spectrum of a C_7D_8 solution of $[Rh(OEP)]_2$-μdppm at –10 °C. 171

Figure 5.7. Sketch of a possible conformation for dppm in $[Rh(OEP)]_2$-μdppm. 172

Figure 5.8. Spectroscopic titration of Rh(OEP)(Cl)(H_2O) with added dppm in CH_2Cl_2 at 25 °C. 173

Figure E.2. Atom labelling scheme for the -(CH(Me)NEt_2) ligand of Rh(OEP)(CH(Me)NEt_2). 206

Figure E.2. The 300 MHz partially decoupled ^1H nmr spectra of the -(CH(Me)NEt_2) ligand of Rh(OEP)(CH(Me)NEt_2), prepared in situ in C_7D_8 solution at 20°C. 207

List of Tables

Table 1.1.	Values of K_1 and K_2 for anation reaction of $Na_3[Rh^{III}(TPPS)(H_2O)_2]$ with Cl^-, Br^-, I^- and NCS^- at 25 °C.	22
Table 1.2.	Values of $\Delta H^{\ddagger}$ and $\Delta S^{\ddagger}$ for substitution of the first H_2O ligand of $Na_3[Rh^{III}(TPPS)(H_2O)_2]$ with Cl^-, Br^-, I^- and NCS^-.	23
Table 1.3.	Binding constants of amines with $Rh^{III}(por)(CH_2C(O)CH_3)$ (por = cis- and trans-5,15-bis(2-hydroxy-1-naphthyl)octaethylporphyrin) in $CHCl_3$ at 15 °C.	23
Table 1.4.	Formation constants for binding of PPh_3 to $Rh^{III}(por)(R)$ to form $Rh^{III}(por)(R)(PPh_3)$.	24
Table 1.5.	Some thermodynamic parameters for insertion into Rh-Rh and Rh-H bonds.	32
Table 2.1.	The $^{31}P\{^1H\}$ shifts of PPh_3 relative to 85% H_3PO_4 in various solvents.	48
Table 2.2.	The ^1H nmr data for H_2TMP in various solvents at 20 °C.	53
Table 2.3.	The ^1H nmr data for $Rh(OEP)(Cl)(H_2O)\cdot H_2O$ in various solvents at 20 °C.	55
Table 2.4.	The ^1H NMR spectral data for $Rh(OEP)(Cl)(PPh_3)$ at 20 °C.	57
Table 2.5.	Room temperature $^{31}P\{^1H\}$ NMR spectral data for $Rh(OEP)(Cl)(PPh_3)$ at 20 °C.	58
Table 2.6.	The ^1H nmr spectral data for Rh(OEP)(H) in various solvents and temperatures.	59
Table 2.7.	The ^1H NMR spectral data for Rh(TMP)(Cl)(iPrOH)·iPrOH in various solvents.	62
Table 2.8.	The ^1H NMR spectral data for Rh(TMP)(Cl) in CH_2Cl_2 and C_7D_8 at various temperatures.	66
Table 3.1.	The visible spectral data for $[Rh(OEP)]_2$ and for the product of the reaction of Rh(OEP)(H) with O_2 in benzene.	73
Table 3.2.	Some IR data for M-OOH and M-OH species from the literature.	76
Table 3.3.	Some ^1H nmr chemical shifts for hydroxyl and hydroperoxo protons of M-OH and M-OOH complexes from the literature.	84
Table 3.4.	Selected nmr data for $Rh(OEP)(Cl)(PPh_3)$ and $[Rh(OEP)(PPh_3)_2]^+$ as observed in CD_2Cl_2 solution of Rh(OEP)(H) with PPh_3 at ca. 20°C.	91
Table 4.1.	The ^1H nmr spectral data for various Rh(OEP)(Cl)(amine) complexes.	115
Table 4.2.	Ligand ^1H nmr spectral data for $RhOEP(CH(Me)NEt_2)$.	118
Table 4.3.	The ^1H nmr spectral data for various Rh(TMP) complexes in C_6H_6 or C_7D_8.	125
Table 4.4	Ligand ^1H spectral nmr data for $Rh(TMP)(CH(Me)NEt_2)$.	127

Table 4.5.	Ligand ^1H nmr spectral data for Rh(OEP)(Cl)($CH_2CH{=}NEt_2$).	133
Table 4.6.	The ^1H NMR spectral data for various Rh(TMP) complexes in the ^1H nmr spectrum illustrated in Fig. 4.15.	138
Table 4.7.	Ligand ^1H nmr spectral data for Rh(TMP)(Cl)($CH_2CH{=}NEt_2$).	139
Table 4.8.	Pseudo first-order rate constants for the disappearance of Rh(por)(Cl)(Et_3N) in CH_2Cl_2.	149
Table 4.9	Pseudo first order rate constants for the reaction of Rh(por)(Cl)(CH_3CN) with PPh_3 and CO in CH_2Cl_2.	151
Table 5.1.	NMR spectral data for Rh(OEP) complexes of monodentate phosphines and other axial ligands.	156
Table 5.2.	Visible spectral data at 25 °C for Rh^{III}(OEP) complexes.	157
Table 5.3.	Variation of K_{obs} for reaction 5.1 in CH_2Cl_2 at 25 °C.	162
Table 5.4.	Various ^1H and $^{31}P\{^1H\}$ nmr spectral data for Rh(OEP) complexes of monodentate diphosphines.	166
Table 5.5.	Various ^1H nmr spectral data for the phenyl protons of monodentate diphosphine ligands in Rh(OEP) complexes.	167
Table 5.6.	Various ^1H and $^{31}P\{^1H\}$ nmr spectral data for Rh(OEP) complexes containing bridging diphosphines.	170
Table A.1.	Rh^{III}(por)(R) species (R = hydrocarbyl), and methods of their synthesis.	192
Table A.2.	Rh^{III}(por)(R) species containing heteroatoms, and methods of their synthesis.	193
Table A.3.	Rh^{III}(EP)(R) species prepared from the "out-of-plane" Rh(I) complexes.	195
Table A.4.	Rh^{III}(TTP)(R) species electrochemically prepared from Rh^{II}(TPP).	197
Table B.1.	The ^1H NMR spectral data for Rh(TMP)(Cl)(phosphine) complexes in C_6D_6.	198
Table D.1.	Variation of K_{obs} for reaction 5.1 in CH_2Cl_2 at 10 °C.	200
Table D.2.	Variation of K_{obs} for reaction 5.1 in CH_2Cl_2 at 15 °C.	201
Table D.3.	Variation of K_{obs} for reaction 5.1 in CH_2Cl_2 at 20 °C.	202
Table D.4.	Variation of K_{obs} for reaction 5.1 in CH_2Cl_2 at 25 °C.	203
Table D.5.	Variation of K_{obs} for reaction 5.1 in CH_2Cl_2 at 30 °C.	204
Table E.1.	Ligand ^1H nmr spectral data for Rh(OEP)(CH(Me)NEt_2).	206

Abbreviations

Ac	acyl group
acac	acetoacetonate
Ar	aryl group
BAP^+	1-benzyl-3-acetylpyridinium ion
BDE	bond dissociation energy
BNA^+	1-benzylnicotinamide
CV	cyclic voltammetry
DMF	dimethylformamide
dppb	1,4-bis(diphenylphosphino)butane
dppe	1,2-bis(diphenylphosphino)ethane
dppm	bis(diphenylphosphino)methane
dppp	1,3-bis(diphenylphosphino)propane
ε	extinction coefficient ($M^{-1}cm^{-1}$); dielectric constant
$E_{1/2}$	half-wave potential (in cyclic voltammetry)
EC	EC mechanism: fast (reversible) electron transfer process followed by an irreversible, first-order chemical reaction
E_p	peak potential (in cyclic voltammetry)
eq'n	equation
esr	electron spin resonance
Φ	quantum yield
FAB	fast atom bombardment (mass spectroscopy)
FID	flame ionization detector (GC)
fig.	figure
FTIR	Fourier transform infrared (spectroscopy)
GC	gas chromatography
H_2EP	etioporphyrin(I)
$H_2MePDEE$	mesoporphyrin(IX)-diethyl ester
$H_2MePDME$	mesoporphyrin(IX)-dimethyl ester
H_2MePME	mesoporphyrin(IX)-methyl ester
H_2OEP	2,3,7,8,12,13,17,18-octaethylporphyrin
H_2por	unspecified porphyrin
H_2TAPP	5,10,15-trianthracenyl-20-(4-methoxyphenyl)porphyrin
H_2TMP	5,10,15,20-tetramesitylporphyrin
H_2ToTP	5,10,15,20-tetra-o-tolylporphyrin

H_2TPP	5,10,15,20-tetraphenylporphyrin
H_2TPPS	5,10,15,20-tetra-p-sulfonatophenylporphyrin
H_2TTP	5,10,15,20-tetra-p-tolylporphyrin
H_2TXP	5,10,15,20-tetra-(3,5 dimethylphenyl)porphyrin
hν	light (photons)
iPr	isopropyl
IR	infrared (spectroscopy)
L, L'	ligand, usually a Lewis base
M (alone)	Molarity
M (as in ML_n)	metal atom
N	Nujol™, used as a label in an IR spectrum
$NAD(P)^+$	nicotinamide coenzyme
nmr	nuclear magnetic resonance (spectroscopy)
NOE	nuclear overhauser enhancement
Ph	phenyl group
pip	piperidine
$^{31}P\{^1H\}$	proton decoupled phosphorus 31 (nmr spectroscopy)
PP	diphosphine
py	pyridine
R	alkyl group
RDS	rate determining step
ref.	reference
SCE	standard calomel electrode
sect.	section
SET	single electron transfer
τ	lifetime; chemical shift.
TBAP	tetrabutlyammonium perchlorate
THF	tetrahydrofuran
TLC	thin layer chromatography
TMS	tetramethylsilane
Vis	visible region (380—780 nm in electronic absorption spectroscopy)
VT	variable temperature
X	halide or pseudo-halide; inorganic anionic group
XPS	x-ray photoelectron spectroscopy
μ-	ionic strength
μ-L	prefix for a bridging ligand, L

Key to abbreviations used for ^1H nmr data:

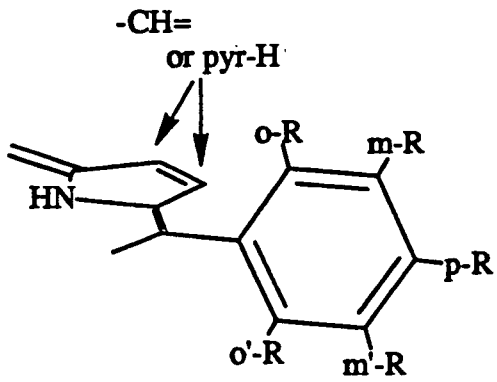

for TMP: m-, m'-R = H; o-, o'-, p-R = CH_3

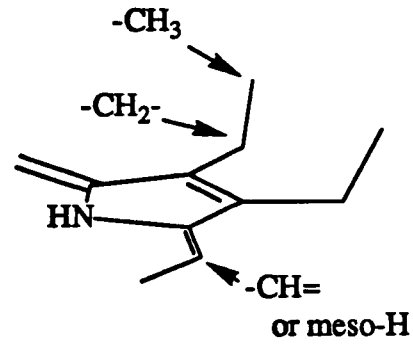

for OEP

The structure of Proton Sponge™ (used in Chapter 4):

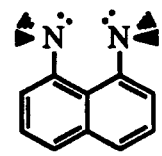

Acknowledgements

I thank Dr. Brian James for his support, guidance and encouragement. Much thanks is due to my fellow graduate students for helpful discussions and support. I particularly thank Dr. M. Camenzind in this regard and Dr. T.P. Wijesekera for help in obtaining the porphyrin ligands. Dr. A. Matsumoto also deserves thanks for his assistance in cyclic voltammetry experiments which, in the end, were not used in this thesis. I also thank the support staff in the department without whom little could be achieved.

A teaching stipend and other financial support from the Department of Chemistry are gratefully acknowledged.

Chapter 1
Introduction and literature review

1.1. Introduction

There is a strong motivation to develop metal complex catalysts that will utilize molecular oxygen under mild conditions for the selective oxidation of organic substrates (1,2), and it is very reasonable to look to analogues of components of natural systems, which normally operate under ambient conditions. In this thesis certain aspects of the chemistry of rhodium porphyrins and small molecules will be investigated. The thesis work will begin with the reaction of hydridorhodium(III) octaethylporphyrin with dioxygen, presented in Chapter 3. Chapters 4 and 5 present chemistry involving amines and phosphines. The first chapter of the thesis presents a review of the current literature of rhodium porphyrin chemistry and provides a relevant background to the research which constitutes this thesis. Of particuler relevance to the compounds discussed in the present work are section 1.2, on the metallation of porphyrins, and sections 1.3.3, 1.3.7 and 1.4.1, on the hydrides, dioxygen and σ-bonded organometallic complexes of rhodium porphyrins, respectively. Much of section 1.5, Stoichiometric Reactions, is critical to the mechanistic investigation.

The porphyrin ligand is a planar macrocycle (Fig. 1.1) with an 18-electron π system that displays aromaticity, and behaves as a quadridentate, soft-base ligand (3). Porphyrins are particularily characterised by intense colours, due to the extensive delocalised π-system. In metalloporphyrins the colours are sensitive to the metal, its oxidation state and the nature of its other ligands (4). The XPS binding energies of the nitrogen 1s electrons in metalloporphyrins show that the nitrogen atoms bound directly to the metal center are all equivalent sp^2 type (5).

The historical motivation for the study of metalloporphyrin complexes of group 8 transition metals was an interest in the mechanisms of the photosynthetic, respiratory, enzymic and organometallic chemistry of biological systems (3). Regarding the last two areas, focus has tended to be on P-450 (Fe) (6,7) and vitamin B-12 (Co) (8) type chemistry, although B-12 chemistry is actually based on the corrin ligand and not the less flexible porphyrin (9). The light harvesting capabilities of porphyrins have of course been of continuing interest (energy storage or photosynthesis (10,a), tumor reduction via photodynamic therapy (10b)). Interest in catalytic

applications of biological and biomimetic oxidations is high and provides the general motivation for the work presented in this thesis (1).

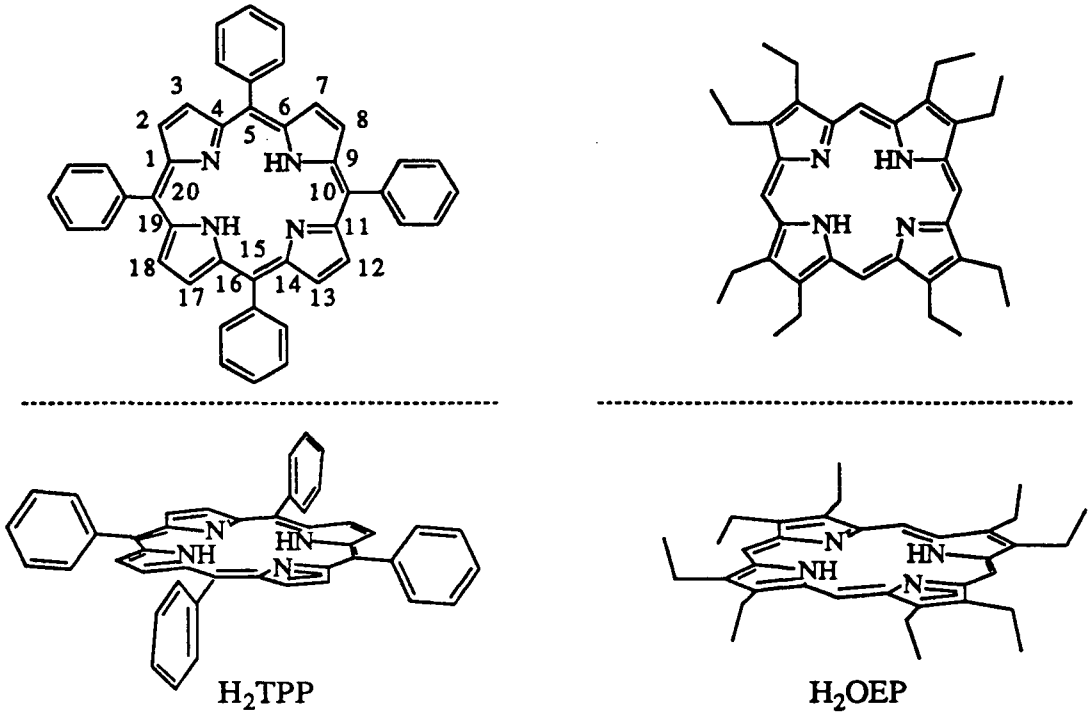

Figure 1.1. The structures of un-metallated tetraphenyl- and octaethyl-porphyrins showing the numbering scheme for the porphine core.

In terms of Rh porphyrin (Rh(por)) species attention has focused on a relatively narrow range of artificial porphyrins, particularily D_{4h} octaalkyl- and tetraaryl-porphyrins (cf. Fig. 1.1) which have simpler spectra to interpret than the natural porphyrins of lower symmetry. "Direct" application to biological systems has been limited to reconstitution of myoglobins with Rh(III) complexes (including Rh(III)-Me as an ^1H nmr probe (11)). At one time interest focused on the use of metalloporphyrins as non-paramagnetic shift reagents because of their strong ring current (sect. 1.4.1, Fig. 1.4 for visualization), the shift of the ^1H nmr resonances of coordinated ligands being a very useful diagnostic feature.

Within the field of organometallic porphyrin chemistry there has been a number of recent reviews looking at the field from the point of view of electrochemistry and structural properties of metalloporphyrins with metal-carbon and metal-metal bonds (12,13), organometallic aspects of P-450 metabolism (7), porphyrins and related macrocycles (3), and organometallic chemistry (13,14). The literature on the chemistry of Rh(por) in particular is expanding of late so that a

comprehensive review is lacking, although aspects have been thoroughly treated within broader reviews such as on organometallic compounds (15), or electrochemistry (12,13). As will be discussed in section 1.6 there is considerable interest in catalytic application of Rh(por) species, especially by workers in Japan. Hydride transfer, superoxide generation, photochemical and Lewis acid (aldol condensation) activity are the areas so far explored. In France, C-C bond formation via cyclopropanation has been investigated. Application of steric control in Rh(por) species is a critical concern in the C-C bond forming processes.

1.2. Metallation

The goal of almost all metallation recipes has been to obtain Rh(III) species, which are usually air stable and easily manipulated for further derivatization at the metal center. The general route to Rh^{III}(por)(X) is based on the reaction of $[Rh(CO)_2Cl]_2$ with the appropriate free base porphyrin. Under mild conditions (room temperature), and in inert noncoordinating solvents, "out-of-plane" (16) Rh(I) dicarbonyl complexes form (for example, Scheme 1.1). These are oxidized to Rh(III) by air (17-21), by photolysis(22,23), electro-oxidation (24), or chemical procedures using acetoacetates, fluorosulphonates, HCO_2R, $(RC(O))_2O$, RCHO, $RC(O)CH_3$, RC(O)X, RX or X_2 (sect. 1.4.1 and 1.5.2), with concomitant shift of the Rh(III) into the plane of the porphyrin.

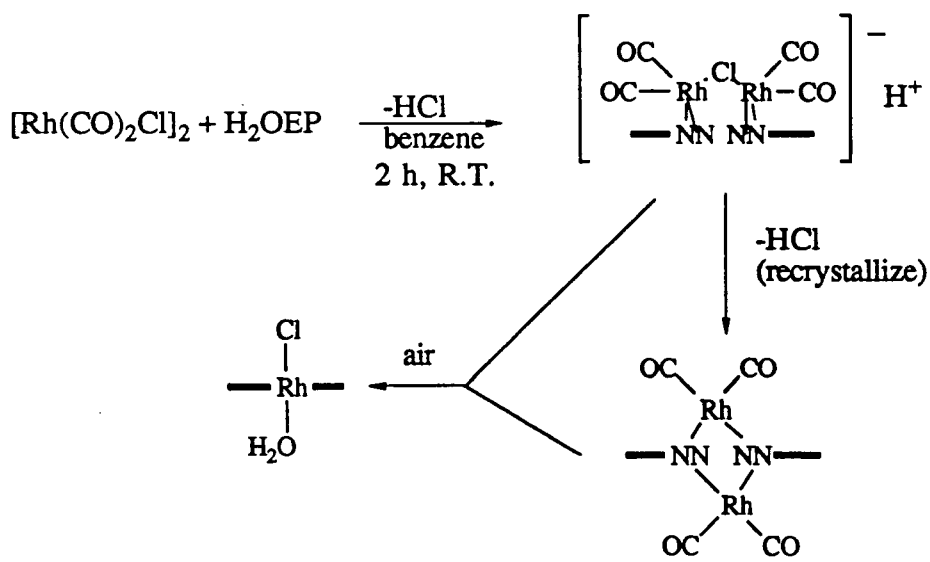

Scheme 1.1. Metallation of H_2OEP using $[Rh(CO)_2Cl]_2$.

Formation of "out-of-plane" Rh(I) dicarbonyl complexes of the kind illustrated has been shown to be general for a number of symmetric and unsymmetrical tetraalkyl- and meso-tetraarylporphyrins, azaporphyrins, oxophlorins, corroles and thiaphlorins (the last two polypyrrole macrocycles give mono-$Rh^{I}(CO)_2$ adducts only) that are not sterically hindered (25-29). After oxidation (often by refluxing in air briefly) one Rh^{I} ends up in the macrocycle as Rh(III). Oxidation by addition of I_2 during work-up has yielded Rh^{III}(por)(I) species (por = meso-, deutero-porphyrin (10,26-29); por = TPP^{2-}, $ToTP^{2-}$, TMP^{2-} (30)) in good yield. The more hindered porphyrins ($ToTP^{2-}$, TMP^{2-}) required prolonged reflux in 1,2-dichloroethane (16–36 h). For less hindered porphyrins, forcing conditions can lead to complications. For example, after $OEPH_2$ and $Rh(CO)_2Cl_2$ were refluxed for 7 h in $CHCl_3$, $[OEPH_4][Rh(CO)_2Cl_2]_2$ has been isolated and characterized by x-ray crystallography (28,31); however, coupling photolysis with similar conditions (benzene/CCl_4 reflux 8 h) gave moderate yields of Rh^{III}(por)(Cl) (por = OEP^{2-}, EP^{2-}) (32). In benzene the paramagnetic complex $Rh^{IV}(TPP)(Cl)(C_6H_5)$ has been obtained after prolonged reflux (33,34). Combining reflux with photolysis in toluene gave benzylrhodium(III) complexes rather than Rh^{III}(por)(Cl), which was obtained under otherwise identical conditions in benzene (32).

A series of Rh^{III}(por)(Cl) complexes, where por = octaethylporphyrin meso- substituted with various Lewis base functional groups (phenolic, quinolyl, methoxy, pyridyl), were prepared from $[RhCl(CO)_2]_2$ in benzene or NaOAc/HOAc (35). Mixtures of atropisomers were obtained which were separable in some cases.

When N-alkyl porphyrins or corroles are reacted with $[Rh(CO)_2Cl]_2$ in $CHCl_3$, only one $Rh^{I}(CO)_2$ unit is bound trans to the N-alkyl group(25,36). The complexes formulated as N,N-$[Rh(CO)_2Cl]_2$[por], or $[(por)(Rh^{I}(CO)_2)][Rh(CO)_2Cl_2]$, were also found (17,36,37); gentle heating of these resulted in formation of alkylrhodium(III) complexes (sect 1.5.6). The rate of metal incorporation into the N-alkyl porphyrins was much faster than into the non-N-alkylated porphyrins.

In summary, the low-valent routes yield "out-of-plane" Rh^{I} dicarbonyl complexes that are moderately air-stable and can be isolated from the product mixtures at short reaction times. Usually longer reaction times and/or higher temperatures are required to increase the proportion of

more desirable in-plane Rh^{III} complexes; however, application of long reflux periods and/or photolysis can also lead to unexpected results. Workup is usually by column chromatography, yields are often variable and unexpected products can result. For example, reaction (1.1) is used to obtain Rh(TPP)(O_2) (41-44). If the carbonyl is not added slowly to the porphyrin much of the rhodium is lost as metal (41).

$$H_2TPP \xrightarrow[\text{HOAc/NaOAc}\\ \text{reflux, } N_2]{[Rh(CO)_2Cl]_2} Rh^{III}(TPP)(O_2) \quad \text{(after chromatography)} \qquad (1.1)$$

In spite of "fine-tuning" required to achieve reliable and good yields the preferred metallation route (relative to those to be discussed below) is via the reaction of $[Rh^{I}Cl(CO)_2]_2$ with H_2por to form ultimately Rh^{III}(por)(X). In addition, the "out-of-plane" Rh^{I} dicarbonyl complexes are quite sensitive to RX oxidative addition, which can be useful preparatively. The use of other Rh(I) complexes as precursors has not been explored. A mention of [Rh(cyclooctene)$_2$Cl]$_2$ as being useful has been made but details are not available (38).

A Rh(III) precursor such as $RhCl_3 \cdot 3H_2O$ has been used in conjunction with CO as reductant (39,40). These reactions are believed to go via a Rh^{I}(por) species, which has not been isolated, and which is subsequently air oxidized to Rh^{III}(por)(Cl) (reaction (1.2)).

$$RhCl_3 \cdot 3H_2O \xrightarrow[\text{reflux}]{\text{CO, EtOH}} \xrightarrow[\text{HOAc/NaOAc}\\ \text{reflux 2 h, air}]{\text{porphyrin}} Rh^{III}(por)(Cl)(H_2O) \qquad (1.2)$$

Addition of I_2 during work-up of an H_2TPP metallation yielded Rh^{III}(TPP)(I) in variable yields (45). Addition of H_2 during work-up of an H_2OEP metallation gave Rh(OEP)(H) (46).

Variations of the general method of Adler et al. (47) for metallating porphyrins in DMF have been used with $RhCl_3 \cdot 3H_2O$. Depending on the exact recipe, and the type of porphyrin used, one obtains Rh^{III}(por)(Cl)($NHMe_2$) (48,49), [Rh^{III}(por)($NHMe_2$)$_2$]Cl (50) (sometimes mixed with [Rh^{III}(por)($NHMe_2$)$_2$][Rh($CO)_2Cl_2$] (51)), or mixtures of Rh^{III}(por)(Cl)($NHMe_2$) and [Rh^{III}(por)($NHMe_2$)$_2$]Cl (52).

For example:

$$RhCl_3\cdot 3H_2O \xrightarrow[\text{reflux, 30 min}]{DMF} \xrightarrow[\text{reflux 24 h, air}]{H_2TPP,\ DMF} Rh^{III}(TPP)(Cl)(NH(CH_3)_2) + [Rh^{III}(TPP)(NH(CH_3)_2)_2]Cl \qquad (1.3)$$

The amine ligand appears to be derived from decarbonylation of the solvent, N,N-dimethylacetamide, N-methylformamide and N-ethylformamide giving $HNMe_2$, H_2NMe and H_2NEt ligands, respectively. However, the more sterically hindered N,N-diethylformamide gave Rh^{III}(por)(Et) (por = OEP^{2-}, TPP^{2-}). The decarbonylation is proposed to occur after metallation because substitution of Rh^{III}(por)(Cl) for "$RhCl_3\cdot xH_2O$ + H_2por" in the metallation procedures gave identical products (53). The non-amine ligated, water soluble $Na_3[Rh^{III}(TPPS)(H_2O)_2]$ has been prepared in a DMF/MeOH/H_2O solvent mixture by a similar procedure (54,55).

1.3. Non-Organometallic Complexes

Four-coordinate ("bare") porphyrin complexes have been proposed for Rh in oxidation states I, II and III. These complexes are unusually reactive and only for the more oxidatively stable Rh(III) state has such a complex been isolated, although it is possible to prepare such stable Rh(I) species in solution. Evidence supporting the coordinative unsaturation includes the strong nucleophilicity of $[Rh^{I}(por)]^-$, the radical chemistry of "Rh^{II}(por)" and the strong electrophilicity of $[Rh^{III}(por)]^+$ as discussed in section 1.5.

Air sensitive "4-coordinate" $[Rh^{I}(por)]^-$ has been formed in situ under inert atmospheres but not yet isolated (sect. 1.3.3 re: H[Rh(TPP)]). Reduction of $Rh^{III}(OEP)(Cl)\cdot 2H_2O$ in EtOH with $NaBH_4/NaOH_{(aq)}$ gives $[Rh^{I}(OEP)]^-$ (17). Alternatively Rh(por)(H) can be deprotonated to give the corresponding Rh(I) anion. Thus Rh(OEP)(H) in C_6H_6 is deprotonated by stirring with alcoholic-hydroxide solutions (56). An elegant approach is to deprotonate Rh(por)(H) (por = TPP^{2-}, TTP^{2-}) in C_6D_6 with KOH solubilised by 18-crown-6-ether (57). Characterization of $[Rh^{I}(por)]^-$ as a symmetric monomer is based on its reactivity as a nucleophile (sect. 1.3.3 and 1.5), as well as uv-vis and ^{1}H nmr spectroscopy; however, detailed structural studies of the solution species are lacking.

The Rh^{II}(por) radical is proposed to exist only as an intermediate in most situations (sect. 1.5). The monomer readily dimerizes to form diamagnetic $[Rh(por)]_2$ (see sect. 1.3.1), but can reportedly be trapped in a low-temperature matrix. Based on uv-vis and esr data, irradiation of Rh^{III}(TPP)(Cl) (at λ <400 nm), or $[Rh(TPP)]_2$ (at λ < 310 nm) in 2-Me-THF, gives Rh^{II}(TPP) at 77 K (58).

The cationic complex $[Rh^{III}(OEP)]X$ (X = ClO_4^-, BF_4^-) can be isolated in ca. 50% yield from the reaction of Rh^{III}(OEP)(Cl) with either $AgClO_4$ or $AgBF_4$ in dry CH_2Cl_2. The anions are non-coordinating and the Rh(III) cation is a powerful electrophile (sect. 1.5) (21). The first reduction of $[Rh^{III}(TPP)]ClO_4$, generated in situ by electro-oxidation of $Rh^{III}(TPP)(C(O)CH_3)$, is an irreversible 1-electron process at -0.67 V (vs SCE) in PhCN to form Rh(II) (59). As for the case of $[Rh^{I}(por)]^-$, detailed solution studies of $[Rh^{III}(OEP)]X$ are lacking.

1.3.1. Homo- and hetero-bimetallic complexes

Dimerization of 5,15-bis(2-pyridyl)octaethylporphyrinato rhodium(III) chloride occurs in $CDCl_3$. The upward facing pyridyl groups on the periphery coordinate to the Rh metal center of another molecule of the monomer (Fig. 1.2); the dimer did not form in pyridine-d_5 (60).

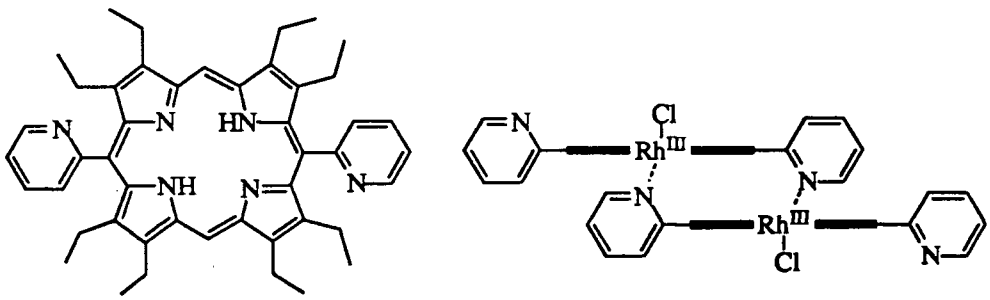

Figure 1.2. The structure of 5,15-bis(2-pyridyl)octaethylporphyrin and of its Rh(III) chloride dimer (adapted from ref. 60).

The only isolated metal-metal bonded homo-bimetallic complexes of Rh(por) are formally in the +2 oxidation state and are formulated as $[Rh(por)]_2$. The 14 d electrons of this complex are proposed to be in the configuration $\sigma^2\pi^4\eta^4\pi^{*4}$, yielding a diamagnetic species with a net single metal-metal bond (61). The BDE for the metal-metal bond of $[Rh(OEP)]_2$ has been estimated,

from ^1H nmr line broadening data, as 16.5 kcal/mol in benzene and 17.5 kcal/mol in cyclohexane (62,63). The diamagnetic dimers are prepared from Rh(por)(H) in aromatic solvents by oxidative cleavage in air (por = OEP^{2-}) (64,65), or by thermal (64) or photolytic (43,57,61) homolytic cleavage (por = OEP^{2-}, TPP^{2-}, TTP^{2-}). For example (reactions 1.4 – 1.5), in toluene the OEP dimer can be prepared by either route.

$$2\ Rh(OEP)(H) + air \longrightarrow [Rh^{II}(OEP)]_2 + H_2O \qquad (1.4)$$

$$2\ Rh(OEP)(H) + heat\ or\ h\nu \longrightarrow [Rh^{II}(OEP)]_2 + H_2 \qquad (1.5)$$

The isolated tetraarylporphyrin complexes have been characterized only by ^1H nmr. Photolysis of (μ-TPP)$[Rh^{I}(CO)_2]_2$ in benzene is reported to yield $[Rh^{II}(TPP)]_2$ dimer via formation of Rh^{II}(TPP) monomer (22). The identity was made on the basis of uv-vis data and reactivity toward O_2 but has been subsequently suggested to be Rh(TPP)(H) also on the basis of the uv-vis data (52). Heating Rh(TPP)(O_2) at 150 °C in vacuo results in sublimation of a diamagnetic Rh(TPP) compound tentatively formulated as $[Rh^{II}(TPP)]_2$, on the basis of reactivity and unpublished spectral data (42).

The isolated Rh(II) dimers have not been examined electrochemically. However, electrochemical reduction of Rh^{III}(TPP)(Cl)($NHMe_2$) or $[Rh^{III}(TPP)(NHMe_2)]_2Cl$ in PhCN, THF, or py gives $[Rh^{II}(TPP)]_2$ via a 1-electron EC mechanism (sect. 1.3.2.3). The dimer has not been isolated but cyclic voltammetry shows a reversible 2-electron reduction of the species at -1.95 V (vs. SCE) in PhCN (0.1 TBAP). Similar reductions occur in THF at -1.83 V and py at -1.90 V. The reduced species is proposed to be a radical anion on the basis of uv-vis data. The $[Rh^{II}(TPP)]_2$ species is irreversibly oxidized during the anodic sweep at E_p = -0.24 V in PhCN, E_p = -0.22V in THF and E_p = -0.40V in py . No cathodic peak was coupled to the oxidation in the second cycle and the product is believed to be $Rh^{III}(TPP)(solvent)^+$. Some dissociation of the dimer to Rh^{II}(TPP) monomer is indicated and the E_p for its oxidation was $\approx$ -1.0 V (52). The monomeric Rh(II) species generated in situ readily reacts with halogenated and unsaturated compounds to generate organometallic products (sect. 1.4).

A hetero-bimetallic Rh(I)-In(III) dimer, $Rh^{I}(OEP)In^{III}(OEP)$, is synthesised by the reaction of $Rh^{I}(OEP)^{-}$, prepared in situ by deprotonation of Rh(OEP)(H) with $NaN(SiMe_3)_2$), and $In^{III}(OEP)(Cl)$ in THF. The spectral and x-ray crystallographic data are consistent with a single metal-metal bond. The $Rh(I)^{-}:\rightarrow In(III)^{+}$ formulation is supported by the quantitatively regioselective reaction with MeI to form Rh(OEP)(Me) and In(OEP)(I) (66).

Hetero-bimetallic complexes of the type $Rh(TPP)(ML_n)$, $ML_n = Mn(CO)_5$, $Co(CO)_4$, $GeCl_3$, have been isolated by reaction of the corresponding metallate anions with $Rh^{III}(TPP)(Cl)$ in THF. Reaction of $SnCl_2$ with $Rh^{III}(TPP)(Cl)$ gives $Rh(TPP)(SnCl_3)$. The complexes are believed to be 5-coordinate, akin to $Rh^{III}(TPP)(X)$ on the basis of preliminary IR, uv-vis and ^1H nmr data, even though the nmr data also indicate that all the complexes are symmetrical (D_{4h}) in solution (67).

1.3.2. Lewis-Base donor complexes

It is relatively easy to form Rh(por)(X)(L) species in situ from Rh(por)(X)(L') species because of lability of L' (see sect. 1.5.1). The point of view of this section leans more towards isolable complexes. Ligand exchange will be treated in section 1.5.1.

1.3.2.1. Halides/pseudo-Halides

As noted in section 1.2 on metallation, $Rh^{III}(por)(X)$ is the usual product of metallation. The chloride complex is usually obtained because $RhCl_3 \cdot xH_2O$ or $[RhCl(CO)_2]_2$ is the common starting material; however, air is usefully replaced by I_2 as oxidant in which case Rh(III) iodide complexes form. A bromide complex, $Rh^{III}(OEP)(Br)(NH_3)$, has been isolated and will be discussed in section 1.3.2.3 on N- and P-donor complexes. There are no reports of the isolation of in-plane Rh(por) halide complexes in oxidation states other than +3, with the exception of $Rh^{IV}(TPP)(Cl)(C_6H_5)$ (33,34).

The XPS binding energies for the Rh 3d electrons in $Rh^{III}(por)(Cl)$ ($por = OEP^{2-}$, TPP^{2-}) are consistent with a Rh(III) oxidation state (68). Also consistent with the Rh(III) oxidation state is the hypso-type uv-vis spectra (17,69). The first oxidation of $Rh^{III}(OEP)(Cl)$ is a reversible 1-electron process at 0.82 V (vs. SCE, CH_2Cl_2) and for the TPP analogue at 0.98 V, giving a porphyrin π-cation radical species, identified by esr and uv-vis (43). The electrochemistry of

$Rh^{III}(TPP)(Cl)(L)$ (L = amine , phosphine) is similar and will be discussed in section 1.3.2.3. The first oxidation is a reversible 1-electron process at the porphyrin to generate a Rh(III) porphyrin cation radical, and the first reduction is an irreversible 1-electron process at the metal giving Rh(II) with loss of the Cl^- ligand.

Little interest has been shown in pseudo-halide complexes of Rh(por). The Cl^- ligand of $Rh^{III}(MePDEE)(Cl)(H_2O)$ has been replaced with SCN^- (N-bonded), CN^-, or N_3^- (38). A thiocyanate complex has been prepared in situ from $Na_3[Rh^{III}(TPPS)(H_2O)_2]$ (sect. 1.5.1), but the bonding mode is uncertain (54,55).

1.3.2.2. O- and S-donors

Most of the complexes containing Rh-O moieties (exclusive of O_2 complexes to be discussed in sect. 1.3.6) are aquo complexes (see below). The carboxylate complex $Rh(EP)(O_2CCH_3)$ has been reported but with few details (28). The ethene complexes $Rh^{III}(OEP)(X)(CH_2{=}CH_2)$ (X = $CF_3CO_2^-$, $CF_3SO_3^-$) have been observed by ^1H nmr (sect. 1.5.3 and 1.5.5) (70). Solvato complexes in THF are known (sect. 1.3.3 and 1.5.6). Oxygen bound intermediates are proposed during the abstraction of the acetyl group from N,N-dimethylacetamide (71), the dehydrogenation of secondary alcohols (sect. 1.6.3.), and the enolization of ketones (sections 1.5.5 and 1.6.5). Dicarboxylate complexes of Rh(III) thiaphlorin have been reported (28).

Aquo complexes of $Rh^{III}(OEP)(Cl)$ and $Rh^{III}(OEP)(R)$ (R = $n\text{-}C_4H_9$, $n\text{-}C_9H_{19}$) have been isolated (17), as well as the water soluble $Na_3[Rh^{III}(TPPS)(H_2O)_2]\cdot 22H_2O$. The pK_{a1} and pK_{a2} for the TPPS complex in H_2O (25 °C; μ = 1.00 M $NaClO_4$) are 7.01 and 9.80, respectively (54,55).

$$[Rh^{III}(TPPS)(H_2O)_2]^{3-} \overset{K_{a1}}{\rightleftharpoons} [Rh^{III}(TPPS)(H_2O)(OH)]^{4-} \overset{K_{a2}}{\rightleftharpoons} [Rh^{III}(TPPS)(OH)_2]^{5-} \quad (1.6)$$

The $[Rh^{III}(TPPS)(H_2O)_2]^{3-}$ complex shows moderate phosphorescence ($\Phi \geq 10^{-2}$) in H_2O at room temperature, as do $Rh^{III}(por)(Cl)(MeOH)$ species (por = OEP^{2-}, TPP^{2-}, $MePME^{2-}$)

formed in situ in MeOH. Strong phosphorescence ($\Phi = 0.23$) was observed for $Rh^{III}(EP)(Cl)(2\text{-Me-THF})$ in 2-Me-THF at 77 °K (50).

There are no examples of isolated complexes containing a Rh-S bond. Metastable complexes of the type $[Rh^{III}(OEP)(thiolate)_2]^+$ (thiolate = thioglycolate ethyl ester, thioglycolate n-octyl ester, thioglycolate octadecyl ester, methyl 3-mercaptopropionate, 2-mercapto acetanilide, thioalide, thiosalicylic acid, Me- and halo-thiophenols) can be prepared in situ by the reaction of $Rh^{III}(OEP)(Cl)$ with the appropriate thiolate in a number of solvents, the thiolates being prepared in situ using Bu_4NOH. The bis-thiolato complexes have a split-Soret hyperporphyrin spectrum similar to that of P-450 and decompose with concomitant catalytic reduction of O_2 to O_2^- (sect. 1.6.2) (72). The position of the Soret peaks (over a 20 nm range) correlate linearly with Hammett σ values of thiophenol substituents indicating an inductive dependance; linear correlation with the dielectric constants of 5 alcohol solvents was also found (over ~10 nm range).

1.3.2.3. N- and P-donors

As mentioned in section 1.2, metallation of H_2por in amide solvents usually gives amine complexes of the type $Rh^{III}(por)(Cl)(amine)$ or $[Rh^{III}(por)(amine)_2]X$ (amine = primary or secondary). The counter ion ($X = Cl^-$) can be exchanged for PF_6^- by treatment with $AgPF_6$ in acetone (51). Irradiation of $Rh^{III}(OEP)(Cl)$ in toluene in the presence of $NHMe_2$ gives $[Rh^{III}(OEP)(NHMe_2)_2]Cl$ but, if $Rh^{III}(EP)(Cl)$ is used in 1,2-dichloroethane, the Cl is not replaced and $Rh^{III}(EP)(Cl)(NHMe_2)$ is obtained (32). The ammonia complexes $Rh^{III}(OEP)(X)(NH_3)$ ($X = Br^-, I^-$) are obtained by a somewhat novel route, by reaction of $Rh^{III}(OEP)(Cl)(H_2O)$ with EtMgX followed by workup in aqueous NH_4Cl (17). Reaction of $[Rh(OEP)]_2$ with EtI, followed by recrystallization (after chromatography) from n-hexane/pyridine, gives $Rh^{III}(OEP)(I)(py)$ (64). Pyridine complexes of the type $Rh^{III}(OEP)(CH_3)(amine)$ (amine = 4-CH_3-py, py, 4-CN-py) can be isolated in the presence of excess pyridine, but equilibrate to a mixture of 5- and 6-coordinate species in solution (17).

Chloro- and methyl-rhodium(III) complexes of trans-5,15-bis(2-hydroxy-1-naphthyl)- and 5,15-bis(1-naphthyl)octaethylporphyrin form 1:1 amine adducts with L-phenylalanine methyl ester and L-leucine methyl ester, as well as with 2-phenylethylamine and 3- or 4-aminoheptane in

$CHCl_3$. The binding of the non-ionic amino acid esters is both at Rh (by the amino group) and at naphtholic functions on the periphery of the porphyrin (by the ester group) (Fig. 1.3) (73).

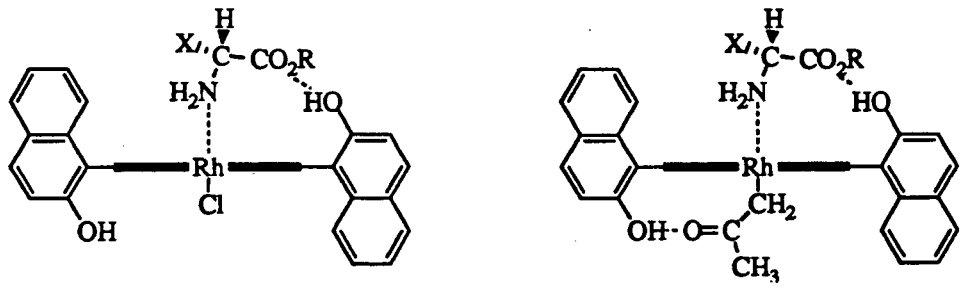

Figure 1.3. The binding of the amino acid esters to chloro- and acetylmethyl-trans-5,15-bis(2-hydroxy-1-naphthyl)octaethylporphyrinrhodium(III) (adapted from ref. 73).

In the particular case of some $[Rh^{III}(por)(NHMe_2)_2]X$ complexes, there is evidence of close association of the anion with the cationic complexes, by hydrogen bonding. For example, X-ray crystallography reveals that the Cl^- of $[Rh^{III}(EP)(NHMe_2)_2]Cl\cdot H_2O$ is in a roughly tetrahedral environment, hydrogen-bonded to two N-H groups on different complexes and two water molecules, and the water molecules are not linked to any other moieties (49). The tightness of ion pairing in $[Rh^{III}(por)(NHMe_2)_2]X$ (por = OEP^{2-}, TPP^{2-}) is believed to increase with X in the order $[Rh(CO)_2Cl_2]^- < PF_6^- < Cl^-$, this being based on IR data, ligand N-H ^1H nmr resonance shapes and positions, and on ligand N-Me and OEP meso C-H mutual 2D NOE correlations in $CDCl_3$ solution (51).

The electrochemistry and spectroelectrochemistry of $Rh^{III}(TPP)(Cl)(NHMe_2)$ and $[Rh^{III}(TPP)(NHMe_2)_2]Cl$ have been studied. Depending on the solvent used, a reversible 1-electron oxidation of the porphyrin occurs at 1.3 – 1 V (vs. SCE) to form a Rh(III) porphyrin cation radical. A 1-electron reduction occurs at an E_p of -1.28 to -1 V (vs. SCE) to give $\frac{1}{2}[Rh^{II}(TPP)]_2$ via an EC process involving a transient Rh(II) species (detected at -78°C by CV), previously mentioned in section 1.3.1 (52).

Strong phosphorescence is observed for $[Rh^{III}(EP)(NHMe_2)_2]Cl$ in 2-Me-THF at 77 K (Φ_p =0.23, τ_p = 0.73(2) ms) (49) and has been discussed in the context of iterative extended Hückel calculations (74).

As described in this Thesis (Chap. 5), addition of PPh_3 to $Rh^{III}(OEP)(Cl)$ in benzene gives $Rh^{III}(OEP)(Cl)(PPh_3)$ which is characterized spectroscopically and crystallographically. The octahedrally coordinated Rh atom is displaced by 0.077 Å from the mean plane of the porphyrin N atoms towards the PPh_3 ligand (75). The cationic complexes $[Rh^{III}(por)(L)_2]PF_6$ (por = OEP^{2-}, EP^{2-}, TPP^{2-}; L = PPh_2Me, $P(OMe)_3$) can be prepared by addition of excess phosphine to acetone solutions of $Rh^{III}(por)(PF_6)$, prepared in situ; alternatively, the OEP complexes can be prepared by photolysis of $[Rh^{III}(OEP)(NHMe_2)_2]PF_6$ in the presence of the phosphine (32). A $[Rh^{III}(TPP)(PPh_3)_2]^+$ complex can also be prepared in situ from $Rh(TPP)(O_2)$ through a $Rh(TPP)(O_2)(PPh_3)$ intermediate (sect. 1.3.7).

The rhodium phosphonate complex $Rh^{III}(OEP)(P(O)(OCH_3)_2)$ is formed by the reaction of $P(OCH_3)_3$ with $[Rh^{II}(OEP)]_2$. An unstable Rh(II) phosphite complex, which loses a methyl radical, is proposed as an intermediate (76). There are no examples of isolated low-valent Rh complexes containing N- or P-donors.

The XPS binding energies for the Rh 3d electrons in $[Rh^{III}(TPP)(PPh_3)_2]PF_6$ and $[Rh^{III}(OEP)(PPh_2Me)_2]PF_6$ are consistent with a Rh(III) oxidation state (68). The electrochemistry of in situ $[Rh^{III}(TPP)(P)_2]^+$ species (P = PPh_3, $PPhMe_2$) varies with the phosphine ligand. The $PPhMe_2$ complex in CH_2Cl_2 (0.1 M TBAP) has a reversible 1-electron oxidation at $E_{1/2}$ = 1.20 V (SCE) to give a Rh(III) porphyrin cation radical, and a reversible 1-electron reduction at $E_{1/2}$ = -1.14 V (SCE) to give a Rh(III) porphyrin anion radical (77). The PPh_3 complex is reduced at E_p = -0.98 V (SCE) via an 1-electron EC process that is metal-centered and is followed by loss of PPh_3; electro-oxidation was not reported on (44).

1.3.3. Hydride complexes

In iPrOH or DMF at 20 °C, dihydrogen reacts with $Rh(TPP)(O_2)$ to give Rh(por)(H), originally formulated as $H[Rh^{I}(TPP)]\cdot 2H_2O$ (41). Reaction of H_2 with $Rh^{III}(OEP)(Cl)$ in methanol at room temperature precipitates Rh(OEP)(H) but in low yield (~20%) (65,78), while better yields (80%) are obtained if in situ $Rh^{III}(OEP)(Cl)$ species is used (46). Reaction of $Rh^{III}(por)(I)$ (por = TPP^{2-}, TTP^{2-}) with sodium formate in MeOH, followed by workup under H_2, gives Rh(por)(H) in 78% yield (57). Rhodium hydride complexes can be prepared also via

protonation of Rh(I) species generated in situ from borohydride reduction of Rh(III) complexes. Typically Rh^{III}(por)(X) (por = OEP^{2-}, X = Cl^- (65,78); por = TPP^{2-}, TTP^{2-}, X = I^- (57)) in EtOH is reduced with $NaBH_4$ followed by protonation with AcOH. Yields of 60 - 80% of Rh(por)(H) are reported. Acidification with AcOD gives Rh(por)(D).

The electronic spectrum of Rh(OEP)(H) is similar to the hypso-type spectra of Rh^{III}(OEP)(R) complexes, and thus the oxidation state of rhodium is considered correctly assigned as three (65). The diamagnetic Rh(por)(H) complexes are all characterized by a solvent dependent doublet hydride ^1H nmr resonance upfield of TMS in the -29 to -42 ppm region, and thus in solution the species are better formulated as Rh(por)(H)(solvent). The ^1H nmr spectrum of Rh(OEP)(H) in benzene is temperature dependent, probably due to exchange with small amounts of $[Rh^{II}(OEP)]_2$ (46) (sect. 1.3.1). The porphyrin ^1H nmr resonances of Rh(TPP)(H) and Rh(TTP)(H) in C_6D_6 are broadened and also the hydride resonance is not seen because of the exchange with dinuclear species (equilibrium 1.7) (57). Thermodynamic data for the equilibrium:

$$[Rh(OEP)]_2 + H_2 \rightleftharpoons 2Rh(OEP)(H) \qquad (1.7)$$

has been measured: $\Delta H° = -13 \pm 4$ kJ mol^{-1}; $\Delta S° = 3 \pm 8$ J K^{-1} mol^{-1}. As the BDE of $[Rh(OEP)]_2$ is known (sect . 1.3.1), the Rh-H bond energy of Rh(OEP)(H) has been estimated to be 259 kJ mol^{-1} (46,63). Conversion of Rh(por)(H) to $[Rh^{II}(por)]_2$ and H_2 is a typical decomposition path observed for the hydrides (sect. 1.3.1 and 1.5).

Although the Rh-H bond can be considered to be largely covalent, the hydrides can be deprotonated by MOH (M = Na^+ in EtOH; M = K^+[18-crown-6-ether] in benzene) (41,57,80), and this is just the reverse of the synthesis of Rh(por)(H) via protonation of $Rh^I(por)^-$. Solutions of Rh(TPP)(H) in DMF are conducting, and the proton is titratable (41). The Rh-H pK_a has not been reported in any solvent system, although the tetraarylporphyrin complexes are considered to be more acidic than the octaalkylporphyin complexes (65).

1.3.4. Carbonyl complexes

Carbonylation of Rh(TPP)(Cl) in CH_2Cl_2 with 1 atm CO precipitates Rh(TPP)(Cl)(CO), $\nu_{CO} = 2100$ cm^{-1}. The CO appears to be labile and the complex was not stable enough to

withstand chromatography (82). The coordinated CO is susceptible to nucleophilic attack at carbon (sect 1.5.3).

Reactions of CO with $[Rh(OEP)]_2$ in toluene give an equilibrium system including 3 species besides $[Rh(OEP)]_2$: a 1:1 adduct $[Rh(OEP)]_2CO$ (ν_{CO} = 2094 cm^{-1}), a metallo-ketone $[Rh(OEP)]_2$-μCO (ν_{CO} = 1733 cm^{-1}) and a double insertion product [Rh(OEP)]-C(O)C(O)-[Rh(OEP)] (sect.1.5.3). In situ characterisation was by ^1H and ^{13}C nmr, and IR (83-85). Another 1,2-ethanedionyl complex, [Rh(TXP)]-C(O)C(O)-[Rh(TXP)], has been similarly characterised (85a). The monomeric Rh^{II}(TMP) complex reacts with CO to form Rh(TMP)(CO), containing a bent 17-electron M-CO unit, found in equilibrium with [Rh(TMP)]-C(O)C(O)-[Rh(TMP)] (85b).

1.3.5. Nitric oxide complexes

Nitric oxide reacts with $[Rh(OEP)]_2$, Rh(OEP)(H) and Rh(por)(Cl) (por = OEP^{2-}, TPP^{2-}) in toluene solution, or the solid state, to give ultimately Rh(por)(NO). On the basis of epr data Rh(por)(NO) is formulated as diamagnetic Rh^{III}(por)(NO^-). The Rh(OEP)(NO) complex undergoes a reversible 1-electron oxidation in CH_2Cl_2 at 0.77 V (vs. SCE) and the TPP analogue is similarly oxidized at 0.94 V, giving porphyrin π-cation radical species. The reaction of the Rh(por)(Cl) complexes with NO proceeds through a paramagnetic porphyrin π-cation radical intermediate species $Rh^{III}(por^{+\cdot})(Cl^-)(NO^-)$. In the presence of excess NO, Rh(por)(NO) reversibly adds further NO to form a paramagnetic porphyrin π-cation radical species $Rh^{III}(por^{+\cdot})(NO^-)_2$. Solutions of Rh(OEP)(NO) are air-sensitive, slowly giving Rh(por)(NO_2) (43).

1.3.6. Isocyanide complexes

The cationic complexes $[Rh^{III}(por)(t\text{-}BuNC)_2]PF_6$ (por = OEP^{2-}, EP^{2-}, TPP^{2-}) can be prepared by addition of excess t-BuNC to acetone solutions of $[Rh^{III}(por)]PF_6$, prepared in situ. Alternatively, the OEP complex can be prepared by photolysis of $[Rh^{III}(OEP)(NHMe_2)_2]PF_6$ in the presence of excess isocyanide (32).

1.3.7. Dioxygen complexes

It should be noted that no crystal structures, elemental analyses or isolated yields have yet been reported for any of the dioxygen species discussed in this section. The paramagnetic dioxygen adduct $Rh(TPP)(O_2)$ can be isolated from the metallation reaction of H_2TPP with $[Rh(CO)_2Cl]_2$ in DMF (41,42). The complex can reportedly also be made by borohydride reduction of "any $Rh^{III}(TPP)(X)$" complex with subsequent addition of O_2 (43). The analogous $Rh(OEP)(O_2)$ complex is thermally unstable, but could be prepared at -80 °C by slow diffusion of dry O_2 into a toluene solution of $[Rh^{II}(OEP)]_2$. The O_2 is believed to be coordinated end-on as a superoxide, based on esr data at -160 °C and IR data (ν_{O-O} = 1075 cm^{-1}) of an impure solid isolated at -20 °C; warming solutions of the superoxide species to room temperature results in formation of the μ-peroxide $Rh^{III}(OEP)$-O_2-$Rh^{III}(OEP)$, as judged by its diamagnetism, disappearance of ν_{O-O} and "unpublished ^1H nmr data indicative of a $Rh^{III}(OEP)(L)$ complex" (42). At low temperature, $Rh(OEP)(O_2)(L)$ (L = py, pip, $(BuO)_3P$) species were detected by esr (42,43).

The electrochemistry of the $Rh(TPP)(O_2)$ complex is similar to that of $Rh^{III}(TPP)(Cl)(NHMe_2)$ and $[Rh^{III}(TPP)(NHMe_2)_2]Cl$. The first reduction is at E_p = -1.14 V (SCE) in PhCN (1.0 M TBAP) and was a 1-electron metal centered EC process forming $[Rh^{II}(TPP)]_2$. The dioxygen complex reacts with PPh_3 forming $Rh^{III}(TPP)(O_2)(PPh_3)$ and then $[Rh^{III}(TPP)(PPh_3)_2]^+$ in the presence of excess PPh_3 (equilibria 1.8a/b; sect. 1.5.1).

$$Rh(TPP)(O_2)(solvent) + PPh_3 \overset{K_1}{\rightleftharpoons} Rh(TPP)(O_2)(PPh_3) + solvent \qquad (1.8a)$$

$$Rh(TPP)(O_2)(PPh_3) + PPh_3 \overset{K_2}{\rightleftharpoons} [Rh(TPP)(PPh_3)_2]^+ + O_2^- \qquad (1.8b)$$

Coordination of the π-acid PPh_3 causes a shift of the first reduction to a lower potential at E_p = -0.88 V; however, because of the nature of the CV experiment it was unclear whether this was due to changes in kinetics, geometry or stabilization of the initial Rh(II) formed in the EC process. The equilibria are unaffected by air. Direct observation of O_2^- was not made; indeed the product solutions are esr silent (44). It should be noted that superoxide is known to react with CH_2Cl_2 (86,87). No mention was made of any $OPPh_3$ formation.

The simple substitution of the dioxygen ligand by PPh_3 (i.e., reaction 1.8b) in aprotic solvents is akin to the behaviour of a Brönsted base, and is consistent with the O_2 ligand of $Rh^{III}(TPP)(O_2)$ being superoxide (87). The origin of the claimed increased stability of the TPP complex versus the OEP complex is not apparent.

1.4. Organometallic Complexes

1.4.1. σ-Bonded complexes (mono-hapto)

A large number of $Rh^{III}(por)(R)$ complexes have been synthesized from Rh(I), Rh(II) or Rh(III) porphyrin precursors. With one exception there are no known isolated complexes with the metal in other oxidation states; a paramagnetic complex $Rh^{IV}(TPP)(Cl)(C_6H_5)$ was reported in the late 1960s (including preliminary crystal structure data), but no work on this or related complexes has appeared since (33,34).

The $Rh^{III}(por)(R)$ complexes have a hypso-type uv-vis spectrum typical of a d^6 system, the -R group being considered to be a purely σ-bonded axial ligand (17,69). The Rh-C bond length in $Rh^{III}(OEP)(CH_3)$ is 2.031 Å (88), and the BDE of Rh-C in the Rh(III) complexes is estimated to be 230–251 kJ mol^{-1} (see below, re: Rh-CHO) (56,62). The electrochemistry of an extensive series of $Rh^{III}(por)(R)$ species (Table A.4 in Appendix A) has been studied. The first reduction (1-electron, reversible) is between -1.39 and -1.44 V (vs. SCE, depending on solvent) and gives a Rh(III) porphyrin radical anion. Depending on R and the timescale Rh-C or C-X (if R = RX) cleavage can follow the first reduction. Normally, the first oxidation (1 e^-, reversible) is between 0.85 and 1.03 V (vs. SCE) and gives a Rh(III) radical cation, but the $Rh^{III}(TPP)(C(O)CH_3)$ complex is irreversibly oxidized at the $C(O)CH_3$ ligand rather than at the porphyrin π-system, resulting in cleavage to form $[Rh(TPP)]^+$ (12,13,59,89-91).

A series of $Rh^{III}(OEP)(R)$ complexes have been used to calibrate an isoshielding map of the variation of ^1H nmr chemical shifts with distance from the porphyrin (Fig. 1.4) (17). The shifts are explained mainly by the diamagnetic anisotropy of the porphyrin ring current and could be estimated using the Johnson-Bovey equation (92). However, the differences, Δτ, between the observed shifts and the parent hydrocarbon shifts deviate from the shift differences, δ, calculated from the Johnson-Bovey equation. There is a correlation, $\Delta\tau = 2.34(\delta)^{1/2} - 1.08$, between the

shifts, and the map was created from the data calculated using the Johnson-Bovey equation, modified by the correlation.

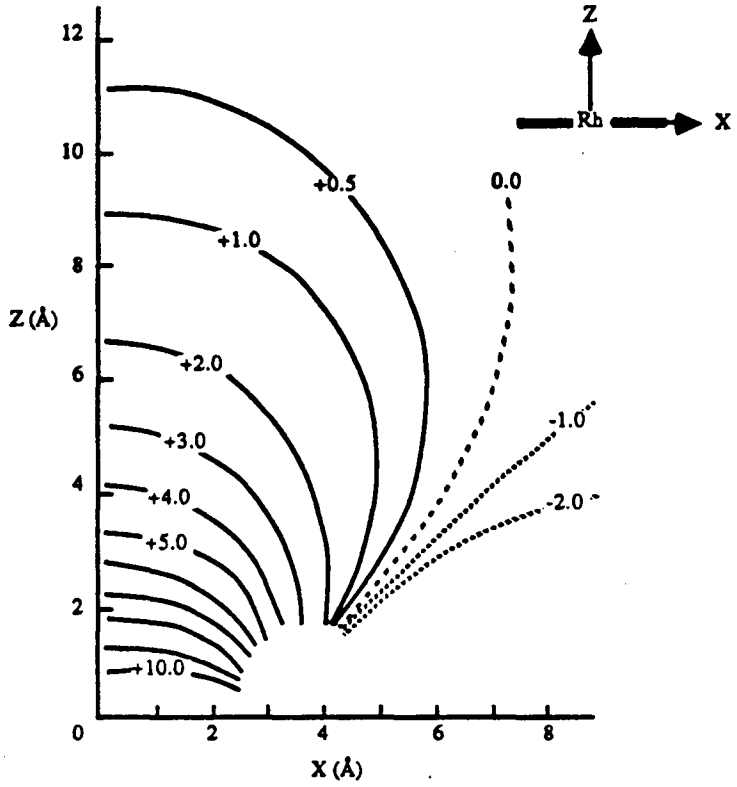

Figure 1.4. The isoshielding lines of the OEP porphyrin ring current of Rh^{III}(OEP)(R) complexes, based on data from a modified Johnson-Bovey equation; note that the contours are of change in shift in τ and that the axes are oriented as indicated in the schematic (adapted from ref. 17).

The chemical methods to synthesize Rh^{III}(por)(R) complexes will be treated first and then electrochemical methods. Some additional examples are also covered in section 1.5. Tables A.1 and A.2 (Appendix A) summarize the Rh^{III}(por)(R) complexes that have been synthesised and the primary reagents used to obtain them. Note that complexes which are "fully" characterized, i.e. isolated with elemental analysis and spectroscopic characterization, are specially marked in the Tables. The reactions corresponding to the tabulated data are briefly discussed in the following paragraphs from the point of view of the general reactivity of the Rh(por) precursor in the context

of Rh-C bond formation. The Rh^{III}(por)(R) complexes are generally 5-coordinate in the solid state but for a few cases H_2O occupies the sixth site (17).

Generally alkylation, or arylation, of Rh^{III}(por)(X) is achieved with RLi but not RMgBr or RMgI, because reaction with the Grignard reagent results in halide exchange instead of Rh-C formation (17). With certain RLi reagents in excess (R = p-$MeOC_6H_4$, o-MeC_6H_4, C_6H_5, or n-Bu), migration of a second incoming R from Rh to the meso position of OEP to form Rh^{III}(OEP-R)(R) has been reported (sect. 1.5.6) (93). Terminal alkynes react with Rh^{III}(por)(Cl) to give either net addition of Rh-Cl across the triple bond or Rh-C(O)R derivatives if H_2O is present. A unique alkene reaction has been reported, vinyl ether in EtOH reacting with Rh^{III}(por)(Cl) in the presence of tertiary amine as co-reagent to give a β-acetal (94). Diazomethane, diazoacetate and diazopropionates react with Rh^{III}(por)(I) to give a variety of products (45,95). The α-metallation of methyl ketones to give Rh-$CH_2C(O)R$ is possible with Rh^{III}(por)(Cl) (por = cis- and trans-5,15-bis(2-hydroxy-1-naphthyl)-octaethylporphyrin, tetrakis(2-hydroxy-phenyl)porphyrin, trans-5,15-di(8-quinolyl)octaethylporphyrin). The presence of phenolic hydroxyl or quinolyl nitrogen in correct orientation and proximity to the site of coordination is essential (35). The very electrophilic [Rh^{III}(OEP)]X (X = ClO_4^-, BF_4^-) complexes react regioselectively with activated and unactivated arenes to give Rh-arenes (21) and with methyl ketones to give Rh-$CH_2C(O)R$ (96).

The reactions utilizing [Rh^{II}(por)]$_2$ or Rh(por)(H) will be treated together because their chemistry is related (sect. 1.5.2 and 1.5.3). Both complexes are sources of the radical species Rh^{II}(por) which is believed to be the active Rh reagent in these reactions. Benzylic halogen (65) or hydrogen (56) can be abstracted and the resulting radical trapped to give Rh-$CHRC_6H_5$ species. The *monomeric* Rh^{II}(TMP) species reacts with CH_4 giving Rh(TMP)(CH_3) and Rh(TMP)(H) (95a). The Rh(II) dimers add across terminal alkynes to form μ-alkene complexes (65) and across the vinyl group in styrene to form a μ-alkane derivative (83). Alkenes with a terminal propylene group give rearranged products still containing a double bond (Rh-CH_2CH=CHR) (65). The hydride complex adds across alkenes to give the corresponding Rh-alkyl (56,83), and across the CO of aldehydes to give α-hydroxy complexes (57). Addition to CO or CNR occurs only at the

terminal C giving Rh-CHO or Rh-CH=NR complexes. Interestingly, the dimer $[Rh^{II}(por)]_2$ in the presence of H_2 (or CO/H_2O or CO/KOH) can be used in place of Rh(por)(H) for the reaction with CO and CNR (57,81,97,98). The formyl group of $Rh^{III}(OEP)(CHO)$ is considered to be like an organic aldehyde with little π-backbonding to $Rh^{III}(OEP)$ on the basis of its short C-O distance (1.175 Å) and high ν_{co} of 1700 cm^{-1}. The BDE of the Rh-C bond has been estimated to be ~243 kJ mol^{-1} (46,63,97).

The $[Rh^{I}(por)]^-$ complex is generated in situ (sect. 1.3), and as a nucleophile will displace halide from RX (17,56). Cyclopropyl rings with extra strain, electron-withdrawing substituents, or containing hetero-atoms (oxiranes and azirines), are opened by $[Rh^{I}(por)]^-$, while C_3H_6 and $C_3H_5C_6H_5$ do not react; a proton from the reaction medium is incorporated stereospecifically trans in the product (99). Medium involvment occurs also for the reaction with terminal alkynes and alkenes, where a net trans addition of $[Rh^{I}(por)]^-$ and a proton occurs across the multiple bond (17).

The "out-of-plane" Rh(I) dicarbonyl complexes of aetioporphyrin (section 1.2) react with acetoacetates, fluorosulphonates, HCO_2R, RC(O)X, $(RC(O))_2O$, RCHO, $RC(O)CH_3$ or RX to form Rh(III)-R or Rh(III)-C(O)R complexes (Table A.3 for summary). Initially the substrate oxidatively adds to the Rh(I) center via C-X or C-H bond cleavage, followed by collapse of the Rh(III) center produced into the porphyrin cavity (sect. 1.5.2). Yields are variable and concomittant carbonylation or decarbonylation can occur, frequently producing mixtures. Induction periods of several hours are noted for the reactions with anhydrides. It is interesting to note that cyclopropyl methyl ketone can be metallated without ring-opening, unlike its reaction with $[Rh^{I}(por)]^-$.

Electrochemically generated $Rh^{II}(TPP)$ (prepared in situ from the 1-electron reduction of $[Rh^{III}(TPP)(NHMe_2)_2]Cl$ in THF, 0.2 M TBAP) reacts with alkyl (but not aryl) halides or dihalides (89,90,100), and with $H_2C{=}CHR$ and $HC{\equiv}CR$ (91) to give $Rh^{III}(TPP)(R)$. The reactions with alkenes or alkynes go with loss of the unsaturated C_2 moiety. Table A.4 summarizes the complexes produced.

1.4.2. Carbene complexes

Heterocarbene complexes have been proposed as intermediates in rhodium porphyrin chemistry (30,45,94,95,101,102) but only one type has been isolated and characterized. The cationic diaminocarbene complexes $[Rh^{III}(por)(:C(NHR)_2)(L)]PF_6$ (por = TPP^{2-}, R = CH_2Ph, L = vacant, $CNCH_2Ph$, $P(OMe)_3$, PPh_3; por = OEP^{2-}, R = CH_2Ph, L = vacant, $P(OMe)_3$; por = TPP^{2-}, OEP^{2-}, R = p-ClPh, L = vacant) were synthesised by prolonged refluxing of $[Rh^{III}(por)(CNR)_2]PF_6$ in MeOH to form the parent $[Rh^{III}(por)(:C(NHR)_2)]PF_6$ complex in 50% yield; addition of L to chloroform solutions of $[Rh^{III}(por)(:C(NHR)_2)]PF_6$ followed by chromatography gave $[Rh^{III}(por)(:C(NHR)_2)(L)]PF_6$. The structure, determined by x-ray diffraction, of $[Rh^{III}(TPP)(:C(NHCH_2Ph)_2)(CNCH_2Ph)]PF_6$ showed the expected planar arrangement of the Rh-$C(N)_2$ metallocarbene unit (103).

1.4.3. π-Bonded complexes (dihapto)

There are no examples of isolated dihapto complexes; however, π-bonded vinyl alcohol (70), vinyl ether (94), alkene or alkyne (17,78,94) species of Rh(I), Rh(II), and Rh(III), have been proposed as intermediates. A few examples have been detected spectroscopically. Electrochemically generated transient, radical π-complexes $Rh(TPP)(H_2C{=}CHC_4H_9)$ and $Rh(TPP)(HC{\equiv}CHC_3H_7)$ have been postulated on the basis of spectroelectrochemical and esr data (sect. 1.5.2) (91). The ethene complexes $Rh(OEP)(X)(CH_2{=}CH_2)$ (X = $CF_3CO_2^-$, $CF_3SO_3^-$) have been detected by VT ^1H nmr (sect. 1.5.3) (70).

1.5. Stoichiometric Reactions

There are a number of mechanistic studies involving Rh(por) species. The emphasis in this area has been on metal-centered processes, although the availability of a wide range of organometallic derivatives (sect. 1.4) suggests that organometallic ligand reactivity should be of increasing interest. Thermal reactions are discussed in the first sub-sections with photochemistry gathered into one sub-section (sect. 1.5.7).

1.5.1. Ligand Substitution and Exchange

Reactions covered in this section do not involve a change in metal oxidation state. At present only processes at Rh(III) centers have been studied in any detail.

The equilibrium constants for the reaction of $Na_3[Rh^{III}(TPPS)(H_2O)_2]$ with Cl^-, Br^-, I^- and NCS^- have been studied in aqueous solution (equilibrium 1.9, Table 1.1).

Table 1.1. Values of K_1 and K_2 for anation reaction of $Na_3[Rh^{III}(TPPS)(H_2O)_2]$ with Cl^-, Br^-, I^- and NCS^- at 25 °C.[a]

X	K_1 (M^{-1})	K_2 (M^{-1})
NCS^-	$1.22 \pm 0.04 \times 10^4$	3.68 ± 0.42
I^-	$4.12 \pm 0.18 \times 10^1$	<0.03
Br^-	1.82 ± 0.10	<0.03
Cl^-	0.74 ± 0.11	<0.03

a. $[H^+] = 0.10$ M, $\mu = 1.00$ M ($NaClO_4$).

$$[Rh^{III}(TPPS)(H_2O)_2]^{3-} \underset{-X}{\overset{K_1}{\overset{+X}{\rightleftharpoons}}} [Rh^{III}(TPPS)(H_2O)(X)]^{4-} \underset{-X}{\overset{K_2}{\overset{+X}{\rightleftharpoons}}} [Rh^{III}(TPPS)(X)_2]^{5-} \qquad (1.9)$$

The rates of substitution by the first anion are considered to be 10^2–10^6 greater than for comparable non-porphyrin systems. Associative activation is proposed, based on the activation parameters (Table 1.2) and that addition of the first anion was first order in [anion] up to 0.90 M. The cause of the labilization is uncertain although it may in part be due to mixing of the d orbitals of the metal and π-ligand orbitals resulting in loss of formal d^6 character of the Rh(III) (55).

Binding constants of L-leucine methyl ester and 4-aminoheptane to form adducts with $Rh^{III}(por)(CH_2C(O)CH_3)$ (por = cis- and trans-5,15-bis(2-hydroxy-1-naphthyl)-octaethylporphyrin) (Fig. 1.5) in $CHCl_3$ have been determined (Table 1.3). Hydrogen bonding bythe ester group of the amino acid ester to naphtholic functions on the periphery of the trans-isomer of the porphyrin was estimated to contribute 8.8 kJ mol^{-1} to the stabilization energy (73), and this represents a trans/cis selectivity of 42 towards the amino acid ester.

Table 1.2. Values of $\Delta H^{\ddagger}$ and $\Delta S^{\ddagger}$ for substitution of the first H_2O ligand of $Na_3[Rh^{III}(TPPS)(H_2O)_2]$ with Cl^-, Br^-, I^- and NCS^-.[a]

X	$\Delta H^{\ddagger}$ (kJ mol^{-1})	$\Delta S^{\ddagger}$ (J mol^{-1} K^{-1})
NCS^-	69.0 ± 0.8	–43.1 ± 2.5
I^-	53.6 ± 3.3	–97.9 ± 10.5
Br^-	57.7 ± 1.3	–94.6 ± 4.6
Cl^-	56.1 ± 2.5	–106 ± 8

a. $[H^+]$ = 0.10 M, μ = 1.00 M ($NaClO_4$).

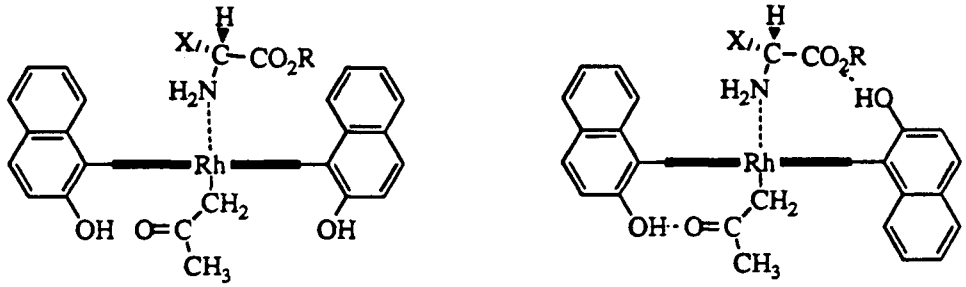

cis trans

Figure 1.5. Cis- and trans-isomers of $Rh^{III}(por)(CH_2C(O)CH_3)$ (por = 5,15-bis(2-hydroxy-1-naphthyl)-octaethylporphyrin).

Table 1.3. Binding constants of amines with $Rh^{III}(por)(CH_2C(O)CH_3)$ (por = cis- and trans-5,15-bis(2-hydroxy-1-naphthyl)-octaethylporphyrin) in $CHCl_3$ at 15 °C.

amine	K (M^{-1})	
	trans	cis
L-leucine methyl ester	5×10^6	1.6×10^5
4-aminoheptane	2.9×10^5	3.9×10^5

The same amines form 1:1 adducts with $Rh^{III}(por)(Cl)$ irreversibly, unlike the reaction with $Rh^{III}(por)(CH_2C(O)CH_3)$, but consistent with the greater trans effect of the $-CH_2C(O)CH_3$ ligand (73).

The formation constants for the binding of PPh_3 to $Rh^{III}(por)(R)$ (por = OEP^{2-}, R = CH_3; por = TPP^{2-}, R = CH_3, C_2H_5, C_4H_9) to give $Rh^{III}(por)(R)(PPh_3)$ have been measured electrochemically in CH_2Cl_2 and PhCN (Table 1.4). The binding constants were an order of magnitude lower in PhCN, indicative of coordination of PhCN to $Rh^{III}(por)(R)$. Interestingly, the formation constant for $Rh(por)(O_2)(PPh_3)$ in CH_2Cl_2 is two orders of magnitude greater than for $Rh^{III}(por)(R)(PPh_3)$, suggesting that a σ-bonded alkyl is a better electron donor than O_2^-. When the concentration of $Rh^{III}(TPP)(R)$ is less than 2×10^{-5} M in CH_2Cl_2, only $[Rh^{III}(por)(PPh_3)_2]^+$ is observed, but neither the liberated R group nor Rh(por) intermediates could be detected (97).

Table 1.4. Formation constants for binding of PPh_3 to $Rh^{III}(por)(R)$ to form $Rh^{III}(por)(R)(PPh_3)$.

por	R	K (M^{-1})		ref
		solvent		
		CH_2Cl_2	PhCN	
OEP	CH_3	1.8×10^3	2.4×10^2	1
TPP	CH_3	3.9×10^3	1.0×10^2	1
	C_2H_5	1.2×10^3	4.2×10^2	1
	C_4H_9	1.0×10^3	4.3×10^2	1
	O_2	3.3×10^5	—	2

1. K.M. Kadish, C. Araullo and C. Yao. Organometallics, **7**, 1583 (1988).
2. J.E. Anderson, C. Yao and K.M. Kadish. Inorg. Chem. **25**, 3224 (1986).

Formation of $[Rh^{III}(TPP)(PPh_3)_2]^+$ from $Rh(por)(O_2)$ or $Rh^{III}(OEP)(Cl)(PPh_3)$ has been studied (equilibria 1.10a/b).

$$Rh(TPP)(O_2)(solvent) + PPh_3 \overset{K_1}{\rightleftharpoons} Rh(TPP)(O_2)(PPh_3) + solvent \qquad (1.10a)$$

$$Rh(TPP)(O_2)(PPh_3) + PPh_3 \overset{K_2}{\rightleftharpoons} [Rh(TPP)(PPh_3)_2]^+ + O_2^- \qquad (1.10b)$$

The equilibrium constants, $K_1 = 3.3 \times 10^5$ and $K_2 = 1.1 \times 10^2$, were determined in CH_2Cl_2 (0.1 M TBAP) at 25 °C (44). The corresponding K_2 value for the reaction of PPh_3 with

$Rh^{III}(OEP)(Cl)(PPh_3)$ at the highest ionic strength studied (ca. 0.02 M TBAP) has been estimated in the present thesis work (sect. 5.2.2.) to be $K_{obs} \approx 1.9 \times 10^2$ at 25 °C. The $\Delta H°$ was estimated as -33 ± 2 kJ mol^{-1} and $\Delta S°$ was -146 ± 8 J mol^{-1} K^{-1} at $\mu = 0.0$ M; the overall exothermicity is thought to result primarily from contributions of the solvation enthalpies of the product ions (75).

1.5.2. Oxidative-Addition and Reductive-Elimination

The porphyrin ligand of the in-plane mono-nuclear Rh(por) species effectively restricts oxidative-addition and reductive-addition to single site processes such as nucleophilic substitution and to chain, or non-chain, single electron transfer (SET). This is in contrast to the usual sense (104) of simultaneous addition of two 1-electron ligands A and B by oxidative addition of a molecule of A–B to the metal center, the reverse process being reductive elimination. In the case of the out-of-plane Rh(I) complexes oxidative-addition in the usual sense can occur but not reductive-elimination because the product of the oxidative-addition is an in-plane species. There have been no reports of in-plane Rh(I) coming out of the plane of the porphyrin to form an out-of-plane species.

Net oxidative addition reactions to $[Rh^{I}(por)]^-$ with RX to form $Rh^{III}(por)(R)$ have been previously mentioned (sect. 1.4.1); however, there have not been any explicit mechanistic studies. On the basis of the products obtained and the oxidation state changes, the reaction is believed to involve nucleophilic substitution by $[Rh^{I}(Por)]^-$ (17,44). In the case of the ring opening of cyclopropanes inversion of configuration at the reaction site occurred for nortricyclanone consistent with S_{N2} type reactivity (reaction 1.11) (99).

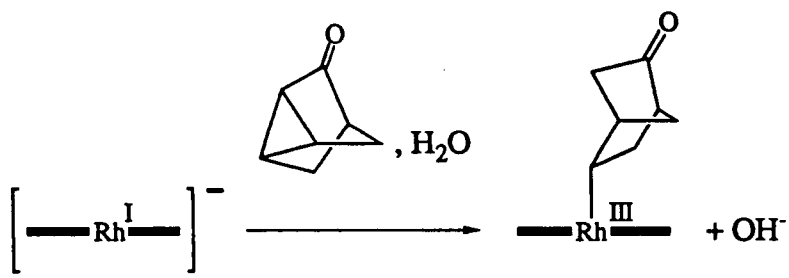

(1.11)

Reaction of $[Rh^{I}(OEP)]^{-}$ with olefins containing electron-withdrawing groups (CH_2=CHX; X = CN, CO_2CH_3) or with phenylacetylene is proposed to go via initial formation of a π-complex (Scheme 1.2).

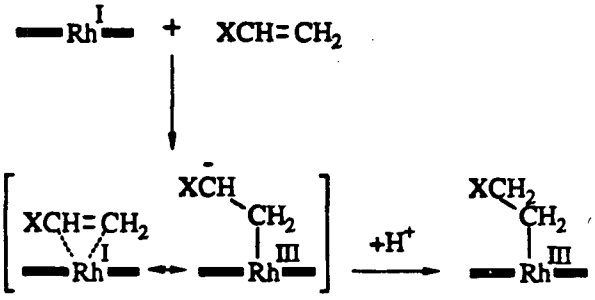

Scheme 1.2. Reaction of $[Rh^{I}(OEP)]^{-}$ with olefins containing electron-withdrawing groups.

Subsequent to the nucleophilic attack by Rh(I), a proton adds trans to Rh as evidenced by formation exclusively of cis-styryl complex from the reaction with phenylacetylene (17).

For "out of plane" $Rh^{I}(CO)_2$ complexes, the substrate C-X or C-H (Table A.4) bonds are proposed to oxidatively add to the Rh(I) center in the normal sense. Observation of concomitant carbonylation or decarbonylation indicates migratory insertion and deinsertion can compete with the subsequent collapse of the Rh(III) center into the porphyrin cavity. It is noteworthy that cyclopropyl methyl ketone can be α-metallated without ring-opening, unlike its reaction with $[Rh^{I}(por)]^{-}$ but consistent with the different modes of reaction (27,29).

Oxidative addition to $[Rh^{II}(por)]_2$ occurs via chain and non-chain SET yielding Rh(III) products (e.g., Tables in Appendix A) with the overall stoichiometry:

$$M^{II}\text{–}M^{II} + A\text{–}B \longrightarrow M^{III}\text{–}A + M^{III}\text{–}B \qquad (1.12)$$

The mono-nuclear radical species $Rh^{II}(por)$ is believed to be a key active Rh reagent in these reactions, the driving force generally being Rh-C formation. Addition of donors has been suggested to promote the cleavage of the $[Rh^{II}(por)]_2$ species (76).

The reaction of $C_6H_5CH_2Br$ with $[Rh(OEP)]_2$ (65,78) in toluene has been investigated and can be described as a free-radical chain mechanism.

initiation/termination: $[Rh(OEP)]_2 \underset{k_{-13}}{\overset{k_{13}}{\rightleftharpoons}} 2\,Rh^{II}(OEP)$ (1.13)

propagation: $Rh^{II}(OEP) + C_6H_5CH_2Br \xrightarrow{k_{14}} Rh^{III}(OEP)(Br) + C_6H_5CH_2\cdot$ (1.14)

$C_6H_5CH_2\cdot + [Rh(OEP)]_2 \xrightarrow{fast} Rh^{III}(OEP)(CH_2C_6H_5) +$

$Rh^{II}(OEP)$ (1.15)

The rate law was $-d[[Rh(OEP)]_2]/dt = k_{obs}[[Rh(OEP)]_2]^{1/2}[C_6H_5CH_2Br]$, where $k_{obs} = (k_{13}/k_{-13})^{1/2}k_{14} = 8.5 \times 10^{-4}\ M^{-1/2}\ s^{-1}$ at 26 °C (83).

In contrast, the reaction of 1-C_3H_7X (X = Cl, Br, I) with *mono-nuclear* $Rh^{II}(TPP)$ generated electrochemically from $Rh^{III}(TPP)(L)_2^+$ in PhCN gave $Rh^{III}(TPP)(R)$ and X^- with no evidence of $Rh^{III}(TPP)(X)$. Coulometry and CV data indicate initial formation of $Rh^{III}(TPP)(R)$ and $X\cdot$ when X was Br or I, but only $Rh^{III}(TPP)(R)$ was detected with X = Cl. A Scheme involving an electron source (S) other than the electrode was formulated to explain this.

$[Rh^{III}(TPP)(L)_2]^+ + e^- \longrightarrow Rh^{II}(TPP) + 2L$ (1.16)

$Rh^{II}(TPP) + RX \longrightarrow Rh^{III}(TPP)(R) + X\cdot$ (1.17a)

$Rh^{II}(TPP) + RX \longrightarrow [Rh^{III}(TPP)(R)]^+ + X^-$ (1.17b)

$X\cdot + S \longrightarrow X^- + S^+$ (1.18a)

$[Rh^{III}(TPP)(R)]^+ + S \longrightarrow Rh^{III}(TPP)(R) + S^+$ (1.18b)

A key relationship is between the $Rh^{III}(TPP)(R)/[Rh^{III}(TPP)(R)]^+$ and $X^-/X\cdot$ couples. The $Rh^{III}(TPP)(R)/[Rh^{III}(TPP)(R)]^+$ couple is near +1.0 V while the $Cl^-/Cl\cdot$ couple is greater than +1.0 V; thus reactions 1.17b/1.18b occur rather than 1.17a/1.18a. For X = Br and I, reaction 1.17a occurs since the $X^-/X\cdot$ couple is less than +1.0 V. It was suggested that the occurrence of a radical chain process in the reaction of $C_6H_5CH_2Br$ with $[Rh^{II}(OEP)]_2$ discussed above, but not for n-C_3H_7X with $Rh^{II}(TPP)$, is due to the greater stability of the $C_6H_5CH_2\cdot$ radical (89). Chemical reaction of $[Rh(OEP)]_2$ with CH_2Cl_2 in benzonitrile or THF likewise gave only $Rh(TPP)(CH_2Cl)$ without formation of Rh(TPP)(Cl) and the reaction was proposed to be between $Rh^{II}(TPP)$ and CH_2Cl_2 rather than "direct reaction" between $[Rh(OEP)]_2$ and CH_2Cl_2 (105).

A mechanism initiated by dissociation of $[Rh(OEP)]_2$, but without formation of organic free radicals, has been proposed for the reaction with alkylaromatics. The rate of reaction with deutereotoluene was first order in $[Rh(OEP)]_2$ at ca. 100 °C. Based on the product distributions and labelling studies, initial reaction apparently occurs at the benzylic carbon, which bears the weakest C–H bond, with subsequent rearrangements when necessary to less sterically constrained β-sites (56).

$$[Rh(OEP)]_2 \rightleftharpoons 2\ Rh^{II}(OEP) \quad \text{(fast)} \quad (1.19)$$

$$Rh^{II}(OEP) + RH \rightleftharpoons [Rh(OEP),{\cdot}HR] \quad \text{(fast)} \quad (1.20)$$

$$[Rh(OEP),{\cdot}HR] + Rh^{II}(OEP) \rightleftharpoons Rh(OEP)(R) + Rh(OEP)(H) \quad \text{(RDS)} \quad (1.21)$$

$$Rh(OEP)(H) \rightleftharpoons 1/2\ [Rh(OEP)]_2 + 1/2\ H_2 \quad \text{(slow)} \quad (1.22)$$

Interestingly, monomeric $Rh^{II}(TMP)$ reacts reversibly with methane in benzene (equilibrium 1.22a). Kinetic studies reveal a large deuterium isotope effect of 8.6 ± 1.5 at 296 K; $\Delta H° \sim -50$ kJ mol^{-1} and $\Delta S° \sim -63$ J K^{-1} mol^{-1} (95a).

$$CH_4 + Rh^{II}(TMP) \rightleftharpoons Rh(TMP)(CH_3) + Rh(TMP)(H) \quad (1.22a)$$

A four-centered linear transition state is proposed:

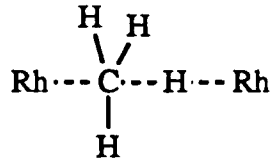

Alkenes with a terminal propylene group react with $[Rh(OEP)]_2$ to give rearranged products still containing a double bond, e.g. $Rh^{III}(OEP)(CH_2CH{=}CHR)$ (R = C_6H_5, CN, n-C_3H_7). A non-chain "$S_{H2'}$" mechanism is proposed (65).

$$[Rh(OEP)]_2 \rightleftharpoons 2\ Rh^{II}(OEP) \quad (1.23)$$

$$Rh^{II}(OEP) + CH_2{=}CHCH_2R \longrightarrow Rh^{III}(OEP)(CH_2\dot{C}HCH_2R) \quad (1.24)$$

$$Rh^{III}(OEP)(CH_2\dot{C}HCH_2R) \longrightarrow Rh^{III}(OEP)(CH_2CH{=}CHR) + \text{“}H{\cdot}\text{”} \quad (1.25)$$

The reaction of terminal alkenes, $H_2C{=}CHR$, and alkynes, $HC{\equiv}CR$, with electrochemically generated $Rh^{II}(TPP)$ gives $Rh^{III}(OEP)(R)$ (for examples see sect. 1.4.1), with loss of the unsaturated C_2 unit. Intermediate Rh(II) π-alkene and π-alkyne complexes have been observed, but the mechanism of the C_2 loss is unknown (91). In contrast, the reaction of styrenes or alkynes with $[Rh(OEP)]_2$ gives bridged Rh(III) products, and is discussed in section 1.5.3 on insertion.

The oxidative addition of H_2 to $[Rh^{II}(por)]_2$ forming Rh(por)(H) and the reverse reductive elimination are key reactions in the chemistry of these two Rh complexes (see especially sect. 1.5.3). As previously mentioned (eq'n 1.7, page 14), a measurable equilibrium (equilibrium 1.26) is established for the OEP complexes with $K = 116 \pm 8$ at 294 K; $\Delta H° = -13 \pm 4$ kJ mol^{-1}; $\Delta S° = 3 \pm 8$ J K^{-1} mol^{-1} (63).

$$[Rh(OEP)]_2 + H_2 \overset{K}{\rightleftharpoons} 2\,Rh(OEP)(H) \qquad (1.26)$$

The mechanism of the H_2 activation is not known, but it has been noted that light (sect. 1.3.1 and 1.6.3) and trace amounts of rhodium metal remaining from the $[Rh(OEP)]_2$ synthesis catalyse the reverse reaction (56).

Reductive elimination occurs during anaerobic thermolysis of Rh(OEP)(R). When R is $-CH(C_6H_5)CH_2CH_3$ or $-CH_2CH_2CH_2(C_6H_5)$, the dimer, $[Rh(OEP)]_2$, and equal amounts of $CH_3CH{=}CHC_6H_5$ and $CH_3CH_2CH_2C_6H_5$ form without formation of coupled products. A mechanism involving formation of a geminate radical pair $[Rh^{II}(OEP),{\cdot}R]$, followed by subsequent reactions with a $Rh^{III}(OEP)(H)$ intermediate was proposed (reactions 1.27–1.29).

$$Rh^{III}(OEP)(CH(C_6H_5)CH_2CH_3) \longrightarrow [Rh^{II}(OEP),{\cdot}CH(C_6H_5)CH_2CH_3] \qquad (1.27)$$

Abstraction of H·, accompanied by rearrangements depending on R, followed by the reaction of the intermediate $Rh^{III}(OEP)(H)$ with the initial complex gives the Rh(II) dimer.

$$[Rh^{II}(OEP),{\cdot}CH(C_6H_5)CH_2CH_3] \longrightarrow Rh^{III}(OEP)(H) + CH_3CH{=}CHC_6H_5 \qquad (1.28)$$

$$Rh^{III}(OEP)(H) + Rh^{III}(OEP)(CH(C_6H_5)CH_2CH_3) \longrightarrow [Rh(OEP)]_2 + CH_3CH_2CH_2C_6H_5 \qquad (1.29)$$

Further evidence for a radical pair formation comes from the ærobic thermolysis of $Rh^{III}(OEP)(CH_2C_6H_5)$ and $Rh^{III}(OEP)(CH(C_6H_5)CH_3)$ which quantitatively gives $C_6H_5C(O)H$ and $C_6H_5C(O)CH_3$ respectively. Dioxygen is presumed to intercept the radical pair to form a peroxy intermediate that decomposes to a carbonyl and possibly a Rh(III) hydroxide (56). Another example of a $Rh^{III}(OEP)(H)$ induced reductive elimination is the formation of methanol and $[Rh(OEP)]_2$ from the reaction of $Rh^{III}(OEP)(H)$ and $Rh^{III}(OEP)(CH_2OH)$ in toluene (106).

1.5.3. Insertion

A number of unsaturated molecules insert into Rh-Rh and Rh-H bonds (e.g., sect. 1.4.1). The reaction of CO with $Rh^{III}(OEP)(H)$ (46,57,63,78,81,97), and of styrene with $[Rh(OEP)]_2$ or $Rh^{III}(OEP)(H)$ (83), has been shown to go via a radical chain mechanism with the intermediacy of mono-nuclear $Rh^{II}(OEP)$. The $Rh^{II}(OEP)$ acts as chain carrier and the product formation depends on oxidative-addition to the Rh(II) center. The unusually strong Rh-C bonds are felt to contribute to the driving force.

The reaction of $[Rh(OEP)]_2$ with styrene in C_6D_6 gives a Rh(III) μ-alkane product. An equilibrium (reactions 1.30–1.33) is attained at 25 °C with $K_{30} = 8.5 \times 10^4\ M^{-1}$ (see Table 1.5 for thermodynamic values).

$$[Rh(OEP)]_2 + CH_2{=}CHPh \overset{K_{30}}{\rightleftharpoons} Rh^{III}(OEP)\text{-}CH_2CH(Ph)\text{-}Rh^{III}(OEP) \qquad (1.30)$$

initiation/termination:
$$[Rh(OEP)]_2 \underset{k_{-31}}{\overset{k_{31}}{\rightleftharpoons}} 2\ Rh^{II}(OEP) \qquad (1.31)$$

propagation:
$$Rh^{II}(OEP) + CH_2{=}CHPh \underset{k_{-32}}{\overset{k_{32}}{\rightleftharpoons}} Rh^{III}(OEP)(CH_2\dot{C}HPh) \qquad (1.32)$$

$$Rh^{III}(OEP)(CH_2\dot{C}HPh) + [Rh(OEP)]_2 \xrightarrow{k_{33}} Rh^{III}(OEP)\text{-}CH_2CH(Ph)\text{-}Rh^{III}(OEP) + Rh^{II}(OEP) \qquad (1.33)$$

The rate law is $-d[[Rh(OEP)]_2]/dt = k_{obs}[[Rh(OEP)]_2]^{3/2}[CH_2{=}CHPh]$, where $k_{obs} = (k_{31}/k_{-31})^{1/2}(k_{32}/k_{-32})k_{33}$, when reactions 1.31 and 1.32 are at equilibrium and reaction 1.33 is rate-limiting. The intermediate $Rh^{III}(OEP)(CH_2\dot{C}HPh)$ radical could be efficiently trapped by $Rh^{III}(OEP)(H)$. In fact, $[Rh(OEP)]_2$ catalyses the reaction of styrene with $Rh^{III}(OEP)(H)$. In the

absence of added Rh(II) dimer, the reaction of CH_2=CHPh with the hydride is slow because only small amounts of $[Rh(OEP)]_2$ are formed in situ from decomposition of $Rh^{III}(OEP)(H)$. A mechanism similar to the previous one can be written.

$$Rh^{III}(OEP)(H) + CH_2{=}CHPh \rightleftharpoons Rh^{III}(OEP)\text{-}CH_2CH_2Ph \qquad (1.34)$$

initiation/termination: $$[Rh(OEP)]_2 \underset{k_{-35}}{\overset{k_{35}}{\rightleftharpoons}} 2\,Rh^{II}(OEP) \qquad (1.35)$$

propagation: $$Rh^{II}(OEP) + CH_2{=}CHPh \underset{k_{-36}}{\overset{k_{36}}{\rightleftharpoons}} Rh^{III}(OEP)(CH_2\dot{C}HPh) \qquad (1.36)$$

$$Rh^{III}(OEP)(CH_2\dot{C}HPh) + Rh^{III}(OEP)(H) \xrightarrow{k_{37}} Rh^{III}(OEP)(CH_2CH_2Ph) + Rh^{II}(OEP) \qquad (1.37)$$

and $-d[Rh^{III}(OEP)(H)]/dt =$

$(k_{35}/k_{-35})^{1/2}(k_{36}/k_{-36})k_{37}(K_{30})^{-1/2}[[Rh(OEP)]_2]_{total}^{1/2}[CH_2{=}CHPh]^{1/2}$, when equilibria (1.30) and (1.35) are established, equilibrium (1.30) lying to the right, and reaction (1.37) is rate-limiting. At 42 °C, $(k_{35}/k_{-35})^{1/2}(k_{36}/k_{-36})k_{37}(K_{30})^{-1/2}$ is 9.8×10^{-2} s^{-1}. The corresponding reaction of cis-stibene was accompanied by cis-trans isomerization of the unreacted stilbene, presumably via equilibrium (1.36).

The reaction of CO with $Rh^{III}(OEP)(H)$ can be described by a similar mechanism involving $Rh^{II}(OEP)$ catalysis (reactions 1.38–41). A measurable equilibrium is found (equilibrium 1.38, Table 1.5 for thermodynamic values). At 36 °C the equilibrium constant (K_{38}) is 5.5×10^2 M^{-1}, and the rate law is $-d[Rh^{III}(OEP)(H)]/dt =$ $k_{obs}[[Rh(OEP)]_2]^{1/2}[Rh^{III}(OEP)(H)][CO]$, where $k_{obs} = (k_{39}/k_{-39})^{1/2}(k_{40}/k_{-40})k_{41}$ (83).

$$Rh^{III}(OEP)(H) + CO \overset{K_{38}}{\rightleftharpoons} Rh^{III}(OEP)(CHO) \qquad (1.38)$$

initiation/termination: $$[Rh(OEP)]_2 \underset{k_{-39}}{\overset{k_{39}}{\rightleftharpoons}} 2\,Rh^{II}(OEP) \qquad (1.39)$$

propagation: $$Rh^{II}(OEP) + CO \underset{k_{-40}}{\overset{k_{40}}{\rightleftharpoons}} Rh^{III}(OEP)(\dot{C}O) \qquad (1.40)$$

Table 1.5. Some thermodynamic parameters for insertion into Rh-Rh and Rh-H bonds.

reagent	substrate	solvent	$\Delta H°$ (kJ mol^{-1})	$\Delta S°$ (J mol^{-1} K^{-1})	ref
$[Rh(OEP)]_2$	$PhCH{=}CH_2$	C_6D_6	-94 ± 11	-63 ± 33	1
Rh(OEP)(H)	CO	"	-54 ± 4	-123 ± 15	2
Rh(TPP)(H)	CO	"	-42 ± 4	-91 ± 15	3

1. R.S. Paonessa, N.C. Thomas and J. Halpern. J. Am. Chem. Soc. **107**, 4333 (1985).
2. M.D. Farnos, B.A. Woods and B.B. Wayland. J. Am. Chem. Soc. **108**, 3659 (1986).
3. B.B. Wayland, S.L. Van Voorhees and C. Wilker. Inorg. Chem. **25**, 4039 (1986).

$$Rh^{III}(OEP)(\dot{C}O) + Rh^{III}(OEP)(H) \xrightarrow{k_{41}} Rh^{III}(OEP)(CHO) + Rh^{II}(OEP) \qquad (1.41)$$

It is possible that the chain radical mechanism just described is extensible to other insertion reactions, such as Rh(II) dimer addition across terminal alkynes to form μ-alkene complexes (65) and hydride complex addition across the CO of aldehydes to give α-hydroxy complexes (57). The utility of further studies in this area can be supported by noting that a cycle can be written, utilising *stoichiometric* reactions, for the conversion of H_2 and CO to methanol (Scheme 1.3).

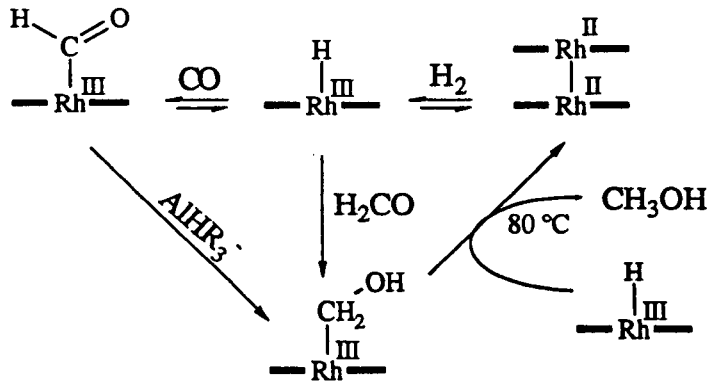

Scheme 1.3. Possible cycle for the reduction of CO by H_2 to CH_3OH from combining known elementary steps; refs: insertion of CO (46,57,63,81,97,98); aluminium hydride reduction (106); reductive elimination of MeOH (106).

In addition, there remains a lack of depth in the mechanistic studies, given the variety of proposals that all involve a Rh(II) radical species. In particular, an explanation is needed for the C—C bond cleavage proposed during the loss of the C_2 unit of terminal alkenes and alkynes (previous section) when reacted with electrochemically generated Rh(II).

Terminal acetylenes react with $Rh^{III}(OEP)(Cl)$ in benzene to give inserted products and oxygen-containing products in the presence of H_2O (Scheme 1.4). Di-substituted acetylenes did not react, presumably due to steric hindrance. The formation of oxygen-containing products is proposed to occur via hydration of carbenoid intermediates. Evidence for the path via $Rh^{III}(OEP)(C{\equiv}CR)$ comes from the isolation of such complexes from the reaction in the presence of Et_3N. Treatment of $Rh^{III}(OEP)(C{\equiv}CC_6H_5)$ with aqueous HCl gives $Rh^{III}(OEP)(C(O)CH_2C_6H_5)$ (94).

A cationic Rh(III) intermediate is also proposed in the reaction of $Rh^{III}(OEP)(Cl)$ in EtOH with $CH_2{=}CHOC_2H_5$ to give $Rh^{III}(OEP)(CH_2CH(OC_2H_5)_2)$. Cationic σ- and π-complexes are considered to be in equilibrium at an intermediate stage (Fig. 1.6). Attack of the solvent on the σ-complex presumably generates the acetal product (94). The acetal can be degraded via an acid promoted process to the β-aldehyde on silica gel.

These Rh(III) reactions are probably related to the direct metallation of arenes by $[Rh^{III}(OEP)]X$ (sect. 1.5.4), where X is at best only weakly coordinating compared to the Cl^- ligand of $Rh^{III}(OEP)(Cl)$. The initial step is likely to be coordination of an unsaturated substrate to the Rh(III) center via a dissociative or associative mechanism, which could be difficult to distinguish when X is weakly coordinating. A possible prototype for the substrate binding may be found in the reversible insertion of ethene into the Rh-O bond of $Rh^{III}(OEP)(CF_3CO_2)(CH_2{=}CH_2)$ (equilibrium 1.42), which has a $\Delta H°$ of -5.9 ± 0.5 kcal over a temperature range of 243 K to 315 K. Replacement of $CF_3CO_2^-$ by $CF_3SO_3^-$ prevents the forward reaction under the same conditions (70). However, no such complexes have been reported for reactions involving acetylenes.

$$Rh^{III}(OEP)(CF_3CO_2)(CH_2{=}CH_2) \rightleftharpoons Rh^{III}(OEP)(CH_2CH_2OC(O)CF_3) \qquad (1.42)$$

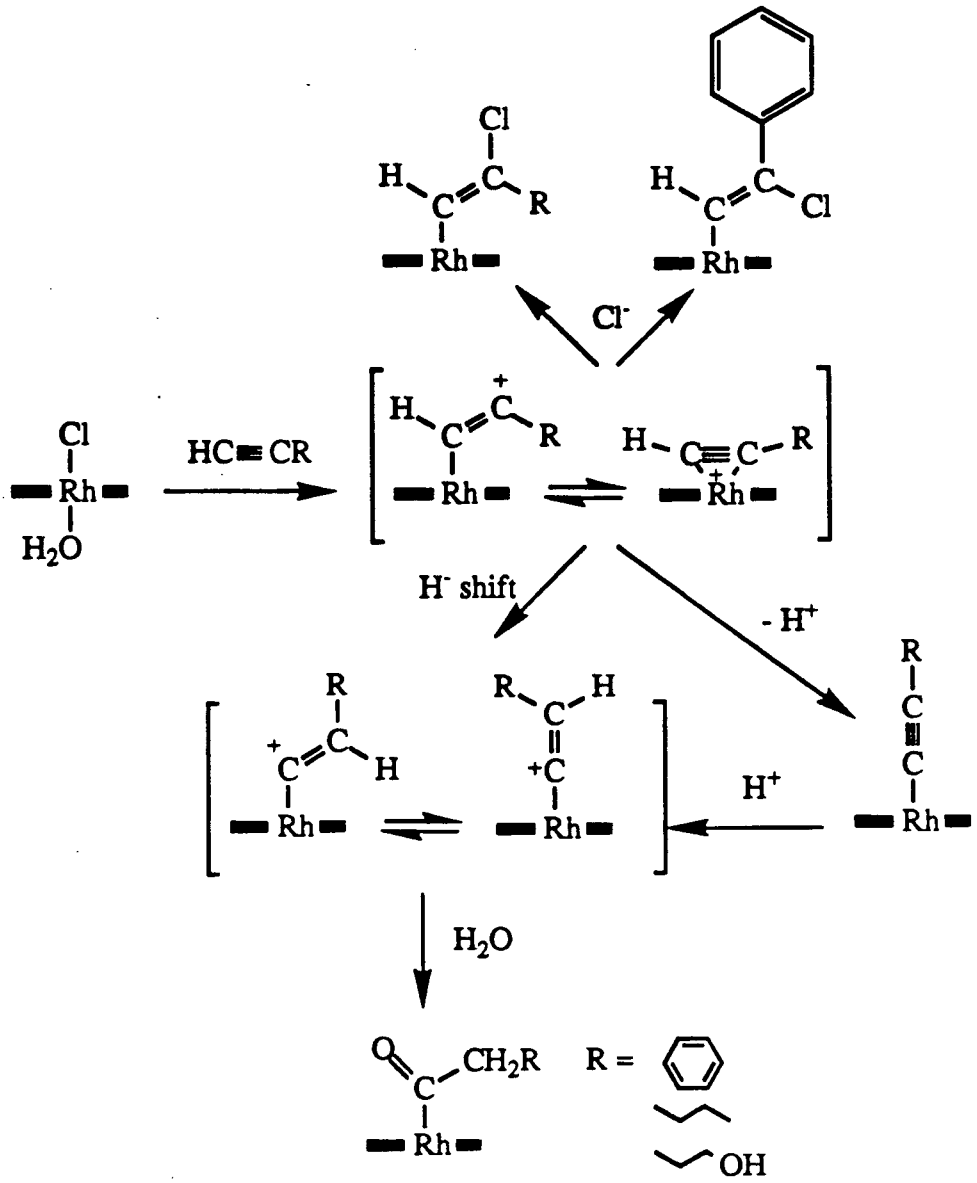

Scheme 1.4. The reaction of terminal acetylenes with Rh^{III}(OEP)(Cl) in benzene (adapted from ref. 94).

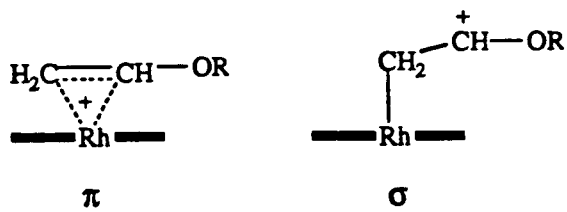

Figure 1.6. Cationic π- and σ-complex intermediates in the reaction of Rh^{III}(OEP)(Cl) and vinylethers (adapted from ref. 94).

1.5.4. Electrophilic Aromatic Metallation

Direct metallation of arenes by $[Rh^{III}(OEP)]X$ ($X = BF_4^-$, ClO_4^-) occurs under mild conditions via ionic electrophilic substitution (107,21). Yields vary from 28 to 70% depending upon the counter ion and substituent on the arene. The reactivities of substituted arenes (C_6H_5X; $X = p\text{-}OCH_3$, $p\text{-}CH_3$, H, Cl, $m\text{-}CO_2CH_3$, $p\text{-}CO_2CH_3$) follow the Hammett σ equation giving a ρ value of -5.43. Substitution was exclusively para, except for the reaction of methyl benzoate, where a 92:8 ratio of meta:para was found for the benzoate product. The metallation was totally inhibited by potentially donor solvents such as methanol, tetrahydrofuran and pyridine, but not by oxygen. There was no deuterium isotope effect using C_6D_6 instead of C_6H_6: the rate determining step is coordination of the arene to form a cationic Rh(III)-arene complex, followed by the rapid loss of a proton to yield the product. The deprotonation is proposed to involve the conversion of an η^2-arene to σ-aryl species (21).

$$[Rh^{III}(OEP)]^+ + C_6H_6 \longrightarrow [[Rh^{III}(OEP)(C_6H_6)]^+] \longrightarrow Rh^{III}(OEP)(C_6H_5) + H^+ \quad (1.43)$$

Electrochemical generation of $[Rh^{III}(TPP)]ClO_4$ in PhCN by electro-oxidation of $Rh^{III}(TPP)(C(O)CH_3)$ is possible. The only chemical reaction examined was the instantaneous reaction with Cl^- to form $Rh^{III}(TPP)(Cl)$ (59).

1.5.5. Reactions at an axial ligand

Reduction of $Rh^{III}(OEP)(CHO)$ with $HAl(iBu)_2$ followed by aqueous workup is reported to give the α-hydroxy complex $Rh^{III}(OEP)(CH_2OH)$ in 30% yield (106). Proton nmr evidence indicates that α-hydroxy complexes of the type $Rh^{III}(por)(CH(R)OH)$ ($por = OEP^{2-}$, R = H, Me; $por = TPP^{2-}$, R = H) undergo slow self condensation in benzene to form bridged ether complexes, which subsequently undergo hydride-transfer disproportionation to form metallo acyl and alkyl species (57,106,108).

$$2\ Rh(OEP)(CH(Me)OH) \rightleftharpoons Rh(OEP)\text{-}CH(Me)OCH(Me)Rh(OEP) \quad (1.43)$$

$$Rh(OEP)\text{-}CH(Me)OCH(Me)Rh(OEP) \longrightarrow Rh(OEP)(Et) + Rh(OEP)(C(O)Me) \quad (1.44)$$

The β-hydroxyethyl complex Rh(OEP)(CH_2CH_2OH) can be dehydroxylated by CF_3CO_2H or CF_3SO_3H in toluene, creating an ethene complex. In the case of CF_3CO_2H, the VT ^1H nmr data showed an equilibrium existed between $Rh^{III}(OEP)(CF_3CO_2)(CH_2{=}CH_2)$ and $Rh^{III}(OEP)(CH_2CH_2OC(O)CF_3)$ (equilibrium 1.42). Addition of hydroxide reformed the β-hydroxyethyl complex (70).

Nucleophilic addition of $NaOC_2H_5$ to $Rh^{III}(TPP)(Cl)(CO)$ in ethanol gives the ethoxycarbonyl complex Rh(TPP)(C(O)OEt), while reaction of $Rh^{III}(TPP)(Cl)(CO)$ with $LiNEt_2$ in $NHMe_2$ gives the analogous carbamoyl species $Rh^{III}(TPP)(C(O)NEt_2)$. In each case the metal carbonyl could be reformed by reaction with dry HCl. No reaction was observed between $Rh^{III}(TPP)(Cl)(CO)$ and NaSEt (82).

Attack of OH^- on Rh(por)(Cl)(CO) (por = OEP^{2-}, TPP^{2-}) in benzene is proposed to occur during the formation of Rh(por)(H) from Rh(por)(Cl)(CO) in the presence of CO and solid KOH, an intermediate carboxylate complex decomposing to yield the hydride and CO_2. Alkyl isocyanides undergo an analogous reaction to give Rh(por)(H) and BuNCO (81,98).

$$Rh(por)(Cl)(CO) + OH^- \longrightarrow [Rh(por)(CO_2H)] + Cl^- \qquad (1.45)$$

$$[Rh(por)(CO_2H)] \longrightarrow Rh(por)(H) + CO_2 \qquad (1.46)$$

Electrophilic attack of O_2 on coordinated NO in Rh(OEP)(NO) gives a nitrite complex as judged by appearance of bands at 1222 and 1325 cm^{-1} in the IR. No further details were given (43).

An α-metallation product is formed by enolization of coordinated acetone via bifunctional activation with Rh^{III}(por)(Cl) (por = 5,15-bis(8-quinolyl)-, 5,15-bis(2-pyridyl)octaethylporphyrin) (for example, Scheme 1.5). The presence of the phenolic hydroxyl or quinolyl nitrogen (acting as Brønsted bases) was essential as is steric restraint to prevent simple combination of the basic and Lewis acid metal centers (e.g. Fig. 1.2). The proposed mechanism involves binding the enolate, which is formed with assistance from the peripheral base followed by an intramolecular rearrangement and loss of H^+ to give the α-metallated product (35).

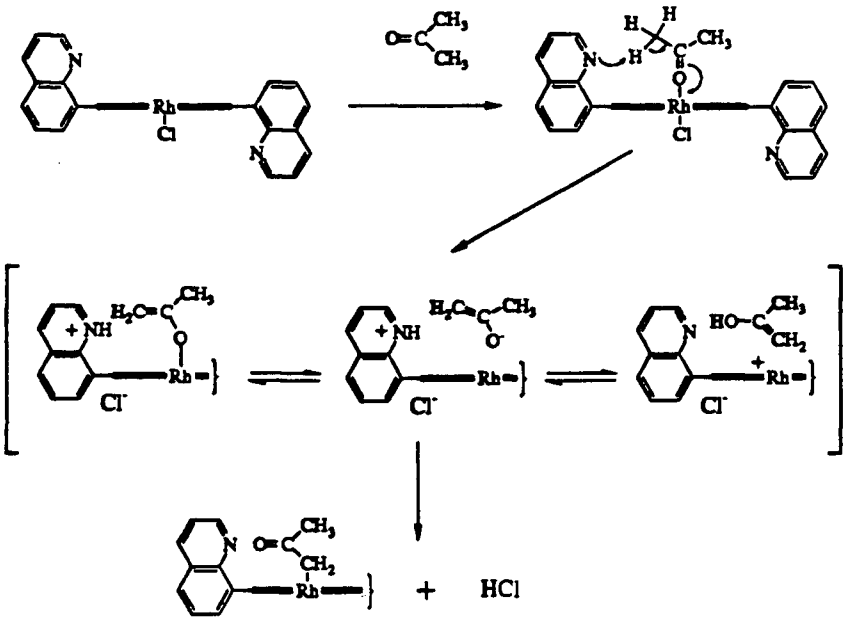

Scheme 1.5. The enolization of acetone via bifunctional activation with Rh^{III}(por)(Cl) (por = 5,15-bis(2-pyridyl)octaethylporphyrin) (adapted from ref. 35).

Ketone α-metallation could be achieved also in the absence of peripheral base using the more electrophilic [Rh^{III}(OEP)]X (X = BF_4^-, ClO_4^-) complex (see also sect. 1.6.5 for a related catalytic system) (96).

1.5.6. Migrations between metal and porphyrin

A considerable interest exists in the title migrations, using non-Rh (i.e. Fe, Co) porphyrins, mainly in relation to suicide inhibition of P-450 enzyme systems (109). As mentioned in sect 1.2, a number of N-alkylated "out-of-plane" $Rh^{I}(CO)_2$ complexes are known and these undergo a facile irreversible oxidative addition of N-C (of the N-alkyl group) to Rh(I) to form the corresponding in-plane Rh^{III}(por)(R) complex. Only one in-plane N-alkylated Rh(por) complex is known, but it is not believed to be formed via alkyl migration from metal to pyrrolic N. In the presence of AcOH, Rh^{III}(OEP)(Me) reacts with ethyldiazoacetate in CH_2Cl_2 to give the stable N-alkylated complex [Rh^{III}(OEP-N-CH_2CO_2Et)(Me)]ClO_4. Unstable, impure, salt-like, green products, which are also believed to be N-alkylated species, were obtained using Rh^{III}(OEP)(I) and Rh^{III}(TPP)(I). A preliminary step to the N-alkylation of the iodide complexes is suggested to be alkylation of Rh via formation of a Rh carbene intermediate. A molecule of protonated diazoester is believed to react directly with a pyrrolic nitrogen made more nucleophilic after the Rh

alkylation. The strength of the Rh-N bond is thought to make a bridged intermediate less favourable than for the Co analogues where carbene insertion into a Co-N bond is found (45). The possibility of interconversion of the Rh(III) N-alkylated complex to Rh(R) has yet to be explored.

Migration of R (R = p-$MeOC_6H_4$, o-MeC_6H_4, C_6H_5, or n-Bu; R ≠ o-$MeOC_6H_4$, or Me) from Rh to the meso position of OEP to form Rh^{III}(OEP-R)(R) has been reported (93). Addition of excess RLi to a dry THF solution of Rh^{III}(OEP)(Me) forms the anionic brown dialkyl complex (p-type hyperporphyrin) which slowly converts to the green phlorin. The mono-meso-substituted Rh^{III}(OEP-R)(R) complexes were isolated after addition of saturated aqueous NH_4Cl (Scheme 1.6). In the case of R = o-$MeOC_6H_4$, or Me, only the brown solution was formed, and addition of NH_4Cl to this solution gave only starting material. A similar transfer of H^- is discussed in sect. 1.6.3.

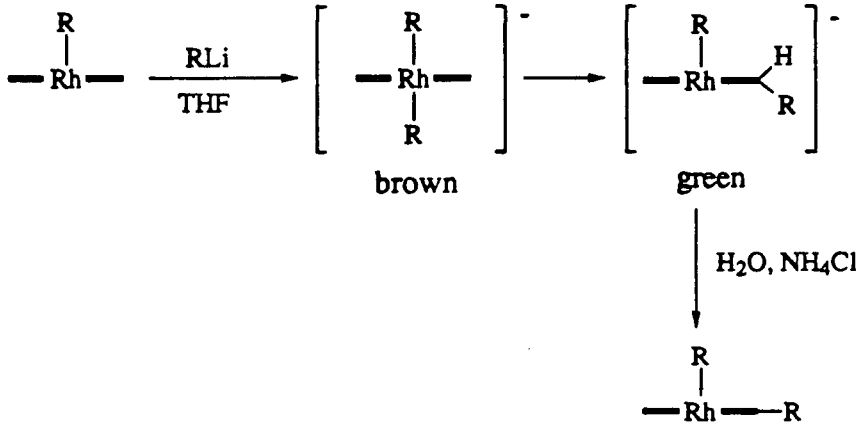

Scheme 1.6. The reaction of Rh^{III}(OEP)(R) with excess RLi.

1.5.7. Photochemistry

Irradiation of Rh^{III}(TPP)(Cl) (at λ <400 nm) or $[Rh(TPP)]_2$ (at λ <310 nm) in 2-Me-THF at 77 K gives Rh^{II}(TPP), as judged by uv-vis and esr data; no photochemical reaction was observed when the Q bands (β and α) were irradiated (58).

Photo-assisted replacement of the amine ligand of $[Rh^{III}(OEP)(NHMe_2)_2]X$ (X = Cl^-, PF_6^-) with tBu-NC, PPh_2Me or $P(OMe)_3$ in 1,2-dichloroethane has been reported, and addition of $NHMe_2$ to Rh^{III}(OEP)(Cl) in toluene to give $[Rh^{III}(OEP)(NHMe_2)_2]Cl$ is also promoted by

photolysis, but with $Rh^{III}(EP)(Cl)$ in 1,2-dichloroethane the chloride is not replaced and $Rh^{III}(EP)(Cl)(NHMe_2)$ is obtained (sect. 1.3.2.3) (32). As described in this thesis (sect. 5.2.3), exposure to laboratory light or sunlight of $Rh^{III}(OEP)(Cl)(PPh_3)$ in benzene, THF, or MeCN, in the presence of 1 atm CO, yields $Rh^{III}(OEP)(Cl)(CO)$, while cessation of irradiation results in reformation of the PPh_3 complex. If CO is absent, then the $Rh^{III}(OEP)(Cl)(solvent)$ species forms in THF or MeCN solutions under similar conditions. In the dark, PPh_3 ligand replacement with CO, THF, or MeCN is not observed (75).

The hydroxymethyl complex $Rh^{III}(OEP)(CH_2OH)$ and $Rh^{III}(por)(CH_3)$ (por = OEP^{2-}, TPP^{2-}) photolytically ($h\nu > 445$ nm) incorporate CO to form corresponding acyl complexes.

$$Rh^{III}(OEP)(CH_2OH) + CO \xrightarrow{h\nu} Rh^{III}(OEP)(C(O)CH_2OH) \qquad (1.47)$$

$$Rh^{III}(por)(CH_3) + CO \xrightarrow{h\nu} Rh^{III}(por)(C(O)CH_3) \qquad (1.48)$$

The formation of the hydroxyacyl complex is complicated by photoinduced transformation back to Rh(OEP)(H) and H_2CO. Reaction between geminate radical pairs within the benzene solvent cage is suggested as the likely mechanism (57).

Irradiation of the arene complexes $Rh^{III}(OEP)(aryl)$ (aryl = $-C_6H_5$, p-OCH_3-C_6H_4, p-CH_3-C_6H_4) in degassed benzene homolytically cleaves the Rh-C bond. The photolysis yielded 4-substituted biphenyls with no evidence of 4,4'-substituted biphenyls that might be expected from coupling of the ligand radicals (21).

1.6. Catalytic Reactions

1.6.1. Reactions of dihydrogen

A paramagnetic complex, subsequently identified as $Rh(TPP)(O_2)$ (42), catalyses the hydrogenation of acetylene in DMF as well as the conversion of H_2/O_2 mixtures to H_2O (41). Details of the catalysis, such as the turnover rates, were not reported in the communication.

1.6.2. Reactions of dioxygen

Catalysis of autooxidation of cyclohexene by $Rh^{III}(TPP)(Cl)(CO)$ and $Rh^{III}(TPP)(Cl)$ is said to produce large amounts of, or cyclohexene hydroperoxide as sole product, although no details are available (110).

Superoxide anion, detected by esr, has been generated in benzene from air using a bis(thiolato)-Rh^{III}(OEP) complex, characterized by a "split Soret band", hyperporphyrin spectrum. The mechanism proposed (Scheme 1.7) involves reduction of Rh^{III} by a thiolato ligand, generated in situ from various thioglycolate esters (thioglycolate ethyl ester, n-octyl ester, octadecyl ester, dithiothreitol) using Bu_4NOH. The generation of superoxide continues until the available thiolato ligand is oxidized to the disulfide form (72).

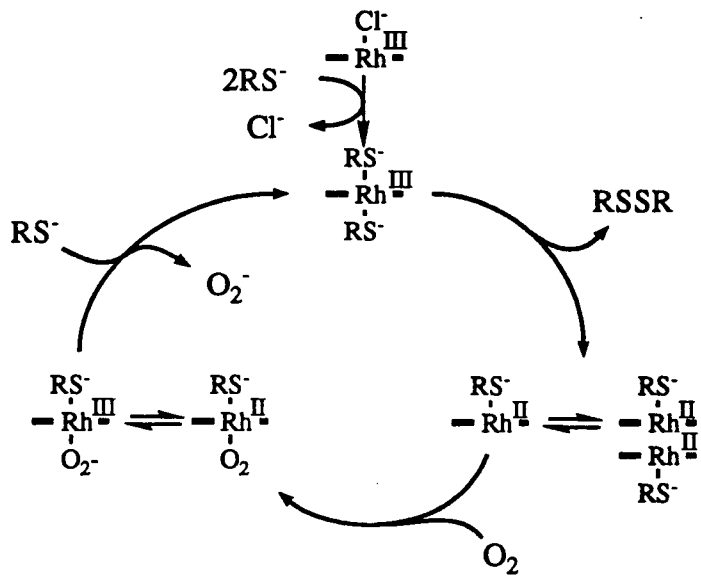

Scheme 1.7. Catalytic cycle for the reduction of dioxygen to superoxide using an in situ Rh^{III}(OEP)/thiolate catalyst complex (adapted from ref. 72).

It is interesting to compare this system with the reaction of $Rh(TPP)(O_2)$ and excess PPh_3, which also displaces the O_2 moiety as O_2^- (sect. 1.3.7), but where the phosphine is not capable of reducing Rh(III) under the conditions used. It should be noted that $[Rh^{III}(TPP)(PPh_3)_2]^+$ does not have a "split Soret band" (77), P-450 hyperporphyrin type spectrum (6), which is a characteristic feature of Rh^{III}(OEP)/thiolate species (72). However,

$Rh(TPP)(O_2)$ could be reformed using an external reductant, for example, via the borohydride reduction of Rh^{III} followed by addition of O_2 (sect. 1.3.7). In Scheme 1.6, the thiolato ligand plays the dual role of ejecting O_2^-, as well as acting as reductant.

1.6.3. Dehydrogenation/Hydride transfer

Secondary alcohols (2-propanol or cyclohexanol) can be photocatalytically dehydrogenated to the ketone and H_2, using $Rh^{III}(TPP)(Cl)$ (Scheme 1.8), via excitation of either B or Q bands. A bimolecular process between Rh(TPP)(H) complexes in the photoexcited (π-π^*) and ground states is involved in H_2 production within the catalytic cycle (111-114).

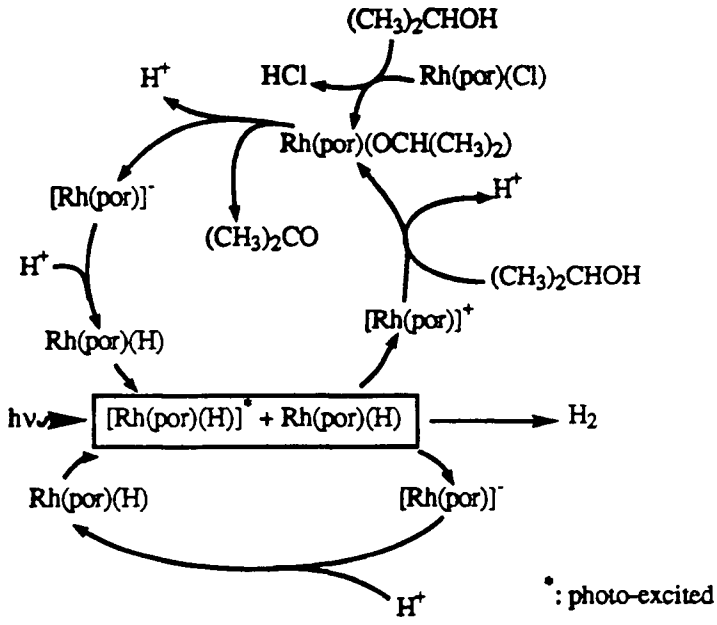

Scheme 1.8. Photocatalytic dehydrogenation of 2-propanol using $Rh^{III}(TPP)(Cl)$ (adapted from refs. 111-114).

Catalytic hydride transfer to $NAD(P)^+$ models has been reported (115). The $Rh^{III}(OEP)(C(O)CH_3)$ complex catalyses the photoreduction of 1-benzylnicotinamide (BNA^+) and 1-benzyl-3-acetylpyridinium ion (BAP^+) to the corresponding 1,4-dihydro derivatives with $B(C_6H_5)_4^-$ as reductant and alcohol as proton source; reduction of BAP^+ in the presence of CH_3OD results in deuteration of the 4-position of BAPH. Hydride donors such as $NaBH_4$, alkoxides and BNAH could be used in place of the alcohol/$B(C_6H_5)_4^-$ system. In the absence of any hydride acceptor, $Rh^{III}(OEP)(C(O)CH_3)$ bleaches when irradiated, a hydride migration from

Rh to the meso carbon of the OEP ligand followed by protonation initiating the bleaching process (also sect. 1.5.6). The stoichiometric reduction of $Rh^{III}(OEP)(Cl)$ in ROH using $NaBH_4$, alkoxide (RO^-; R = CH_3, CH_3CH_2, $(CH_3)_2CH$), or BNAH to form $Rh^{I}(OEP)^-$ occurs under photochemical conditions or in the dark, and, in an inert solvent, Rh(OEP)(H) is formed from the reaction with BNAH; these stoichiometric reactions are believed to be hydride transfers. The $Rh^{III}(OEP)(C(O)CH_3)$ complex is stable to the same reagents in the dark.

1.6.4. Borane transfer reactions

The ærobic reduction of ketones (acetophenone, cyclohexanone, methylcyclohexanones, cyclopentanone, 3-heptanone, and norcamphor) with $NaBH_4$ in THF to the corresponding alcohol is catalysed by Rh(por)(Cl) (por = OEP^{2-} or TPP^{2-}). A key step is the transfer of borane from a proposed intermediate $Rh^{III}(por)(BH_4)$ complex to the ketone to form a dialkoxyborane; oxidative "hydrolysis" of the B-O bonds with O_2 (or an O_2/N_2 mixture or air) coupled to oxidation of Rh(por)(H) yields the alcohols (for example Scheme 1.9). The product distributions obtained

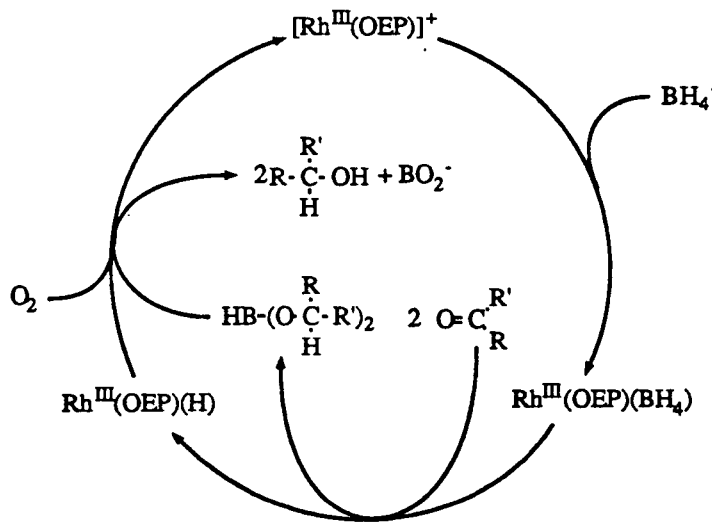

Scheme 1.9. The ærobic reduction of ketone with $NaBH_4$ in THF to the corresponding alcohol catalysed by Rh(OEP)(Cl) (adapted from ref. 116).

from the reaction were compared with the reductions by $LiAlH_4$, $NaBH_4$, diborane and disiamylborane ((3-methyl-2-butyl)-borane). The alcohol product stereoisomer distributions were comparable, the more stable trans isomers being favoured when less hindered ketones were used.

Reduction of 2-methylcyclohexanone gives the less thermodynamically favoured cis isomer for both the Rh^{III}(por)-catalysed and the bulky disiamylborane systems. Catalytic transfer of borane to Et_3N was also reported (116). Olefins have also been catalytically converted to the corresponding alcohols, the "hydration" being anti-Markovnikov (117). A one-pot conversion of 1-methylcyclohexene to (E)-2-methylcyclohexanol with 100% regioselectivity and up to 97% stereoselectivity was performed. Acetylenes could also be converted to alcohols.

1.6.5. Carbon-carbon bond formation

The aldol condensation of cyclohexanone is catalyzed by $[Rh^{III}(OEP)]ClO_4$ under mild conditions. Other ketones such as acetone and methyl ethyl ketone simply undergo metallation at the methyl groups, the resulting complexes being easily cleaved by H^+ or Br_2. The key mechanistic step is believed to be enolization of the ketones promoted by activation with $[(Rh^{III}(OEP)]^+$ acting as a Lewis acid (Scheme 1.10). A chiral modification is being pursued (96,118).

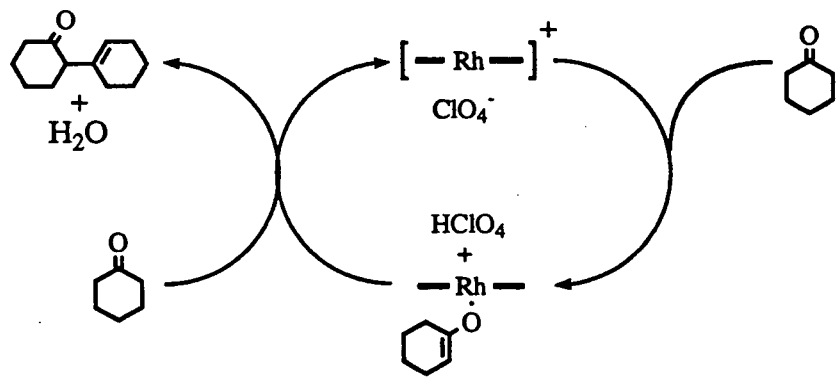

Scheme 1.10. Catalytic C–C bond formation via enolization of ketone (adapted from ref. 118).

Cyclopropanation of cis-olefins (1-hexene, cyclohexene, 1,4-cyclohexadiene, norbornene, 2-methyl-cis-3-pentene, benzene, styrene, phenanthrene, and the pyrroles of Zn(TPP)) by ethyldiazoacetate is catalysed by Rh^{III}(por)(I) (por = $(CN)OEP^{2-}$, TPP^{2-}, TTP^{2-}, TMP^{2-}) using excess olefin at 60°C. A large cis-product selectivity relative to that obtained using more classical CuCl and Rh^{II}(pivalate) systems as catalysts, was observed, and the results were interpreted in

terms of steric hindrance between the olefin substituents and the porphyrin ligand of the proposed Rh-carbene intermediate (30,45,102).

Insertion of "CHCOOEt", from ethyldiazoacetate, into the C-H bonds of long chain alkanes (C_8-C_{18}), chloroalkanes (C_5-C_{10}), and aromatics (toluene, p-xylene, mesitylene) is also catalyzed by Rh^{III}(por)(I) (por = TPP^{2-}, TMP^{2-}, $TDCPP^{2-}$) at ~65°C. The yields are erratic, but selectivity for the terminal methyl group increases with the steric crowding of the Rh center within a carbene intermediate. Direct insertion of the carbene fragment into a C-H bond was proposed rather than H atom abstraction followed by recombination, because an isotope effect of only 2-3 was found for deuterated n-decane as the substrate (101).

1.7. Summary

Much of the chemistry of Rh(por) necessarily involves "single-site" and one-electron chemistry from the point of view of the metal-centerd chemistry. Products of what would otherwise be migratory insertion chemistry are still accessible via one-electron radical processes (chain and cage) in spite of the formal lack of cis-coordination sites. Lewis acid/base, two-electron chemistry is also possible both at Rh(I) and Rh(III) centers and with appropriately functionalised porphyrins. The importance of the relatively high strength of the Rh-C bond is apparent from the array of organometallic products observed and the variety of routes to those compounds. In addition, the porphyrin macrocycle enhances the lability of the d^6 Rh(III) complexes relative to "comparable non-porphinitic systems".

1.8 Goals of the present work

The aim of this thesis is to examine the possibility of forming Rh(por)(OOH) or Rh(por)(OOH)(L) (L = phosphine or amine) species by reaction between O_2 and a rhodium hydride, as is discussed in Chapter 3 of this thesis. As the formation of the Rh(III) hydride species often involves a lower oxidation state of Rh, the collateral discovery of the reduction of Rh(por)(Cl) by tertiary amines was also investigated. This lead to identification of some novel amine and CH_2Cl_2 derived organometallic complexes of Rh(por) and a partial mechanistic description of the reaction with Et_3N and CH_2Cl_2. The work is presented in Chapter 4 and, in the end, provided a more fruitful line of investigation than the original one. Of importance to both the O_2 and amine reactions is the common involvement of Rh(II) monomeric and dimeric species.

Chapter 2
Experimental methods

2.1. General Techniques Used

2.1.1. Infrared spectra

Spectra over the range (3800 – 200) cm^{-1} were obtained using Nujol mulls and KBr disks on a Nicolet 5DX FTIR spectrometer.

2.1.2. Electronic spectra

Spectra over the range (800 – 200) nm were obtained on a Perkin Elmer 552A UV/VIS spectrophotometer, fitted with a Perkin-Elmer Model C550-0555 Thermoelectric single cell holder and a Model C570-0701 Digital Controller, or on a Hewlett-Packard 8452A diode array spectrophotometer. Conventional cells were used under ærobic conditions while air-sensitive samples were handled in a tonometer such as illustrated in Figure 2.1. Unless otherwise noted, all the visible spectra in this thesis were obtained using a 0.1 cm path cell. Typically the solid sample to be dissolved was placed in the quartz cell on the left as drawn and the solvent, and added liquid reagents as required, transferred into the volume on the right for degassing by repetitive freeze-pump-thaw cycles. The solvent and solid sample were mixed by tipping the apparatus to pour the solvent onto the solids in the cell side and shaking vigorously. Mixing times varied from 17 s to several minutes depending upon the rapidity of dissolution: Rh(por) species tended to dissolve slowly (3–10 min) in aromatics but rapidly (15–50 s) in CH_2Cl_2 or $CHCl_3$. Most of the visible spectroscopy studies in this thesis were performed in this fashion when speed of observation was not a critical parameter. Stopped-flow techniques were used when speed and consistent mixing were critical (i.e., the kinetic studies in Chapter 4). If stock solutions were used, then degassing was done in other containers and the solutions transferred into the tonometer for mixing. The apparatus was wrapped with black plastic electricians tape if the samples were light-sensitive.

The spectra of solutions in nmr tubes were obtained, without disturbing the integrity of the sample, using the HP diode array spectrometer. A spectrum was obtained on the thin film of solution flowing down the wall of the nmr tube after gently shaking the sample. Artifacts frequently occurred and very slight motion of the tube during the scan was helpful in reducing

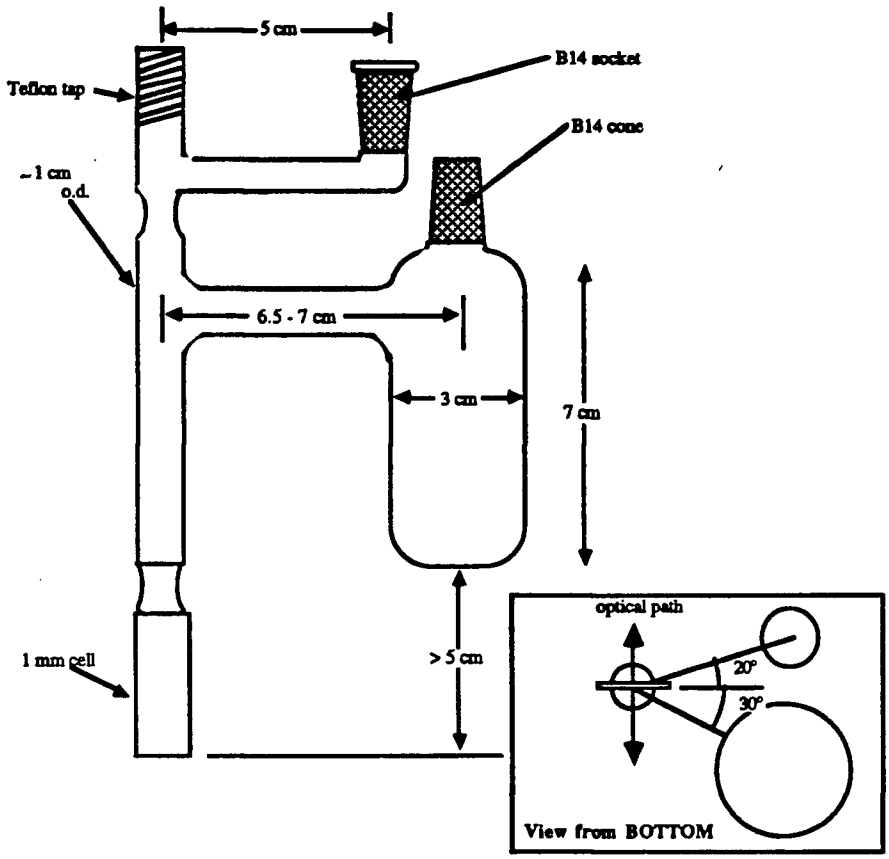

Figure 2.1. Tonometer for anærobic sample handling. Designed to fit compactly in the sample compartments of PE 552A, HP 8452A and Cary 17D spectrophotometers.

these, because the HP spectrometer uses multi-pulse averaging to collect data. The quality of a spectrum obtained this way was acceptable for wavelength and relative peak intensity determination of the porphyrin chromophore but not for concentration determination. Weak and broad bands were poorly resolved.

Solid-state spectra were obtained on mulls supported on filter paper. A solid sample would be mulled in Nujol and then a small piece of filter paper was soaked in the mull. The paper could be "stuck" on a face of a cell, for support in the spectrometer, and run against a blank of

Nujol on a similar sized piece of the same type of filter paper. The quality of a spectrum obtained this way was acceptable for wavelength determination of the porphyrin chromophore but not for concentration determination. Weak and broad bands were again poorly resolved.

2.1.3. NMR spectra

Most ^{1}H, $^{13}C\{^{1}H\}$ and $^{31}P\{^{1}H\}$ spectra were obtained on a Varian XL-300 machine. Some ^{1}H and $^{31}P\{^{1}H\}$ spectra were obtained on Bruker WP-80 and WH-400 machines. Proton and carbon spectra were normally referenced to residual solvent peak positions (124) and reported in units of δ relative to TMS generally to 0.01 ppm accuracy, although the precision of the data was below 1 Hz. Phosphorus spectra were referenced to external triphenylphosphine in the appropriate solvents and reported relative to 85% phosphoric acid (Table 2.1) generally to 0.1 ppm accuracy.

The difference in shifts between the residual phenyl and methyl resonances of C_7D_8 was found to be slightly temperature dependent (Fig. 2.2). This was noticeable during some VT ^{1}H nmr experiments if the spectral reference and lock were on different solvent peaks. Less variation between experiments occurred if the stopcock grease peak† at about 0.28 ppm (at 20 °C) was used as the reference and assumed to have a temperature invariant shift. A stopcock grease peak at about 0.09 ppm in CD_2Cl_2 and CH_2Cl_2 was similarily used as a reference.

Some difficulty arose in quantifying the concentration changes of species during reactions under an O_2 atmosphere. In particular, comparison of initial spectra obtained under inert atmophere, or in vacuo, with those after addition of O_2 required the use of internal standards which had resonance intensities that were relatively insensitive to the increase in relaxation rates caused by the paramagnetic O_2 (126). In this thesis, the practical solution was to use the nearly ubiquitous stopcock grease peaks in the 0.0 to 1.6 ppm region of ^{1}H nmr spectra, which appeared to be insensitive to the presence of O_2. The peaks, although generally weak, provided a convenient means to approximately normalize routine spectra before and after addition of O_2 to a particular sample. The same aquisition parameters were used across any series of experiments where comparisons were desired.

† Apiezon N.

Table 2.1. The $^{31}P\{^{1}H\}$ shifts of PPh_3 relative to 85% H_3PO_4 in various solvents.

Solvent	δ ppm [a]
C_6D_6	-6.05
CD_2Cl_2	-5.64
$CDCl_3$	-5.46

a. Determined (125) relative to phosphoric acid held in a coaxial capillary tube at 20 °C.

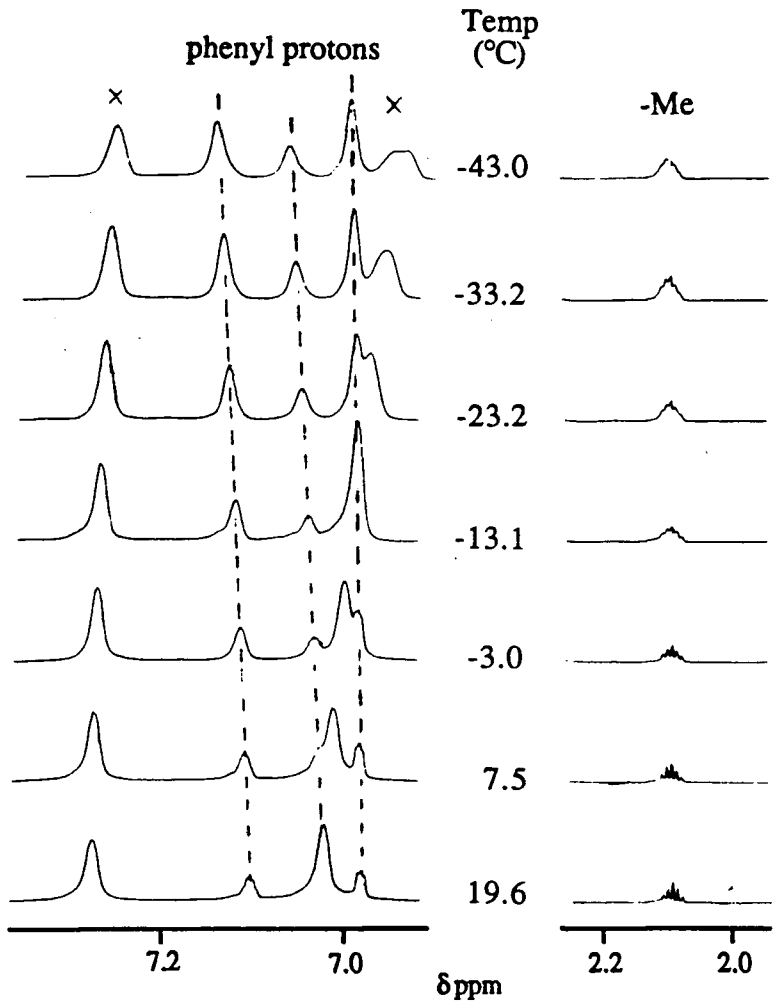

Figure 2.2. Example of temperature variation of the ^{1}H nmr shifts of C_7D_8, plotted with reference to toluene-d_8 δ_{CH3} = 2.09 ppm. x = m,m'-H resonances of diamagnetic Rh(TMP)(Cl).

Sealed tube samples were prepared on a vacuum line. Solid samples were placed in an nmr tube with an attached B14 socket joint. This tube was attached to a vacuum line and evacuated, and a pre-measured volume of nmr solvent was vacuum transferred onto the sample, under static vacuum. After the solvent transfer, and with the sample still frozen by liquid nitrogen, dynamic vacuum was re-established and the tube sealed off with a torch.

2.1.4. Mass spectroscopy

Analyses of samples using FAB desorption were performed in this department's Mass Spectroscopy facility supervised by Dr. Eigendorf.

2.1.5. Micro-analysis

Micro-analyses for carbon, hydrogen, nitrogen, oxygen and chlorine were performed by Mr. P. Borda of this department. Samples containing TMP required addition of V_2O_5 as a combustion aid to prevent a low analysis for nitrogen.

2.1.6. Chromatography

For column separations neutral, Brockman Activity I Alumina (80-200) mesh from Fisher Scientific was used fresh from the bottle. Activity II and III were prepared by vigorously shaking Activity I with 2.3% and 4.5% H_2O by weight, respectively. Aluminium oxide 60 F_{254} neutral (type E) TLC plates were used for analyses.

Silica gel 60 (Merck) (70-230 mesh) was also used for column separations with silica gel 1B2-F (J.T. Baker Chemical Co.) TLC plates being used for analyses.

Gas chromatography was done using an HP 5890A GC equipped with a FID and a HP 3392A digital integrator. The column was a 15 m OV 101 capillary, used with about a 100:1 split ratio at the inlet. Samples of the volatile fractions to be examined were injected following vacuum distillation from metal complexes. Typically 0.8 to 1 mL bulk samples (nmr sample size scale) were prepared using the bulb-to-bulb distillation apparatus illustrated in Figure 2.3. About 1 μL was then injected for analysis.

Typical programmed conditions for separation of Et_3N from Et_2NH in toluene on the HP 5890A GC were:

Detector temp:	220 °C
Inlet temp:	200 °C
Initial column temp:	70 °C
Initial time:	8 min
Rate of temp change:	20 °C/min
Final temp:	220 °C
Final time:	5 min

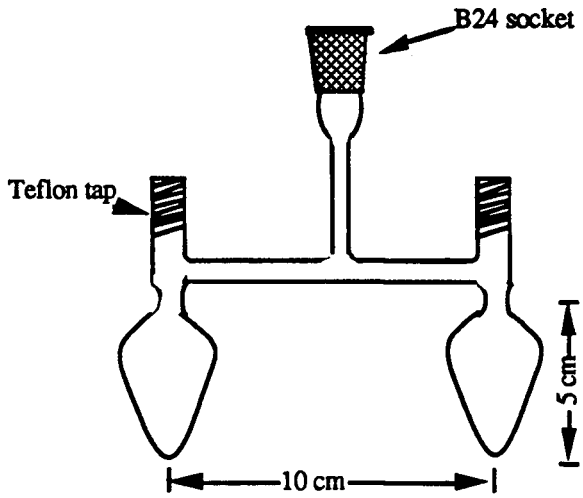

Figure 2.3. A small scale bulb-to-bulb distillation apparatus.

2.1.7. Electrochemistry

Conductivity measurements were made at 25°C under anærobic conditions using a Thomas Serfass conductivity bridge and a cell (constant: 1.0) from Yellow Springs Instrument Co.

2.1.8. Stopped-flow measurements

A model 100/110 Durrum Stopped-flow apparatus was used for the measurements. The output of the single beam spectrophotometer was displayed on a Tektronix D11 storage oscilloscope as voltage vs. time traces. Polaroid photos of the display screen were taken using a Tektronix oscilloscope camera. Numerical data were obtained by measurement on the photographs and subsequently converted to absorbance data. Temperature was controlled to ± 0.1 °C using water circulated by a high-speed pump.

Air-sensitive solutions were handled using the setup illustrated in Figure 2.4. Solutions prepared anærobically were transferred under Ar into the reagent reservoirs (large Schkenk tubes) on the left using cannula, after thoroughly purging all the conecting tubes, drive syringes and stopped-flow valve block etc., with Ar. A slight pressure of Ar was used to transfer the reagent solutions through Teflon cannula into the drive syringes. As much as possible the drive syringes were kept filled and under positive pressure from the large reservoirs in order to maintain any leakage from the drive syringes outward. Due to the solution saturation with a gas (Ar, or CO, see below), bubble formation in the reaction chamber was a recurring problem. Data were accepted if the voltage vs. time oscilloscope traces from 3 consecutive "shots" overlapped, and the data were reasonably smooth.

The precision of the absorbance data is ~± 0.015 absorbance units (largely due to noise) and the accuracy is estimated to be ± 0.03 units based on the spectrum of a solution containing a known concentration of Rh(TMP)(Cl)(CH_3CN). However some variation in the baseline voltage occurred from time to time which introduces an offset of ~0.1 absorbance unit. Accordingly, the absorbance at several wavelengths was periodically rechecked during the 4–5 h required to obtain a spectrum and the order of the data collection within a wavelength range was randomized. The wavelength data are accurate to ± 1 nm, based on the same calibration solution.

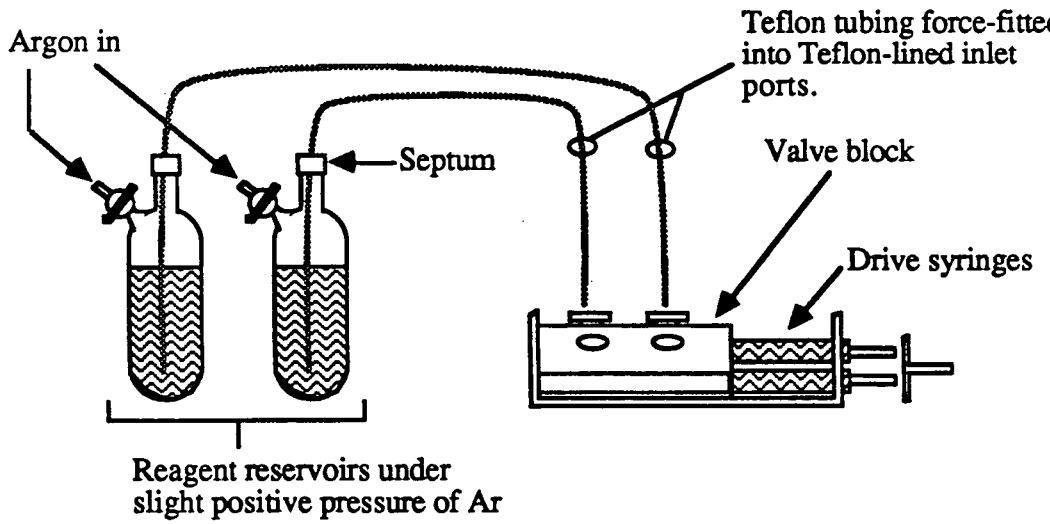

Figure 2.4. The arrangement of reagent reservoirs for handling air-sensitive solutions during stopped-flow experiments using the Durrum Stopped-flow apparatus.

Reagent solutions saturated with CO at 1 atm were used for the investigation of the substitution reactions of Rh(por)(Cl)(CH_3CN) (sect. 4.4). The solubility of CO in CH_2Cl_2 at 25 °C is estimated as ~7.3×10^{-3} M at a $P_{CO} \approx 0.47$ atm (corrected for the vapour pressure of CH_2Cl_2) (127). After the reactant solutions were mixed in the reaction chamber of the stopped-flow apparatus, the [CO] was ~3.65×10^{-3} M, 100 times greater than the typical [Rh(por)(Cl)(CH_3CN)] of ~2×10^{-5} M used in the stopped-flow experiments.

2.2. Materials

2.2.1. Solvents

Benzene and toluene were either spectroscopic or ACS reagent grade and were dried by distillation from benzophenone ketyl or standing over molecular sieves. Dichloromethane was reagent grade and was passed down a column of Alumina I (neutral) before drying by distillation from P_2O_5. N,N'-dimethylacetamide was used immediately after vacuum distillation from CaH_2.

Deuterated solvents were obtained from MSD Isotopes. The C_7D_8, C_6D_6, $CDCl_3$ and CD_2Cl_2 where dried over molecular sieves before use.

All dry solvents were stored under Ar or vacuum in Schlenkware. Deoxygenated, dry solvents were transferred by bulb-to-bulb vacuum transfer or cannula. If dry solvents were to be degassed after transfer to a container, then syringes or cannula were used for the transfers.

2.2.2. Gases

N_2 (N.F. grade), CO (C.P. grade), and O_2 (Ultra High Purity grade) were obtained from Linde. Ar, from Linde, was passed through a molecular sieve and Drierite drying columnn before use. H_2, from Linde, was passed through an Engelhard Catalytic DEOXO purifier before use.

2.2.3. Other materials

2.2.3.1. Amines

The liquid amines used were distilled from KOH before use. Generally small amounts were prepared and used fresh and kept in the dark as much as possible.

2.2.3.2. Phosphines

The phosphines were reagent grade from Strem Chemicals Inc.

2.2.4. Porphyrins

H_2TPP and H_2OEP were gifts from Dr. D. Dolphin. The 5, 10, 15, 20-tetramesitylporphyrin (H_2TMP) was synthesised using a literature method (119). The spectral data for the porphyrin matched the reported data.

Nmr. ^1H: (Table 2.2).

Vis. λ_{max}/nm in CH_2Cl_2: 513, 546, 589, 646.

Table 2.2. The ^1H nmr spectral data for H_2TMP in various solvents at 20 °C.[a]

solvent	–CH=	m-H	p-CH_3	o-CH_3	>N-H
C_6D_6[b]	8.71	7.14	2.46	1.88	-1.73
C_7D_8[c]	8.82	d	2.42	1.89	-1.6
$CDCl_3$[c]	8.60	d	2.60	1.83	-2.53

a. All singlets, integrations matching the assignments, at 300 MHz.
b. In vacuo.
c. In air.
d. Obscured by solvent.

2.2.5. Rhodium porphyrin complexes

Rhodium trichloride ($RhCl_3 \cdot xH_2O$; 42.61% Rh) was obtained from Johnson Matthey Chemicals Ltd. and was used without further purification. Literature methods were used to prepare $[RhCl(cyclooctene)_2]_2$ (120) and $[RhCl(CO)_2]_2$ (121).

2.2.5.1. Rh(OEP)(Cl)(L)

Typical preparations are described below.

2.2.5.1.1. L = H_2O, Rh(OEP)(Cl)(H_2O)·H_2O

The synthesis of Rh(OEP)(Cl)(H_2O)·H_2O was based on a literature method (17,18). In that method $[RhCl(CO)_2]_2$ was stirred with H_2OEP in C_6H_6 for 2 hours at room temperature, the solution was.concentrated and then chromatographed on silica (100 mL dry volume of silica slurried in C_6H_6) with C_6H_6 followed by acetone/C_6H_6 (1:3). Solvent was removed from the

second fraction, eluted with acetone/C_6H_6, under reduced pressure using a rotary evaporator and the solids further dried in vacuo at room temperature. Recrystallization from EtOH, yields the purple Rh(OEP)(Cl)(H_2O)·H_2O. Reported yields were variable ranging from 21.7% (17) to 44% (18). In our hands, yields of 10% to 55% were obtained. Best yields were obtained by placing the reaction flask in a well lit place (a bubbler system exhausting to a fumehood isolated the flask) and monitoring the progress of reaction by visible spectroscopy for as long as 3 days! Workup was often complicated by formation of CO-containing organometallic porphyrins and non-porphyrin products. Subsequently an improved procedure was published (21). The same quantities of reagents were used as described above but the reaction times were changed from 2 h stirring at room temperature to 6 h at room temperature then concentration to 30% volume and followed by reflux for 2 h before chromatography. Yield was 75-80% but workup was still complicated by formation of CO-containing organometallic porphyrin and non-porphyrin products.

The elemental analysis and spectral data for the Rh(OEP)(Cl)(H_2O)·H_2O obtained matched the reported data with the exception of the visible spectrum which tended to have slightly lower λ_{max} values than reported (121a). For convenience this complex will be referred to as Rh(OEP)(Cl)(H_2O) in Chapters 3–6, unless it is necessary to emphasize the presence of the lattice H_2O.

Anal. calc.(%) for $C_{36}H_{48}N_4RhClO_2$: C 61.15, H 6.84, N 7.92, O 4.52; found: C 61.14, H 7.02, N 7.61, O 4.80.

Nmr. ^1H: (Table 2.3 and Fig. 2.5).

Vis. λ_{max}/nm (log ε) in $CHCl_3$ ([Rh] = 1.52×10^{-4} M, 25°C in vacuo): 400 (5.13), 517 (4.13), 550 (4.40).

IR. (Fig. 2.6).

Table 2.3. The ^1H nmr data for Rh(OEP)(Cl)(H_2O)·H_2O in various solvents at 20 °C, unless otherwise noted.

solvent	machine freq. (MHz)	–CH=	$-CH_2-$	$-CH_3$	other	temperature
C_6D_6	300	10.50 s	4.07 m, 3.98 m	1.93 t		
C_7D_8[a]	300	10.43 s	4.05 m[b]	1.96 t		
$CDCl_3$	300	10.35 s	4.15 m	2.00 t		
$CDCl_3$	80	10.36 s	4.18 q	2.03 t	0.3 s br	
CD_2Cl_2	80	10.43 s	4.19 q	2.05 t	0.69 s br	27 °C
		10.42 s	4.19 q	2.05 t		0 °C
		10.39 s	4.19 q	2.05 t	-5.69 s (Rh-OH_2), 1.46 s (H_2O)	-40 °C
$CDCl_3$[c]	?	10.31 s	4.15 q	1.99 t		

a. Solid heated at 140°C in vacuo for 2 h before dissolution.

b. Two multiplets, almost resolved.

c. Ref. 21.

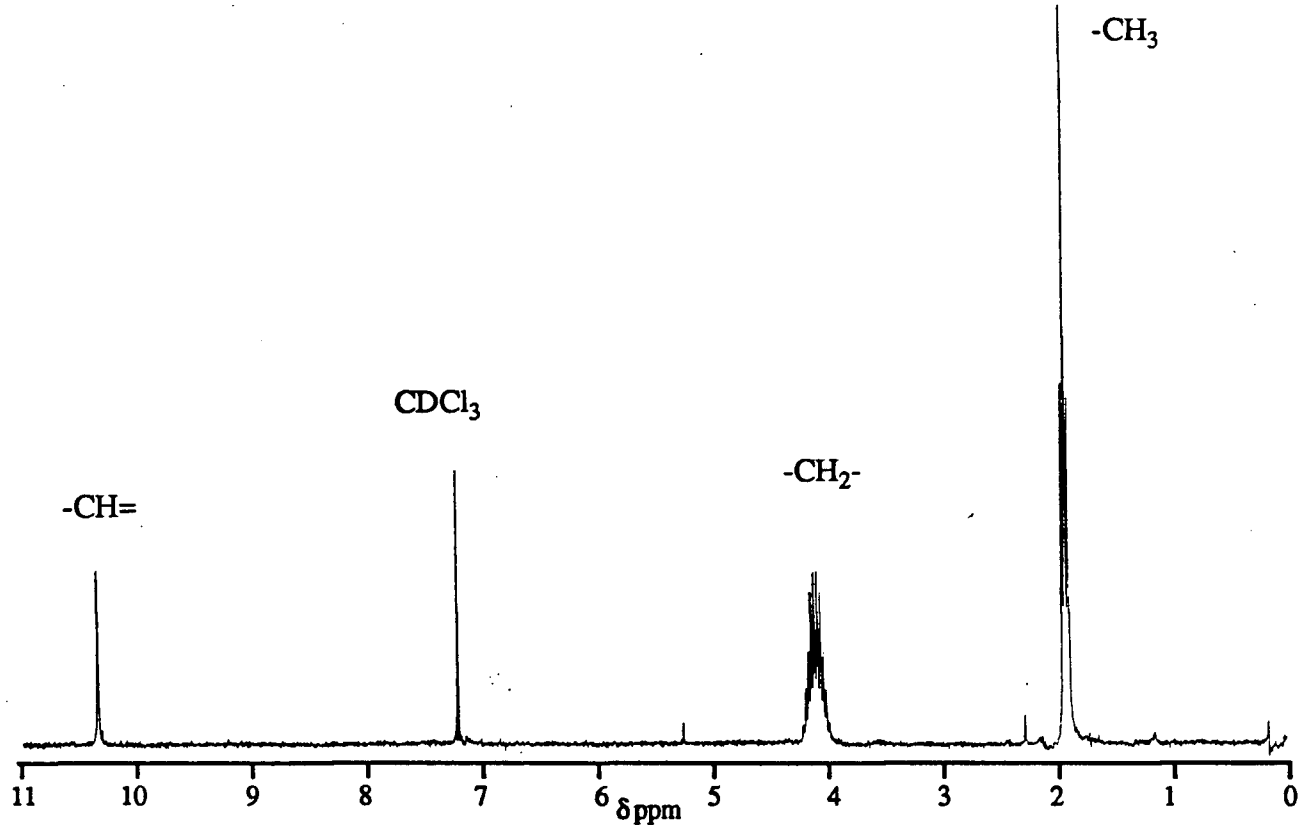

Figure 2.5. The 300 MHz ^1H nmr spectrum of Rh(OEP)(Cl)(H_2O)·H_2O in $CDCl_3$, at 20 °C.

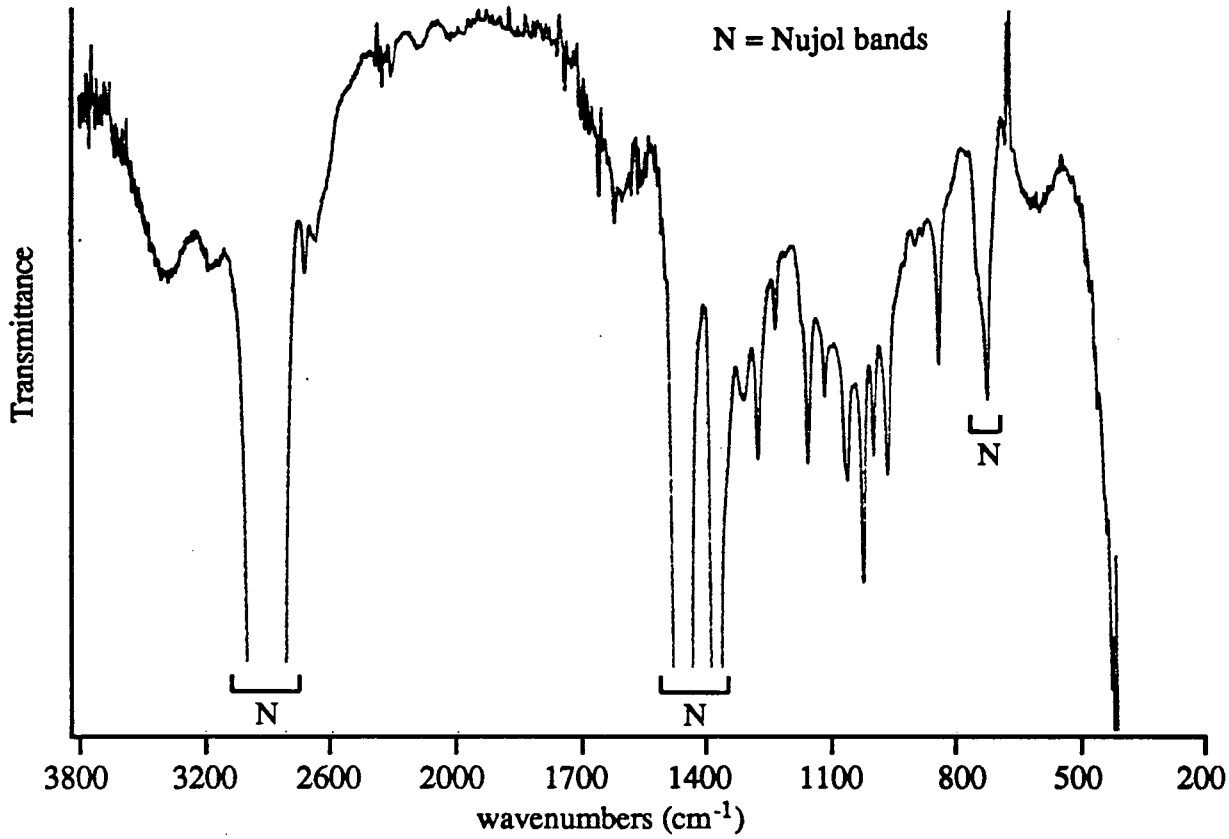

Figure 2.6. The IR spectrum (in Nujol) of Rh(OEP)(Cl)(H_2O)·H_2O.

2.2.5.1.2. L = CH_3CN, Rh(OEP)(Cl)(CH_3CN)

The Rh(OEP)(Cl)(H_2O)·H_2O complex (225 mg, 0.36 mmol) was suspended in 25 mL benzene in a 50 mL Erlemeyer flask. Addition of 2 mL CH_3CN resulted in a clear red-orange solution which was chromatographed on a silica gel column (ca. 100 mL dry volume of silica slurried in C_6H_6). A pale yellow-brown fraction eluted with C_6H_6 and was discarded, following which elution with 5% CH_3CN in C_6H_6 was begun and collection of a broad orange-brown band continued until a green or bright purple band began to elute. This band was left on the column and discarded. The 5% CH_3CN in C_6H_6 fraction, after removal of solvent in vacuo, yielded 118 mg of red-brown Rh(OEP)(Cl)(CH_3CN) (52%).

Anal. calc.(%) for $C_{38}H_{47}N_5RhCl$: C 64.09, H 6.65, N 9.83; found: C 64.65, H 6.83, N 9.30.
Nmr. ^1H (300 MHz, C_6D_6 at 20 °C): 10.53 (s, 4H, –CH=), 4.11 (m, 8H, –CH_2–), 4.00 (m, 8H, –CH_2–), 1.98 (t, 24H, –CH_3), -2.96 (s, 3H, $C\underline{H}_3CN$).

Vis. λ_{max}/nm (log ε) in CH_2Cl_2 ([Rh] = 4.82×10^{-5} M, 25°C in Ar): 400 (5.10), 518 (4.17), 550 (4.42).

2.2.5.1.3. L = PPh_3, Rh(OEP)(Cl)(PPh_3) (122)

The $Rh(OEP)(Cl)(H_2O)\cdot H_2O$ complex (82 mg, 0.11 mmol) and PPh_3 (33.5 mg, 0.12 mmol) were placed in a small Schlenk tube under argon. The solids were dissolved in 20 mL freshly dried benzene. After ca. 15 min the solution was filtered and the filtrate volume reduced in vacuo to ~3 mL. The product was precipitated by addition of freshly dried hexanes, collected on a frit, and washed 3 times with 2 mL portions of hexanes before drying in vacuo. Yield was 52 mg (50%) of red purple powder.

The complex was found to be light-sensitive in dilute solution. Dissolution in CH_3CN gave non-conducting solutions.

Anal. calc.(%) for $C_{54}H_{60}N_4RhClPO_{0.5}$: C 68.17, H 6.46, N 5.89; found: C 68.82, H 6.42, N 5.94 (contains 0.5 H_2O).

Nmr. ^1H and $^{31}P\{^1H\}$: (Tables 2.4 and 2.5).

Vis. λ_{max}/nm (log ε) in C_6H_6 ([Rh] = $(0.9 - 6.0) \times 10^{-3}$ M, 25°C in vacuo): 351 (4.59), 422 (5.20), 533 (4.32), 564 (4.38); in Nujol mull: 350, 418, 535, 564.

Table 2.4. The ^1H NMR spectral data for Rh(OEP)(Cl)(PPh_3) at 20 °C.

solvent	machine frequency (MHz)	–CH=	$-CH_2-$	$-CH_3$	o-H	m-H	p-H
CD_3CN	300	9.96 s	4.10 m, 3.97 m	1.91 t	3.58 m	6.42 m	6.84 m
CD_2Cl_2	300	9.93 s	4.09 m, 3.95 m	1.94 t	3.62 m	6.39 m	6.82 m
C_6D_6	80	10.06 s	3.93 m	1.90 t	3.90 m	6.28 m	

Table 2.5. Room temperature $^{31}P\{^1H\}$ NMR spectral data for Rh(OEP)(Cl)(PPh_3) at 20 °C.

solvent	machine frequency (MHz)	Rh-P	$^1J_{Rh-P}$
CD_3CN	121.421	9.68 d	124
CD_2Cl_2	121.421	9.52 d	124
C_7H_8	32.21	9.05 d	116

2.2.5.2. Rh(OEP)(H)

Literature methods were used to prepare Rh(OEP)H (78). The hydride was prepared by protonation of $[Rh(OEP)]^-$, itself prepared in situ in basic EtOH solution by borohydride reduction of Rh(OEP)(Cl)(H_2O)·H_2O, using HOAc. The orange Rh(OEP)(H) precipitates from the EtOH solution. An alternative "one-pot" preparation starting from $[RhCl(CO)_2]_2$ and H_2OEP in glacial acetic acid was also used (46). Precipitation of Rh(OEP)(H) was induced by bubbling H_2 into the solution. However, the product contained a large amount of unidentified insoluble black material characterised by IR bands at 2065 (m, sharp) and 1785 cm^{-1} (vs, broad). This material could be separated from the hydride by washing the mixture through celite with CH_2Cl_2, under H_2, and removal of the CH_2Cl_2 from the filtrate with a flow of H_2.

The hydride is air- and light-sensitive in solution but the solid is stable in dry air for several days. It is normally stored in the absence of light and under an Ar atmosphere. It is soluble in pyridine, THF, $CHCl_3$, CH_2Cl_2, DMA or acetone, less soluble (slow dissolution) in aromatics and is poorly soluble in EtOH, alkanes or CH_3CN.

The elemental analysis and spectral data for the Rh(OEP)(H) obtained matched the reported data (78).

Anal. calc.(%) for $C_{36}H_{45}N_4Rh$: C 67.91, H 7.12, N 8.8; found: C 67.23, H 7.20, N 8.62.

Nmr. ^1H: (Table 2.6).

Vis. λ_{max}/nm (log ε) in CH_2Cl_2 ([Rh] = 1.73×10^{-4} M, 25 °C in vacuo): 391 (5.11), 508 (4.15), 542 (4.68).

IR. ν_{RhH} at 2226 cm^{-1} (Fig. 2.7).

Table 2.6. The ^1H nmr data for Rh(OEP)(H) in various solvents and temperatures.

solvent	machine frequency (MHz)	–CH=	$-CH_2-$	$-CH_3$	Rh-H($^1J_{Rh-H}$)	temperature (°C)
C_6D_6	200[a]	10.15 s[b]	3.95 q	1.87 t	-41.28 d (44)	
C_6D_6	400	10.22 s	4.01 q	1.95 t	-41.24 d (44)	20
CD_2Cl_2	400	9.97 s	4.01 q	1.90 t	-41.80 d (44)	20
	"	9.73 s	3.89 m	1.78	-42.03 bs	-40
	80	9.98 s	-	-	n.o.	17
	"	9.98 s	-	-	-41.0	0
	"	9.82 s	-	-	-41.3	-40
	"	9.54 s	-	-	n.o.	-70
THF-d_8	400	10.00 s	4.05 m	1.92 t	-39.1 d (32)	28
pyr-d_5	80	10.33 s	4.05 m	1.93 t	-33.1 d (23)	20
	"	10.34 bs	3.95 bs	1.83 bs	-32.8 d (23)	-20

n.o. = not observed

a. Ref. 46.

b. Temperature dependent: $\delta H = 10.3117 - 62.61\ (1/T)$ (ref. 46).

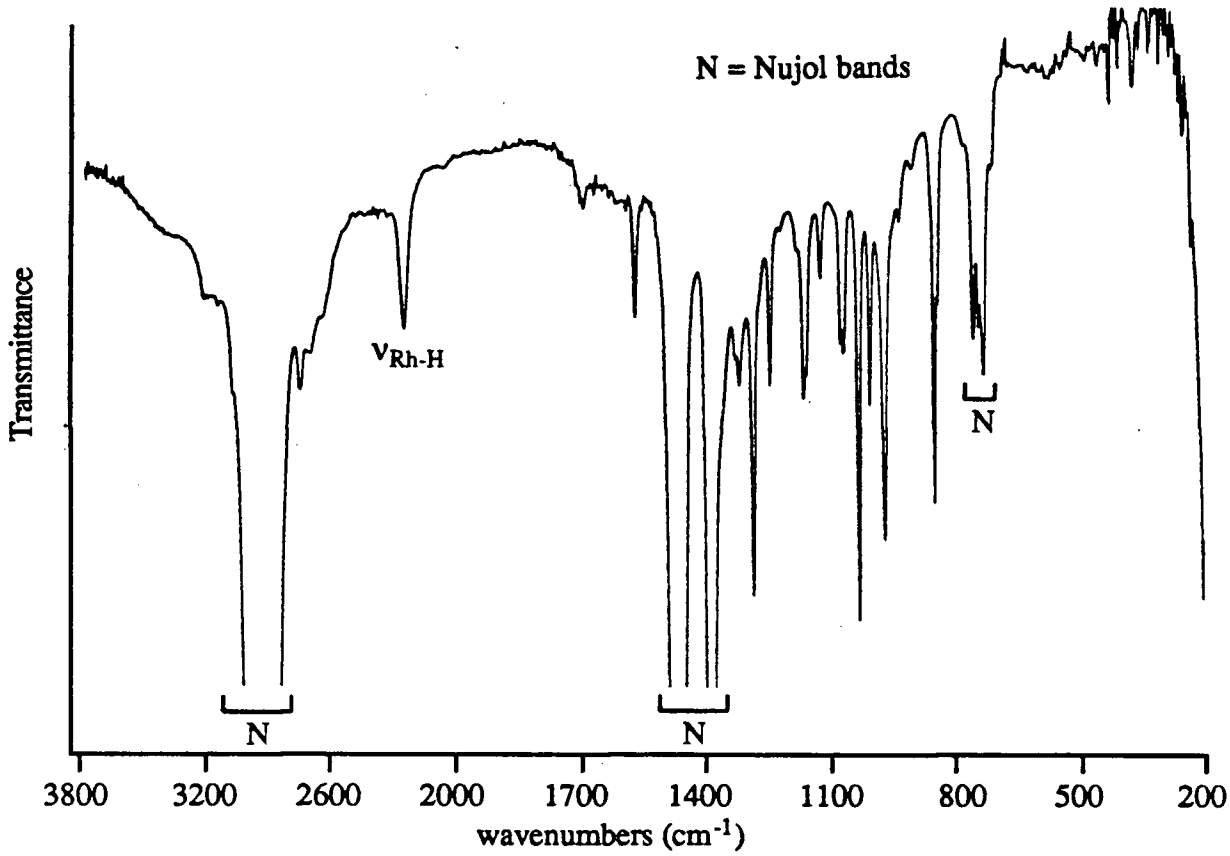

Figure 2.7. The IR spectrum of Rh(OEP)(H) (in Nujol).

2.2.5.3. Rh(TMP)(Cl)(L)

Considerable effort went into finding a metallation procedure that would yield reasonable quantities of Rh(TMP)(Cl)(L) derivatives with easily replaceable ligands. The successful methods presented below (sect. 2.1.5.3.1–2) are adaptions of the syntheses for $Rh(OEP)(Cl)(H_2O)\cdot H_2O$ discussed above. A promising procedure was the reaction of $RhCl_3\cdot 3H_2O$ with H_2TMP in DMF which was directly adapted from the reported preparation of $Rh(TPP)(Cl)(N(CH_3)_2H)$ (with $[Rh(TPP)(N(CH_3)_2H)_2]Cl$ as co-product) (52). Although ca. 80% of the H_2TMP was metallated it proved impossible to purify the products which were principally: (i) $Rh(TMP)(Cl)(N(CH_3)_2H)$ (^1H nmr in $CDCl_3$: 8.63 (s, 8H, -CH=), ~7.3 (m,m'-H obscured), 2.60 (s, 12H, p-CH_3), 1.98 (s, 12H, o-CH_3), 1.74 (s, 12H, o'-CH_3), -2.78 (d, 6H, N-CH_3), -5.4 (s, 1H, N-H)); (ii) $[Rh(TMP)(N(CH_3)_2H)_2]Cl$ (ionic, very low solubility in C_6H_6; ^1H nmr in $CDCl_3$: 8.81 (s, 8H, -CH=), 7.30 (s, 8H, m-H), 2.63 (s, 12H, p-CH_3), 1.92 (s, 24H, o-CH_3), -3.08 (d, 12H,

N-CH_3), -3.89 (s, 1H, N-H); mass measurement expected for $C_{60}H_{66}N_6Rh$: 973.44, found (FAB): 973); (iii) $[Rh(TMP)(N(CH_3)_2H)_2][Rh(Cl)_2(CO)_2]$ (ionic, very low solubility in C_6H_6; ^1H nmr in $CDCl_3$: similar to $[Rh(TMP)(N(CH_3)_2H)_2]Cl$; IR (Nujol): ν_{CO} at 2064 and 1983 cm^{-1}, ν_{CO} reported for $[Rh(OEP)(N(CH_3)_2H)_2][Rh(Cl)_2(CO)_2]$ (51): 2064 and 1982 cm^{-1}).

We recently became aware of the synthesis of Rh(TMP)(I) in 1,2-dichloroethane that utilizes I_2 as oxidant (30), but have not repeated this synthesis.

2.2.5.3.1. L = iPrOH, Rh(TMP)(Cl)(iPrOH)

Most of the work in this investigation that involved Rh(TMP) species used the title isopropanol complex as starting material. Unfortunately the synthesis of Rh(TMP)(Cl)(iPrOH) is unreliable, working only 2 times out of 5. Use of CH_3CN instead of iPrOH (sect. 2.1.5.3.2.) led to reproducible results, although the synthesis has not been optimized. The products of the 3 "failed" experiments were not fully characterized; however, TLC data are consistent with Rh(TMP)(iPrO) as a major product (see below; comments in sect. 2.1.5.3.3. are also relevant).

The $[RhCl(CO)_2]_2$ complex (108 mg, 0.38 mmol) and H_2TMP (211 mg, 0.27 mmol) were placed in a 100 mL reaction flask having a Kontes Teflon valve as the only entrance. Then 28 mL dry toluene was vacuum transferred onto the solids. The flask was wrapped in foil to exclude light and the mixture stirred in vacuo for 18h at room temperature. The foil was removed and the temperature raised to 70°C for 2 days, after which the reaction flask was cooled to room temperature. The flask was opened to the atmosphere for about 10 min while the solution was stirred. The reaction flask was closed and the contents left to stir until the the visible spectrum of the reaction solution had ceased changing from bands at 520 (major), 545 (weak), 590 (broad) and 640 (broad) nm to bands at 544 and 578 nm. About 30 mg of solid K_2CO_3 were added to neutralize the H^+ from H_2TMP, and 0.2 mL of 2-propanol was added. The mixture was stirred until the green tinge of the solution was gone, then about 5 mL of solvent were removed by vacuum transfer, which resulted in disappearance of the 544 and 578 nm bands and generation of a 534 nm peak. The solution was filtered to remove K_2CO_3 and fine greenish solids, before passing the reaction solution down a silica gel column (75 – 100 mL dry volume of silica slurried in C_6H_6), eluting with C_6H_6; the column was wrapped with aluminium foil to protect it from direct

light. A yellow-orange band came off first, then a red-orange complex group (1 broad and 2 narrow overlapped bands). The bands of this group sometimes spread out on the column during elution; adding 2-propanol to the benzene eluant (1-5%) brought the bands together and they were collected together. The remaining material at the top of the column was discarded. Prior to removal of solvent from the two fractions, 3-6 drops of 2-propanol were added to each.

Solvent was removed under reduced pressure using a rotary evaporator and the solids further dried in vacuo at room temperature. The first band yielded 28 mg of a purple solid (a mixture, including H_2TMP and Rh(TMP)(iPrO) as judged by nmr), and the second band 145 mg of a microcrystalline lilac-purple Rh(TMP)(Cl)(iPrOH)·iPrOH (51%). For convenience this complex will be referred to as Rh(TMP)(Cl)(iPrOH) in Chapters 3–6, unless necessary to emphasize the presence of the lattice iPrOH .

Rh(TMP)(Cl)(iPrOH)·iPrOH

Anal. (V_2O_5 combustion additive required) calc.(%) for $C_{62}H_{68}N_4RhClO_2$: C 71.63, H 6.59, N 5.39; found: C 70.96, H 6.40, N 5.24.

Nmr. ^1H: (Table 2.7 and Fig. 2.8).

Vis. λ_{max}/nm (log ε) in C_6H_6 ([Rh] = 1.24×10^{-4} M, 25 °C in vacuo): 422 (5.33), 534 (4.39), 565 (3.41); in CH_2Cl_2 ([Rh] = 5.55×10^{-4} M, 25 °C in vacuo): 423 (5.46), 532 (4.40), 565 (3.40).

Table 2.7. The ^1H NMR spectral data for Rh(TMP)(Cl)(iPrOH)·iPrOH in various solvents.[a]

solvent	–CH=	m,m'-H	p-CH_3	o,o'-CH_3	coordinated iPrOH
C_6D_6	8.94	7.23, 7.03	2.44	2.22, 1.71	
CD_3OD[b]	8.63	7.29	2.60	1.90	
C_7D_8	8.83	7.24, 7.06	2.47	2.22, 1.69	
C_7D_8[c,d]	8.91	7.22, 6.99	2.46	2.29, 1.68	-2.25 d (6H,-CH_3), -2.67 m (1H, >CH-), -6.33 m (1H, -OH)

a. All singlets and at 20 °C except where noted otherwise, integrations matching assignments, at 300 MHz.
b. All resonances broad.
c. -34 °C.
d. One non-coordinated iPrOH is also present: methyl resonance at 0.762 d, other resonances not observed.

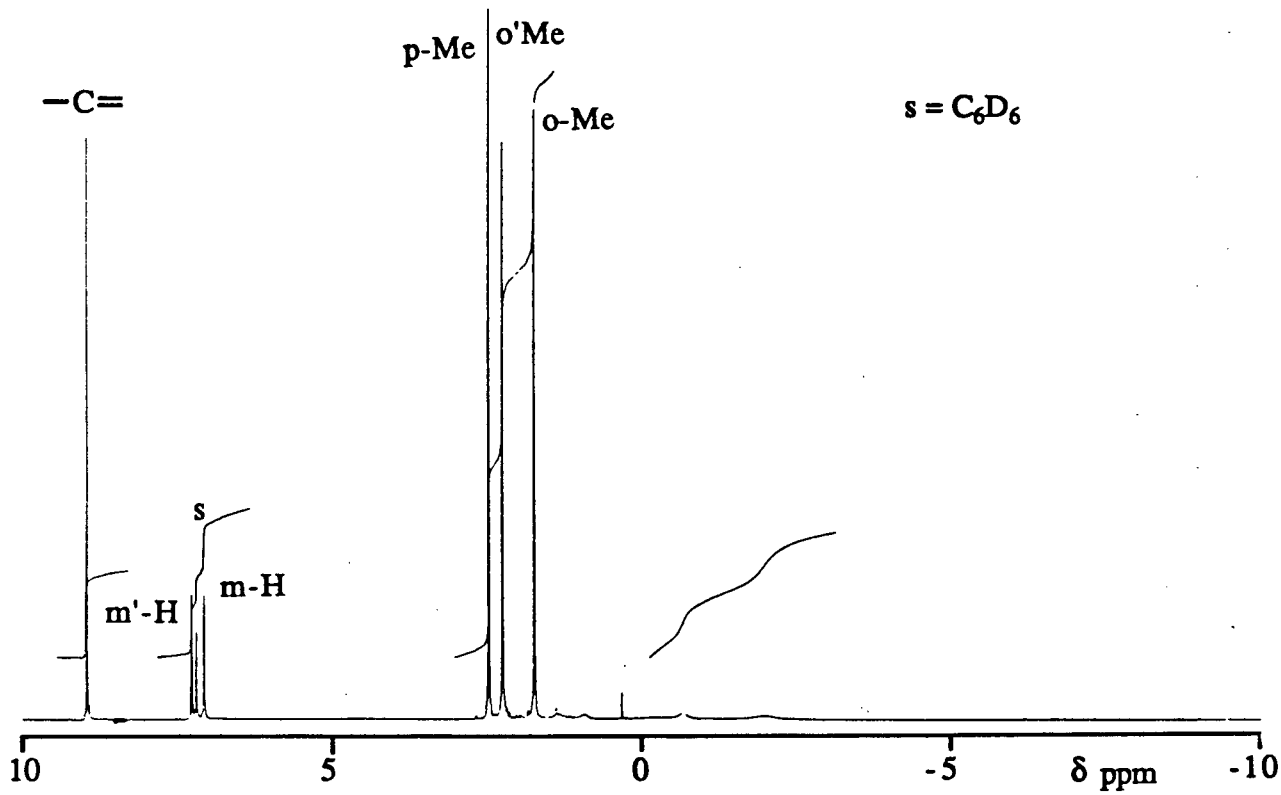

Figure 2.8. The ^1H nmr spectrum of Rh(TMP)(Cl)(iPrOH)·iPrOH in C_6D_6, at 20 °C.

Rh(TMP)(iPrO)

Nmr. ^1H (300 MHz, C_6D_6, 20 °C): 8.81 (s,8H, =CH-), 7.21 (s, 4H, m-H), 7.13 (s, 4H, m'-H), 2.45 (s, 12H, p-CH_3), 2.21 (s, 12H, o-CH_3), 1.92 (s, 12H, o'-CH_3), 2.40 (m, 1H, O-CH<), -0.88(d, $^3J_{HH}$ = 6 Hz, 6H, -CH_3).

IR. ν_{CO} at 1050 cm^{-1} (within the expected region for isopropoxide ligand (123))

2.2.5.3.2. L = CH_3CN, Rh(TMP)(Cl)(CH_3CN)

The synthetic method was the same as for the synthesis of Rh(TMP)(Cl)(iPrOH) except CH_3CN was used in place of iPrOH. Yield of the bright orange-red Rh(TMP)(Cl)(CH_3CN) was 50%.

Anal. (V_2O_5 combustion additive required) calc.(%) for $C_{58}H_{55}N_5RhCl$: C 72.53, H 5.77, N 7.29; found: C 72.25, H 5.76, N 7.06.

Nmr. ^1H (300 MHz, $CDCl_3$ at 20 °C): 8.59 (s, 8H, –CH=), ~7.25 (m,m'-H, obscured by solvent), 2.60 (s, 12H, p-CH_3), 1.88 (s, 12H, o-CH_3), 1.83 (s, 12H, o'-CH_3), -0.179 (s, 2H, Rh-$C\underline{H}_3CN$).

Vis. λ_{max}/nm (log ε) in CH_2Cl_2 ([Rh] = 4.82×10^{-5} M, 25°C in Ar): 400 (5.48), 539 (4.37), 572 (3.59).

IR. (Fig. 2.9).

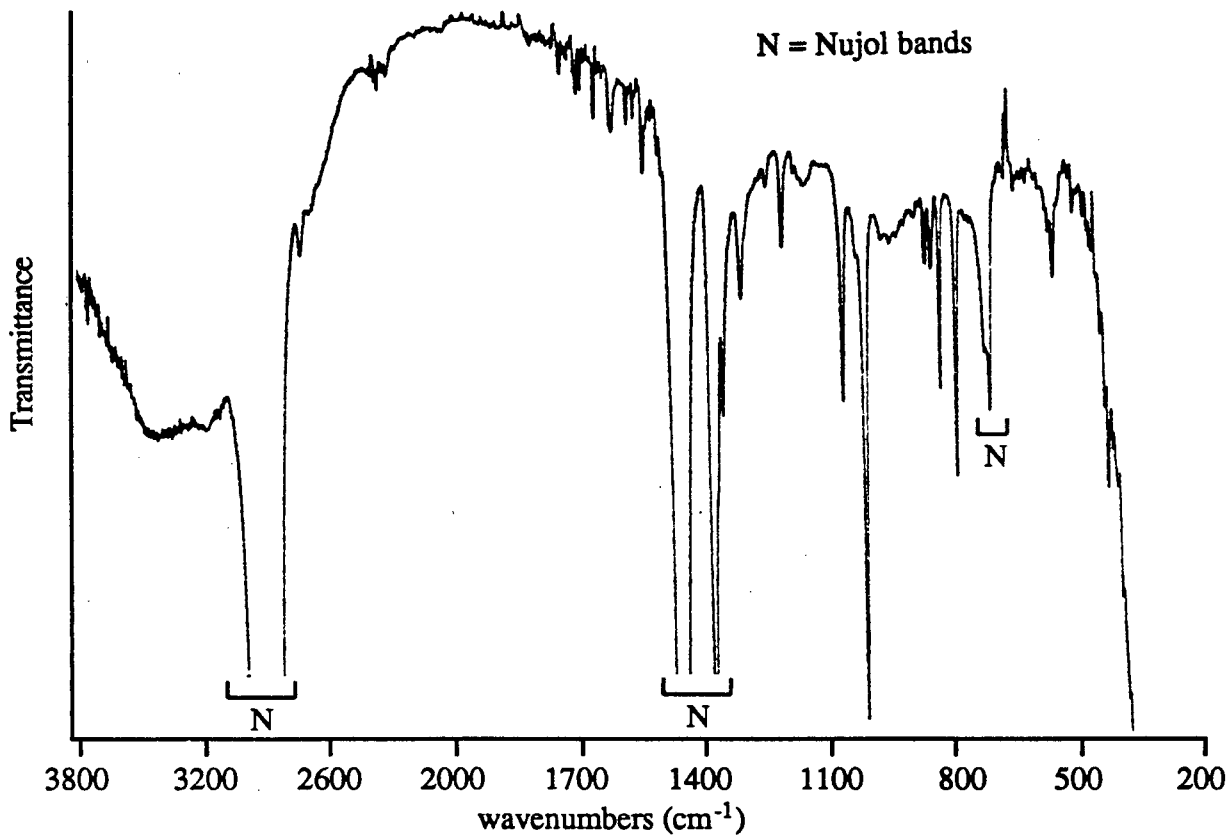

Figure 2.9. The IR spectrum (in Nujol) of Rh(TMP)(Cl)(CH_3CN).

2.2.5.3.3. L = none, Rh(TMP)(Cl)

This complex could be prepared by in vacuo pyrolysis of either Rh(TMP)(Cl)(CH_3CN) or Rh(TMP)(Cl)(iPrOH). However, if amounts of Rh(TMP)(Cl)(iPrOH) larger than 1–3 mgs were pyrolysed, a mixture of products (not characterized) was obtained. At high temperature the Rh(III) complex in the solid state is possibly reduced by its isopropanol ligand. Reduction of Rh^{III}(TPP)(Cl) by isopropanol is known in solution (sect. 1.6.3).

The Rh(TMP)(Cl)(CH_3CN) complex (30 mg, 0.03 mmol) was placed in a tube fitted with a Teflon valve and a B19 socket (Fig. 2.10). The tube was evacuated and then heated at 210 °C under dynamic vacuum (10^{-5} torr) for ~3 h to give very hygroscopic dull red-brown Rh(TMP)(Cl). Manipulations of the complex were performed in a glovebox.

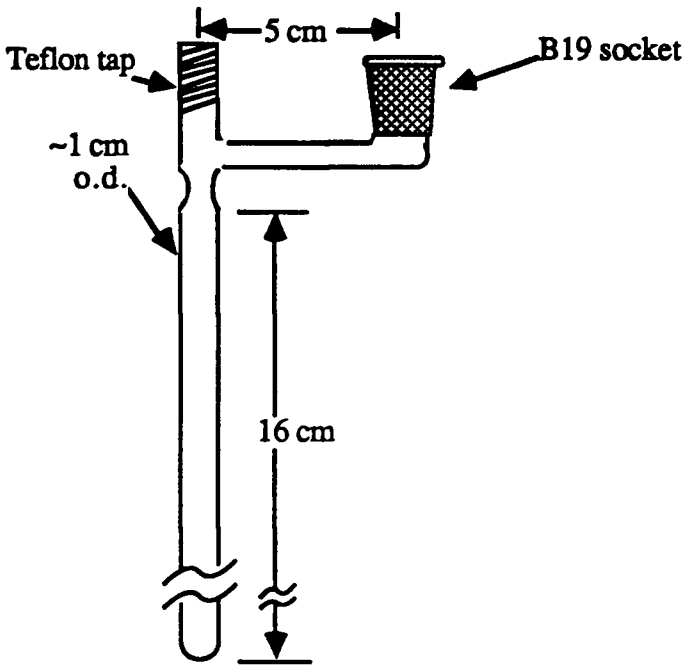

Figure 2.10. Vacuum pyrolysis tube.

Anal. (V_2O_5 combustion additive required) : calc.(%) for $C_{56}H_{52}N_4RhCl$: C 73.16, H 5.70, N 6.09, Cl 3.86; found: C 73.46, H 5.85, N 6.06, Cl 3.70.

Nmr. ^1H (Table 2.8).

Vis. λ_{max}/nm in C_7H_8 at 25 °C: 525 (Soret region not examined).

The Rh(TMP)(Cl)(iPrOH) complex (3 mg, 0.003 mmol) was similarly heated to 220 °C under dynamic vacuum (10^{-5} torr) for 3 h to give Rh(TMP)(Cl).

Anal. (V_2O_5 combustion additive required) : calc.(%) for $C_{56}H_{52}N_4RhCl$: C 73.16, H 5.70, N 6.09, Cl 3.86; found: C 73.39, H 5.67, N 5.95, Cl 3.66.

Table 2.8. The ^1H NMR spectral data for Rh(TMP)(Cl) in CH_2Cl_2 and C_7D_8 at various temperatures.[a]

solvent	–CH=	m-H	m'-H	p-CH_3	o-CH_3	o'-CH_3	temperature (°C)
C_7D_8	8.78	7.28	7.02	2.48[b]		1.51	20
	8.79	7.27	7.00	2.47	4.46	1.50	8
	8.79	7.26	6.99	2.47	2.45	1.50	-13
	8.80	7.23	6.96	2.46	2.43	1.49	-23
	8.81	7.22	6.91	2.45	2.42	1.59	-33
	8.81	7.20	6.89	4.44	2.41	1.49	-43
CD_2Cl_2	8.70	7.31	7.30	2.62	1.94	1.77	21
	8.71	7.31[c]		2.62	1.93	1.79	7
	8.72	7.33[c]		2.63	1.92	1.81	-18
	8.73	7.33[c]		2.63	1.90	1.84	-38

a. All singlets; the integrations matching assignments at 300 MHz.
b. p-CH_3 and o-CH_3 resonances overlap.
c. m-H and m'-H resonances overlap.

2.2.5.4. Rh(TMP)(H)

This complex was never isolated pure or in large quantity. It was prepared in situ for visible spectroscopy experiments by borohydride reduction (5 mg $NaBH_4$) of 0.8 mg [Rh(TMP)$(N(CH_3)_2H)_2$]Cl in 3.2 mL EtOH containing 0.2 mL 1N NaOH. The resulting air-sensitive solution (presumed to contain [Rh(TMP)]$^-$ intermediate: λ_{max} at 498 nm) was carefully acidified with AcOH, forming air-sensitive Rh(TMP)(H) in situ.

A solid sample of uncertain purity was prepared for a nmr experiment by exposing 5 mg solid Rh(TMP)(Cl) to an H_2 atmosphere for 1.5 weeks. The dull red-brown Rh(TMP)(Cl) became reddish orange impure Rh(TMP)(H).

Nmr. ^1H (impure Rh(TMP)(H), 300 MHz, C_7D_8 at 20 °C): 8.66 (s, 8H, –CH=), ~7.15 (m,m'-H, obscured by solvent), 2.47 (s, 12H, p-CH_3), 2.11 (s, 12H, o-CH_3), 1.77 (s, 12H, o'-CH_3), -40.18 ppm (d, 1H, J_{Rh-H} = 44 Hz, Rh-H) (123a).

Vis. λ_{max}/nm in C_2H_5OH at 25 °C (in situ Rh(TMP)(H)): 415 (Soret), 528, 558(sh).

Chapter 3
Reactions involving Rh(OEP)(H)

3.1. Introduction

This chapter contains studies principally of the reactions of Rh(OEP)(H) with O_2. Reactions of some other small molecules with the hydride are included where these have some relevence.

Reactions effected by homogeneous transition metal catalysts utilizing direct oxidation by molecular oxygen are not well understood relative to other areas of homogeneous transition metal catalysis (1). There is a strong motivation to develop metal complex catalysts that will utilize molecular oxygen under mild conditions for the selective oxidation of organic substrates (1,2). Much attention has focused on monoxygenase-type chemistry where two-electron oxidation of substrates (containing C-H, C=C, >N-, >S) by O_2 occurs, with one oxygen atom evolving as H_2O (e.g. P-450 cytochromes) (128):

$$RH + O_2 + NADPH + H^+ \xrightarrow{\text{P-450}} ROH + H_2O + NADP^+ \qquad (3.1)$$

Although the natural systems are not long-lived (P-450 has a lifetime of ~20 min during oxidation (129)) and so the "catalytic system" includes the support of biological replication, the elementary steps involved in the enzymic process are of obvious interest. The key steps in the P-450 enzymic catalytic cycle that effect the conversion of O_2 to useful transferable "O equivalents" are believed to involve a possible Fe^{III}-OOH intermediate (Scheme 3.1; the bound substrate and other components are not shown) (6,7,130).

The M-OOH intermediate has been proposed to occur in a number of transition metal non-porphyrin and porphyrin containing systems (116,131,132). Of particular interest in this laboratory were systems where M-H with O_2 were involved in the oxidation of hydrocarbons and where metal hydroperoxides are likely intermediates in these O_2/hydride systems. The M species

$$\cdots\cdots \longrightarrow Fe^{II} + O_2 \longrightarrow Fe^{III}\text{-}O\text{-}O^- \xrightarrow{e^-} Fe^{III}(O_2^{2-})$$

$$Fe^{III}(O_2^{2-}) + H^+ \longrightarrow Fe^{III}\text{-}O\text{-}O\text{-}H$$

$$Fe^{III}\text{-}O\text{-}O\text{-}H + H^+ \longrightarrow [Fe^{V}{=}O \longleftrightarrow Fe^{III} + O] + H_2O$$

$$[Fe^{V}{=}O] \longrightarrow\longrightarrow \cdots\cdots$$

Scheme 3.1. Part of the catalytic cycle of cytochrome P-450.

may be recycled via M-H formation using H_2 and the use of H_2/O_2 mixtures for the reductive-activation of dioxygen has been documented (132). Scheme 3.2 is a schematic of a cycle based on an Ir, non-porphyrin, system.

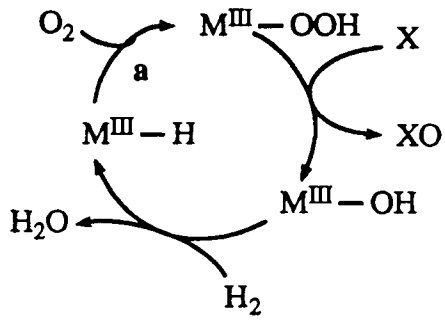

Scheme 3.2. Postulated O_2/hydride system (adapted from ref. 132).

The formation of MOOH via step **a** in Scheme 3.2 is the principle interest in the present work. The observation of MOOH formation from M-H and O_2 has occurred in a few cases: $[Co(H)(CN)_5]^{3-}$ and $[Rh(H)(CN)_4(H_2O)]^{2-}$ (133), $[Rh(NH_3)_5(H)]^{2+}$ (134), $[Rh(NH_3)_4(H_2O)(H)]^{2+}$ (135), $Ir(H)(Cl)_2(C_8H_{12})$ (136) and has been postulated in others (132). In addition, during the course of this study, Ir(OEP)(OOH) (137) was reported to be produced from Ir(OEP)(H) and O_2. To our knowledge, M-OOH species have yet to be crystallographically characterised.

The choice of Rh(OEP)(H) as the hydride was made on the grounds of potential mechanistic simplicity, reactivity and availability. It is a known compound in the literature (sect. 1.3.3). The porphyrin ligand strongly restricts the formation of vacant coordination sites cis to the axial positions by virtue of its planar tetradentate nature. Rh is a second row metal and substitution

kinetics for Rh(III) can be relatively slow. Toluene solutions of the hydride react with O_2 to form $[Rh(OEP)]_2$, at room temperature (64). In addition, a thermally unstable $Rh(OEP)(O_2)$ complex is formed from the reaction of $[Rh(OEP)]_2$ and O_2 at low temperature (42). The TPP analogue, $Rh(TPP)(O_2)$, in DMF catalyses the conversion of H_2/O_2 mixtures to H_2O (41,42). The hydride and dioxygen Rh(TPP) complexes are interconvertable by alternate use of H_2 and O_2 (41). The Rh(OEP)(H) complex itself is formed by direct reaction of H_2 with Rh(OEP)(Cl) in MeOH.

3.2. Results and Discussion

3.2.1. Reaction of Rh(OEP)(H) with O_2

The reaction of O_2 with Rh(OEP)(H) was examined in benzene, toluene and CH_2Cl_2.

3.2.1.1. In benzene and toluene

When nmr samples of Rh(OEP)(H) in dry C_6D_6 are exposed to O_2 at 20 °C the solution colour quickly darkens. The ^1H nmr spectrum of the hydride is replaced with that of $[Rh(OEP)]_2$ (Fig. 3.1), characterised by the relatively low shift of the porphyrin meso proton resonance due to the ring-current effects of the cofacial porphyrins of the diamagnetic Rh(II) dimer, and by the two well-separated sets of $-CH_2-$ resonances of the ethyl side-chains. The multiplet $-CH_2-$ resonances are consistent with the presence of a diamagnetic metallo-octaethylporphyrin complex, that is asymmetrically substituted with regard to the porphyrin plane, i.e., two different axial ligands are present, in this case another metallo-porphyrin (138-141). Within such complexes the methylene protons of the ethyl side-chains become anisochronous and appear as an ABX_3 multiplet (139,142). In this particular example the especially wide separation into 2 multiplets probably reflects the increased ring-current effects in the environment between the cofacial porphyrins (cf. Fig. 1.4). In symmetrically substituted species the $-CH_2-$ protons appear as a single quartet due to coupling with the adjacent $-CH_3$ group. Using stopcock grease as an internal "standard" (sect. 2.1.3), comparison of the ^1H nmr spectra from several experiments shows that $[Rh(OEP)]_2$ has formed in up to 100% yield during the reaction (Fig. 3.1). A small amount of the dimer was present (less than 2%) before addition of O_2 because of the equilibrium between Rh(OEP)(H), $[Rh(OEP)]_2$ and H_2 (reaction (1.7)). Coincident with the formation of $[Rh(OEP)]_2$, a small peak

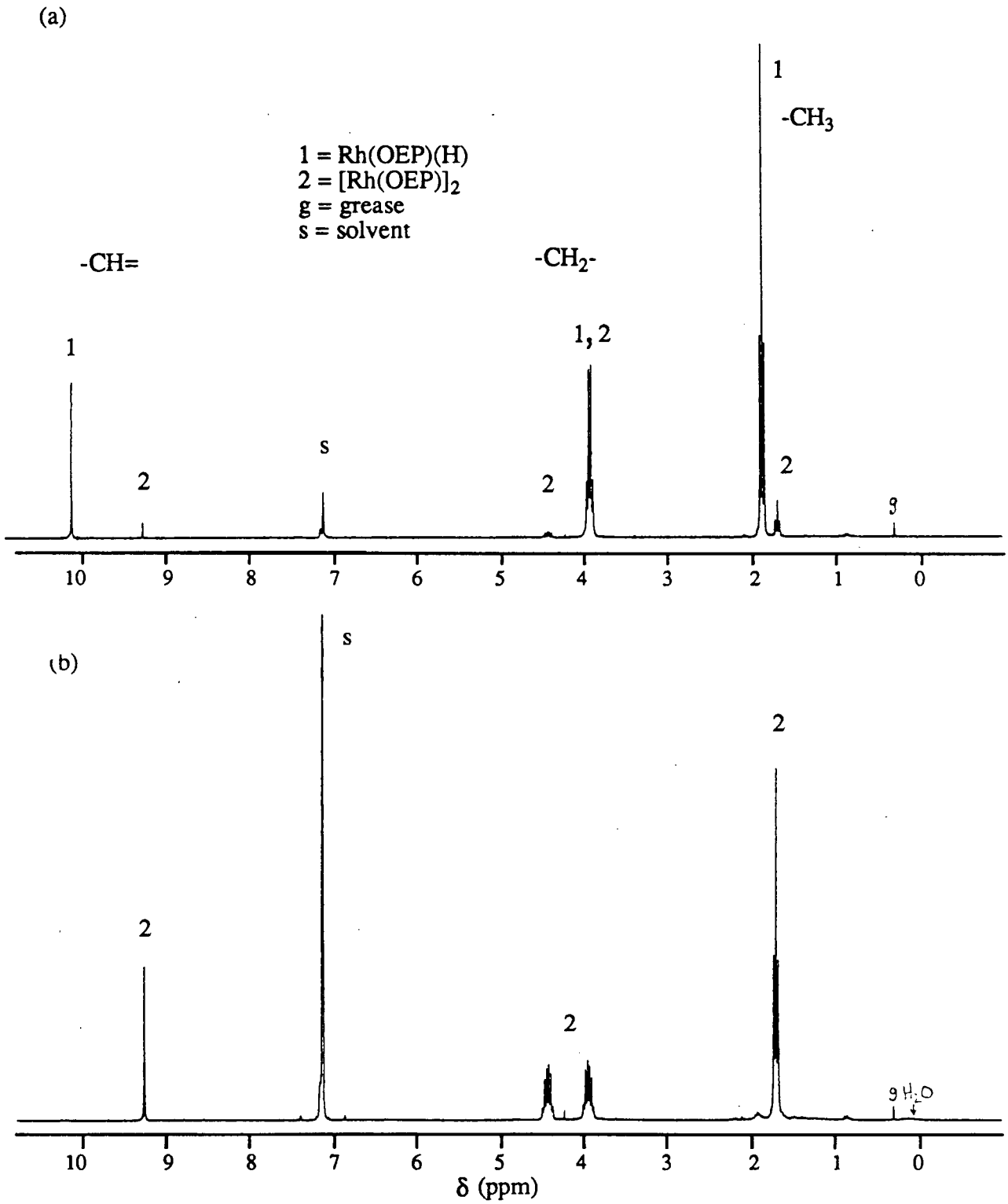

Figure 3.1. The 300 MHz ^1H nmr spectra of (a) Rh(OEP)(H) in C_6D_6 and (b) 30 min after addition of O_2 at 20°C. [Rh] ≈ 2×10^{-3} M, P_{total} = 1 atm.

in the 0–0.5 ppm region, due to H_2O (not always observed apparently because of exchange) increases in intensity and shifts downfield towards the position of free H_2O (~0.45 ppm) indicating the formation of H_2O during the reaction. The amount of $[Rh(OEP)]_2$ remains constant when a sample is left in air for a further 2 h period. The visible spectrum of the solution *in* the nmr tube (Fig. 3.2) showed Soret bands at 352 and 390 nm with weak β and α bands at ~520 and ~550 nm similar to those reported for $[Rh(OEP)]_2$ (64). These observations are in accordance with the reported oxidative cleavage of the Rh-H bond to form $[Rh(OEP)]_2$ with the presumed formation of H_2O (64).

Sometimes precipitation occurs during the reaction. Presumably the purple precipitate is $[Rh(OEP)]_2$ because its solid state IR shows only bands expected for the OEP ligand.

The reaction could also be monitored by visible spectroscopy, which was in fact the first method used in this work to examine the reaction. The spectrum of the reaction product in these experiments has the α band at 552 nm (Fig. 3.3), which is similar, but not identical, to the spectrum obtained for the nmr sample (Fig. 3.2) and to the spectrum of $[Rh(OEP)]_2$ (Table 3.1). Assuming, on the basis of the nmr data, that the principle product will be $[Rh(OEP)]_2$, then the presence of an extra complex in solution is suggested by the data in Table 3.1. It turns out that the reaction of Rh(OEP)(H) with O_2 is very sensitive to solvent purity. A number of experiments were pursued before the marked sensitivity was realized; the effects are briefly presented.

If the change of absorbance at the α band (542 nm) of the hydride is monitored during the reaction, the absorbance vs. time curve observed is very dependent on the benzene purity. Figure 3.4a illustrates the change in absorbance when the benzene used has been washed with conc. H_2SO_4 prior to drying by distillation from benzophenone ketyl. A very fine suspension was found after 20 min. In benzene freshly distilled only from benzophenone ketyl there is a rapid drop in intensity at 542 nm followed by a "transition segment" and then a slower increase to ca. 65% of initial intensity (Fig. 3.4b). The spectrum of the product (solid line, Fig. 3.5) is similar (at least in peak positions) to that of the starting Rh(OEP)(H). In addition there is no precipitation and the spectrum is stable to added H_2. If undistilled benzene is used, then a completely different absorbance vs. time curve with an induction period, followed by sigmoidal decrease is seen and

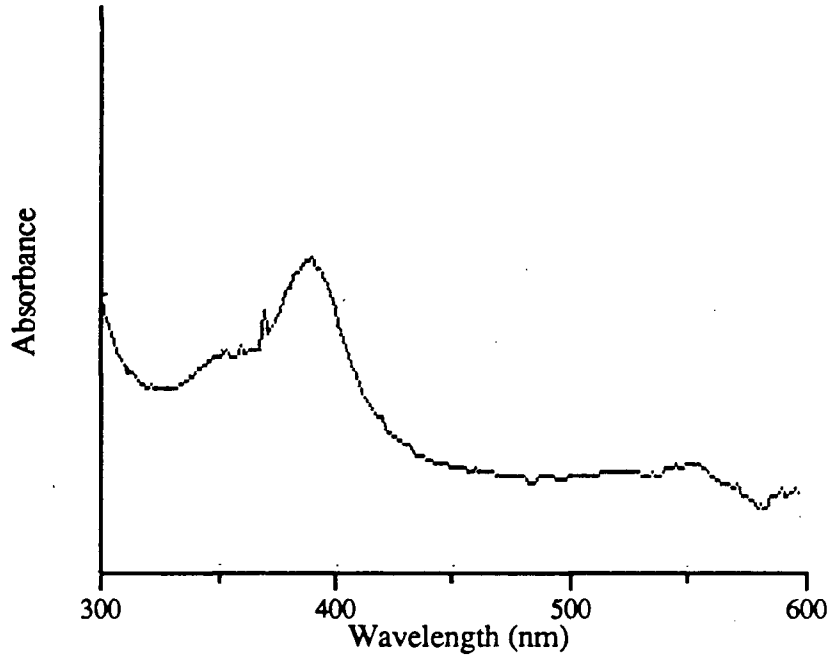

Figure 3.2. The visible spectrum of the nmr sample illustrated in Fig. 3.1b, for the reaction of Rh(OEP)(H) and O_2 in C_6D_6. [Rh] $\approx 2 \times 10^{-3}$ M, P_{total} = 1 atm.

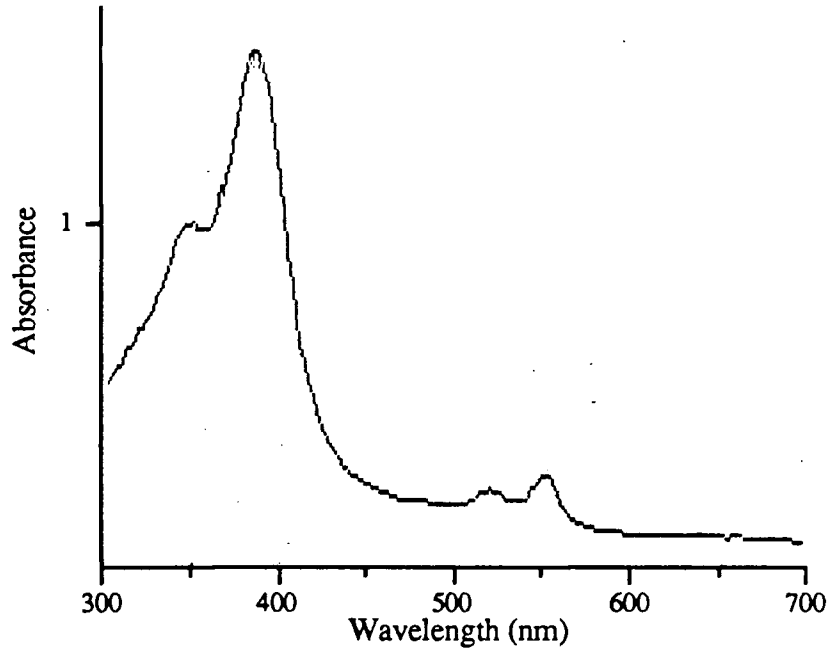

Figure 3.3. The visible spectrum of the products of the reaction of Rh(OEP)(H) and O_2 in C_6H_6 30 min after addition of O_2. [Rh] = 2.70×10^{-4} M, P_{total} = 1 atm, 25 °C.

Table 3.1. The visible spectral data for $[Rh(OEP)]_2$ and for the product of the reaction of Rh(OEP)(H) with O_2 in benzene purified by washing with conc. H_2SO_4 and then distilling from benzophenone ketyl.

complex	λmax(log ε)				
	Soret		β	α	
$[Rh(OEP)]_2$	352(4.01)	388(4.09)	521(3.77)	550(3.76)	ref. (64)[a]
product	351(4.52)	391(4.71)	520(3.73)	552(3.84)	this work

a. The log ε values given in ref. 64 for the Soret region in ref. 64 are incorrectly stated judging from the spectrum shown.

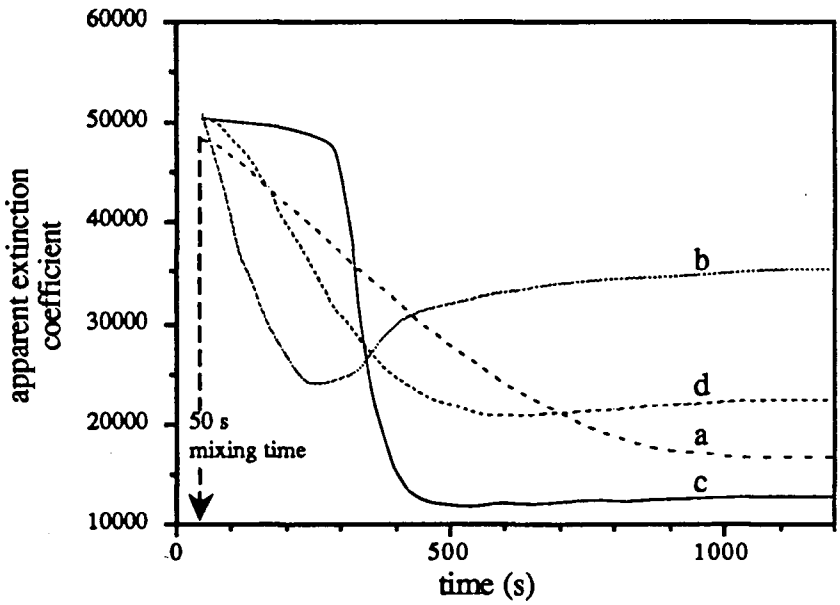

Figure 3.4. Change in apparent extinction coefficient at 542 nm during the reaction of Rh(OEP)(H) with O_2 in benzene from various sources: (a) washed with conc. H_2SO_4 then dried over ketyl, (b) only dried over ketyl, (c) ACS Spectroscopic grade and (d) is (b) stored under Ar. [Rh] ≈ 2.6×10^{-4} M, P_{total} = 1 atm, 25 °C.

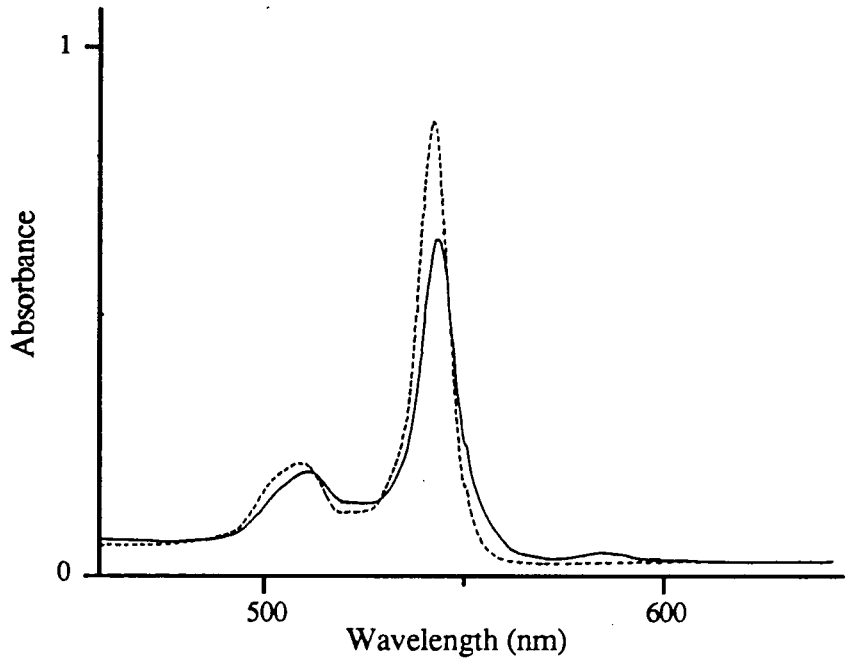

Figure 3.5. The visible spectra of (···) Rh(OEP)(H) in C_6H_6 (in vacuo) dried only over ketyl and (—) 30 min after addition of O_2. [Rh] = 1.42×10^{-4} M, P_{total} = 1 atm, 25 °C.

concomittant precipitation occurs (Fig. 3.4c). The soluble product shows a Soret at 392 nm and β and broad α bands at 524 and 546 nm. The precipitate exibits a band in the IR spectrum (Fig. 3.6) at 3605 cm^{-1} which is attributable to an -OH moiety: some literature data (Table 3.2) indicate that the 3605 cm^{-1} band observed is probably due to the presence of Rh-OH rather than Rh-OOH because all but one hydroperoxo species have ν_{OH} bands that fall below 3600 cm^{-1} (132).

If benzene that has been purified only by distillation from ketyl is stored under Ar for more than a day or two before use, then the change of the α band is a smooth sigmoidal decrease (Fig. 3.4d) and precipitation again occurs. The precipitate does not show an IR band at 3605 cm^{-1}. The soluble products have a weak α band at 544 nm, with a prominant shoulder at 554 nm, probably due to some $[Rh(OEP)]_2$.

In toluene solution, qualitatively similar effects were observed by visible spectroscopy. Use of toluene dried with benzophenone ketyl or molecular sieves gives soluble products which have spectra similar to the product spectrum obtained from the analogous experiments in benzene. Monitoring the changes at the α band reveals differences between the ketyl- and sieves-dried

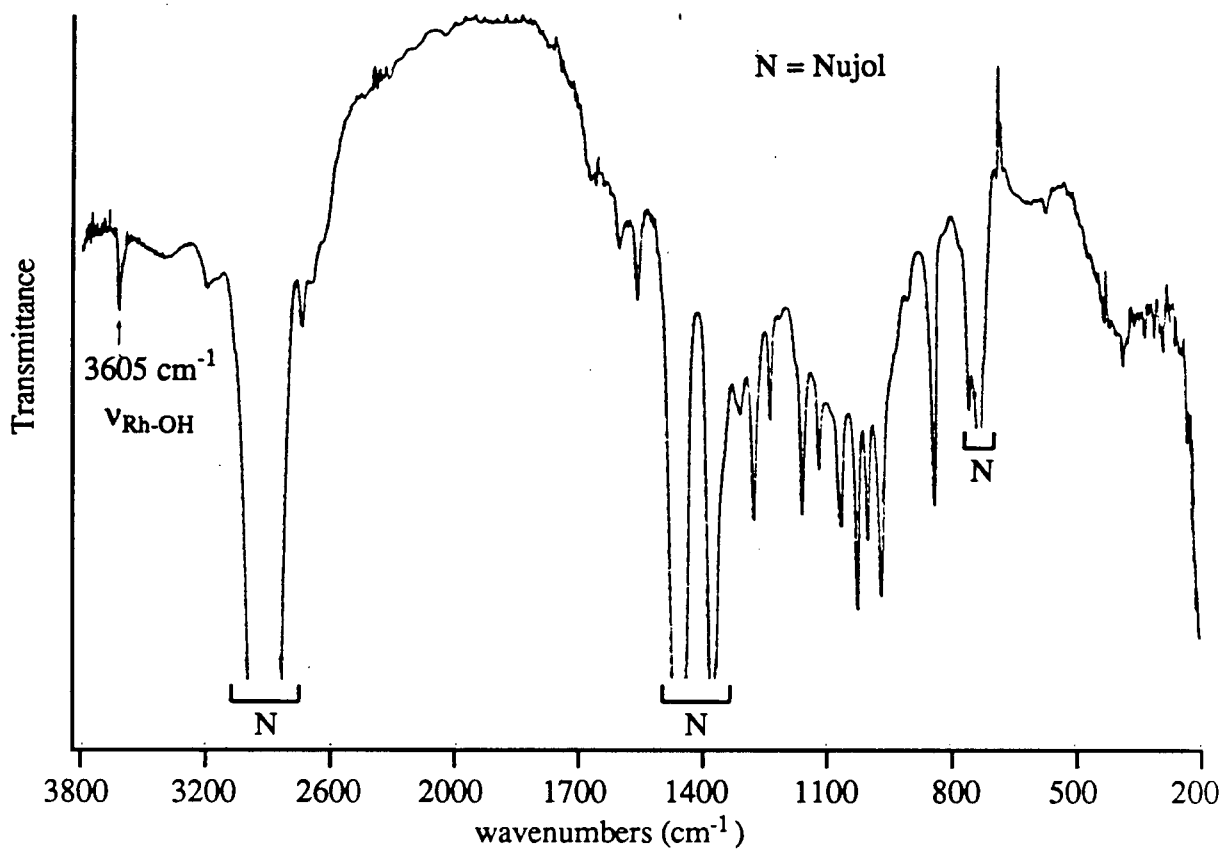

Figure 3.6. The IR spectrum of a purple precipitate (in Nujol) isolated from the reaction of Rh(OEP)(H) and O_2 in benzene (ACS Spectroscopic grade).

systems (Figure 3.7), the reaction in the ketyl-dried solvent showing a very fast initial reaction. If toluene is used without purification, then the reaction leads to precipitation and the soluble components have a spectrum similar to that for the comparable experiment in benzene.

In summary, the reaction is very sensitive to solvent impurities and possibly trace impurities in the Rh(OEP)(H) when run at the concentrations used for visible spectroscopy (i.e., ~2×10^{-4} M). In C_6D_6, at the higher concentrations used in the nmr experiments (i.e., 2×10^{-3} M), the Rh(II) dimer forms. Otherwise, the products are uncharacterised Rh(III) complexes and some $[Rh(OEP)]_2$. One product of the impurity "driven" reactions may be Rh(OEP)(OH) judged by the observation that the IR spectra of the precipitates did show a band above 3600 cm^{-1}.

Table 3.2. Some IR spectral data for M-OOH and M-OH species from the literature.

complex	ν_{OH} bands (cm^{-1}) for: OH	OOH	ref
$Fe^{III}(TMP)(OH)$	3650, 3610		1
$Fe^{IV}(TAPP)(OH)$	3660		2
$[Ru^{IV}(OEP)(OH)]_2$-μO	3606		3
$[Os^{IV}(OEP)(OH)]_2$-μO	3598		3
$[Os^{IV}(OEP)(OH)]$-μO-$[Os^{IV}(OEP)(OCH_3)]$	3602		3
$[Co(en)_3][Co(CN)_5(OOH)]\cdot 3H_2O$		3600 vs, 3440 br	4
$Rh(Cl)(acac)(PPh_3)_2(OOH)$		3470	5
$Rh(Cl)(acac)(PPh_3)_2(OH)$	3550		5
$Rh(Cl)(acac)(PPh_3)(OH)$	3502		5
$K_2[Rh(CN)_4(OOH)(H_2O)]$		3500 vs, 3380 br	4
Ir(OEP)(OOH)		3596	6
"Ir^{III}-OOH"		3495	7
"Ir^{III}-OH"	3680, 3605		7
"Pt-OOH"		3585–3517	8
"Pt-OH"	3628–3602		8
$Ge(TPP)(OH)_2$	3600		9
$Sn(TPP)(OH)_2$	3610		10

1. J.T. Groves, R.C. Haushalter, M. Nakamura, T.E. Meno and B.J. Evans. J. Chem. Soc. **103**, 2884 (1981).
2. Y. Harel and R.H. Felton. J. Chem. Soc. Chem. Commun. 206 (1984).
3. H. Sugimoto, T. Higashi, M. Mori, N. Nagano, Z. Yoshida and H. Ogoshi. Bull. Chem. Soc. Jpn. **55**, 822 (1982).
4. H.L. Roberts and W.R. Symes. J. Chem. Soc. (A), 1450 (1968).
5. H. Suzuki, S. Matsuura, Y. Moro-Oka and T. Ikawa. Chem. Lett. 1011 (1982).
6. J.P. Collman and K. Kim. J. Am. Chem. Soc. **108**, 7847 (1986).
7. M.T. Atlay, M. Preece, G. Strukul and B.R. James. Can. J. Chem. **61**, 1332 (1983).
8. G. Strukul, R. Ros and R.A. Michelin. Inorg. Chem. **21**, 495 (1982); R.A. Michelin, R. Ros and G. Strukul. Inorg. Chim. Acta, **37**, L491 (1979).
9. M. Hartmann, G. Meyer and D. Wöhrle. Makromol. Chem. **176**, 831 (1975).
10. L.R. Milgrom and R.N. Sheppard. J. Chem. Soc. Chem. Commun. 350 (1985).

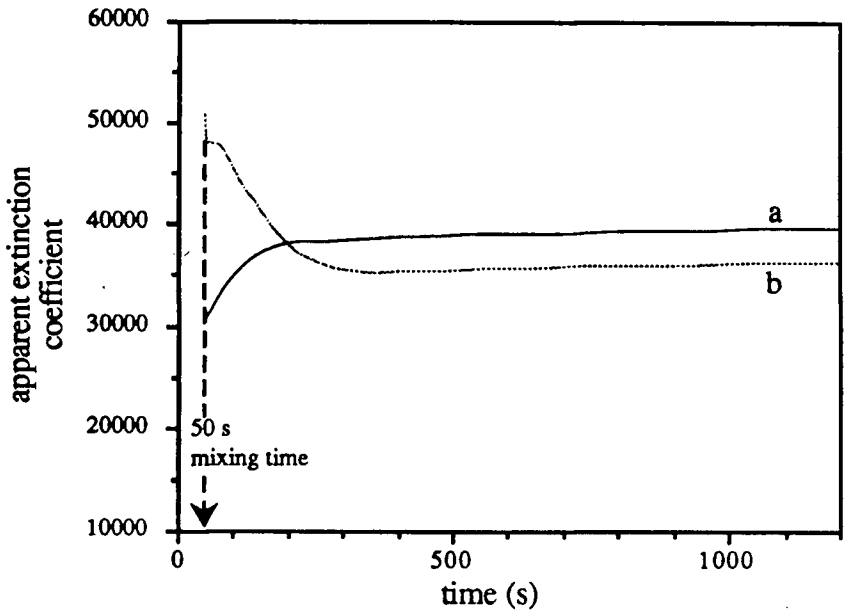

Figure 3.7. Change in apparent extinction coefficient at 542 nm during the reaction of Rh(OEP)(H) with O_2 in toluene from various sources: (a) dried over ketyl, (b) dried over molecular sieves. [Rh] ≈ 2.0×10^{-4} M, P_{total} = 1 atm, 25 °C.

3.2.1.2. In CH_2Cl_2

The reaction of Rh(OEP)(H) with O_2 in dichloromethane is rapid. Some precipitation usually occurs at the concentrations used for nmr experiments and the precipitate shows IR spectral bands due only to the OEP ligand. The change in ^1H nmr spectrum that occurs upon reaction of Rh(OEP)(H) with O_2 at room temperature is shown in Figures 3.8a and 3.8b. There is a marked reduction in the intensity of the porphyrin resonances in keeping with the observation of precipitation. However, in some experiments, a similar reduction in intensity is seen when no precipitation occurs. The integration of the meso proton resonances of the porphyrin is very low compared to that of the ethyl side chains and there are several weak, broad, resonances in the 4-2 ppm region. Examination of a spectrum covering a range greater than ± 60 ppm at very good S/N revealed no other resonances beyond those already noted in Figure 3.8b. Also the $[Rh(OEP)]_2$ present initially does not appear to have changed in concentration during the reaction unlike the corresponding reaction in benzene.

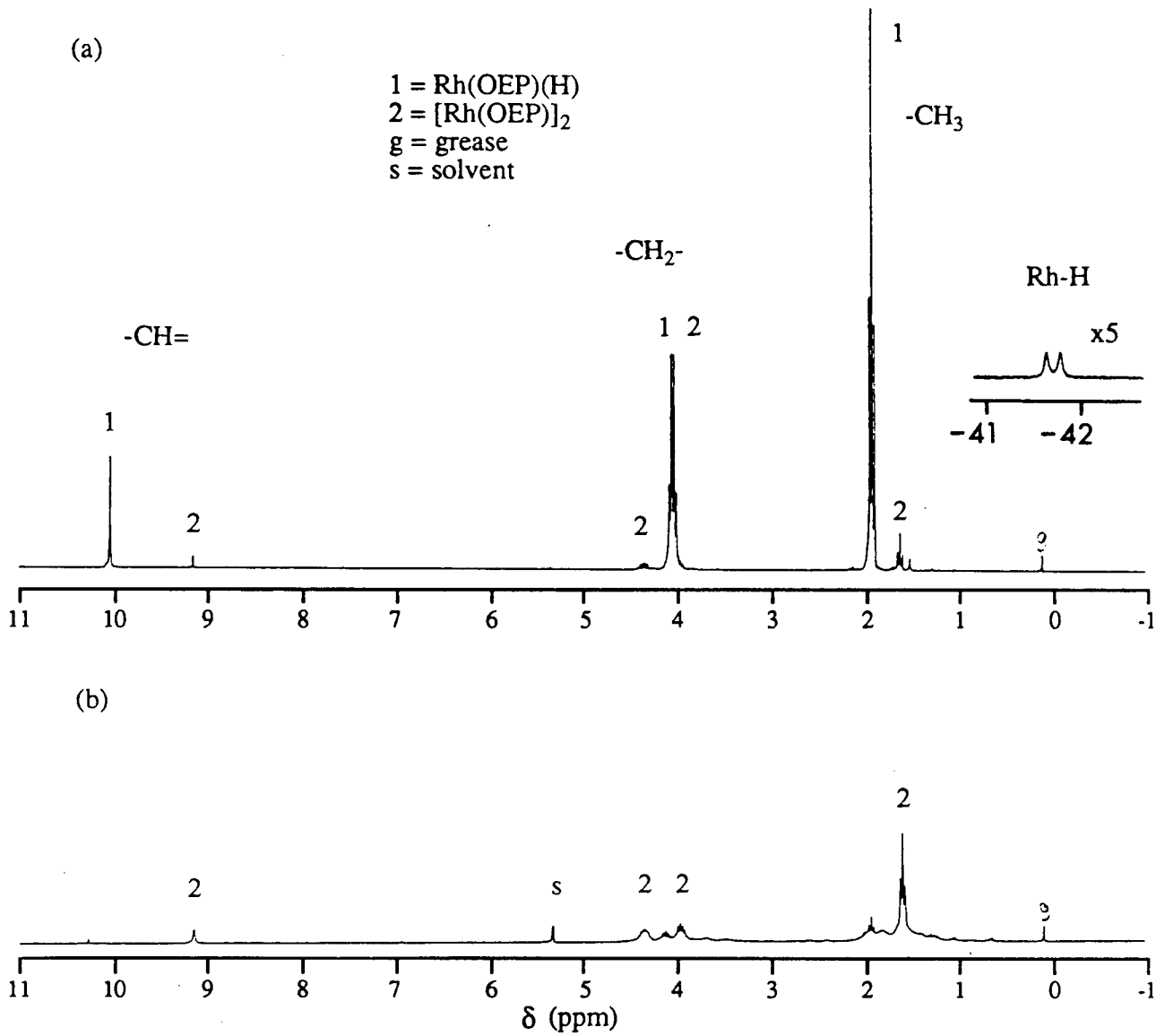

Figure 3.8. The 300 MHz ^1H nmr spectra of (a) Rh(OEP)(H) in CD_2Cl_2 and (b) 15 min after addition of O_2 at 20°C. [Rh] ≈ 2×10^{-3} M, P_{total} = 1 atm.

The reaction of Rh(OEP)(H) with O_2 in freshly dried CH_2Cl_2 can be followed by visible spectroscopy; no precipitation occurs initially and isosbestics are not observed. The product has a Soret band at 402 and the β and α bands at 520 and 553 nm (Fig. 3.9) which are not those expected for $[Rh(OEP)]_2$, being more consistent with the hypso-type spectrum of a Rh(III) species (69). The solvent could be removed and the residue redissolved in fresh solvent to give the same spectrum, thus the reaction with O_2 is irreversible. The product when redissolved in

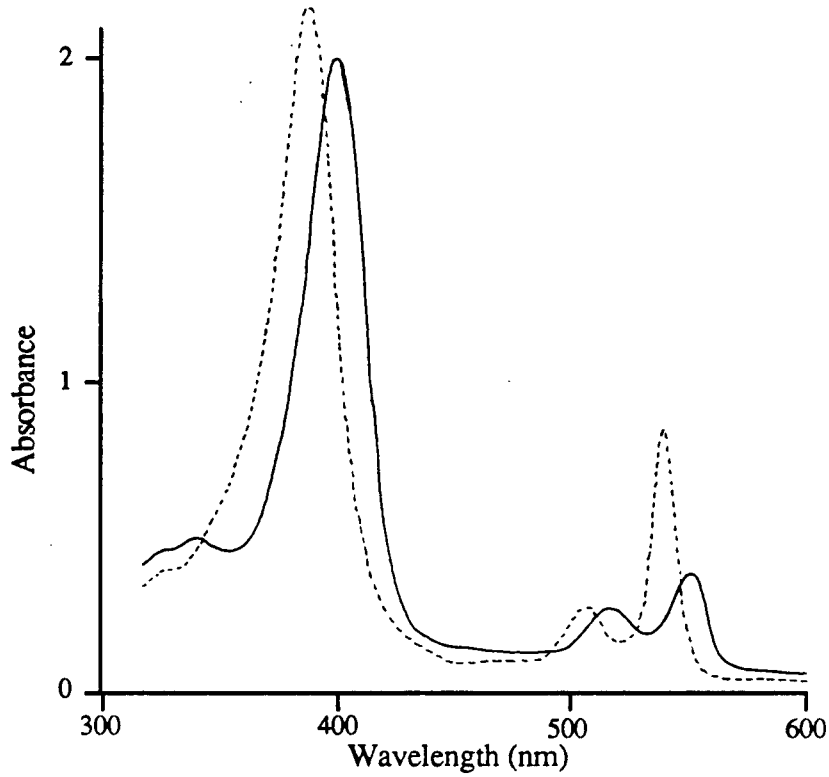

Figure 3.9. The visible spectra of (····) Rh(OEP)(H) in CH_2Cl_2 and (—) 30 min after addition of O_2. [Rh] = 1.73×10^{-4} M, P_{total} = 1 atm, 25 °C.

fresh solvent showed little reaction with 1 atm of H_2 at room temperature, with only a small absorbance increase in the 540 nm region and decrease in the 555 nm region occurring. During the course of the O_2 reaction, a sigmoidal decrease in the intensity of the Rh(OEP)(H) α band is seen (Fig.3.10). Precipitation is always observed at the end of the reaction and slowly continues over several hours. The "$t_{1/2}$" of the curve progressively increases with decrease in $[Rh]_o$ (traces **a-d**) but the curves cross in several places. Using undistilled solvent gave a similar curve (trace b vs. trace **e**) within the experimental scatter.

The course of the reaction in dichloromethane and in aromatic solvents is not similar. In particular, $[Rh(OEP)]_2$ is not a major product in CH_2Cl_2. There is an inconsistency between the visible spectroscopic data in dichloromethane, which suggest a Rh(III) product, and the nmr data in dichloromethane where the resonances after addition of O_2 are not consistent with a Rh(III) porphyrin species. Possibly oxidation of the porphyrin occurs during the nmr experiments in CD_2Cl_2 which raises the possibility of O_2 activation at the metal, perhaps involving a

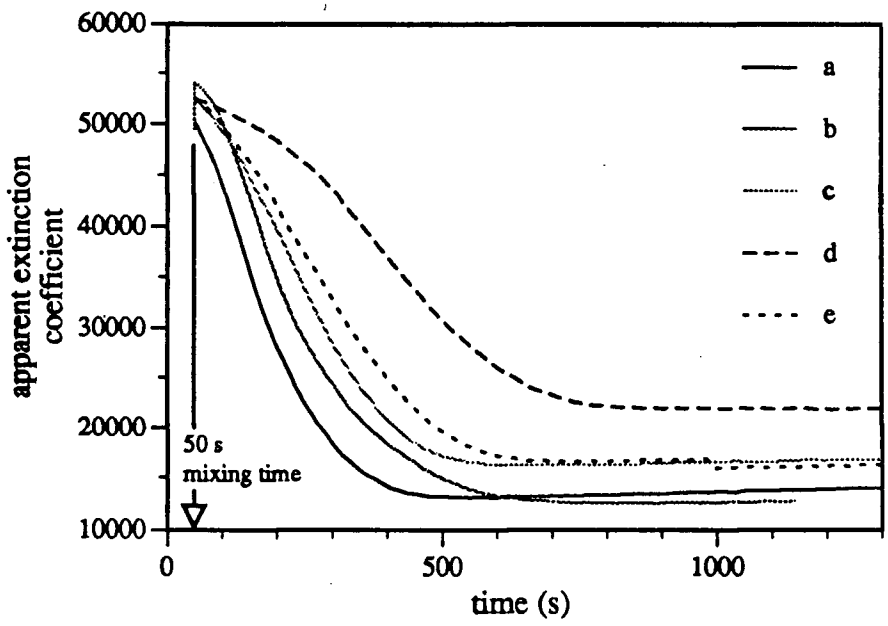

Figure 3.10. Change in apparent extinction coefficient at 542 nm during the reaction of Rh(OEP)(H) with O_2 in freshly dried CH_2Cl_2 for various $[Rh]_o$: (a) 3.40×10^{-4} M, (b) 2.68×10^{-4} M, (c) 1.62×10^{-4} M, (d) 5.6×10^{-5} M and (e) 2.62×10^{-4} M (reagent grade solvent). P_{total} = 1 atm, 25 °C.

Rh(OEP)(OOH) intermediate. In fact, low temperature nmr data provide evidence for an unstable metal-hydroperoxide, and these data will be presented in the following paragraphs.

A sample of Rh(OEP)(H) with CD_2Cl_2 and O_2 was prepared by vacuum transferring the solvent onto the hydride and sealing the tube under ca. 0.6 atm of O_2, while the sample remained frozen at liquid N_2 temperature. The sample was allowed to thaw between -50°C and -40°C, and then changes followed for ca. 3 h at -40°C. It is probable that the solutions were not homogeneous at this temperature; however, sufficient material dissolved to react with the O_2 diffusing into the cold solution. Resonances due to Rh(OEP)(H) decrease and the signals typical of a new diamagnetic Rh(III) species, "Rh(OEP)(X)", increase; having a meso resonance at 10.24 ppm and a single proton at -1.81 ppm (Fig. 3.11). The shifts of the meso protons of Rh(OEP)(H) and "Rh(OEP)(X)" species are not temperature-dependent over the range -50 to -20 °C. If the sample is allowed to warm above -20 °C precipitation occurs and the resonances of Rh(OEP)(H) and "Rh(OEP)(X)" decrease. The 80 MHz ^1H nmr spectrum, taken at room temperature, of the

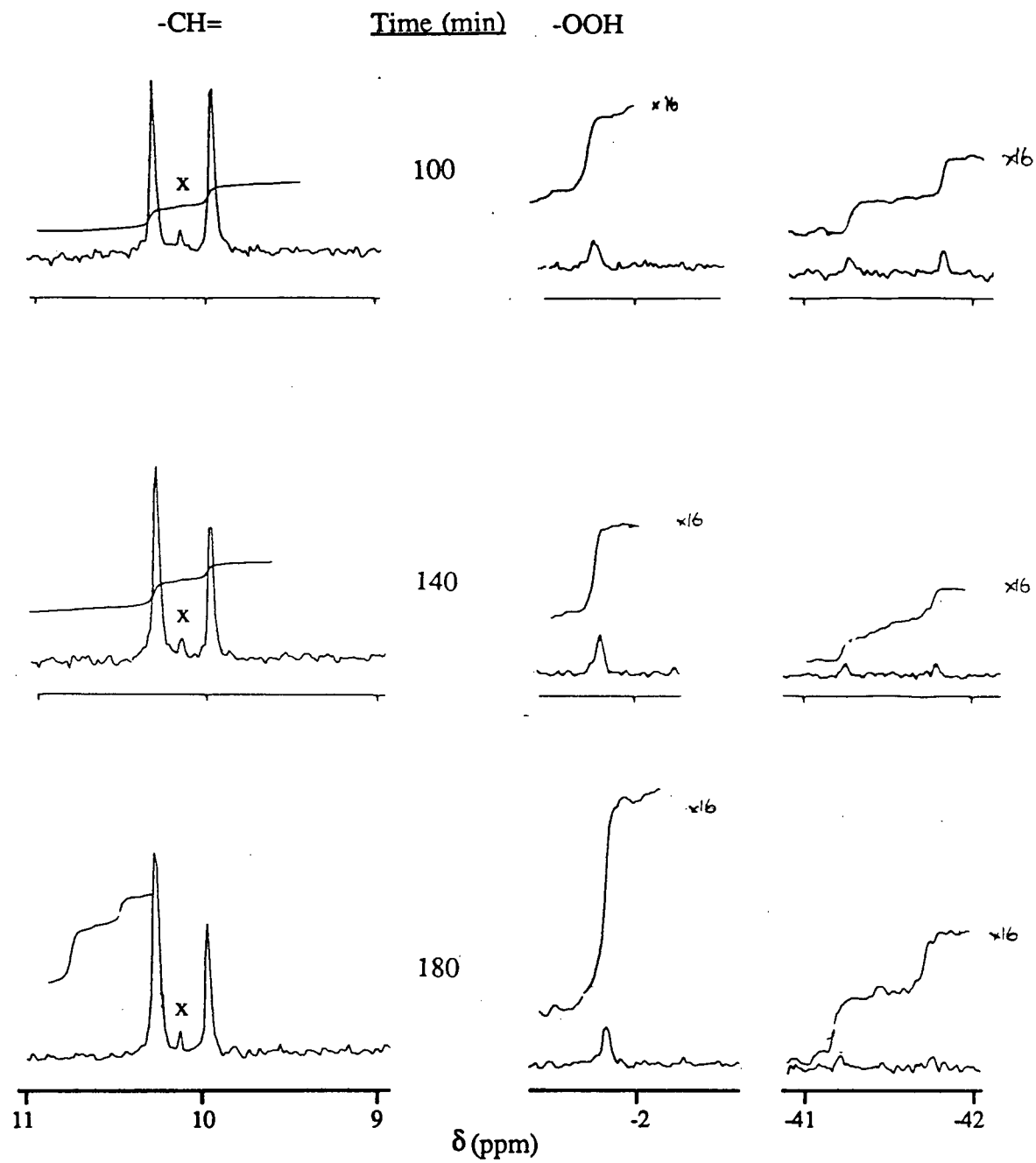

Figure 3.11. Changes in the 80 MHz ^1H nmr spectra during the reaction of Rh(OEP)(H) with O_2 at -40 °C in CD_2Cl_2; x = unknown impurity.

remaining soluble species showed weak porphyrin resonances due an impurity, which was present in the initial material (labelled x on Fig. 3.11), and another equally weak meso resonance at 10.30 ppm. The IR spectrum of the residue (solvent removed at room temperature) showed ν_{OH} bands at 3603 cm^{-1} (sharp) and 3375 cm^{-1} (broad) (Fig. 3.12), attributed to Rh(OEP)(OH).

Repeating the experiments at higher field (400 MHz) resulted in the detection of more upfield resonances (Fig. 3.13). Resonances at -1.92 and -6.15 ppm seem related to the 10.21 ppm meso signal because their relative intensities vary together consistently for different samples. The spectrum of Rh(OEP)(H) in the absence of O_2 does not show the -6.15 peak even when H_2O is present, but at -40 °C Rh(OEP)(Cl)(H_2O) shows a resonance due to Rh-OH_2 at -5.69 ppm in CD_2Cl_2 (Table 2.2). Therefore, the "Rh(OEP)(X)" complex is believed to be Rh(OEP)(OOH)(H_2O) with the resonance at -1.92 ppm tentatively assigned to be -OOH on the basis of its position and the relative intensity.

The ^1H chemical shifts of MOOH species are not well known and only one example of ^1H nmr data for a Rh-OOH species is in the literature, which is to our knowledge the only ^1H nmr data in the literature for OOH coordinated to a metal. This is a non-porphyrin complex and the shift of the hydroperoxide proton is reported in Table 3.3 along with some M(por)$(OH)_n$ data for comparison. A rough correction to the δ 6.43 value, for the presence of the porphyrin ring current, can be made using Figure 1.4 and models of Rh(OEP)(OOH) having Rh-O-O-H dihedral angles of 0° and 180° (143), the method yielding a $\Delta\delta$ of -4 to -8 ppm depending on conformation. On this basis, the "expected" range for the -OOH proton within Rh(OEP)(OOH) species is between 2.43 and -1.57 ppm. The observed resonance at -1.92 ppm is close to this range and, by comparison with the shift of the H_2O ligand mentioned above and the -OH ligand shifts listed in Table 3.3, it seems reasonable to assign the -1.92 ppm signal to an -OOH resonance. The porphyrin resonances of the proposed Rh(OEP)(OOH)(H_2O) complex are broadened, but the -CH_2- resonances are a broadened quartet suggesting that the axial ligands are not very different in bulk, which is also consistent with the OOH assignment. The source of the H_2O is uncertain but there is sufficient H_2O initially present in the CD_2Cl_2. The H_2O ligand is probably exchanging at -40 °C because at the lower field the H_2O resonance was to broad to observe.

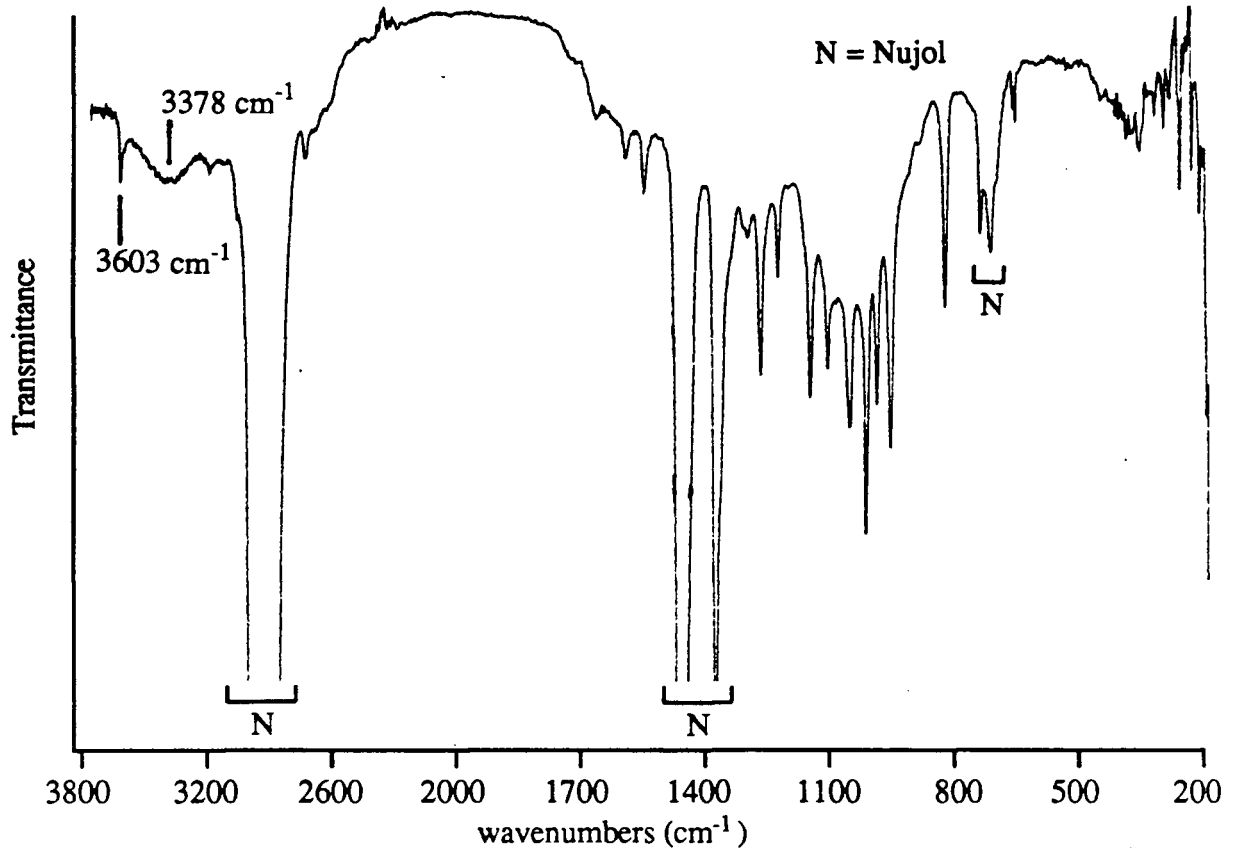

Figure 3.12. The IR spectrum of the residue (in Nujol) from the reaction of Rh(OEP)(H) and O_2 in CD_2Cl_2.

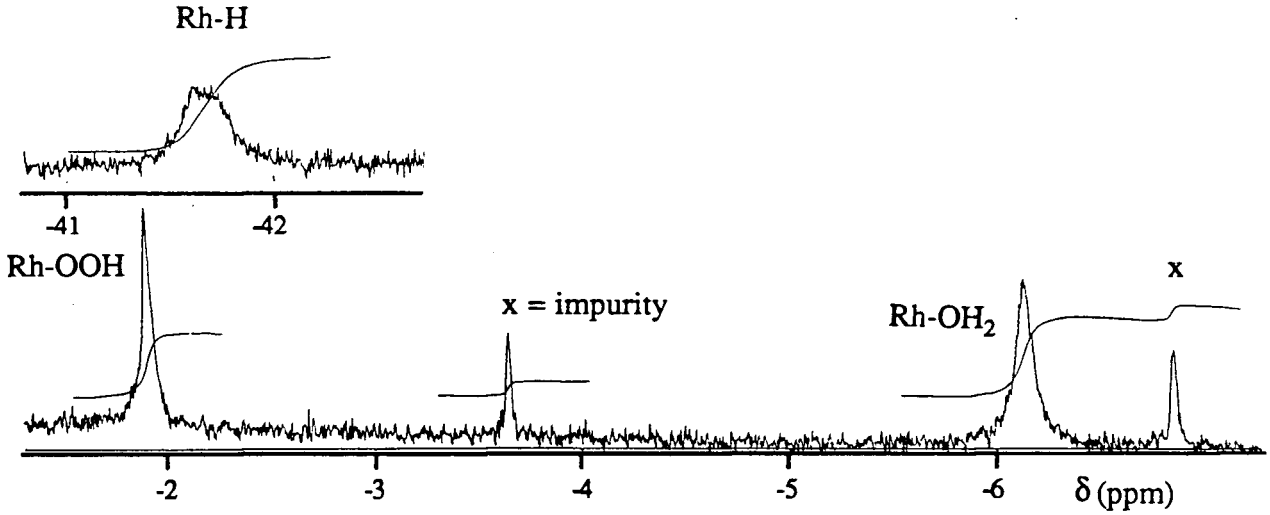

Figure 3.13. Expansion of an upfield region of a 400 MHz ^1H nmr spectrum during the reaction of Rh(OEP)(H) with O_2 in CD_2Cl_2 at -40 °C.

Table 3.3. Some ^1H nmr chemical shifts for hydroxyl and hydroperoxo protons of M-OH and M-OOH complexes from the literature.

complex	solvent	δ(ppm)	ref
$Rh(Cl)(acac)(PPh_3)_2(OOH)$	$CDCl_3$	6.43	1
$Ge(TPP)(OH)_2$	$CDCl_3$	-7.35	2
$Ge(porphine)(OH)_2$	$CDCl_3$	-7.81	2
$Sn(TPP)(OH)_2$	$CDCl_3$	-7.46[a]	3
$[Ru^{IV}(OEP)(OH)]_2$-μO	$CDCl_3$	-4.20	4
$[Os^{IV}(OEP)(OH)]_2$-μO	$CDCl_3$	-3.4 br	4
$[Os^{IV}(OEP)(OH)]$-μO-$[Os^{IV}(OEP)(OCH_3)]$	$CDCl_3$	-3.5 br	4

a. 37 Hz ^1H–$^{117,119}Sn$ coupling constant.

1. H. Suzuki, S. Matsuura, Y. Moro-Oka and T. Ikawa. Chem. Lett. 1011 (1982).
2. J.E. Maskasky and K.E. Kenney. J. Am. Chem. Soc. **95**, 1443 (1973).
3. L.R. Milgrom and R.N. Sheppard. J. Chem. Soc. Chem. Commun. 350 (1985).
4. H. Sugimoto, T. Higashi, M. Mori, N. Nagano, Z. Yoshida and H. Ogoshi. Bull. Chem. Soc. Jpn. **55**, 822 (1982).

A problem with the described warm-up type of experiment is inconsistent thawing and mixing. However, if the Rh(OEP)(H) solution was made up at room temperature, and cooled to -40°C before diffusing O_2 into the solution, then the reaction took a different course, although a homogenous solution could be achieved as was intended. During the cooling, the signal of the meso proton of Rh(OEP)(H) is revealed to be temperature-dependent (Fig. 3.14a), unlike the behaviour in the warm-up experiment. The temperature dependence of the ^1H nmr spectrum of Rh(por)(H) has been noted previously and suggested to be due to exchange with $[Rh(por)]_2$ (46). When O_2 is injected at below -40°C and the subsequent reaction monitored at -40 °C, the meso shift moves to lower fields and quickly decreases in intensity with no appearance of any product, including the hydroperoxide (Fig. 3.14b). The amount of $[Rh(OEP)]_2$ relative to the "impurity" remains constant throughout. Precipitation probably occurs and examination of the sample at end of the reaction confirmed the presence of a reddish precipitate. No sharp ν_{OH} band is seen in the IR spectrum of the residue. The effect of the method (warm-up vs. cool-down) on the outcome may reflect the establishment of the equilibrium between Rh(OEP)(H) and $[Rh(OEP)]_2$ and its

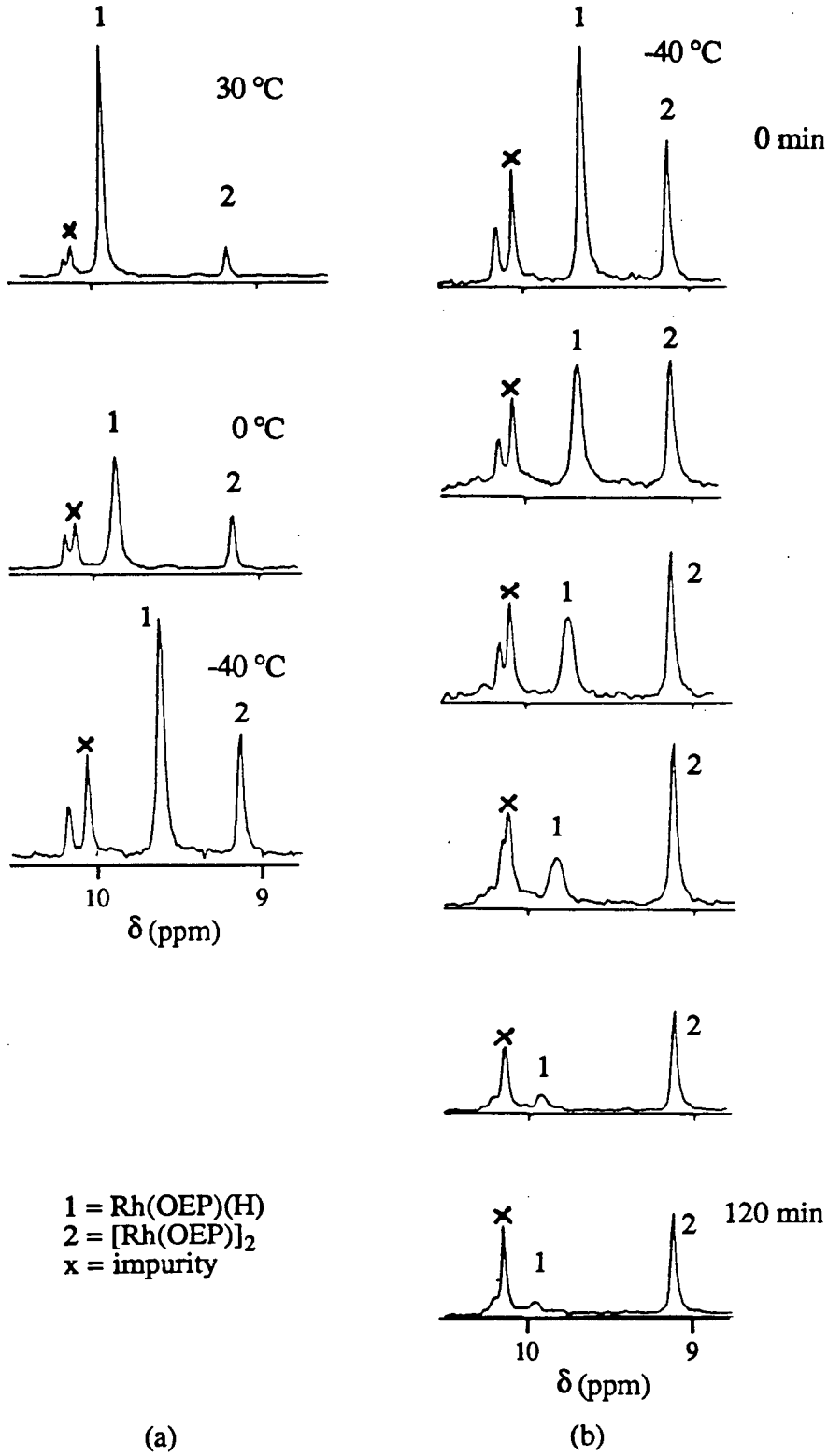

Figure 3.14. Changes in the methine region of the 80 MHz ^1H nmr spectra during (a) cooling a solution of Rh(OEP)(H) in CD_2Cl_2 to -40 °C and (b) addition of O_2 at -40 °C.

effect on the mechanism. At low temperature, the hydride/dimer equilibrium is not established and little dimer is present.

In dichloromethane, the possibility exists that Rh(OEP)(CH_2Cl) may form by reaction with the solvent. Such a reaction will be described subsequently in this chapter and in chapter 4 of this thesis. To check this possibility, the nmr experiments were rerun using CH_2Cl_2 as solvent instead of CD_2Cl_2 and presaturation of the solvent resonance is applied to improve S/N. If a Rh-CH_2Cl complex forms, then a proton resonance in the -2 to -3 ppm region (sect. 4.2.3 and ref. 32) should be found in the fully protio system while none should be found in the deuterated system. In fact, no such signal is seen, suggesting there is no reaction with the solvent either before or after addition of O_2 at the time scales used in the reactions. The hydride is stable for months in CD_2Cl_2 solution if kept in the dark and in the absence of O_2. If a CD_2Cl_2 solution of the hydride is exposed to fluorescent lighting then the slow formation of [Rh(OEP)]$_2$ over several days is observed by ^1H nmr. If left for periods of months, the amount of dimer decreases and resonances of Rh(OEP)(Cl) appear at 10.42 ppm; even after this time some Rh(OEP)(H) is still present, but there is no evidence of a Rh-CH_2Cl complex.

In summary, there is nmr evidence for formation of a thermally unstable Rh(OEP)(OOH)(H_2O) complex from the reaction of Rh(OEP)(H) with O_2 at low temperature in CD_2Cl_2, if the reagents are mixed at low temperature. Any other approach attempted led to products other than the hydroperoxide complex.

3.2.2. Reaction of Rh(OEP)(H) with O_2 in presence of PPh_3

The motivation for this study was to observe the effect of having a potentially reactive or coordinating substrate on the course of the reaction of Rh(OEP)(H) (or Rh(OEP)(H)(L)) with O_2. Triphenylphosphine is useful in both contexts and a marked change in reactivity from the non-phosphine system is found. This is due in part to the interaction between Rh(OEP)(H) and PPh_3 which is presented in the following section before describing the reactions with O_2 (sect. 3.2.2.2 and 3.2.2.3) because the identities of several complexes need establishing first.

3.2.2.1. Reaction of Rh(OEP)(H) with PPh_3

The experiments described in this section cover two quite separate time periods of study and, to a degree, separate approaches. Early work was coincident with the finding of the proposed Rh(OEP)(OOH)(H_2O) complex described in sect. 3.2.1.2. Nmr experiments were done on sealed tube samples containing a 2-3 fold excess of PPh_3 over Rh(OEP)(H). The $^{31}P\{^1H\}$ nmr experiments were carried out on a low-field instrument (32.3 MHz) and the resonances of Rh(OEP)(H)(PPh_3) (see below) were barely detectable at low temperature (Fig. 3.15), and thus the identity of the species was not recognized at that time. The work was suspended until the experiments were being written up for this chapter of the thesis, at which time some of the series of nmr experiments were repeated at higher field (300 MHz for ^1H and 121.42 MHz for $^{31}P\{^1H\}$) which enabled the identification of most species which had previously been unidentified.

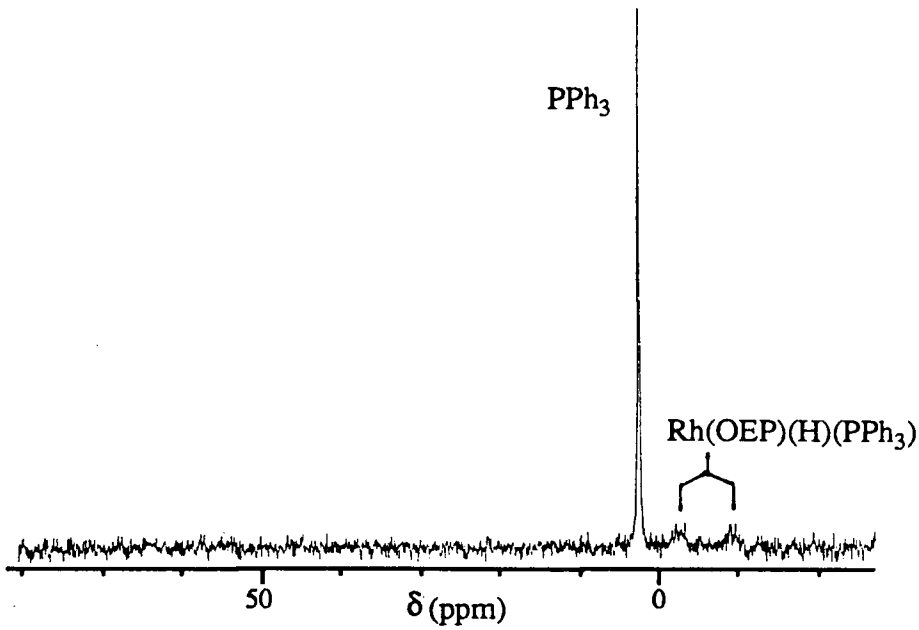

Figure 3.15. The 32.3 MHz $^{31}P\{^1H\}$ nmr spectrum of Rh(OEP)(H) with excess PPh_3 in CD_2Cl_2 at -60 °C.

3.2.2.1.1. In CH_2Cl_2 solvent

Figures 3.16 and 3.17 show the ^1H and $^{31}P\{^1H\}$ nmr data at -60 °C for a CD_2Cl_2 solution of Rh(OEP)(H) (~$7x10^{-3}$ M) containing slightly less than an equivalent amount of PPh_3

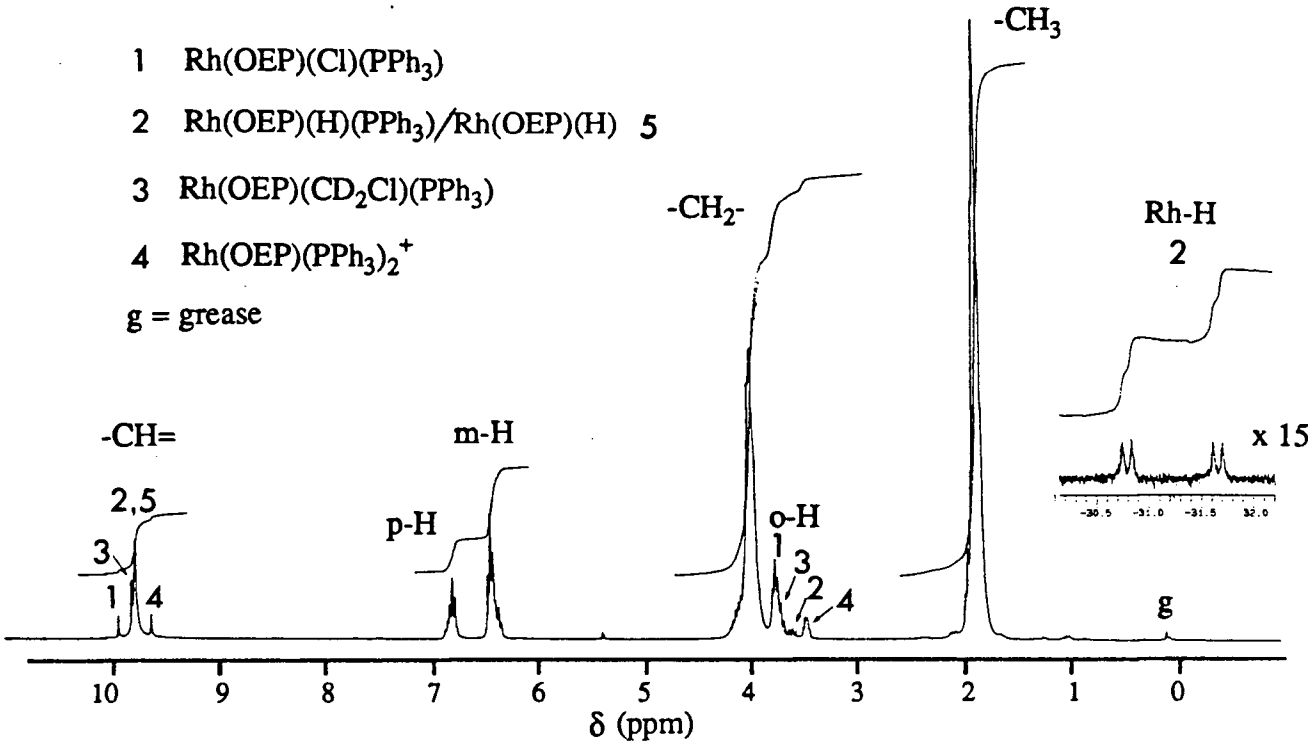

Figure 3.16. The 300 MHz ^1H nmr spectra of Rh(OEP)(H) with PPh_3 in CD_2Cl_2 at -60 °C. [Rh] ≈ 7×10^{-3} M, [PPh_3] ≈ 5.3×10^{-3} M.

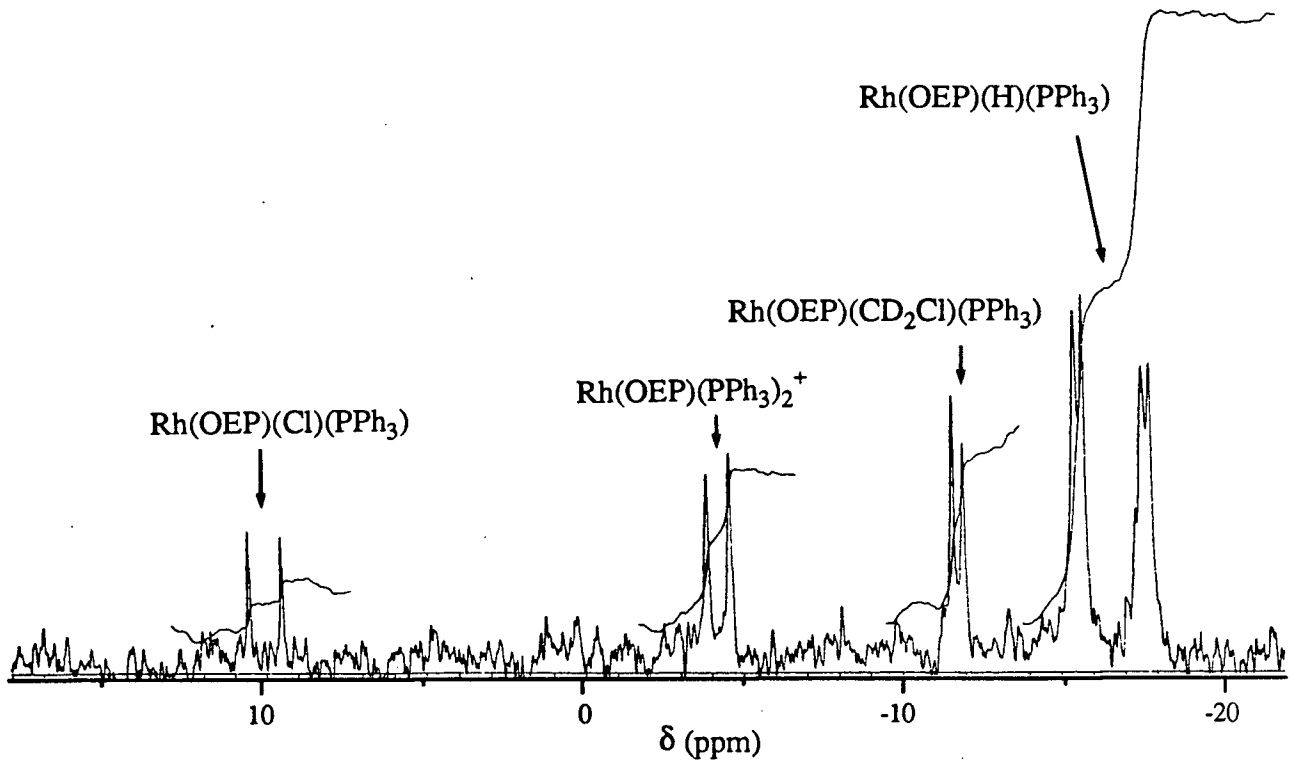

Figure 3.17. The 121.42 MHz $^{31}P\{^1H\}$ nmr spectra of Rh(OEP)(H) with PPh_3 in CD_2Cl_2 at -60 °C. [Rh] ≈ 7×10^{-3} M, [PPh_3] ≈ 5.3×10^{-3} M.

(~5.3×10^{-3} M). In the ^1H spectrum which is typical of those of solutions of diamagnetic $Rh^{III}(OEP)$ species, a doublet of doublets ($^1J_{Rh\text{-}H} \approx 28$ Hz, $^2J_{P\text{-}H} \approx 260$ Hz) at -31.23 ppm can be matched with a corresponding multiplet at -16.66 ppm ($^1J_{Rh\text{-}P} \approx 31$ Hz, $^2J_{P\text{-}H} \approx 260$ Hz) in the $^{31}P\{^1H\}$ nmr spectrum. The large $^2J_{P\text{-}H}$ coupling unequivocably identifies the complex as $Rh(OEP)(H)(PPh_3)$. The $^2J_{P\text{-}H}$ coupling is observed in the $^{31}P\{^1H\}$ nmr data because the upfield shift of the ^1H hydride resonance (<-30 ppm) takes it out of the range of the decoupled region used which is 7 ± 10 ppm in the ^1H nmr spectrum. As the sample is cooled the shifting positions of the PPh_3 and principle meso resonances in the ^1H nmr spectra (**4**, Fig. 3.18) and the PPh_3 resonances in the $^{31}P\{^1H\}$ nmr (Fig. 3.19) probably reflect the effect of temperature dependence of the equilibria involving PPh_3 magnified by the fact that Rh(OEP) species are in excess over the PPh_3 and thus little free PPh_3 remains at -60 °C. The temperature dependent changes are reversible. However, the ^1H resonances of the porphyrin are still broadened at -60 °C, even though the $^2J_{P\text{-}H}$ coupling is observed and the PPh_3 resonances appear to be in their respective slow exchange regimes. Because both Rh(OEP)(H) and $Rh(OEP)(H)(PPh_3)$ hydride resonances can be detected but only one average meso resonance for these two species (Fig. 3.18) it is assumed that the PPh_3 is exchanging, but at a rate that is less than $\approx 600\ s^{-1}$ (i.e. $\pi \cdot J_{P\text{-}H}/\sqrt{2}$) (144), because $^2J_{P\text{-}H}$ is resolved. The meso resonance attributable to the averaging of the meso resonances of the equilibrating hydrides comprises ~80% of the total porphyrin species and the visible spectrum of the nmr sample at room temperature resembles a superposition of the spectrum of Rh(OEP)(H) on a $Rh(OEP)(X)(PPh_3)$ spectrum such as $Rh(OEP)(Cl)(PPh_3)$ (Fig. 3.20; see Table 5.2 on p. 157).

Three minor species (**1**,**2** and **3**, Fig. 3.18) are also observed in the nmr spectra, comprising about 20% of the total Rh(OEP) species based on the integration of the meso ^1H nmr resonances at 6.7 °C (Fig. 3.18), and these species show little evidence of chemical exchange. The same minor species, in about the same amounts relative to total porphyrin, can be observed by ^1H nmr in samples with a greater excess of Rh(OEP)(H) initially. Two sets of ^1H and $^{31}P\{^1H\}$ resonances (Table 3.4) in these spectra can be correlated with $Rh(OEP)(Cl)(PPh_3)$ and $[Rh(OEP)(PPh_3)_2]^+$, which are described in Chapter 5. The counter ion to the bis-phosphine cation in these in situ studies is not definite but is probably Cl^- (Chapter 5 and sect. 1.3.2.).

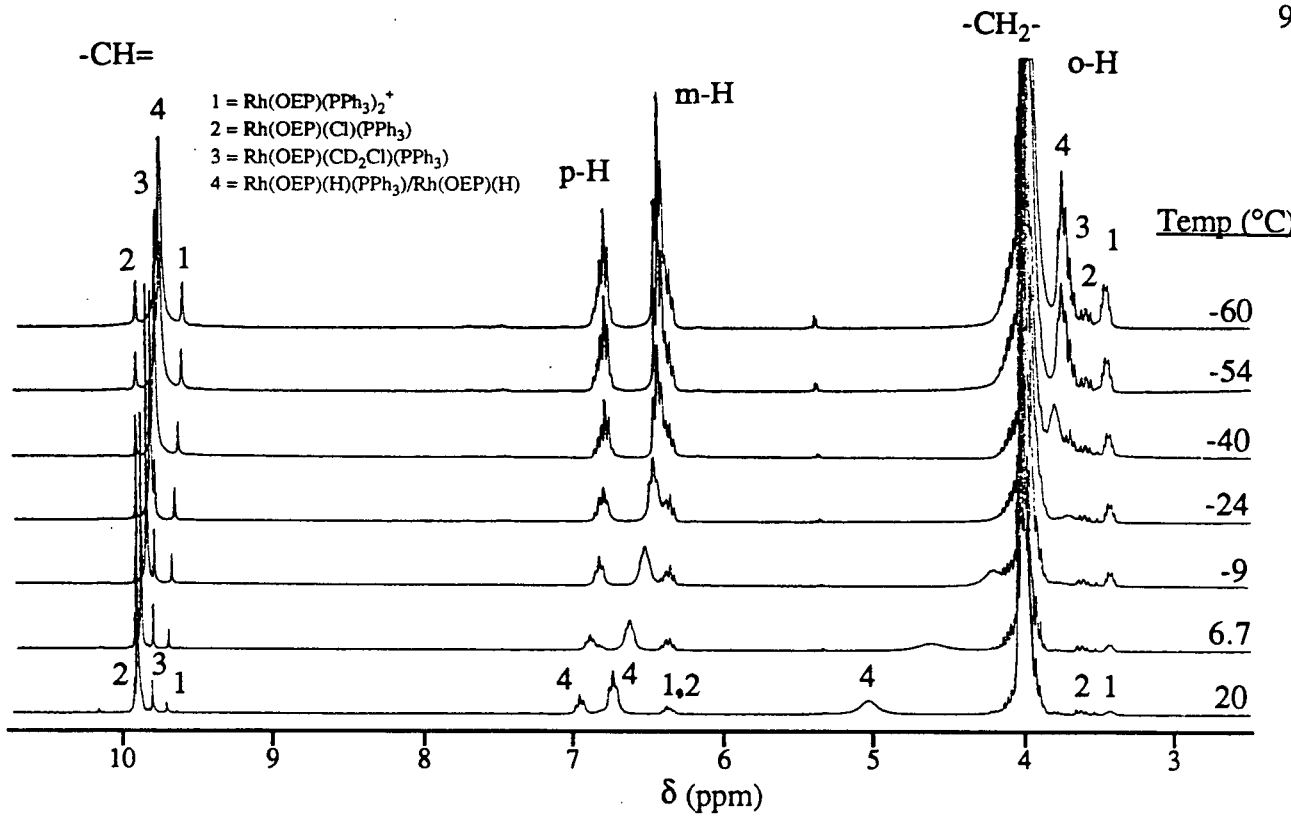

Figure 3.18. The 300 MHz ^1H VT nmr spectra of Rh(OEP)(H) with PPh_3 in CD_2Cl_2 over the temperature range 20 to -60 °C. [Rh] ≈ 7×10^{-3} M, [PPh_3] ≈ 5.3×10^{-3} M.

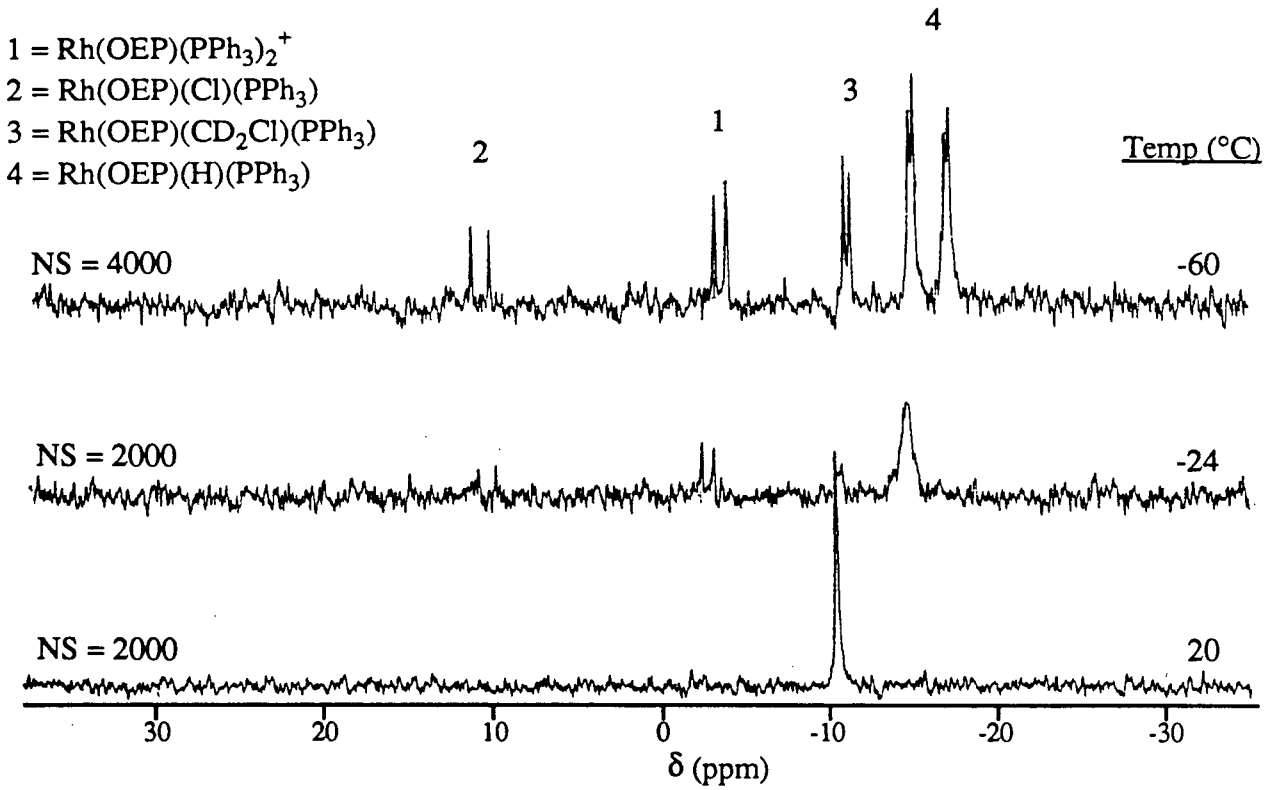

Figure 3.19. The 121.42 MHz $^{31}P\{^1H\}$ VT nmr spectra of Rh(OEP)(H) with PPh_3 in CD_2Cl_2 over the temperature range 20 to -60 °C. [Rh] ≈ 7×10^{-3} M, [PPh_3] ≈ 5.3×10^{-3} M.

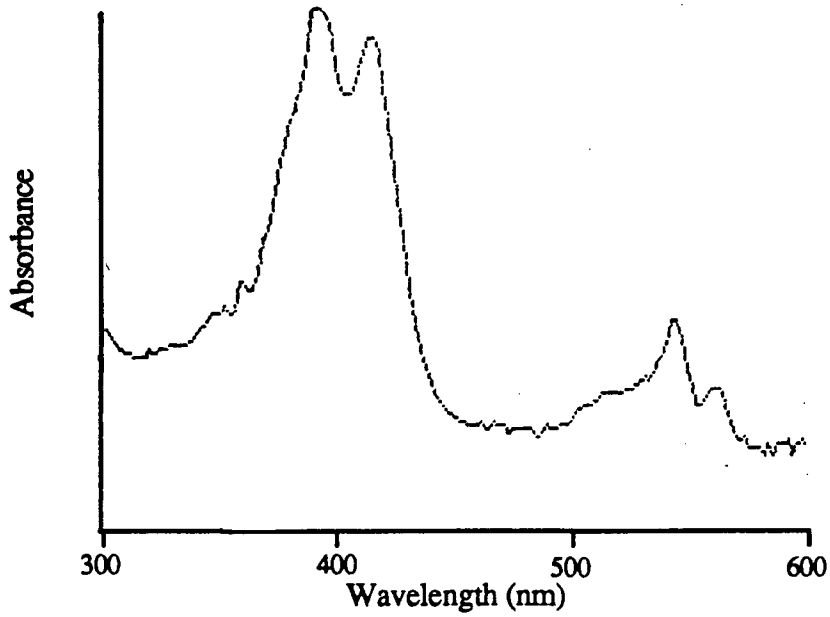

Figure 3.20. The visible spectrum of the nmr sample illustrated in Figs. 3.18/19 for Rh(OEP)(H) with PPh_3 in CD_2Cl_2.

Table 3.4. Selected nmr data for Rh(OEP)(Cl)(PPh_3) and $[Rh(OEP)(PPh_3)_2]^+$ as observed in CD_2Cl_2 solution of Rh(OEP)(H) with PPh_3 at ca. 20°C.

Complex	^1H δ	–CH=	o-H	m-H[a]	p-H[a]
Rh(OEP)(Cl)(PPh_3)		9.94 s	3.62 m	6.39	6.83
$[Rh(OEP)(PPh_3)_2]^+$		9.72 s	3.44 br	6.39	6.83
	$^{31}P\{^1H\}$	$\delta(^1J_{Rh-H})$			
Rh(OEP)(Cl)(PPh_3)		9.33 (124)			
$[Rh(OEP)(PPh_3)_2]^+$		-2.6 (88)			

a. Resonances of Rh(OEP)(Cl)(PPh_3) and $[Rh(OEP)(PPh_3)_2]^+$ overlap.

The remaining complex is identified as Rh(OEP)(CD_2Cl)(PPh_3) in CD_2Cl_2 and Rh(OEP)(CH_2Cl)(PPh_3) in CH_2Cl_2 based on the observation of a doublet at -4.44 ppm ($^2J_{Rh-H}$ = 2.5 Hz) in the ^1H nmr spectra of samples in CH_2Cl_2 (Fig. 3.21). The Rh(TPP)(CH_2Cl) complex

is known and has a doublet at -2.81 ($^2J_{Rh-H}$ = 2.9 Hz) ppm for the -CH_2Cl ligand resonance in C_5D_5N (100). A similar TMP complex is reported on in chapter 4 of this thesis and has a ligand resonance at ~2.9 ppm. The up-field shift of the ligand methylene resonances of Rh(OEP)(CH_2Cl)(PPh_3) is likely due to the coordination of PPh_3 trans. Similar shifts are observed when substituted pyridines coordinate to Rh(OEP)(CH_3) (17) and when Rh(TMP)(CH_2Cl)(NEt_3) forms completely at low temperature (Fig. 4.18).

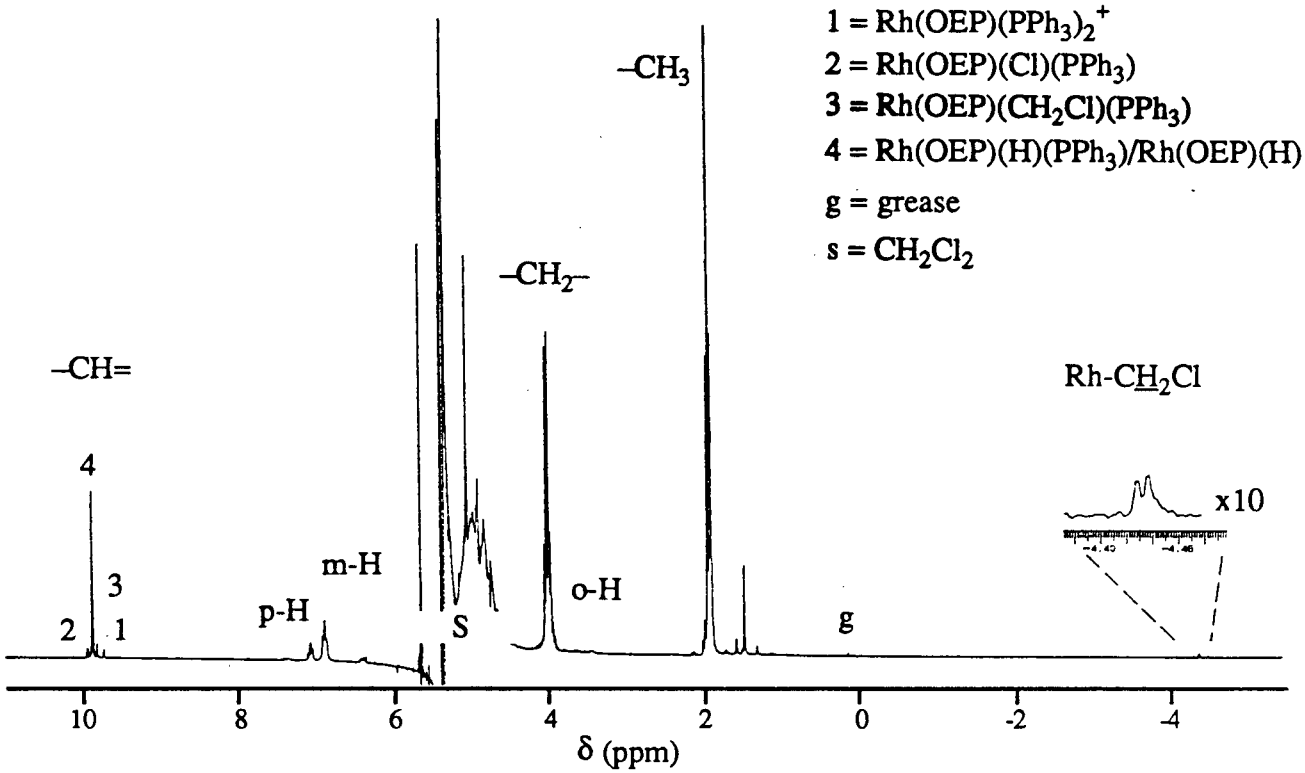

Figure 3.21. The 300 MHz ^1H nmr spectrum of Rh(OEP)(H) with PPh_3 in CH_2Cl_2 at 20 °C. [Rh] ≈ 2×10^{-3} M, [PPh_3] ≈ 5.4×10^{-3} M.

Several points are notable about the minor species. In the absence of PPh_3, Rh(OEP)(H) does not react with CH_2Cl_2 to form Rh(OEP)(CH_2Cl) (sect. 3.2.1.2), which suggests that Rh(OEP)(CH_2Cl)(PPh_3) arises from a PPh_3-induced solvent reaction. The relative amount of the minor species does not vary with the proportion of PPh_3 but is roughly in proportion to the amount of Rh(OEP)(H) initially present. This suggests that the reaction induced by the PPh_3 is not stoichiometric in PPh_3 but may therefore be catalytic in a Rh species.

3.2.2.1.2. In benzene and toluene

The visible spectrum of benzene or toluene solutions containing Rh(OEP)(H) and 1.5 to 3 equivalents of PPh_3 (i.e., the initial spectrum in Fig. 3.34) appears to be the superposition of principally the spectrum of Rh(OEP)(H) and a spectrum similar to that of Rh(OEP)(Cl)(PPh_3) (Table 5.2, p. 157). The ^1H nmr spectra of similarily composed samples in C_6D_6 or C_7D_8 show exchange broadened resonances for the porphyrin and PPh_3 (Fig. 3.22) at room temperature. A weak broad hydride resonance at ~-34 ppm is downfield of its position in the absence of PPh_3 ($\delta \approx$ -42 ppm), consistent with addition of a donor ligand trans to the hydride (17). Cooling a C_7D_8 solution of the hydride and ~2 equivalents of PPh_3 to -60 °C results in sharpening of the meso resonance at 9.95 ppm and the appearance of new resonances at 8.9 ppm and 4.45 ppm (Fig. 3.22). Below this temperature the spectrum decreases in intensity and quality. The hydride resonance moves downfield upon cooling and at -60 °C became a broad doublet with $^2J_{P\text{-}H} \approx 250$ Hz at -30.3 ppm. The spectrum in general still shows the effects of exchange; especially note the phenyl resonances of PPh_3 which are largely indistinguishable. Examination of the $^{31}P\{^1H\}$ spectrum at -60 °C of the sample (Fig. 3.23) reveals a very broad (~1032 Hz) "resonance" at -13.3 ppm. Superimposed on this "resonance" are the broadened resonances of Rh(OEP)(H)(PPh_3), doublet at -17.7 ppm ($^2J_{P\text{-}H} \approx 250$ Hz) (see previous section) and a resonance at -8.96 ppm.

In summary, there is evidence for Rh(OEP)(H)(PPh_3) as a minor component in equilibrium with RhOEP(H) in the aromatic solvents, judging by the sharpening of the meso resonance at 9.95 ppm, chemical shifts consistent with Rh^{III}(OEP) species, and the behaviour of the hydride resonances. This is similar to the behaviour in CH_2Cl_2 but the bulk of the PPh_3 appears to be exchanging with other complexes which cannot be distinguished via the data at hand. The ^1H nmr spectrum at the lowest temperatures shows the presence of a new resonance at 8.9 ppm which could be the averaged meso signal of a $[Rh(OEP)]_2PPh_3$ complex, akin to the known $[Rh(OEP)]_2CO$ complex (85). The resonance at -8.96 ppm in the ^{31}P spectrum could then be assigned to this complex and the 4.45 ppm resonance in the ^1H nmr spectrum to one of the $-CH_2-$ resonances of the $[Rh(OEP)]_2$ moiety. Addition of donors has been suggested to promote the cleavage of $[Rh(OEP)]_2$, to produce paramagnetic Rh(II) species (76). It could be that the PPh_3

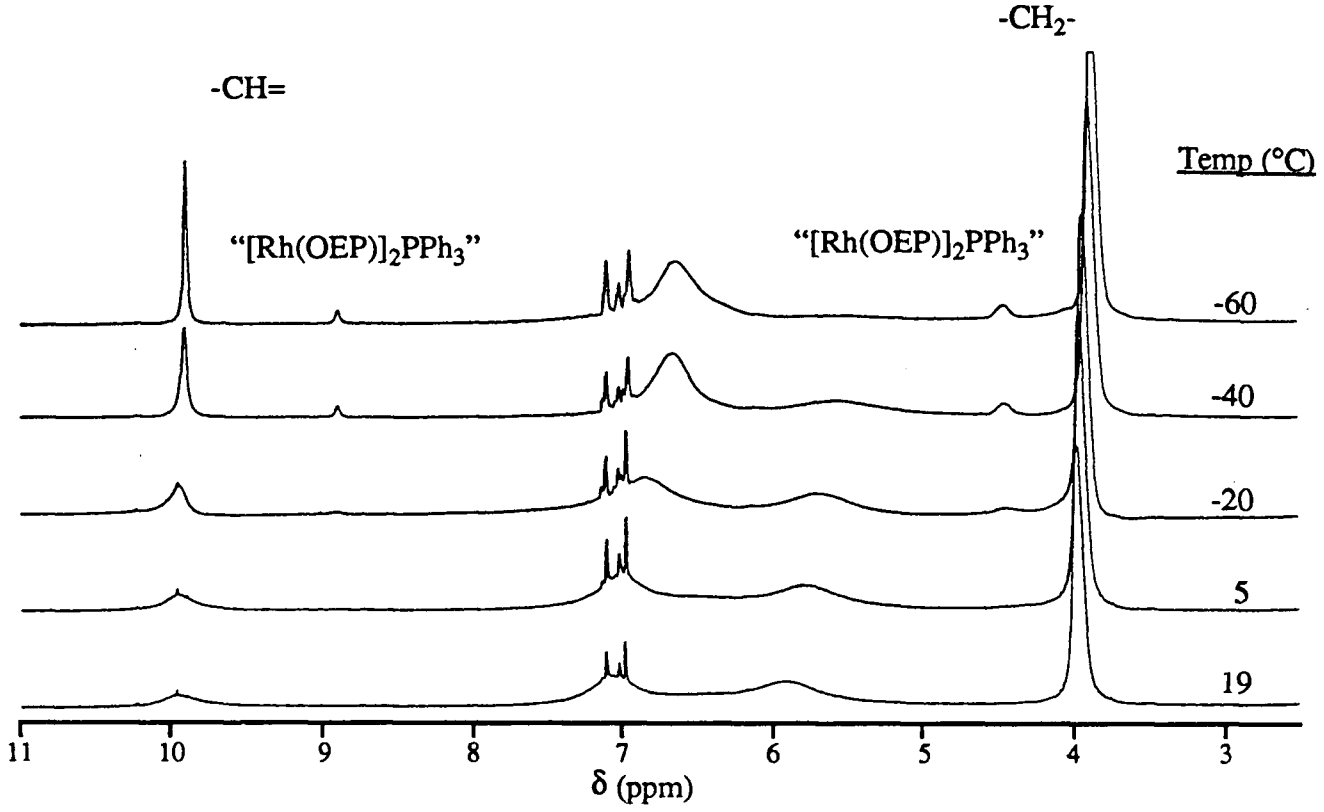

Figure 3.22. The 300 MHz ^1H nmr spectra of Rh(OEP)(H) with PPh_3 in C_7D_8 over the temperature range 20 to -60 °C. [Rh] ≈ 3×10^{-3} M, [PPh_3] ≈ 6×10^{-3} M.

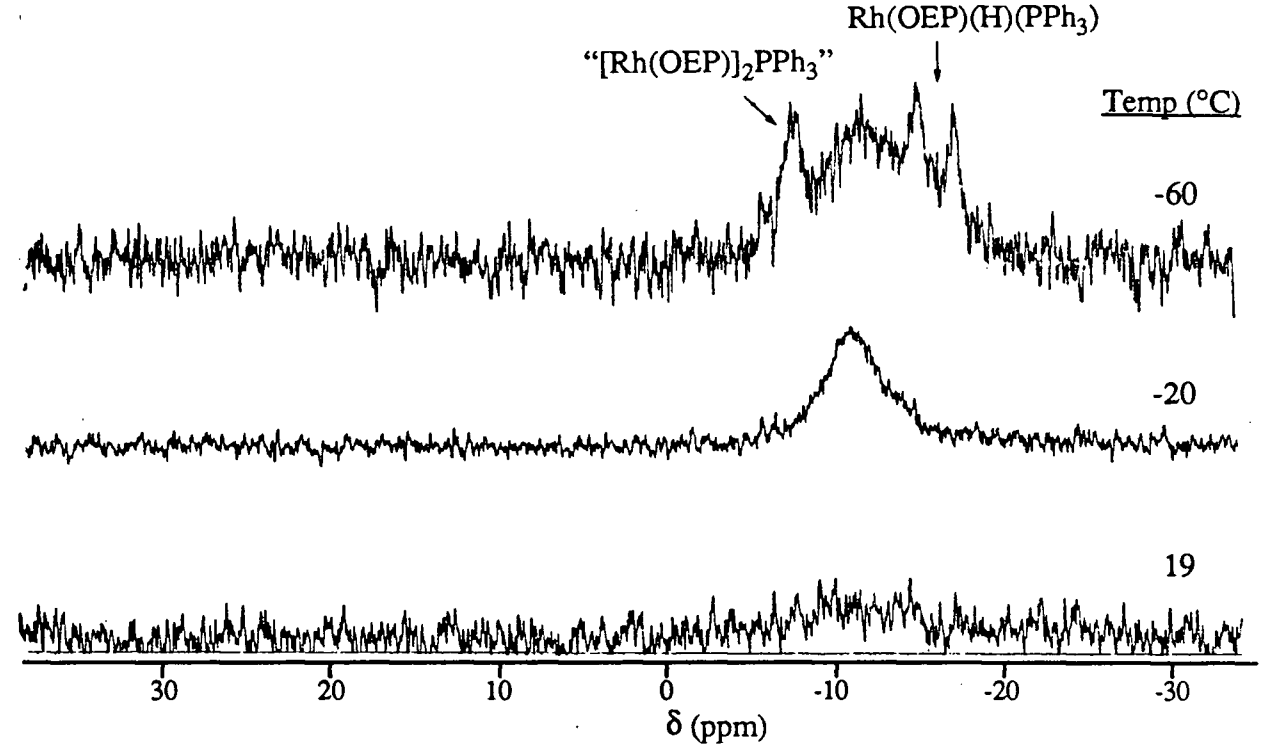

Figure 3.23. The 121.42 MHz $^{31}P\{^1H\}$ nmr spectra of Rh(OEP)(H) with PPh_3 in C_7D_8 over the temperature range 20 to -60 °C. [Rh] ≈ 3×10^{-3} M, [PPh_3] ≈ 6×10^{-3} M.

resonances that have not "frozen out" at low temperature are being affected by exchange amongst neutral paramagnetic Rh(II) species.

3.2.2.2. Reaction with O_2 in CH_2Cl_2

When O_2 is added to dichloromethane solutions of Rh(OEP)(H) and PPh_3, the colour deepens but the solutions remain homogeneous, which is unlike the behaviour in the absence of PPh_3. Figures 3.24 and 3.25 show the changes in the ^1H and $^{31}P\{^1H\}$ nmr spectra of a sample prepared in CH_2Cl_2 (the full spectrum is shown in Fig. 3.21). After addition of O_2 the averaged meso ^1H nmr resonance at 9.87 ppm due to a Rh(OEP)(H)/Rh(OEP(H)(PPh_3) equilibrium (sect. 3.2.2.1.1) is gone, and the meso resonances of Rh(OEP)(Cl)(PPh_3) at 9.94 ppm and that of Rh(OEP)(CH_2Cl)(PPh_3) at 9.85 ppm are increased by roughly equivalent amounts. Changes in the $^{31}P\{^1H\}$ nmr parallel these changes, a doublet at 9.33 ppm due to Rh(OEP)(Cl)(PPh_3) becoming prominent after addition of O_2, and a broad singlet lying between the positions of free PPh_3 and of Rh(OEP)(CH_2Cl)(PPh_3), and the doublet of $[Rh(OEP)(PPh_3)_2]^+$ lying at -2.6 ppm. The visible spectrum (Fig. 3.26) after the reaction is similar to the spectrum of Rh(OEP)(Cl)(PPh_3).

The appearances of the nmr spectra are different when the PPh_3 is not in excess when O_2 is added to the Rh(OEP)(H)/PPh_3 system. Figures 3.27 (^1H nmr) and 3.28 ($^{31}P\{^1H\}$ nmr) illustrate this case. The meso proton signal for Rh(OEP(Cl)(PPh_3) increases substantially from its initial intensity as does its $^{31}P\{^1H\}$ nmr resonance. The meso ^1H nmr resonance for Rh(OEP)(CH_2Cl)(PPh_3) is apparently missing after addition of O_2 but a broad resonance at 9.95 ppm in the ^1H nmr spectrum is believed to be the exchange averaged meso resonances of Rh(OEP)(CD_2Cl)(PPh_3) and Rh(OEP)(CD_2Cl). Because of the deficiency of PPh_3, the Rh(OEP)(CD_2Cl)(PPh_3) complex cannot fully form and an exchange averaged meso resonance at ~9.96 ppm is more downfield towards the meso resonance of Rh(OEP)(CD_2Cl) at ~10.15 ppm in CD_2Cl_2 (sect. 4.2.3) than when the [PPh_3] is higher (Fig. 3.24). The position of the singlet in the $^{31}P\{^1H\}$ nmr at -10 ppm is more towards the position of Rh(OEP)(CD_2Cl)(PPh_3) (Fig. 3.28) consistent with a Rh(OEP)(CD_2Cl)(PPh_3)/Rh(OEP)(CD_2Cl) equilibrium at low [PPh_3]. The visible spectrum of the nmr sample after addition of O_2 (Fig. 3.29) can be interpreted as the

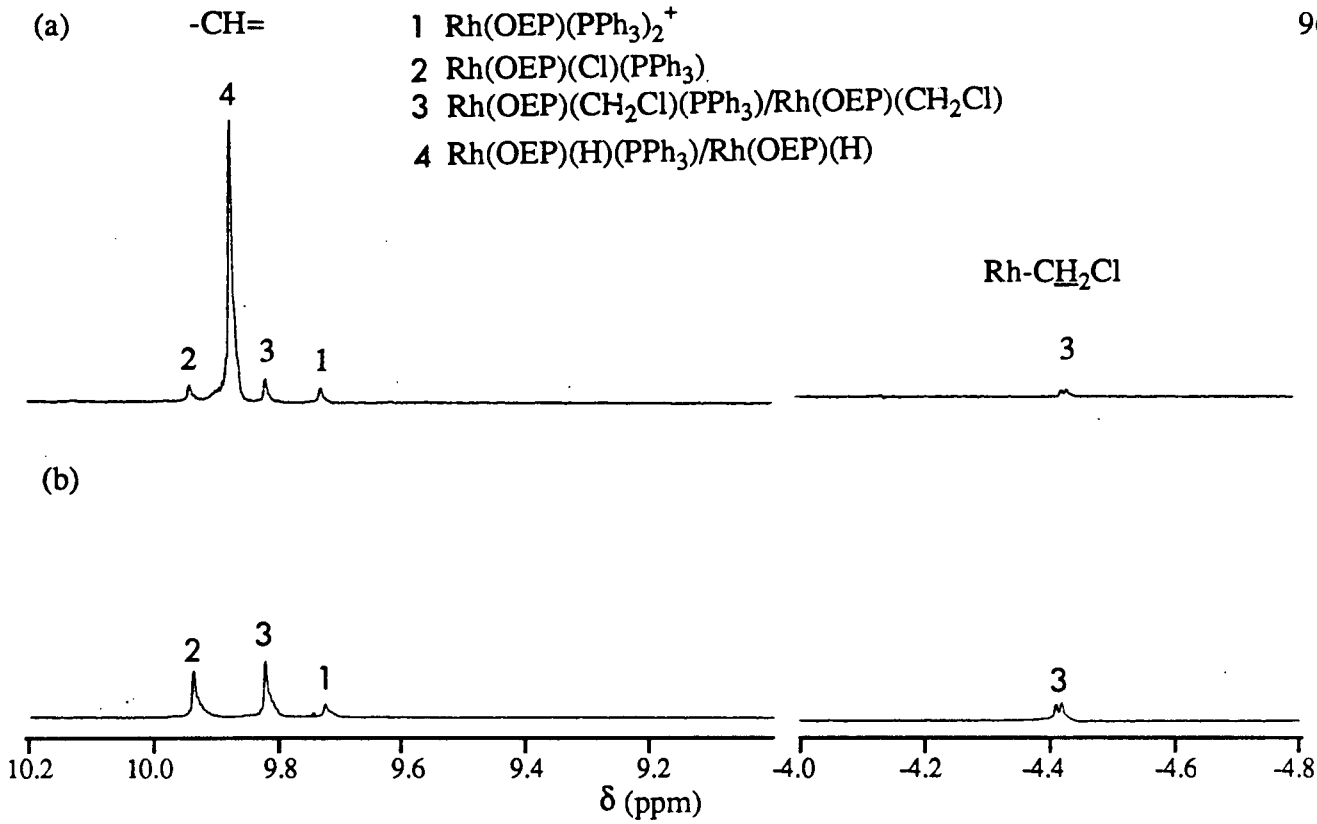

Figure 3.24. Selected regions of the 300 MHz ^1H nmr spectra of (a) Rh(OEP)(H) with PPh_3 in CH_2Cl_2 and (b) 20 min after addition of O_2 at 20°C. [Rh] ≈ 2×10^{-3} M, [PPh_3] ≈ 5.4×10^{-3} M, P_{total} = 1 atm.

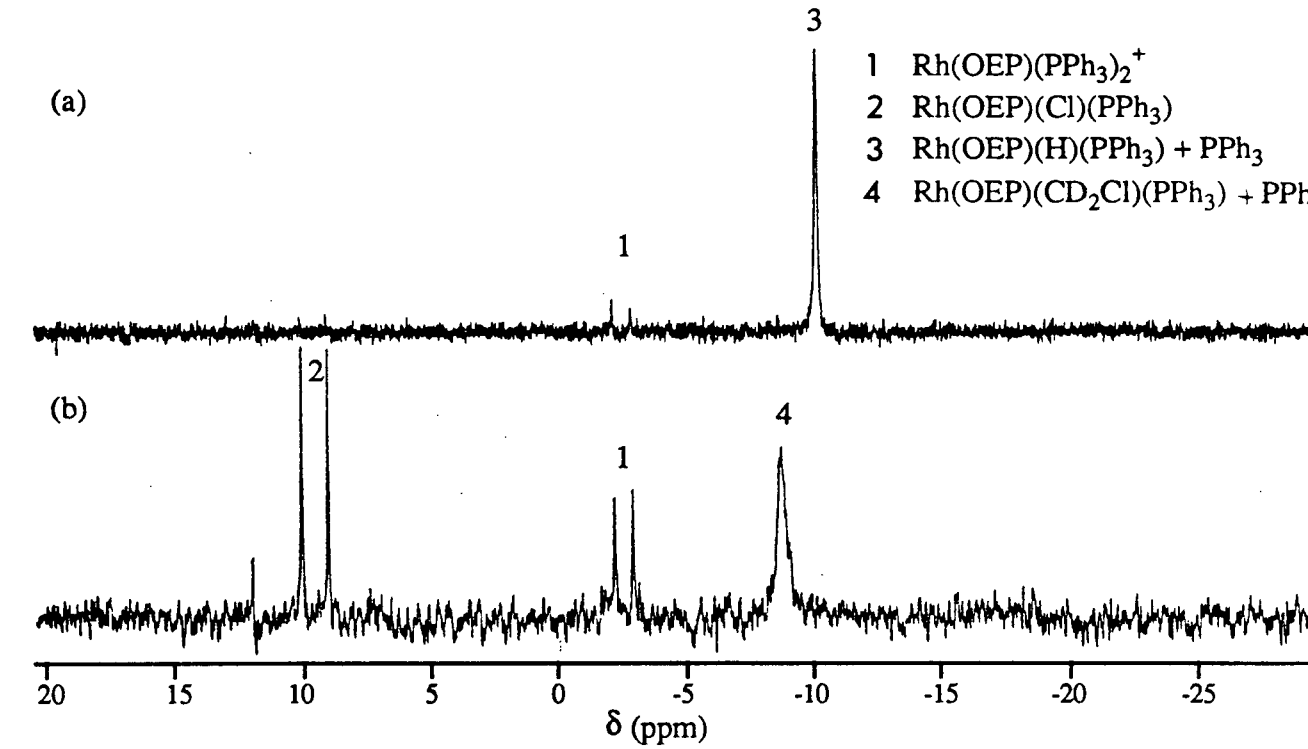

Figure 3.25. The 121.42 MHz $^{31}P\{^1H\}$ nmr spectra of (a) Rh(OEP)(H) with PPh_3 in CH_2Cl_2 and (b) ~ 30 min after addition of O_2 at 20°C. [Rh] ≈ 2×10^{-3} M, [PPh_3] ≈ 5.4×10^{-3} M, P_{total} = 1 atm.

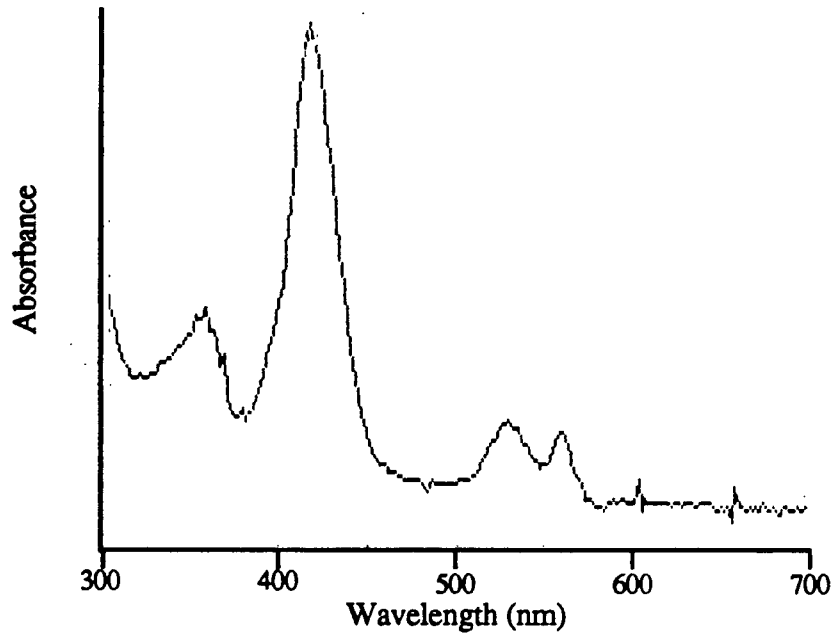

Figure 3.26. The visible spectrum of the nmr sample illustrated in Figs. 3.24/25, after the reaction of Rh(OEP)(H) with PPh_3 and O_2 in CH_2Cl_2.

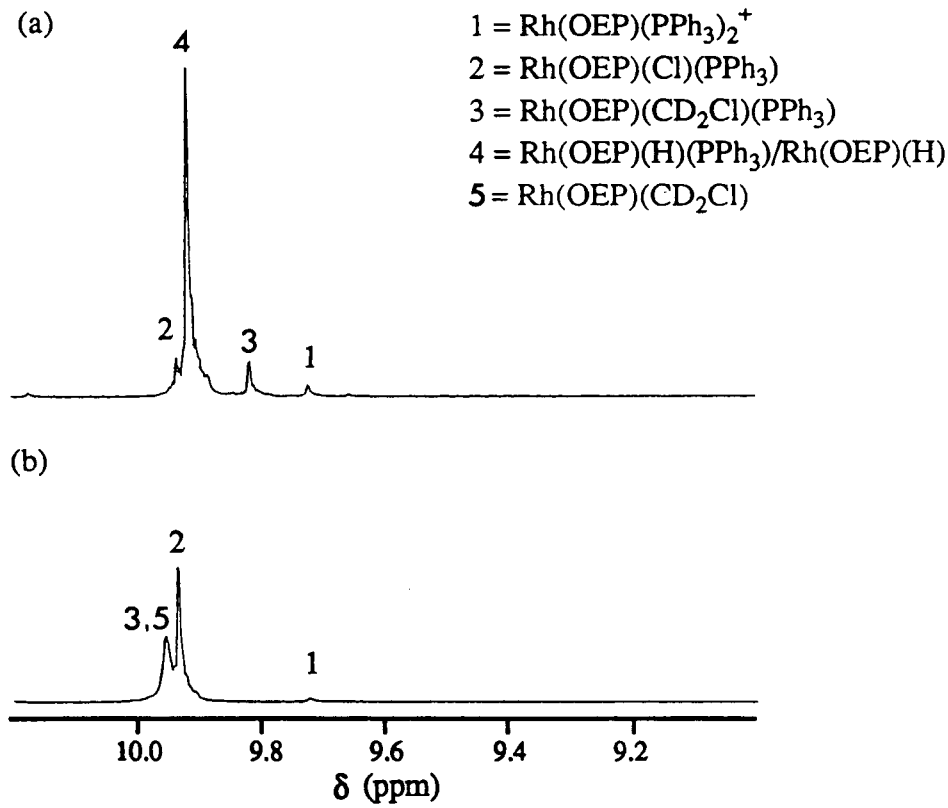

Figure 3.27. A selected region of the 300 MHz ^1H nmr spectra of (a) Rh(OEP)(H) with PPh_3 in CD_2Cl_2 and (b) 20 min after addition of O_2 at 20°C. [Rh] ≈ 6×10^{-3} M, [PPh_3] ≈ 4×10^{-3} M, P_{total} = 1 atm.

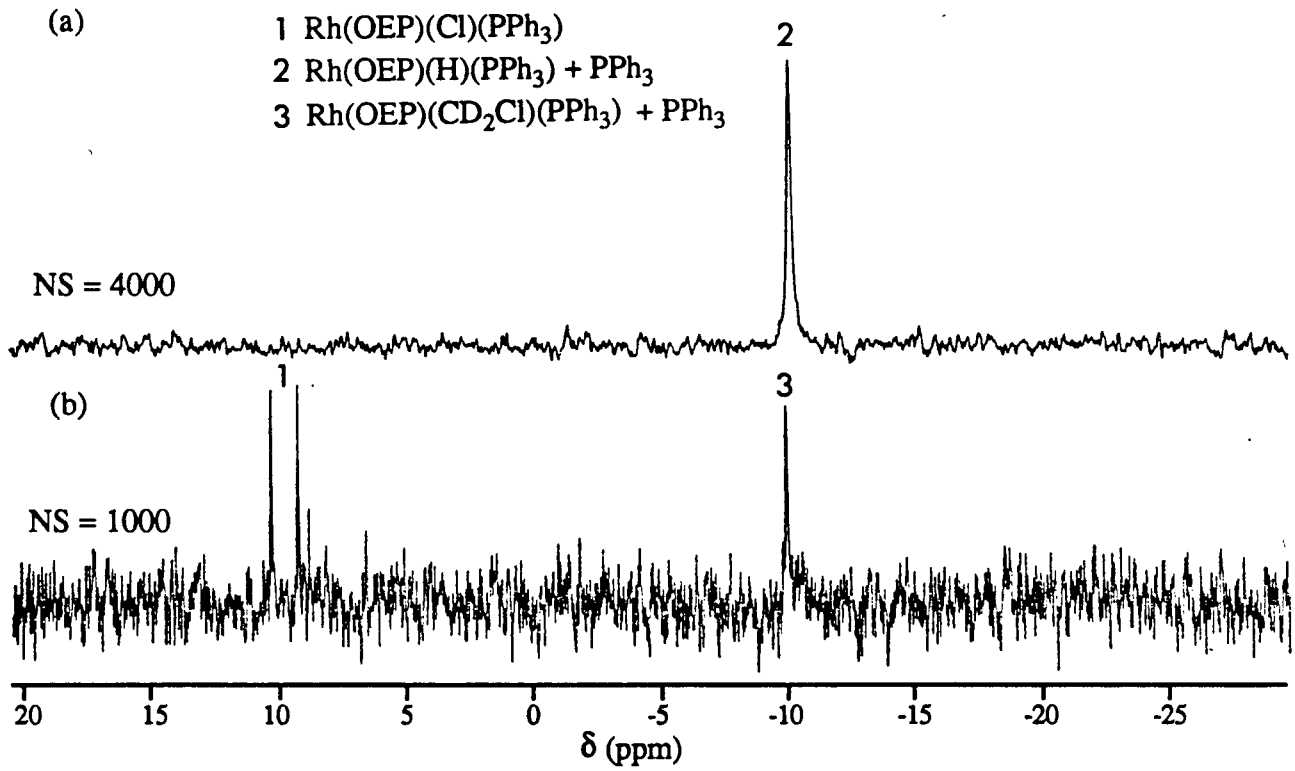

Figure 3.28. The 121.42 MHz $^{31}P\{^{1}H\}$ nmr spectra of (a) Rh(OEP)(H) with PPh_3 in CD_2Cl_2 and (b) ~ 30 min after addition of O_2 at 20°C. [Rh] ≈ 6×10^{-3} M, [PPh_3] ≈ 4×10^{-3} M, P_{total} = 1 atm.

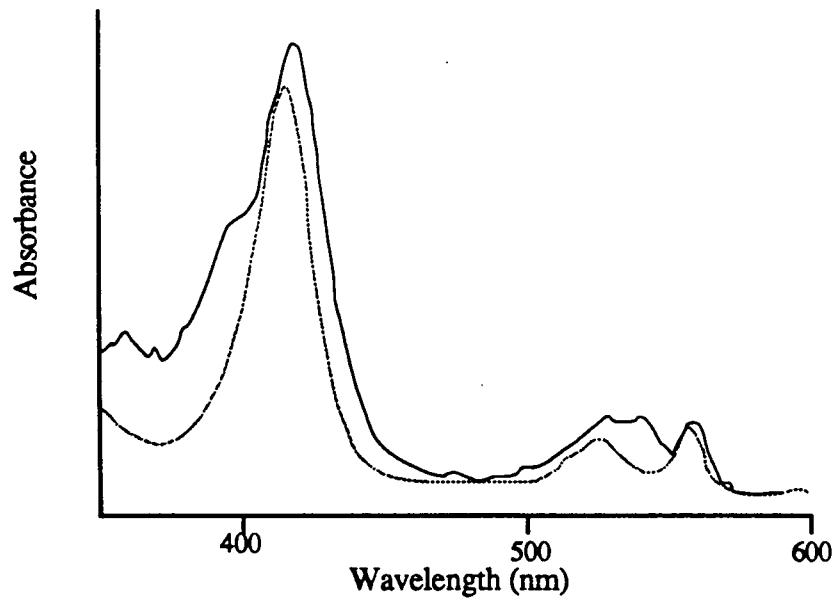

Figure 3.29. The visible spectrum of the nmr sample illustrated in Figs. 3.27/28 for the reaction of Rh(OEP)(H) with PPh_3 and O_2 in CD_2Cl_2 with the spectrum of Rh(OEP)(Cl)(PPh_3) (dotted line) overlaid.

superposition of the spectra of Rh(OEP)(Cl)(PPh_3) and Rh(OEP)(CD_2Cl), where the ~540 nm band is probably the α band of Rh(OEP)(CD_2Cl) (sect. 4.4), consistent with low [PPh_3] relative to [Rh].

A similar visible spectrum is observed for a CH_2Cl_2 solution of Rh(OEP)(H) and 0.9 equivalents of PPh_3 after exposure to O_2 (solid line, Fig. 3.30a). The spectrum of a sample containing a higher [PPh_3] (2.5 equivalents, dotted line, Fig. 3.30b) is much lower in intensity at ~540 nm, the position of the α band of Rh(OEP)(CH_2Cl), probably due to formation of Rh(OEP)(CH_2Cl)(PPh_3).

In summary, the course of the reaction of Rh(OEP)(H) with O_2 in dichloromethane is markedly affected by the addition of PPh_3. In the presence of PPh_3, postulated decomposition of the porphyrin is inhibited and reactivity is directed toward the solvent. Equimolar quantities of Rh(OEP)(Cl)(PPh_3) and Rh(OEP)(CH_2Cl) (PPh_3 ligated when the [PPh_3] is sufficient) are formed.

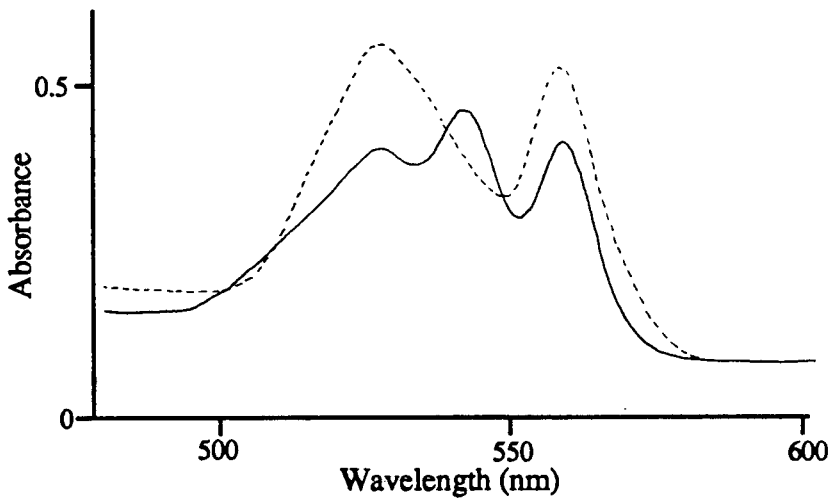

Figure 3.30. The visible spectrum of the products of the reaction of Rh(OEP)(H) with PPh_3 and O_2 in CH_2Cl_2: (a) (—) [Rh] = 3.40×10^{-4} M, [PPh_3] = 3.19×10^{-4} M and (b) (···) [Rh] = 4.64×10^{-4} M, [PPh_3] = 11.41×10^{-4} M. P_{total} = 1 atm, 25 °C.

3.2.2.3. Reaction with O_2 in benzene and toluene

Addition of O_2 to Rh(OEP)(H) and PPh_3 in benzene or toluene gives a homogeneous solution containing a complex mixture, as judged by the nmr spectra. Figures 3.31a and 3.31b show the ^1H nmr spectra of a sample in C_7D_8, before and after reaction, respectively; the $^{31}P\{^1H\}$ nmr spectra show only noise before and after addition of O_2 and are not illustrated (note that the content of Figure 3.31a has been discussed in sect. 3.2.2.1.2). The composition of the reacted sample changes with time and after 5 days its $^{31}P\{^1H\}$ nmr spectrum (Fig. 3.32) was found to contain a singlet at 24.2 ppm assignable to $OPPh_3$ and what is believed to be a doublet at 5.4 ppm ($^1J_{Rh\text{-}P}$ = 95 Hz) partially overlapped by a singlet at 5 ppm. The corresponding ^1H nmr spectrum (Fig. 3.31c) shows $OPPh_3$ phenyl proton resonances at 7.67 and about 7 ppm (overlapped by solvent), while the free PPh_3 phenyl proton resonances at 7.39 and about 7 ppm (overlapped by solvent) observed in the ^1H nmr spectrum immediately after addition of O_2 (Fig. 3.31a) are now gone. Note that only a trace of the oxide is present immediately after addition of O_2. Relative to the total area of the three sharp meso resonances at ca. 9.99 ppm, the set of broad resonances at 10.2, 7.62, 5.5 and 4.72 ppm have decreased as has the meso resonance at 9.97 ppm (Figs. 3.31b vs. 3.31c). Additional resonances which are similar to those of phenyl protons of PPh_3 coordinated to diamagnetic Rh^{III}(OEP) species (Table 5.1) have grown in at 6.48 and 6.23 ppm overlapping the existing ones (Fig. 3.31c).

Resonances at -1.28 and -1.44 ppm (Fig. 3.31b) are similar in position to those of the proposed hydroperoxide observed at low temperature in CD_2Cl_2 (sect. 3.2.1.2). However, this hydroperoxide is unstable above -20 °C and it is hard to reconcile the presence of a similar complex at room temperature in the presence of PPh_3 and H_2O (146). Thus the Rh(OEP) species produced in the O_2-reaction are not known. Speculative possibilities include Rh(II) species, which would account for the broad resonances. Unfortunately there are no reports of ^1H nmr data on paramagnetic Rh(II) porphyrin species to compare with. Metallation of a phenyl group of PPh_3 is plausible, especially because attack on dichloromethane solvent has already been shown to occur (sect. 3.2.2.2). Sterically reasonable structures could be para- or meta-metallated species.

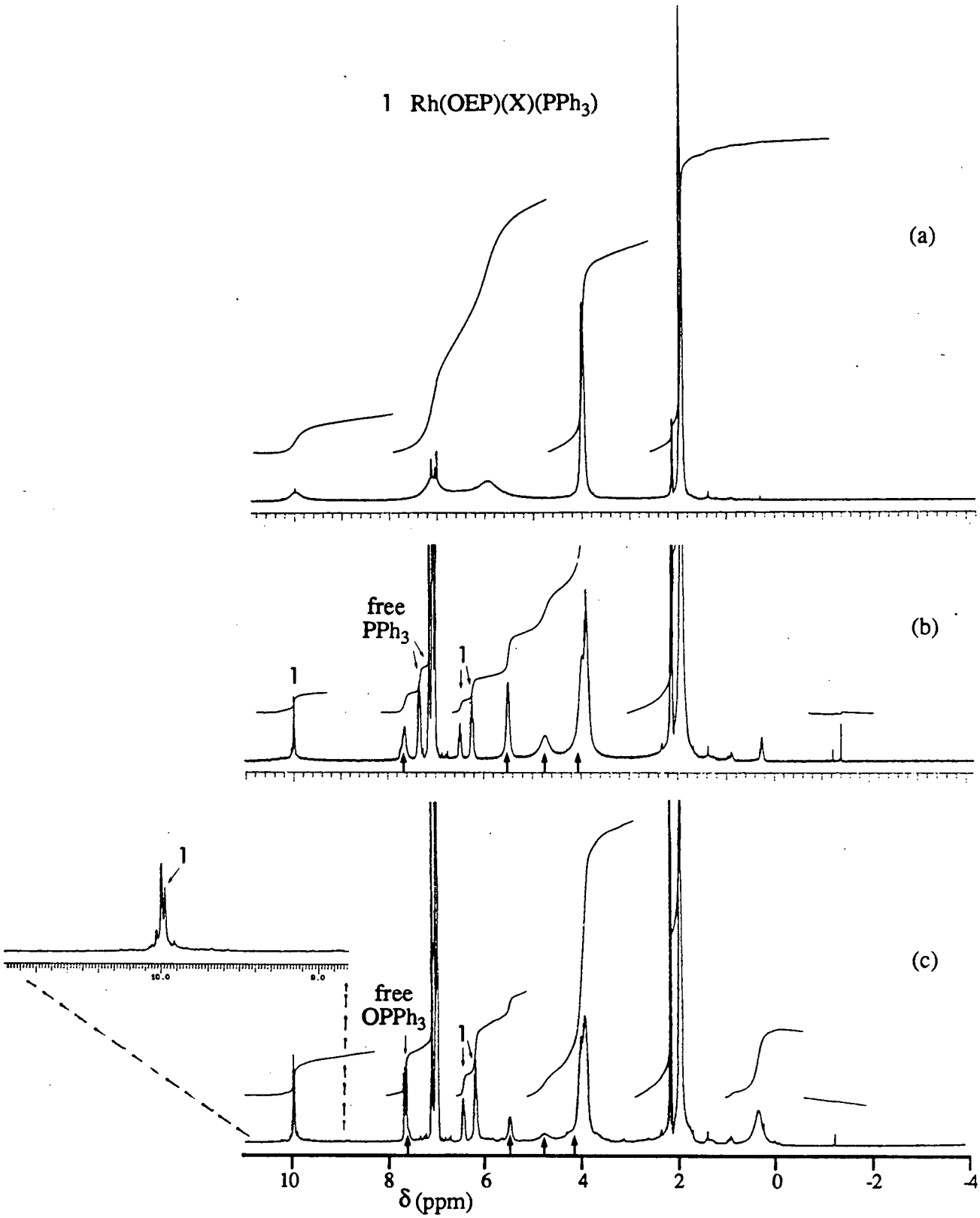

Figure 3.31. The 300 MHz ^1H nmr spectra at 19°C of (a) Rh(OEP)(H) with PPh_3 in C_7D_8, (b) 30 min after addition of O_2 at 19°C and (c) 5 days later . [Rh] ≈ 3×10^{-3} M, [PPh_3] ≈ 6×10^{-3} M, P_{total} = 1 atm.

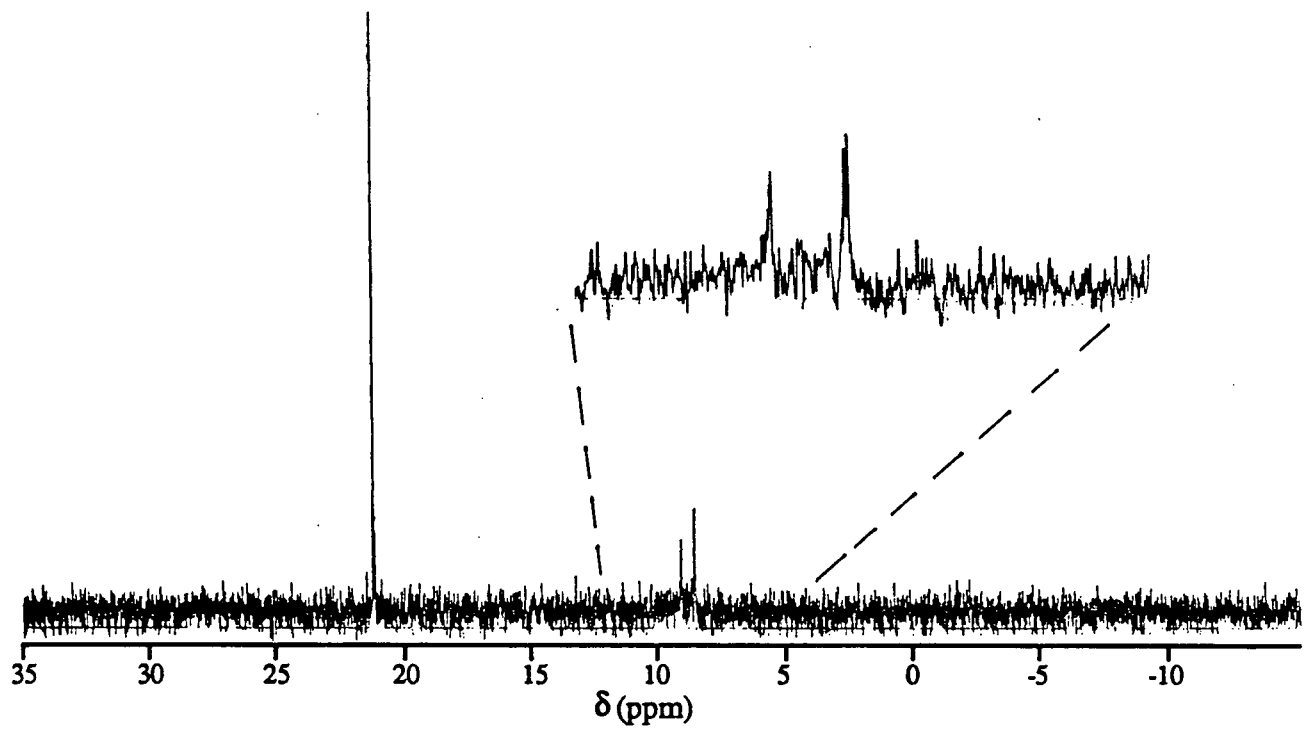

Figure 3.32. The 121.42 MHz $^{31}P\{^{1}H\}$ nmr spectrum at 19°C of Rh(OEP)(H) with PPh_3 in C_7D_8 5 days after addition of O_2. [Rh] ≈ 3×10^{-3} M, [PPh_3] ≈ 6×10^{-3} M, P_{total} = 1 atm.

The p-metallated phenyl complexes Rh(OEP)(C_6H_4-p-X) (X = CH_3, OMe or Cl) show o-H resonances between -0.43 and -0.49 ppm in $CDCl_3$ (107) and the observed resonances at ca. -1.3 to -1.4 ppm are not far from this, and the remaining resonances of the metallated ligand (10.2, 7.62, 5.5 and 4.72 ppm) could be affected by exchange at the dangling phosphine. The singlet at 5 ppm in the $^{31}P\{^{1}H\}$ nmr spectrum, and the new phenyl resonances observed in the ^{1}H nmr spectrum, could be assigned to such a complex (147).

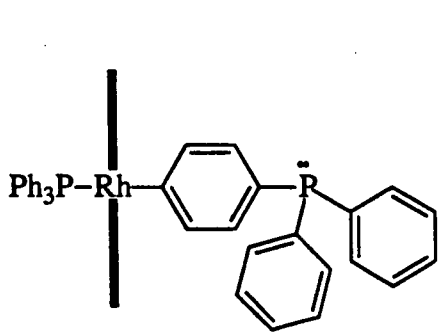

p-metallated

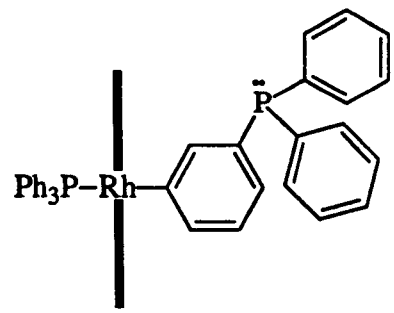

m-metallated

The visible spectrum (Fig. 3.33) of the nmr sample immediately after addition of O_2 is similar to those obtained in CH_2Cl_2 where PPh_3 was in excess. Following the same reaction by visible spectroscopy gives a product spectrum similar to the nmr sample (Fig. 3.34). The rather broad Soret peaks of these spectra cover the 420 nm region where the Soret of a PPh_3 ligated complex is expected (Table 5.2, p.157).

Clearly the effect of PPh_3 on the reaction of Rh(OEP)(H) and O_2 in toluene is different from the non-PPh_3 system in aromatic solvents and that in dichloromethane. The nmr spectra are not obviously interpretable at this time, although the presence of Rh(II) and PPh_3 metallated complexes are possibilities.

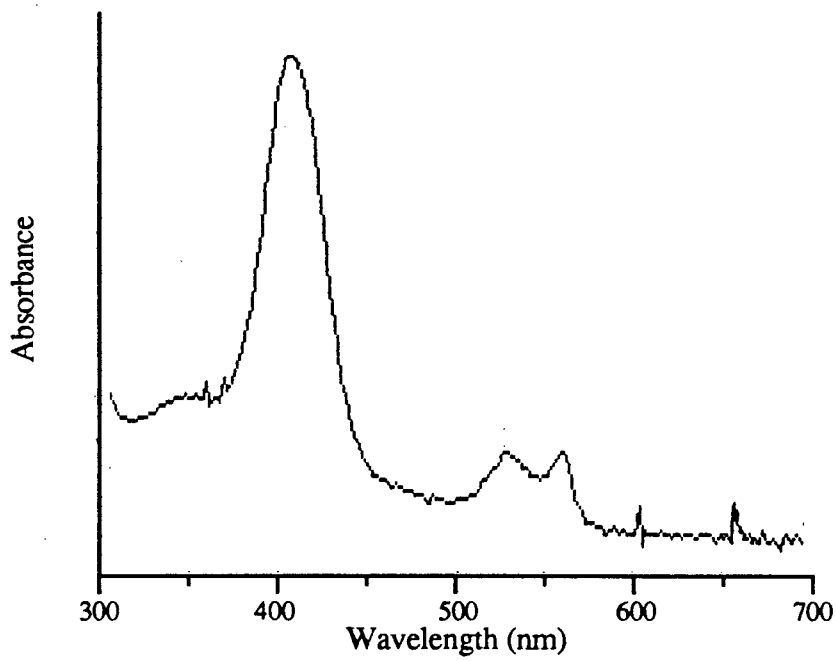

Figure 3.33. The visible spectrum of the nmr sample illustrated in Fig. 3.30b, for the reaction of Rh(OEP)(H) with PPh_3 and O_2 in C_7D_8.

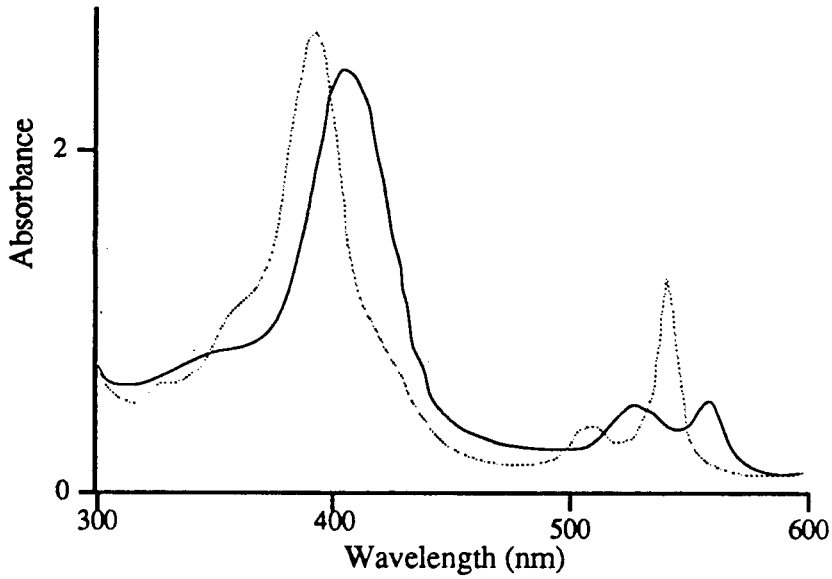

Figure 3.34. The visible spectrum of (···) Rh(OEP)(H) with PPh_3 in C_6H_6 and (—) 30 min after addition of O_2. [Rh] = 2.86×10^{-4} M,[PPh_3] = 8.4×10^{-4} M, P_{total} = 1 atm, 25 °C.

3.2.3. Reaction of Rh(OEP)(H) with CO and O_2/air

The reaction of Rh(por)(H) with CO in C_6H_6 to form Rh(por)(CHO) has been extensively reported upon in the recent literature (57,63,81,83,97,98). During the early part of the experimental work of this thesis, this reaction was examined to obtain reference data and was found to be very sensitive to air or O_2 at levels commensurate with accidental contamination such as incomplete purging of gas inlet lines. At the time the evidence was uninterpretable, and the work was not pursued further. In the last few years, high pressure nmr and ^{13}C labelling studies have been published which allow partial interpretation of the earlier observations which are presented here.

A benzene solution of Rh(OEP)(H) under an atmosphere of CO in a Schlenk flask was briefly exposed to air by opening the tap on the flask to air and the solvent removed using a stream of CO. The IR spectrum of the oily residue (Fig. 3.35) has several bands in the regions where CO and carbonyl stretching bands are expected. Bands at 2089, 1731(sh) and 1709 cm^{-1} can be assigned to $[Rh(OEP)]_2CO$, $[Rh(OEP)]_2\mu CO$ (85) and Rh(OEP)(CHO) (97), respectively. The band at 2336 cm^{-1} can be independently shown to be CO_2 in solution. Atmospheric CO_2 does not

dissolve sufficiently in Nujol to be observed, and thus the 2336 cm^{-1} band may come from the decomposition of a complex during the mulling but more probably was an impurity in the CO and became trapped in the oily residue. There is no evidence of the ν_{Rh-H} of Rh(OEP)(H) which would be expected at 2226 cm^{-1}. The other bands in the 2000 cm^{-1} region are unassigned and there are probably a number of additional bands in the (1550 – 1750) cm^{-1} region, besides those assigned above, that are not due to porphyrin bands.

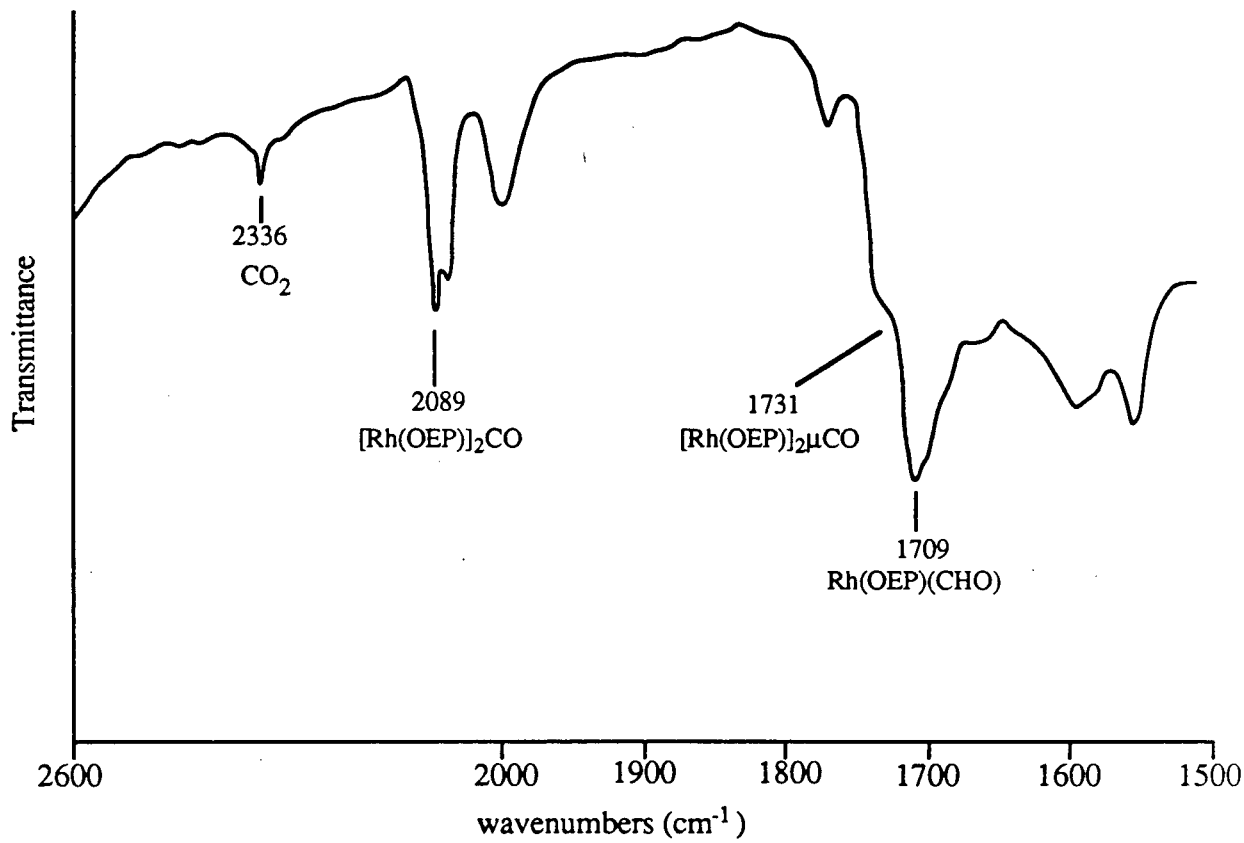

Figure 3.35. The IR spectrum of the residue (in Nujol) from the reaction of Rh(OEP)(H) and air-contaminated CO in benzene.

The reaction of CO (0.6 atm) with Rh(OEP)(H) (~10^{-3}M) in benzene to form Rh(OEP)(CHO) is complete within 20 min and the meso ^1H nmr resonance of the formyl complex is at 10.30 ppm (Fig. 3.36a). The progress of the reaction for similar samples in benzene under CO atmospheres contaminated by small amounts of air or O_2 can be followed by ^1H nmr. Figure 3.36b shows the progress for the first hour and Figure 3.36c shows the spectra of a similar sample

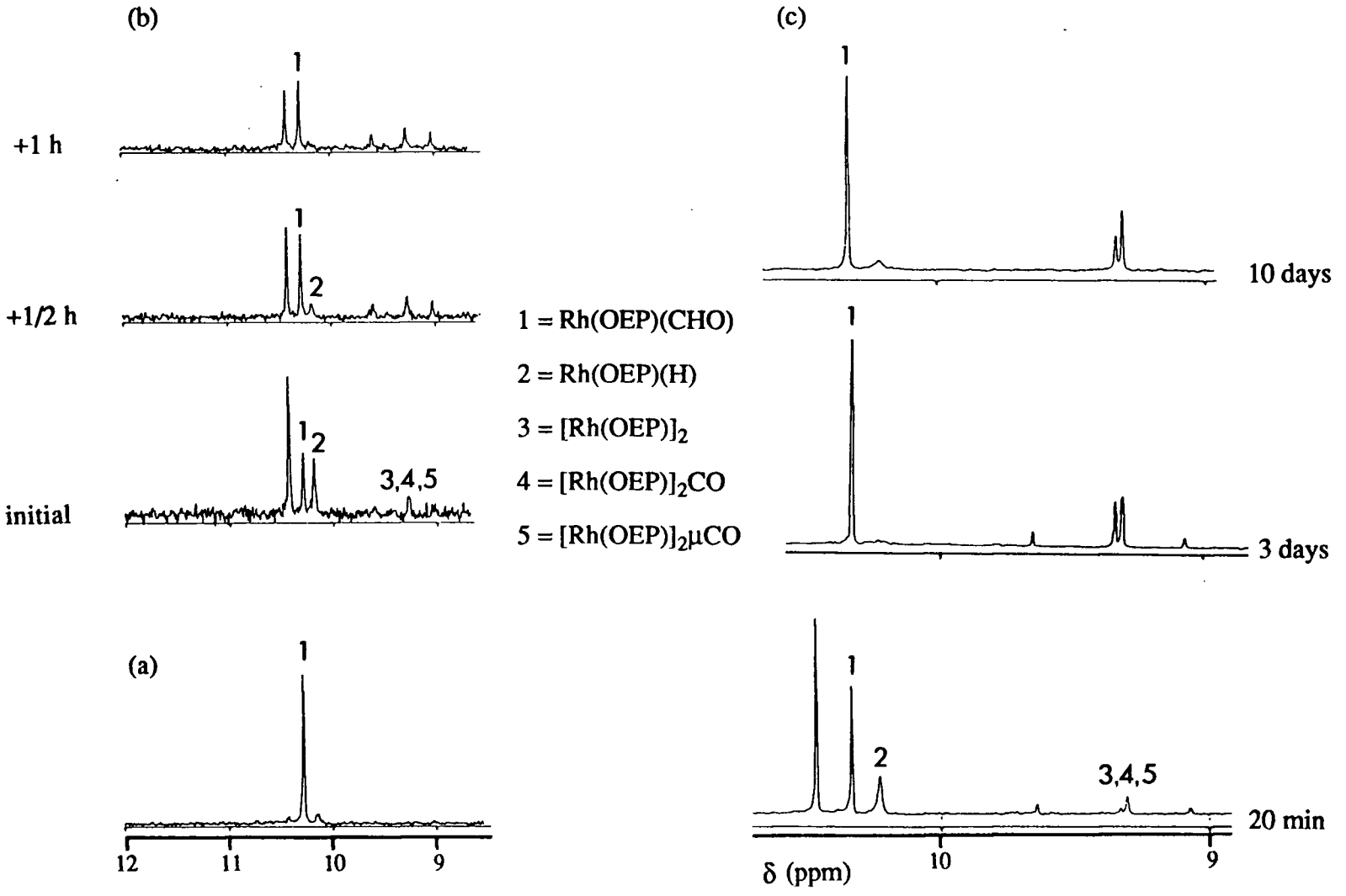

Figure 3.36. The changes in ^1H nmr spectra during the reaction in C_6D_6 of Rh(OEP)(H) with CO contaminated with O_2: (b) in the first hour (80 MHz) and (c) over 10 days (400 MHz). Spectrum (a) (80 MHz) is of Rh(OEP)(CHO) formed in situ using pure CO. [Rh] ≈ 2×10^{-3} M, P_{total} = 0.6–1 atm, ambient temperature.

at ~20 min, 3 days and 10 days after mixing. The meso resonances at 10.19 and 10.30 ppm are due to Rh(OEP)(H) and Rh(OEP)(CHO) (97), respectively, and resonances due to the formyl (δ = 2.85 ppm) and hydride protons ($\delta \approx$ -41 ppm) are found upfield. Resonances at ~9.30 ppm are probably those of $[Rh(OEP)]_2$, $[Rh(OEP)]_2CO$ and $[Rh(OEP)]_2\mu CO$; that at 9.31 ppm is the exchange average of the meso protons of $[Rh(OEP)]_2$ and $[Rh(OEP)]_2CO$, and the slightly downfield meso that slowly grows in over several days is that of the CO bridged species (85). There are 2 resonances of equal intensity, at 9.07 and 9.61 ppm, in this region that appear to correlate (Fig. 3.36b) with the dissappearance of the initial major meso resonance at 10.44 ppm. The 2 resonances are probably due to an unsymmetric dirhodium species (see below).

Besides the meso resonance at 10.44 ppm, there is a signal at ~-0.5 ppm integrated at about 1 proton relative intensity, and this resonance is present only when the meso signal at 10.44 ppm is present; when the latter disappears so does the high-field peak. The ethyl side-chain resonances are complex due to the overlapping resonances of the many different OEP ligands present and the symmetry of the species is not directly apparent. This species is tentatively assigned as Rh(OEP)(C(O)OH) which has been reported as an intermediate observed during the reaction of Rh(OEP)(H) and CO/KOH in benzene to form the formyl complex, although supporting data were not published (98). There are unassigned bands ca. 1700 cm^{-1} in the IR spectrum illustrated in Figure 3.35 that could be assigned to a carboxy species. The unsymmetric dirhodium species mentioned above is believed to be [Rh(OEP)]-C(O)O-[Rh(OEP)]. The meso signal at 9.07 ppm is near to those of analogous $-CH_2CH_2-$ and -CH=CH- bridged dimers (57,65) and would therefore be assigned to the Rh-C containing moiety, and the remaining meso resonance at 9.61 ppm to the Rh-O containing moiety.

3.3. General Discussion

The behaviour of the O_2 reactions as followed by visible spectroscopy, the sensitivity to initial starting conditions, and the observation of Rh(II) and $Rh-CH_2Cl$ containing products, strongly indicate radical mechanisms.

A radical chain mechanism is plausible, where the reaction of O_2 with the Rh center follows a series of steps similar to those for the $[Rh(OEP)]_2$ catalysed reaction of styrene with

Rh(OEP)(H) in benzene to give a net Rh-H addition across an unsaturated bond in the substrate (83):

Initiation/termination:

$$2Rh(OEP)(H) \rightleftharpoons [Rh(OEP)]_2 + H_2 \quad (3.2)$$

$$[Rh(OEP)]_2 \rightleftharpoons 2Rh(OEP)\cdot \quad (3.3)$$

Propagation:

$$Rh(OEP)\cdot + O_2 \rightleftharpoons Rh(OEP)(O_2) \quad (3.4)$$

$$Rh(OEP)(O_2) + Rh(OEP)(H) \longrightarrow Rh(OEP)(OOH) + Rh(OEP)\cdot \quad (3.5)$$

The chemistry of reactions (3.2) and (3.3) is well established in the literature (sect. 1.5.2 and 1.5.3). The chemistry of equation (3.4) has been reported to occur at low temperature in dry toluene and formation of a symmetric μ-peroxo species is postulated to occur on warming to room temperature. This could occur via equation (3.6), written by analogy to the reaction of styrene with $[Rh(OEP)]_2$ in benzene, to give a bridged dirhodium species (83).

$$Rh(OEP)(O_2) + [Rh(OEP)]_2 \rightleftharpoons [Rh(OEP)]_2(\mu\text{-}O_2) + Rh(OEP)\cdot \quad (3.6)$$

However, in the present work, the nmr data appear to show $[Rh(OEP)]_2$ to be stable (at least for several hours) in the presence of 1 atm of O_2 at room temperature, implying that at least equilibrium (3.4), if correctly formulated, lies very much to the left side. When one also considers that $Rh(TPP)(O_2)$ is an isolable stable species then one is forced to consider the contradictory nature of the data on the OEP system. In section 4.2.1 $[Rh(OEP)]_2$ is also noted react very slowly with O_2 in C_6D_6 under an O_2 atmosphere *if* H_2O is added but reacts instantly under *dry* conditions. Water is also present in the solutions after the reaction of O_2 with Rh(OEP)(H) and may be competing with O_2 (in reaction (3.4)), or $Rh(OEP)(O_2)$ (in reaction (3.7)) for a coordination site.

There are only ^1H nmr data at low temperature to support the existence of a thermally unstable Rh(OEP)(OOH) species (sect. 3.2.1.2) but, assuming its existence, then this hydroperoxide or a decomposition product could react further with Rh(OEP)(H) (reaction (3.7)). In essence, the reactions consume H· and release "Rh(OEP)" and H_2O in excess of the

propagation steps of reactions (3.4) and (3.5) in a reaction analogous to the decomposition of H_2O_2 to H_2O and O_2 and is consistent with the formation of $[Rh(OEP)]_2$ and H_2O in good yield from the reaction of Rh(OEP)(H) with O_2 (sect. 3.2.1.1) (64).

$$Rh(OEP)(OOH) + Rh(OEP)(H) \longrightarrow [Rh(OEP)]_2 + H_2O + \tfrac{1}{2}O_2 \qquad (3.7)$$

The reaction of Rh(OEP)(H) with O_2 in CH_2Cl_2 did not lead to $[Rh(OEP)]_2$ at room temperature. Instead, uncharacterisable species were observed by nmr, probably because of the reaction of radical intermediates of the reaction with CH_2Cl_2, or reaction of O_2^-, dissociated from $Rh(OEP)(O_2)$, with CH_2Cl_2 (86). There does not appear to be any rapid reaction between $[Rh(OEP)]_2$ or, by implication, monomeric $Rh^{II}(OEP)$, with the CH_2Cl_2 solvent.

The addition of PPh_3 to solutions of Rh(OEP)(H) promotes a rapid reaction with the CH_2Cl_2 solvent giving $Rh(OEP)(Cl)(PPh_3)$, $Rh(OEP)(CH_2Cl)(PPh_3)$ and $[Rh(OEP)(PPh_3)_2]^+$ in ~20% yield relative to the hydride species. Addition of O_2 to these solutions appears to further promote the solvent reaction to the extent that the $Rh(OEP)(Cl)(PPh_3)$ and $Rh(OEP)(CH_2Cl)(PPh_3)$ become the major species (in equimolar amounts) in solution without the apparent decomposition that occurs in the absence of PPh_3, and without the concomittant formation of $OPPh_3$. Strong donors, such as $P(OMe)_3$, have been suggested to promote the cleavage of $[Rh(OEP)]_2$ and subsequent radical reactions of $Rh^{II}(OEP)$ in C_6H_6 (sect. 1.5.2) (76). It seems reasonable to propose several equilibria, reactions (3.8–3.10), the effect of O_2 addition being to increase the effective [Rh(OEP)] via reactions (3.2–3.6), so long as the reaction of PPh_3 with the dimer and the subsequent solvent reactions are much faster than the "decomposition" reactions that occur in the absence of PPh_3.

$$[Rh(OEP)]_2 + PPh_3 \rightleftharpoons Rh(OEP)(PPh_3) + Rh(OEP) \qquad (3.8)$$

$$Rh(OEP)(PPh_3) + CH_2Cl_2 \rightleftharpoons Rh(OEP)(Cl)(PPh_3) + \cdot CH_2Cl \qquad (3.9)$$

$$Rh(OEP) + \cdot CH_2Cl \rightleftharpoons Rh(OEP)(CH_2Cl) \qquad (3.10)$$

Chapter 4
The reaction of Rh^{III}(por)(Cl)(L) complexes with tertiary amines

4.1. Introduction

In this chapter the mechanisms of the reactions of some tertiary alkylamines (principally Et_3N) with Rh^{III}(por)(Cl)(L) are explored. The formation of $[Rh^{II}(OEP)]_2$ species under mild conditions is observed with some amines and a number of novel organometallic derivatives of Et_3N have been found. Tertiary amine oxidative dealkylation to the dialkylamine is observed. Detailed spectroscopic examination of the reaction of Rh(por)(Cl)(L) with Et_3N revealed a complex manifold of reactions. However, enough mechanistic information about the reaction has been extracted to provide a useful framework from which more exhaustive studies can be undertaken in the future.

Comparison is made between results obtained using two porphyrins: OEP and TMP. The principle reason for the choice is steric rather than electronic, formation of $[Rh^{II}(por)]_2$ being blocked in the case of TMP, because the ortho-methyl groups of the mesityl groups of TMP hinder a sufficiently close approach (119). Although tetraaryl- and octaethyl-porphyrins, on coordination to metals, differ in their cis effects (69), similar chemistry at Rh occurs for both Rh(OEP) and tetraaryl Rh(TPP) species (Chapter 1) and so the use of TMP to prevent dimerization is not considered to change the chemistry to any significant degree other than by steric effects.

In addition, the reactions were studied in chlorinated (CH_2Cl_2) and non-chlorinated (benzene, toluene) solvents. As observed in Chapter 3 and elsewhere (sect. 1.4.1), some Rh(II) species react with CH_2Cl_2 solvent and similar reactivity is observed in the presence of Et_3N.

The results and discussion section of the chapter is in two parts: so-called product analysis and kinetic analysis. The product analysis results cover reaction times greater than 5-15 min after mixing and were largely obtained using nmr and scanning uv-vis spectroscopy. The kinetic analysis results cover times down to ~10 ms using stopped-flow techniques and from 15 s

to 5 min using diode array and conventional scanning uv-vis spectroscopy. This "kinetic/product" division also reflects the typical reaction sequence observed. The metalloporphyrin reagent was consumed in an initial rapid reaction sequence (over seconds/minutes), and then the initial products underwent less rapid reactions (over minutes/hours). The emphasis was semi-quantitative because not enough products and intermediates were confidently identified for quantitative kinetic analysis.

4.2. Results and Discussion of Product Analysis

4.2.1. Amine reaction with Rh(OEP)(Cl)(L) in benzene or toluene

Under ærobic conditions, Rh(OEP)(Cl)(H_2O) in C_6D_6 can be seen by ^1H nmr spectroscopy to rapidly coordinate Et_2NH to form only diamagnetic Rh(OEP)(Cl)(Et_2NH), after addition of 1 equivalent of the neat amine (Fig. 4.1). The $-CH_2-$ resonances of the ethyl side-chains appear as a multiplet indicative of asymmetric substitution with regard to the porphyrin plane, i.e., two different axial ligands are present causing the $-CH_2-$ resonances to appear as an ABX_3 multiplet (138-141). The coordination of the single Et_2NH ligand is shown by the shifting of the Et_2NH resonances by the strong porphyrin ring-current from their normal positions to positions up-field of TMS. The triplet at -2.71 ppm is assigned to the Et_2NH ligand methyl protons, and the two overlapped multiplets at -3.80 ppm are assigned to the diastereotopic methylene protons of the single coordinated Et_2NH ligand; the NH proton is at -6.4 ppm. The complex is stable in solution for days in the absence of light, but a black solid precipitates if a sample is left in laboratory light.

Repeating the experiment using 1 equivalent of Et_3N also yields Rh(OEP)(Cl)(Et_2NH) as the main product (after 4h: 60% yield estimated by ^1H nmr) (Fig. 4.2). A small amount of intractable black precipitate is visible at this point, but was insignificant relative to the amount of dissolved material. Some Et_2NH and unreacted Et_3N are detected by GC in samples prepared similarly to those used in the nmr experiments but with up to a 20-fold excess of Et_3N. The amount of Et_2NH was always less than the initial Rh species and thus there was no evidence of any catalytic dealkylation.

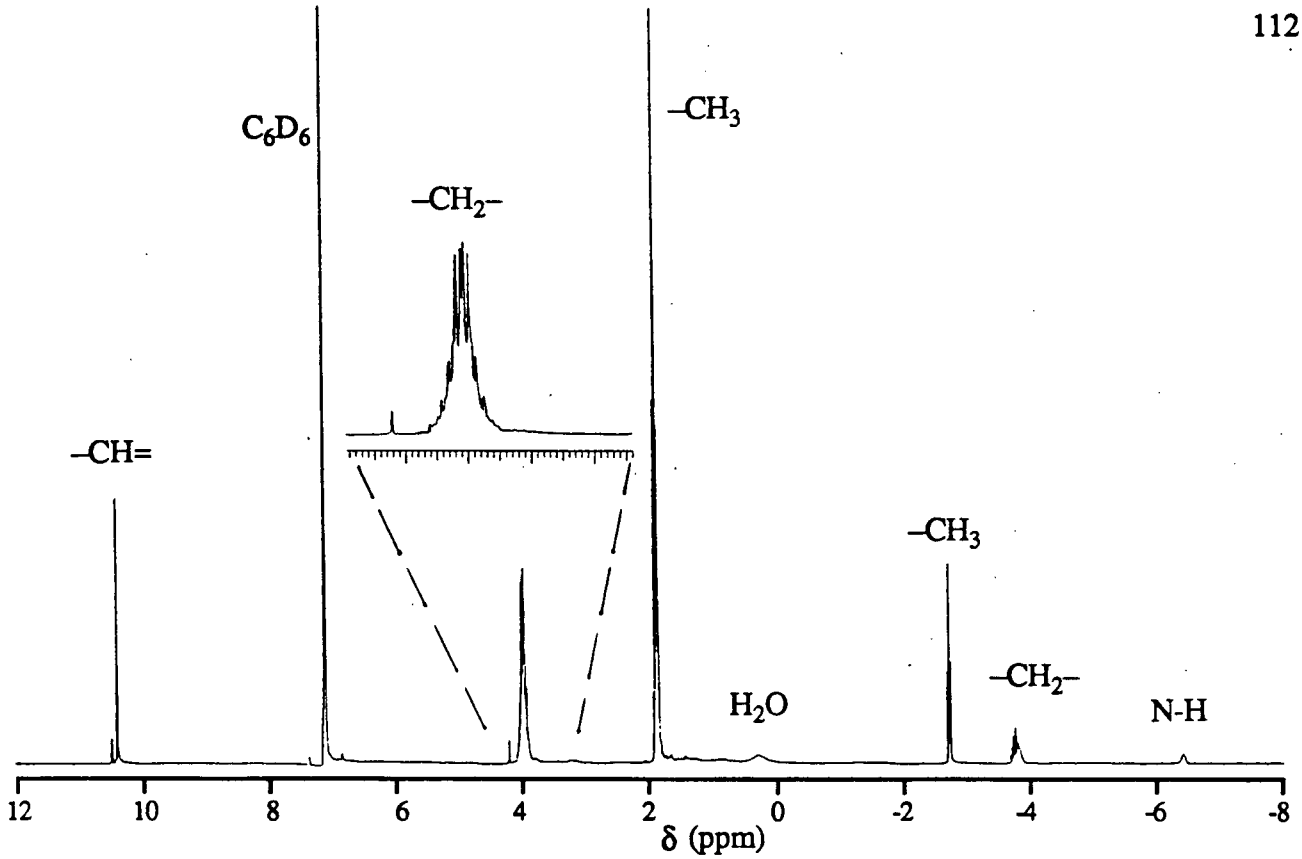

Figure 4.1. The 300 MHz ^{1}H nmr spectrum of Rh(OEP)(Cl)(Et_2NH) in C_6D_6 at 20 °C. Prepared in situ, [Rh] ≈ 3×10^{-3} M, [Et_2NH] ≈ 3×10^{-3} M.

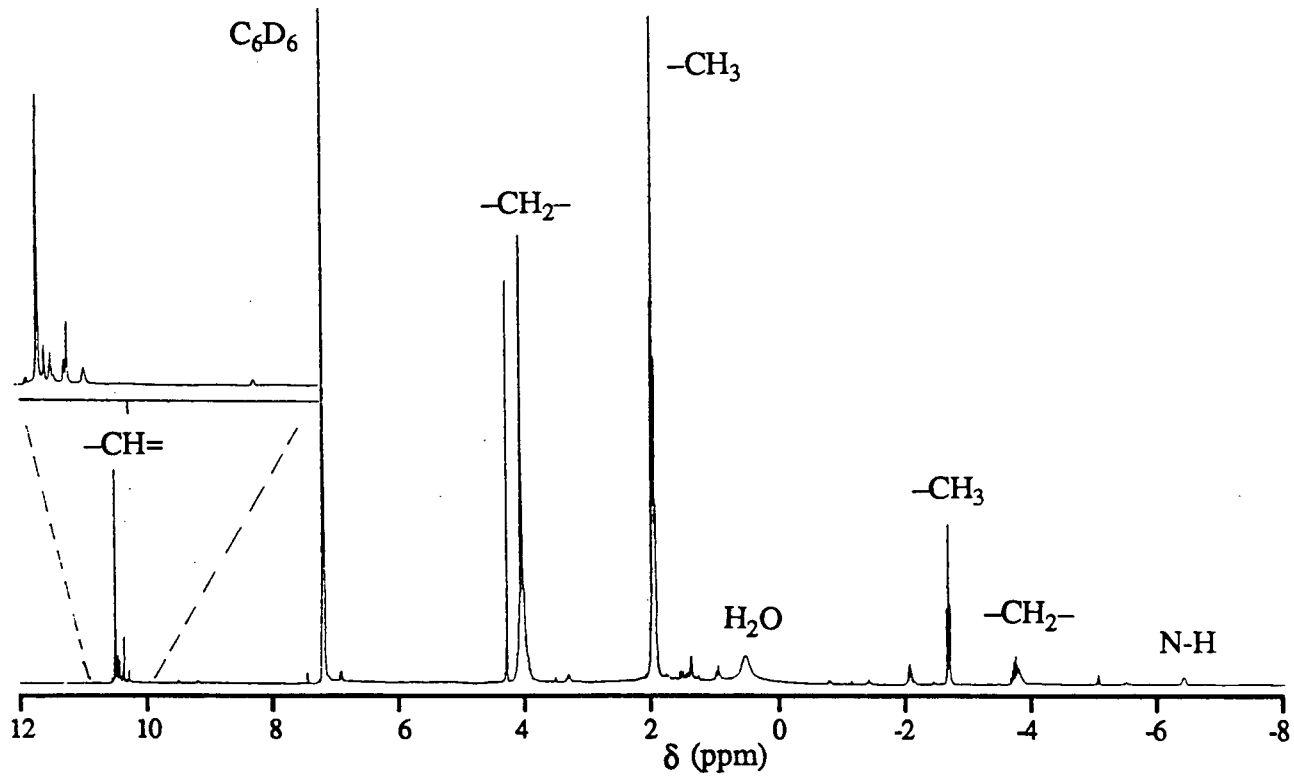

Figure 4.2. The 300 MHz ^{1}H nmr spectrum of a C_6D_6 solution of Rh(OEP)(Cl)(H_2O), 4 h after addition of Et_3N. [Rh] ≈ 4×10^{-3} M, $[Et_3N]_0$ ≈ 4×10^{-2} M, 20 °C.

The Rh(OEP)(Cl)(Et_2NH) product is observable also by visible spectroscopy, using either of the two amines in excess over Rh(OEP)(Cl)(H_2O). Nearly identical hypso-porphyrin spectra with β and α bands at 522 and 552 nm respectively (Fig. 4.3) were obtained for the Rh(OEP) products consistent with formation of Rh(OEP)(Cl)(Et_2NH) regardless of the amine used. The reaction with Et_2NH is complete within the mixing time of ~3 min (sect. 2.2.2), which is consistent with the rapid formation of Rh(OEP)(Cl)(Et_2NH) as expected on the basis of the nmr experiments, but for the Et_3N reaction, complex changes are observed during the first 6 h of the reaction, with little change thereafter. When the Et_3N and Rh(OEP)(Cl)(H_2O) are mixed, the Rh(OEP)(Cl)(H_2O) bands at 519 and 552 nm are immediately replaced by bands at 522 and 553 nm (but probably not those of Rh(OEP)(Cl)(Et_2NH)). A subsequent slow decrease at 553 nm is accompanied by an increase at ~552 and ~544 nm. The latter band is light sensitive and decreases on exposure to light, i.e., when the sample is removed from the spectrometer to check homogeneity. The intensity at 552 nm increases as that at 544 nm decreases, without further exposure to room light, until the final spectrum shown in Figure 4.3 is obtained after ~6 h.

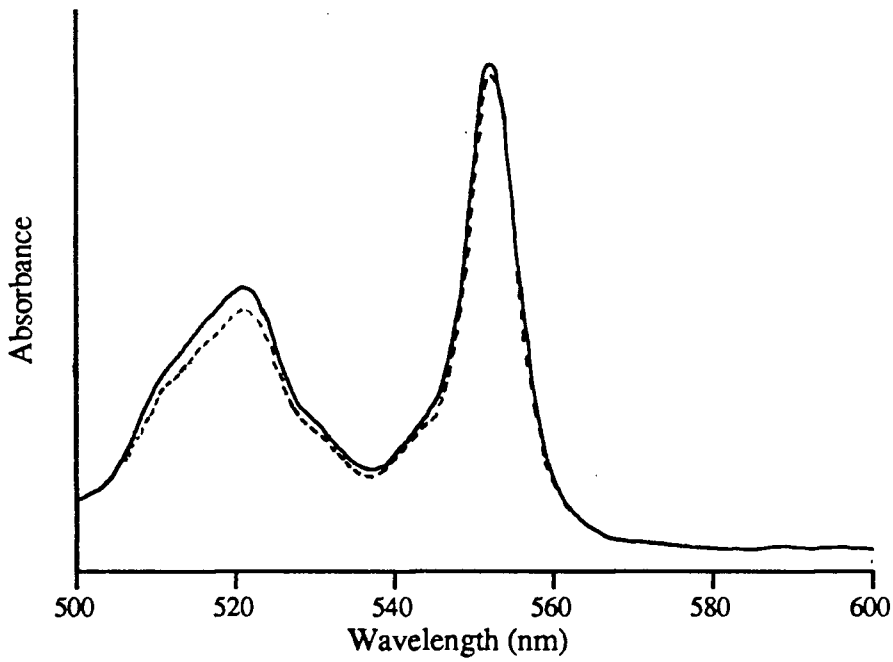

Figure 4.3. The visible spectrum in C_6H_6 at 25 °C of (···) Rh(OEP)(Cl)(Et_2NH) a few minutes after preparation in situ, [Rh] ≈ 3.5×10^{-4} M, [Et_2NH] ≈ 7×10^{-3} M and (—) a solution of Rh(OEP)(Cl)(H_2O) ~6 h after addition of Et_3N ([Rh] = 3.54×10^{-4} M, [Et_3N] ≈ 7.19×10^{-3} M); the Soret at 403 nm is not illustrated.

Dealkylation of amines commonly involves initial oxidation of the amine (148). A redox process involving the metalloporphyrin is indicated because Et_3N does not spontaneously dealkylate under similar conditions without Rh(OEP)(Cl)(H_2O). Indeed, $[Rh(OEP)]_2$ is detected by ^1H nmr spectroscopy as one of the intermediates in the experiments just described, and is the first major product observed by nmr under anærobic conditions (see following discussion). Several other amines were "screened" for a similar reactivity by adding a few μL of the amine to C_6D_6 solutions of Rh(OEP)(Cl)(H_2O) ([Rh] ≈ 5×10^{-3} M) under Ar and examining the ^1H nmr spectra of the reaction solutions, within the first hour, for the formation of $[Rh(OEP)]_2$ or de-alkylated products. Aniline, N-methyl-diphenylamine and N-ethyl piperidine all form complexes of the type Rh(OEP)(Cl)(amine) (Table 4.1), although the N-ethyl piperidine complex decomposes within 24 h. Proton Sponge and tributylamine give $[Rh(OEP)]_2$ as a major product and, in the latter step, the Rh(OEP)(Cl)($^nBu_2NH$) complex is also observed (Table 4.1). Only the reaction of Et_3N will be discussed further in this chapter, because its reaction appeared to be more amenable to study, particularly by ^1H nmr spectroscopy.

When equimolar quantities, or a small excess, of Et_3N relative to Rh(OEP)(Cl)(H_2O) are reacted together in a nmr tube under dry, anærobic conditions in C_6D_6, or C_7D_8, the concentration of $[Rh(OEP)]_2$ grows in as the initial major product observed by ^1H nmr spectroscopy (Fig. 4.4a), being complete in <15 min. Typically, the yield of dimer was high. For example, the proportion of $[Rh(OEP)]_2$ estimated from integration of the meso peaks in in the 10.6–9.0 ppm region of Figure 4.4a was 77%. Some of the resonances assignable to Rh(OEP)(Cl)(Et_2NH), in ~5 % yield, are identifiable (10.37 (s, –CH=) and coordinated Et_2NH at -2.68 (t, $–CH_3$), -3.8 (m, $–CH_2–$)). The remaining "Rh(OEP)" species were not identifiable although the positions of the meso proton resonances are appropriate for Rh^{III}(OEP) species. Broad resonances at 2.40 and 0.96 ppm are attributed to ethyl groups of an uncoordinated amine but from these data it is not clear whether the resonances where those of Et_3N (2.39 q, 0.96 t) or Et_2NH (2.64 q, 0.98 t). Over a few days at room temperature, in the dark, the resonances of the $[Rh(OEP)]_2$ decrease as those of Rh(OEP)(Cl)(Et_2NH) and a new species Rh(OEP)(CH(Me)NEt_2) (see below) increase in intensity (Fig 4.4b). The amine resonances at 2.40 and 0.96 ppm are no longer present. The composition

Table 4.1. The ^1H nmr spectral data for various Rh(OEP)(Cl)(amine) complexes.[a]

amine	–CH=	-CH_2-	-CH_3	other
$PhNH_2$	10.24 s	4.04 m, 3.91 m	1.92 t	-4.92 s (NH_2), 1.68 d (o-H), 5.49 t (m-H), 5.87 t (p-H)
Ph_2NMe[b]	10.12 s	~4 m[c]	1.95 t[c]	-3.19 s (NMe), 2.46 s (o-H), 5.64 m (m-H), 5.99 m (p-H)
EtNpip	10.41 s	4 03 m	1.92 t	[d]
$^nBu_2NH$[e]	10.32 s	~3.97 m	1.95 t	-6.12 s (N-H), -4.06 m/-3.60 m (N-CH_2-), -2.46 m (-CH_2-), -0.87 m (-CH_2-), -0.23 t (-CH_3)
Et_2NH[f]	10.42s	4.02 m	1.92 t	-6.40 s (N-H), -3.80 m (N–CH_2–), -2.71 t (–CH_3)
Et_2NH[g]	10.27	~4.13 m[h]	~1.97 t[h]	-6.57 s (N-H), -3.90 m (N–CH_2–), -2.28 t (–CH_3)

a. Formed in situ in C_6D_6 at 20 °C unless otherwise noted; 300 MHz, integrations match appropriate assignments.

b. In equilibrium with Rh(OEP)(Cl)(H_2O).

c. Overlaps with ethyl resonances of Rh(OEP)(Cl)(H_2O).

d. The EtNpip ligand resonances are labelled according to the perspective diagram ; the tentative assignments are based on integrations, selective decoupling and chemical shifts.

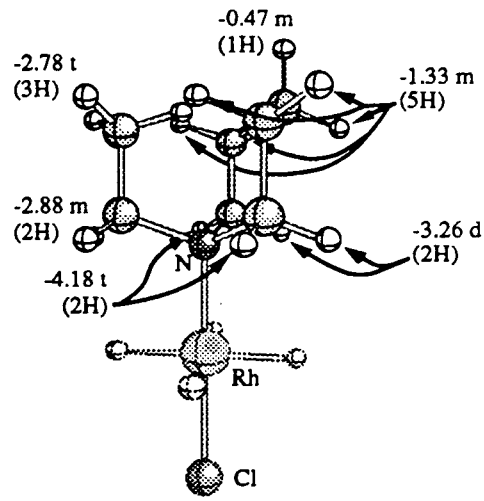

e. [Rh(OEP)]$_2$ also present.

f. Slightly temperature dependent.

g. In CD_2Cl_2, Sect. 4.2.3.

h. Overlapped by ethyl side chain resonances of other species.

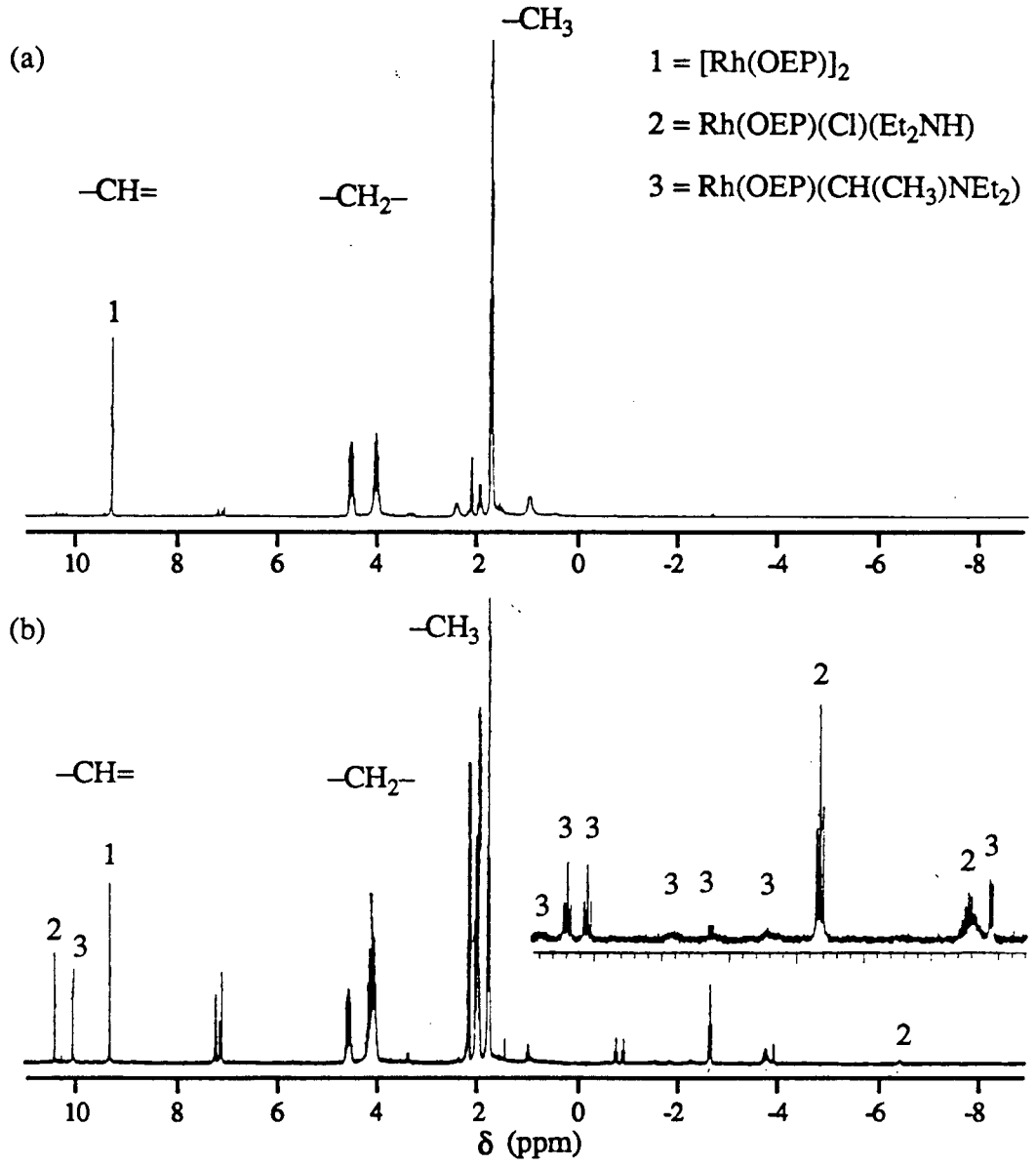

Figure 4.4. The 300 MHz ^{1}H nmr spectrum of a C_6D_6 solution of Rh(OEP)(Cl)(H_2O) (a) 15 min after addition of Et_3N and (b) 7 days later. [Rh] ≈ 8×10^{-3} M, [Et_3N] ≈ 10^{-2} M, 20 °C, in vacuo in a sealed nmr tube.

of such solutions in sealed tubes remained unchanged for periods of months implying that the above mentioned free amine was Et_3N. Samples with slightly more initial Et_3N have proportionately more Rh(OEP)(CH(Me)NEt_2) at this point.

The new complex, Rh(OEP)(CH(Me)NEt_2) is identified by selective decoupling, COSY and integration of its ^1H nmr spectrum (Fig. 4.4b, Table 4.2, Appendix E). The ligand methyl resonance at -3.96 ppm (d, 3H) is close to that of the ligand methyl resonance of Rh(OEP)(CH(Me)C_6H_5) (-4.30 ppm) (56). A COSY experiment and selective decoupling linked the doublet to a weak signal at -2.30 ppm which is assigned to the neighbouring methylene proton. The ethyl group resonances comprise two methyl resonances at ~-0.9 ppm (t, 3H) that are each coupled to one of two pairs of well separated (one separated by 0.27 ppm and the other by 1.69 ppm) weak resonances assigned to four non-equivalent $-CH_2-$ protons of the ethyl groups. The large range of $-CH_2-$ proton shifts suggests that steric congestion of the ethyl groups with each other, the β-methyl, and the porphyrin plane are greater for this ligand than the steric interactions within the Et_2NH ligand of Rh(OEP)(Cl)(Et_2NH), but the triplet nature of the associated methyl resonances indicates that sufficient ligand motion still remains to average the coupling constants. The analogous, but more sterically restricted, TMP complex has a similar ligand spectrum and will be discussed in a later section (sect. 4.2.2). A conformation where the $-CH_3$ groups of the ethyl groups are roughly equidistant from the plane of the porphyrin is suggested by their nmr shifts and a labelled model is illustrated below Table 4.2. Note that within one methylene pair ($H_{1'}$ and $H_{2'}$) the protons must be at very different distances from the porphyrin plane because they differ considerably in shift; the choice of position assigned in the diagram is arbitrary but requires that one ethyl group be canted relative to the other.

The Et_3N reaction with Rh(OEP)(Cl)(H_2O) was also monitored by visible spectroscopy under anærobic conditions. In the presence of Et_3N (1–20 equivalents), the β and α bands of Rh(OEP)(Cl)(H_2O) at 519 and 552 nm decrease in intensity and red-shift, becoming broader and less intense bands at 526 and 557 nm within ~30 min (e.g., Fig. 4.5). The band positions and apparent extinction coefficients of the spectrum after 30 min of reaction are approximately the same over the range of added Et_3N, although further small decreases in absorbance slowly occur over several hours at higher [Et_3N]. The β and α band positions and apparent ε values of the spectrum (Fig. 4.5) are not those expected for $[Rh(OEP)]_2$ (Table 3.1) which is the product expected on the basis of the nmr experiments nor do they correspond to Rh(OEP)(Cl)(Et_2NH) (Fig. 4.3). The

Table 4.2. Ligand ^{1}H nmr spectral data for Rh(OEP)(CH(Me)NEt$_2$).[a]

proton	δ	integral
$H_{2'}$	-0.61 m	1H
H_3	-0.81 t	3H
$H_{3'}$	-0.95 t	3H
$H_{2(1)}$	-1.60 m	1H
$H_{1(2)}$	-1.87 m	1H
$H_{1'}$	-2.28 m	1H
H_α	-2.30 m	1H
H_β	-3.96 d	3H

a. 300 MHz; measured in C_7D_8 solution at ~20°C; see Appendix E for details.

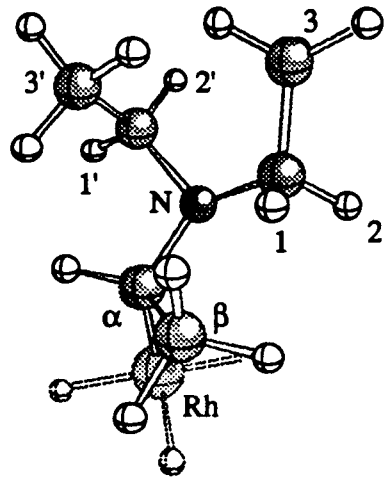

principle band in the Soret region is at 412 nm and this along with the 526 nm (β) and 557 nm (α) bands are typical of the hypso type spectra of Rh^{III} species (3,69). However, the intensity of the spectrum is decreased relative to that of the starting Rh(III) complex and bands at about 350 and 392 nm are present as expected for [Rh(OEP)]$_2$ (inset, Fig. 4.4); therefore the spectrum is believed to be the superposition of that of the Rh(II) dimer and Rh^{III}(OEP) species. A white precipitate formed during the some of the experiments when 1-2 equivalents of amine were used. This was not isolated but was most likely to be amine hydrochloride (see p. 131).

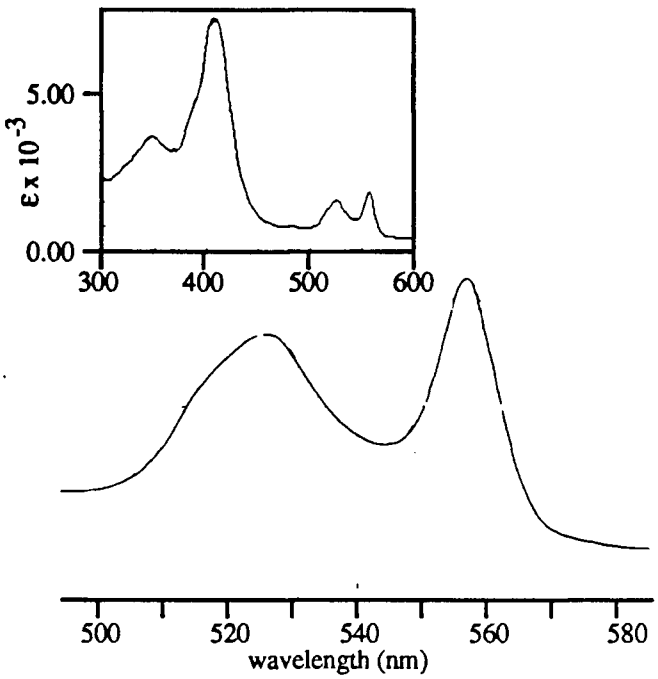

Figure 4.5. The visible spectrum of a C_6H_6 solution of Rh(OEP)(Cl)(H_2O) wth Et_3N, 30 min after the addition of Et_3N. [Rh] = [Et_3N] = 4.31×10^{-4} M, 25 °C, in vacuo.

As will be discussed in section 4.3, use of Rh(OEP)(Cl)(CH_3CN) instead of Rh(OEP)(Cl)(H_2O) or addition of excess CH_3CN slowed the initial reaction with Et_3N in C_6H_6 as monitored by visible spectroscopy but did not affect the "product" spectra appreciably.

Clearly the nmr and visible spectroscopy experiments in the absence of air do not show Rh(OEP)(Cl)(Et_2NH) as the sole or main product, so it appears that air is critical for its formation. The most likely components of air that could be important to completion of the reaction, as it was originally observed, are O_2 and H_2O, alone or in combination. However, addition of air after formation of [Rh(OEP)]$_2$, Rh(OEP)(Cl)(Et_2NH) and Rh(OEP)(CH(Me)NEt_2) does not result in formation of Rh(OEP)(Cl)(Et_2NH) as the major product. A nmr sample which was known to have equilibrated to a mixture of [Rh(OEP)]$_2$, Rh(OEP)(Cl)(Et_2NH) and Rh(OEP)(CH(Me)NEt_2) in vacuo, whose spectrum is illustrated in Figure 4.4, was opened in air and the ^1H nmr spectrum rerun (Fig 4.6). The [Rh(OEP)]$_2$ and Rh(OEP)(Cl)(Et_2NH) species are still present in roughly unchanged proportions, but the Rh(OEP)(CH(Me)NEt_2) meso proton resonance at 10.00 ppm is no longer evident. A new meso proton resonance appears at 10.21 ppm along with a number of very small signals in the meso proton region. Resonances at the positions expected for

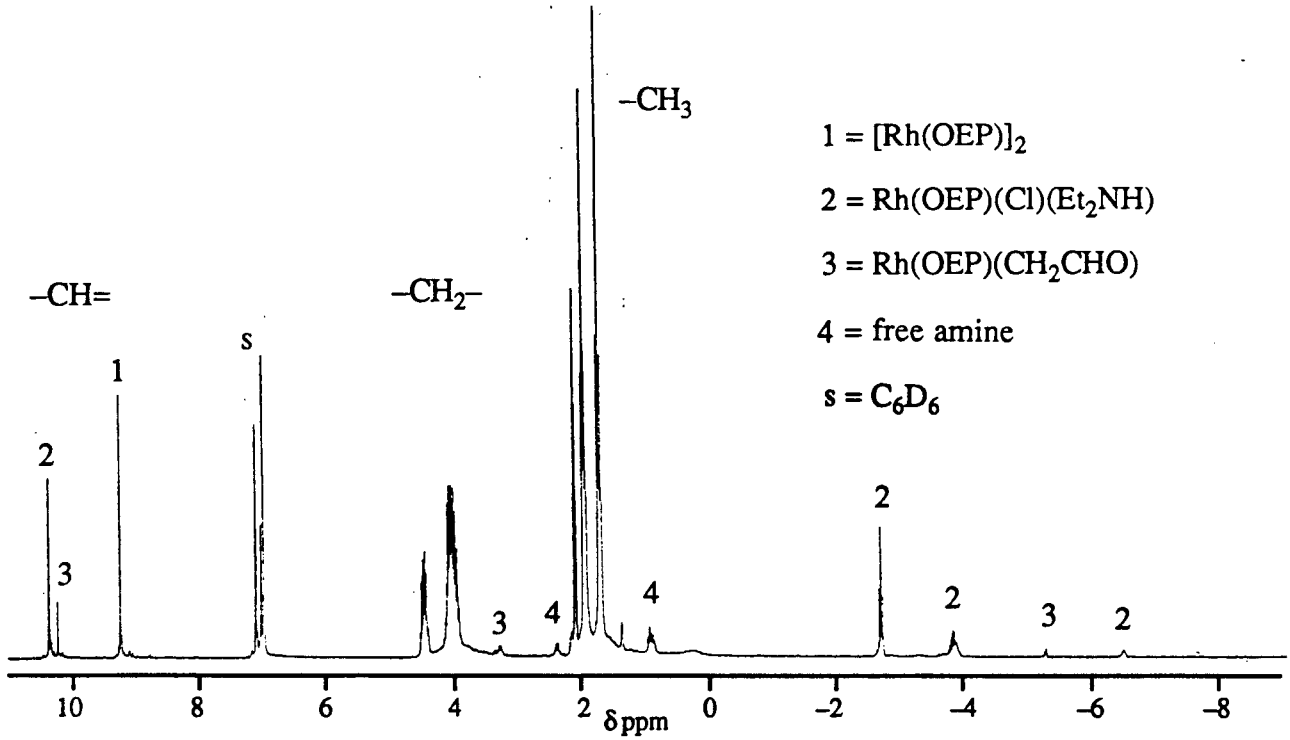

Figure 4.6. The 300 MHz ^1H nmr spectrum of the C_6D_6 solution sample illustrated in Figure 4.4, immediately after exposing to air. [Rh] ≈ 9×10^{-3} M, $[Et_3N]_o \approx 10^{-2}$ M, 20 °C, in air.

free amine (2.40, 0.99) also appear. The spectrum remains unchanged for hours. The meso resonance at 10.21 ppm and a new doublet of doublets (~2H integration, $J_{H\text{-}H} \approx J_{Rh\text{-}H} = 4.2$ Hz) at -5.22 ppm, found to be coupled to another triplet (~1H integration) at 3.35 ppm, are assigned as Rh(OEP)(CH_2CHO). The β-aldehyde complex has previously been isolated from the reaction of $[RhOEP]_2$ with CH_2=CH-OEt in C_6H_6 (149); the ligand resonances in $CDCl_3$ solution are reported to be 2.90 ppm (t , CHO, $J_{H\text{-}H} = 5$ Hz) and -5.55 ppm (dd, Rh-CH_2-, $J_{Rh\text{-}H} = 4$ Hz). Note that Rh(OEP)(CH_2CHO) resonances are also present in the spectrum illustrated in Figure 4.2.

Similar results are obtained using O_2, in the presence of added H_2O, instead of air. Adding deoxygenated water to an equilibrated sample, under Ar in a septum capped nmr tube, of similar composition to that whose spectrum is shown in Figure 4.4 results in no changes in the ^1H nmr spectrum except for the appearance of H_2O resonances. Sweeping the Ar atmosphere out with O_2 and shaking the sample result in the rapid removal of Rh(OEP)(CH(Me)NEt_2) and the

appearance of Rh(OEP)(CH_2CHO) while the resonances of [Rh(OEP)]$_2$ and Rh(OEP)(Cl)(Et_2NH) appear unchanged, just as observed for the samples exposed to air. New, broad resonances at -2.1 and -2.9 ppm are also observed and are attributed to free amine exchanging with amine bound to a Rh(OEP) species. The species in question is believed to be Rh(OEP)(CH_2CHO)(amine), because the -CHO proton resonance couplings were not resolved due to broadening and such exchange is observed for the TMP complex (see below). When the sample was checked 1 month later [Rh(OEP)]$_2$ is not present but Rh(OEP)(Cl)(Et_2NH) and Rh(OEP)(CH_2CHO) were still present in roughly unchanged proportions.

In contrast, exposure of a C_6D_6 solution containing [Rh(OEP)]$_2$, Rh(OEP)(Cl)(Et_2NH) and Rh(OEP)(CH(Me)NEt_2) to dry O_2 alone (i.e., with H_2O only from Rh(OEP)(Cl)(H_2O)·H_2O), results in the immediate consumption of [RhOEP]$_2$ as well as the Rh(OEP)(CH(Me)NEt_2) species. The only Rh(OEP) products, observed by nmr spectroscopy, are Rh(OEP)(Cl)(Et_2NH) and Rh(OEP)(CH_2CHO). Again some amine appeared to be exchanging with Rh(OEP)(CH_2CHO). When the sample was checked one month later, Rh(OEP)(Cl)(Et_2NH) and Rh(OEP)(CH_2CHO) were still present in roughly unchanged proportions.

Analogous visible spectroscopy experiments confirm the nmr observations in a limited way. If O_2 is added to a C_6H_6 solution of Rh(OEP)(Cl)(H_2O) that has been allowed to react with ~7 equivalents of Et_3N, in vacuo, for ~100 min (i.e., a similar extent of reaction to that illustrated by Fig. 4.5) then a new, more complex visible spectrum results (Fig. 4.7). The spectrum remains unchanged for hours, and is not changed when the sample is exposed to room light nor when 2 equivalents of Et_3N are added. The band at 552 nm is believed to be due to Rh(OEP)(Cl)(Et_2NH) (cf. Fig. 4.3) and that at 544 nm to Rh(OEP)(CH_2CHO), because the complex is reported to have an α band at 544 nm in $CHCl_3$ (150). A possible shoulder at ~390 nm on the Soret "band" at ~407 nm, illustrated in the inset of Figure 4.7, is close to the Soret of Rh(OEP)(CH_2CHO) reported at 386 nm. The shoulder at ~554 nm indicates that other species are present, perhaps Rh(OEP)(CH_2CHO)(amine). So, to the extent that Rh(OEP)(Cl)(Et_2NH) and Rh(OEP)(CH_2CHO) appear to be present, the visible experiments are consistent with the nmr data, but only at the lower ratios of [Et_3N] to [Rh]. Although a spectrum similar to the solid line in

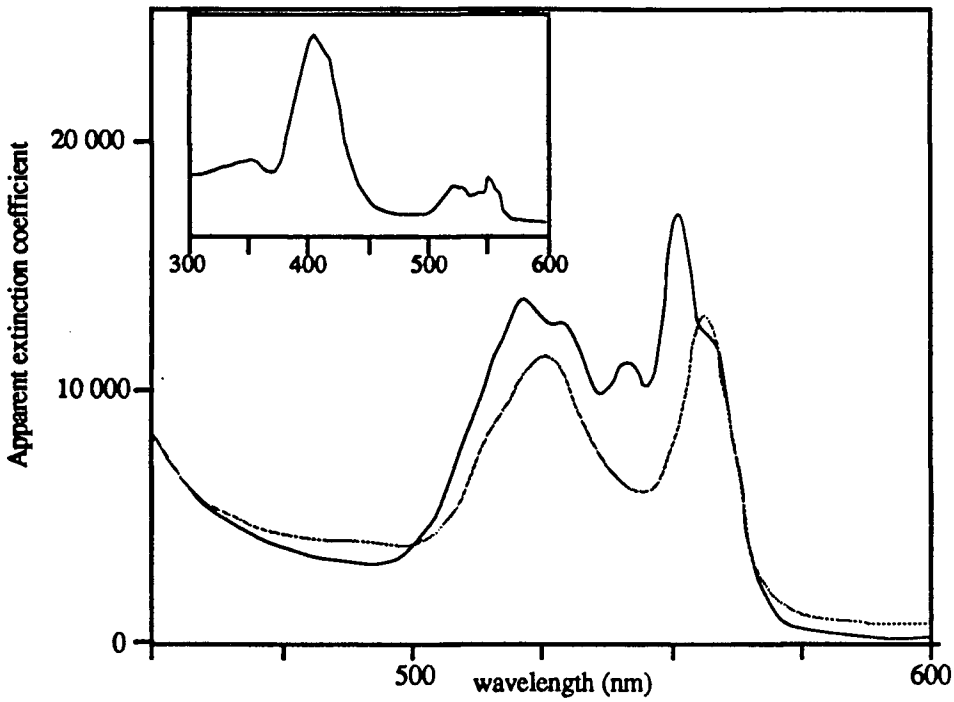

Figure 4.7. The visible spectrum of a C_6H_6 solution of (····) Rh(OEP)(Cl)(H_2O) wth Et_3N, 100 min after the addition of Et_3N and then (—) 90 min after addition of O_2. [Rh] = 4.74×10^{-4} M, $[Et_3N]_o = 3.30 \times 10^{-3}$ M, 25 °C.

Figure 4.7 is obtained for a sample with 20 equivalents of Et_3N initially added under O_2, this solution with the higher [Et_3N] is light-sensitive. Exposure to room light triggered a thermal reaction that led to a spectrum identical to that of Rh(OEP)(Cl)(Et_2NH) (i.e., Fig. 4.3) upon leaving the solution standing over-night in the dark.

In summary, the reaction of Et_3N with Rh(OEP)(Cl)(H_2O) gives products that indicate amine C-H and C-N cleavage (Rh(OEP)(CH(Me)NEt_2), Et_2NH as Rh(OEP)(Cl)(Et_2NH), and Rh(OEP)(CH_2CHO)) and net 1-electron reduction of Rh(III) to Rh(II) species ([Rh(OEP)]$_2$). The high yield of [Rh(OEP)]$_2$ using equimolar quantities of Et_3N and Rh(OEP)(Cl)(H_2O) under anærobic conditions, while available Et_3N reacts further to form Rh(OEP)(CH(Me)NEt_2), indicates a Et_3N:Rh(III) stoichiometry of < 1:1 for the reduction. The reduction reaction is slow in the presence of a competing donor ligand (CH_3CN) implying coordination of Et_3N is required for reduction. In fact, subsequent coordination of Et_2NH to form Rh(OEP)(Cl)(Et_2NH) probably prevents dealkylation catalysis under the conditions used.

The results also show that there is a requirement for an oxidant (i.e., air or O_2) to produce at least some of the C-N cleavage products, but that oxidation *after* formation of Rh(OEP)(CH(Me)NEt_2) does not always lead to the same products as when air is present initially during the reaction of Et_3N with Rh(OEP)(Cl)(H_2O). The stability of Rh(OEP)(CH(Me)NEt_2) in the presence of H_2O implies that the O atom in the Rh(OEP)(CH_2CHO) species is from the added O_2.

The effect of excess H_2O on the fate of [Rh(OEP)]$_2$, in the presence of O_2, during the conversion of Rh(OEP)(CH(Me)NEt_2) to Rh(OEP)(CH_2CHO), is marked but not easily rationalisable. The [Rh(OEP)]$_2$ dimer is known to be stable to O_2 (cf. Chapter 3) but the TPP dimer is reported to react with dry O_2 in toluene to form Rh(TPP)(O_2) (42,151).

4.2.2. Amine reaction with Rh(TMP)(Cl)(L) in benzene or toluene

The [Rh(OEP)]$_2$ dimer is the product of the reaction of some tertiary amines with Rh(OEP)(Cl)(H_2O). However, a [Rh(TMP)]$_2$ dimer is not expected to form because the steric interactions of the ortho-methyl groups of TMP would prevent a close approach to form a Rh-Rh bond, and indeed the reaction of Et_3N with Rh(TMP)(Cl)(iPrOH) intially differs from that with the OEP complex.

Unlike Rh(OEP)(Cl)(H_2O), the TMP complex reacted very slowly in a redox process with Et_3N in benzene under air, taking days rather than hours. The ^1H nmr spectrum of a C_6D_6 solution of Rh(TMP)(Cl)(iPrOH) 10 min after addition of ~2 equivalents of Et_3N is shown in Figure 4.8a. A Rh(TMP)(Cl)(Et_3N) complex is formed initially, but most of its ^1H nmr resonances are broadened because of exchange processes, particularily the ortho-methyl proton resonances at ~2.52 and ~1.5 ppm and the resonances up-field of TMS at about -1.6 and -2.4 ppm due to a single coordinated Et_3N. The assignments (Table 4.3) in the illustration are made using VT nmr data, and are consistent with a diamagnetic complex, asymmetrically substituted with regard to the porphyrin plane. The large difference between the ortho-methyl resonances of the TMP ligand (1.05 ppm at -14 °C) reflect the steric bulk of the Et_3N ligand relative to the trans Cl^-. Comparably large separations of 0.914, 1.189 and 0.950 ppm were also observed for Rh(TMP)(Cl)(PPh_3), Rh(TMP)(Cl)(P^nBu_3) (Table B.1) and "Rh(TMP)(Cl)(C_7D_8)" (Table 2.7).

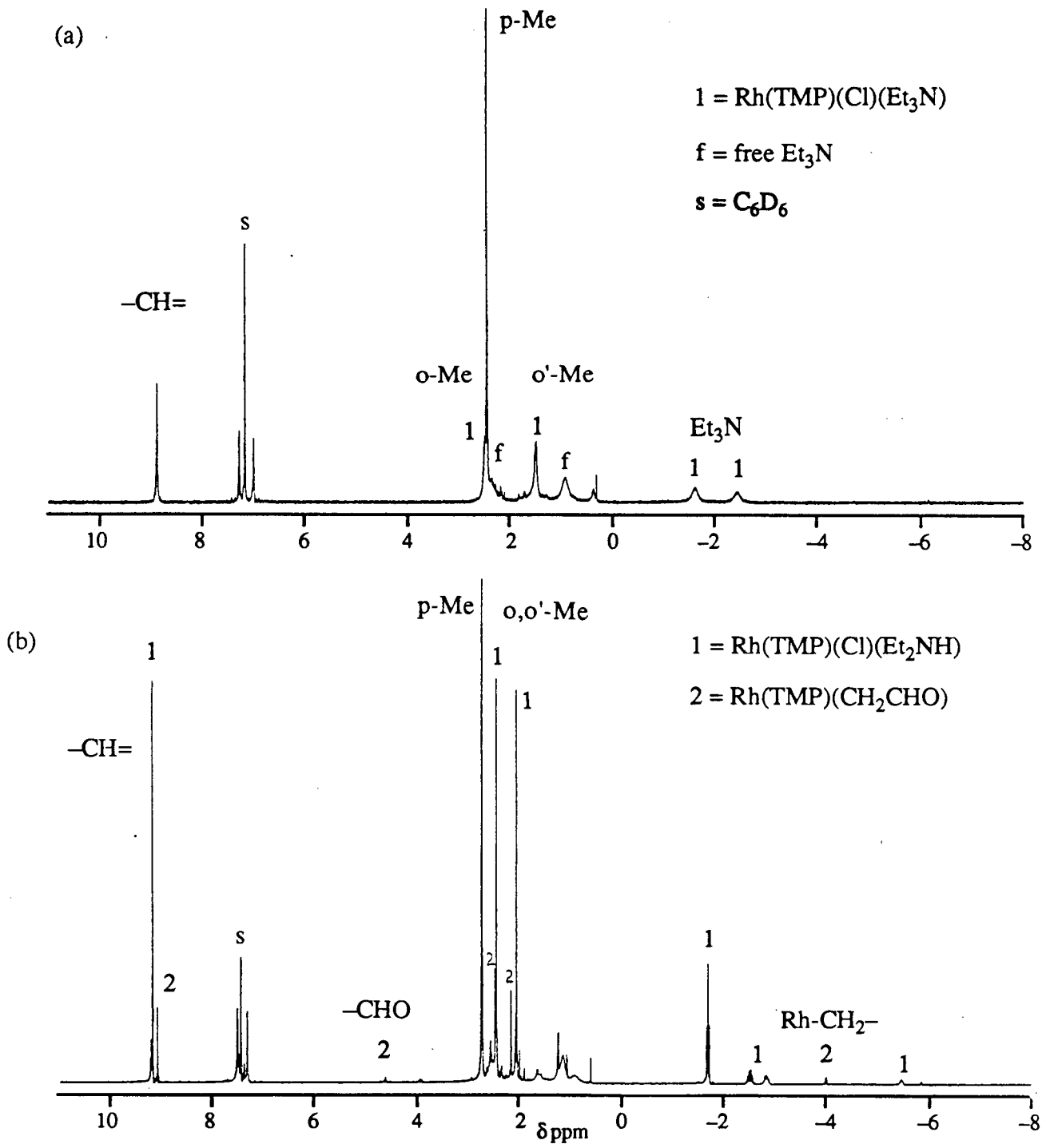

Figure 4.8. The 300 MHz ^1H nmr spectrum of a C_6D_6 solution of Rh(TMP)(Cl)(iPrOH) (a) 10 min after addition of Et_3N and (b) 3.5 days later. [Rh] ≈ 4×10^{-3} M, [Et_3N] ≈ 8×10^{-3} M, at 20 °C, in air.

Table 4.3. The ^1H NMR spectral data for various Rh(TMP) complexes in C_6H_6 or C_7D_8.[a]

complex	–CH=	m,m'-H	p-CH_3	o,o'-CH_3	other
Rh(TMP)(Cl)(Et_3N)[b]	8.79	7.27, 6.97	2.50	2.46, 1.45	-1.69 t (-CH_3), -2.51 q (–CH_2–)
Rh(TMP)(Cl)(Et_2NH)[c]	8.87	7.22, 7.03	2.44	2.16, 1.77	-1.99 t (-CH_3), -2.80 m (–CH_2–), -3.12 m (-CH_2–), -5.80 ppm s (NH)
Rh(TMP)(CH_2CHO)[c]	8.77	d	2.50[d]	2.18, 1.87	-4.29 dd (–CH_2–), 4.32 t (–CHO)

a. At 20 °C, unless otherwise noted; 300 MHz; all singlets unless noted otherwise; integrations match assignments.

b. In situ in C_7D_8, at -14 °C.

c. In situ in C_6D_6.

d. Obscured by resonances of Rh(TMP)(Cl)(Et_2NH).

Very little change occurs in the ^1H nmr spectrum over the next hour but after 3.5 days the spectrum in Figure 4.8b is observed. The principle species seen is Rh(TMP)(Cl)(Et_2NH) with some Rh(TMP)(CH_2CHO) as a minor product. The resonances of Rh(TMP)(Cl)(Et_2NH) (Table 4.3) are assigned by comparison to that of the complex rapidly formed in situ by the addition of 3 equivalents of Et_2NH to Rh(TMP)(Cl)(iPrOH). The diamagnetic complex has two ortho-methyl resonances at 2.16 and 1.77 ppm indicative of non-symmetric substitution with regard to the porphyrin plane. Coordination of one Et_2NH ligand is shown by the up-field shift of the Et_2NH resonances from their normal positions due to the ring-current of TMP. The ligand assignments: -1.99 (t, 6H, -CH_3), -2.80 and -3.12 (2 m, 4H, -CH_2-) and -5.80 ppm (s, 1H, NH) are similar to those of the OEP congener (sect. 4.2.1). The wider separation of the –CH_2– resonances (0.32 ppm) of the Et_2NH ligand of the TMP complex compared to those of the OEP complex (overlapped; Fig. 4.1) reflects the greater steric hindrance caused by the ortho-methyl groups of TMP. The multiplet at -2.80 ppm has a smaller coupling constant to NH indicating that it is the resonance of the methylene proton cis to the NH proton. The methyl resonances of the displaced iPrOH are overlapped by broadened free Et_3N resonances at ~1.2 ppm, but the septet (5 lines

detected) methine proton resonance is at 3.68 ppm. The assignments, established by selective decoupling, for the β-aldehyde ligand of Rh(TMP)(CH_2CHO) (Table 4.3) are similar to those of the OEP congener; the difference of the ortho-methyl proton resonances of TMP is relatively small (0.31 ppm).

The ærobic Et_3N reaction was also followed by uv-vis in C_6H_6 but very little redox change was seen in the first hour, consistent with the nmr experiments. The β and α bands of Rh(TMP)(Cl)(iPrOH) at 531 and 562 nm are instantly replaced by new bands at 536 and 569 nm, and this spectrum is essentially unchanged for hours. A similar spectrum is obtained from addition of Et_2NH to Rh(TMP)(Cl)(iPrOH) in C_6H_6. If the spectrum of Rh(TMP)(Cl)(Et_3N) is similar to that of Rh(TMP)(Cl)(Et_2NH), which is likely, then the initial change is consistent with formation of Rh(TMP)(Cl)(Et_3N).

When the reaction of Rh(TMP)(Cl)(iPrOH) with 1.4 – 3.5 equivalent of Et_3N under dry, anærobic conditions in C_6D_6 or C_7D_8 is examined by ^1H nmr a few minutes after addition of Et_3N, the spectra show broadened resonances like the previously discussed experiment in air. When the sample is examined one day later, the Rh(TMP)(Cl)(Et_3N) resonances are completely replaced by resonances of several new complexes indicated by the multiple pyrrole proton resonances at ~8.6 ppm (Fig. 4.9), and the principal complex is believed to be Rh(TMP)(CH(Me)NEt_2). The pattern of the ligand resonances is similar to that of Rh(OEP)(CH(Me)NEt_2) but shifted down-field by 0.55 – 0.88 ppm (Table 4.4) and is readily assigned by selective decoupling. The pyrrole proton is at 8.54 ppm, the para-methyl protons at ca. 2.96 ppm, and the inequivalent ortho-methyls at 2.35 and 1.64 ppm.

A smaller amount of Rh(TMP)(Cl)(Et_2NH) was also present in this day-old solution and a number of unidentified complexes were present in minor amounts. The identity of the other major species which has a "pyrrole" resonance at 8.53 ppm has not been solved. At longer times, less of this complex is present. Pairs of ortho-methyl resonances (12 H each) can be found for Rh(TMP)(Cl)(Et_2NH) and Rh(TMP)(CH(Me)NEt_2) in the spectrum illustrated in Figure 4.9. A singlet at 1.99 ppm of ~ 24 H intensity (o-Me) relative to the 8 H resonance at 8.53 ppm can also be found, suggesting a symmetrical (D_{4h}) complex; however this single resonance is a

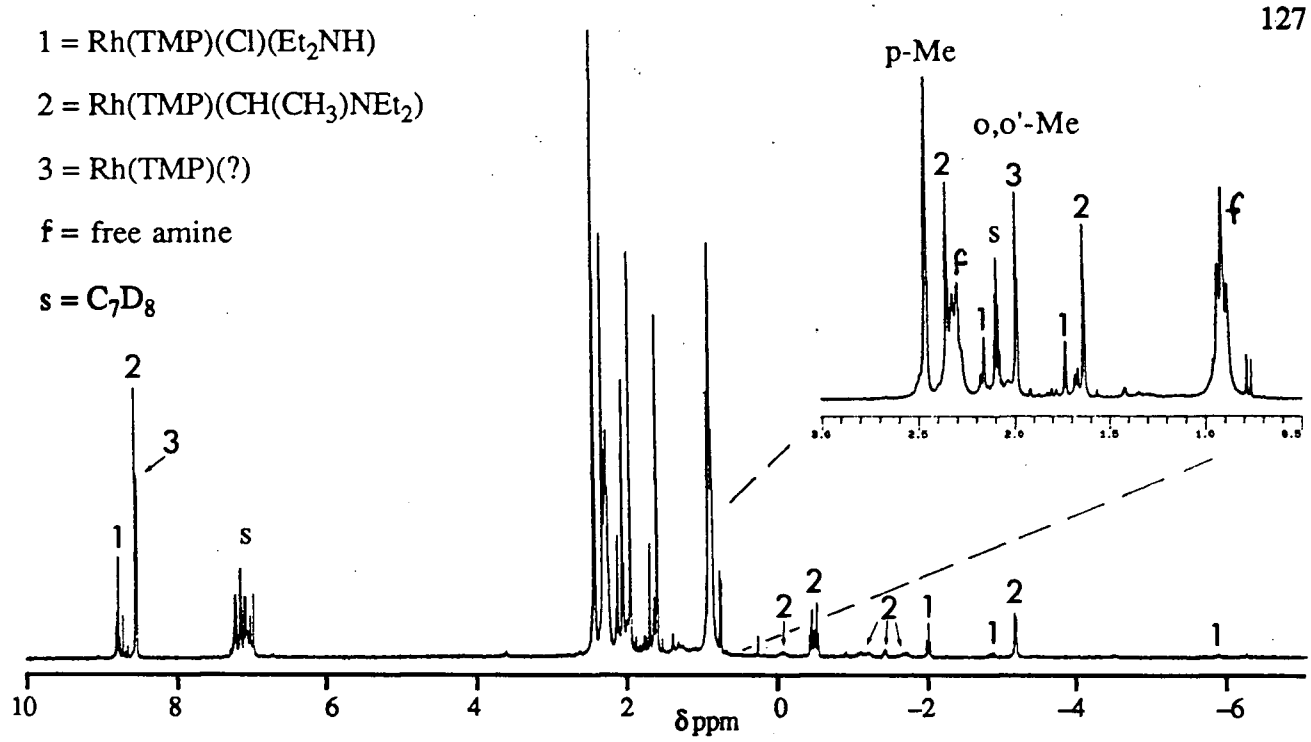

Figure 4.9. The 300 MHz ^1H nmr spectrum of a C_7D_8 solution of Rh(TMP)(Cl)(iPrOH) 1 day after addition of Et_3N. [Rh] ≈ 3×10^{-3} M, [Et_3N] ≈ 1×10^{-2} M, at 18 °C, sealed in vacuo.

Table 4.4 Ligand ^1H nmr spectral data for Rh(TMP)(CH(Me)NEt_2).[a]

proton	δ(ppm)	integral
$H_{2'}$	-0.06 m	1H
H_3	-0.44 t	3H
$H_{3'}$	-0.51 t	3H
$H_{2(1)}$	-1.08 m	1H
$H_{1(2)}$	-1.17 m	1H
H_α	-1.40 m	1H
$H_{1'}$	-1.66 m	1H
H_β	-3.12 d	3H

a. 300 MHz; measured in C_7D_8 solution at ca. 20°C; the labels are the same as in Table 4.2.

consequence of two coincident temperature-dependent signals. A variable temperature experiment on a similar sample revealed that the resonances of the "symmetric" complex are very temperature-dependent in comparison to the other two major Rh species resonances which are comparatively invariant. The same, perhaps paramagnetic, species is found in small amounts immediately after addition of Et_3N. The combined ortho-methyl resonance region data for the species are plotted in Figure 4.10. Fitting straight lines to the two sets of data using a linear least squares calculation indicates that the two resonances became coincident at ~19 °C, about the same temperature that the data of Figure 4.9 were collected. Unfortunately only three resonances are discernable, others likely being obscured by more intense signals. In particular, para-methyl resonances of different complexes are often nearly coincident. The variations with temperature could be accounted for by chemical exchange, although within the context of this thesis, such a 'crossing' of TMP ortho-methyl resonances of the same complex is never observed. Para-magnetism is a real possibility because Rh^{II} species are clearly involved (i.e., in the OEP system) and a diamagnetic $[Rh(por)]_2$ complex is unlikely for por = TMP^{2-}. A likely possibility is *monomeric* $Rh^{II}(TMP)$, but the detailed assignments cannot be made on the basis of the limited data.

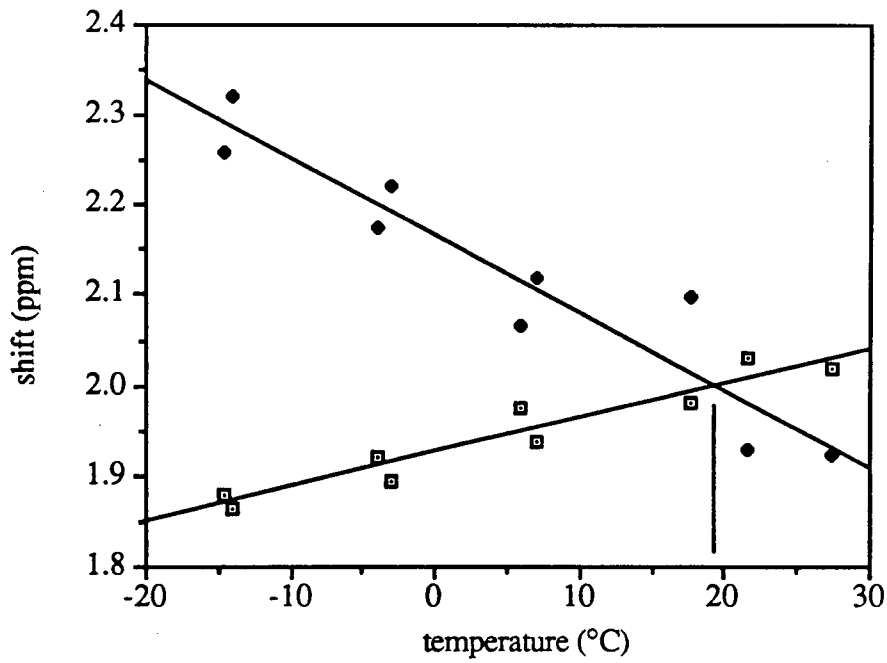

Figure 4.10. Plot of the ^1H nmr shifts of the ortho-methyls of the unknown complex vs. temperature. (◆) o-H, (▫) o'-H.

The visible spectra of the nmr solutions containing mixtures of Rh(TMP)(Cl)(Et_2NH) and Rh(TMP)(CH(Me)NEt_2), just described, show two maxima probably corresponding to two overlapped β bands. The one at 536 nm is the same as that previously obtained for Rh(TMP)(Cl)(Et_2NH), formed in situ from Et_2NH and Rh(TMP)(Cl)(iPrOH); a broader band at ~520 nm presumably belongs to Rh(TMP)(CH(CH_3)NEt_2).

Addition of O_2 to a "day-old" nmr sample containing principally Rh(TMP)(CH(CH_3)NEt_2) and Rh(TMP)(Cl)(Et_2NH) causes an immediate disappearance of the resonances of Rh(TMP)(CH(Me)NEt_2) and putative Rh^{II} species from the ^1H nmr spectrum (Fig. 4.11). A species whose resonances are close to those of Rh(TMP)(CH_2CHO) (Table 4.3), and is in the same relative proportion to the total Rh as was Rh(TMP)(CH(Me)NEt_2) before addition of O_2, can be found in the new spectrum, and resonances of coordinated Et_3N are at -1.74 (t, -CH_3) and -2.40 (q, -CH_2-). The integration of the Et_2NH ligand resonances is more than can be accounted for by just Rh(TMP)(Cl)(Et_2NH), but the coordinated Et_2NH and Et_3N resonances together are approximately equivalent to the total equivalents of RhTMP(Cl)(Et_2NH) plus the "Rh(TMP)(CH_2CHO)" species (assigning the 8.67 ppm peak to the latter). On this basis, the "Rh(TMP)(CH_2CHO)" species is a mixture of Rh(TMP)(CH_2CHO)(Et_3N) (~30%) and Rh(TMP)(CH_2CHO)(Et_2NH) (~70%). The resonances of the -CH_2CHO ligand are broadened and the couplings not resolved, consistent with some degree of exchange, probably with Et_3N and Et_2NH as ligands, resulting in only an average pyrrole resonance for the two complexes. In confirmation, careful examination of the resonances of the coordinated Et_2NH revealed 2 sets of resonances, the new set slightly offset from those of Rh(TMP)(Cl)(Et_2NH). The resonances at 2.25 and 1.88 ppm are assigned to the ortho-methyl protons of the Rh(TMP)(CH_2CHO)(Et_2NH) complex and those of the Et_3N complex at ca. 2.48 (partially obscured by para-methyl proton resonances) and 1.64 ppm. At least 3 other minor species account for ~38% of the total Rh, based on pyrrole integration, and a number of resonances up-field of TMS are seen but not assignable at present.

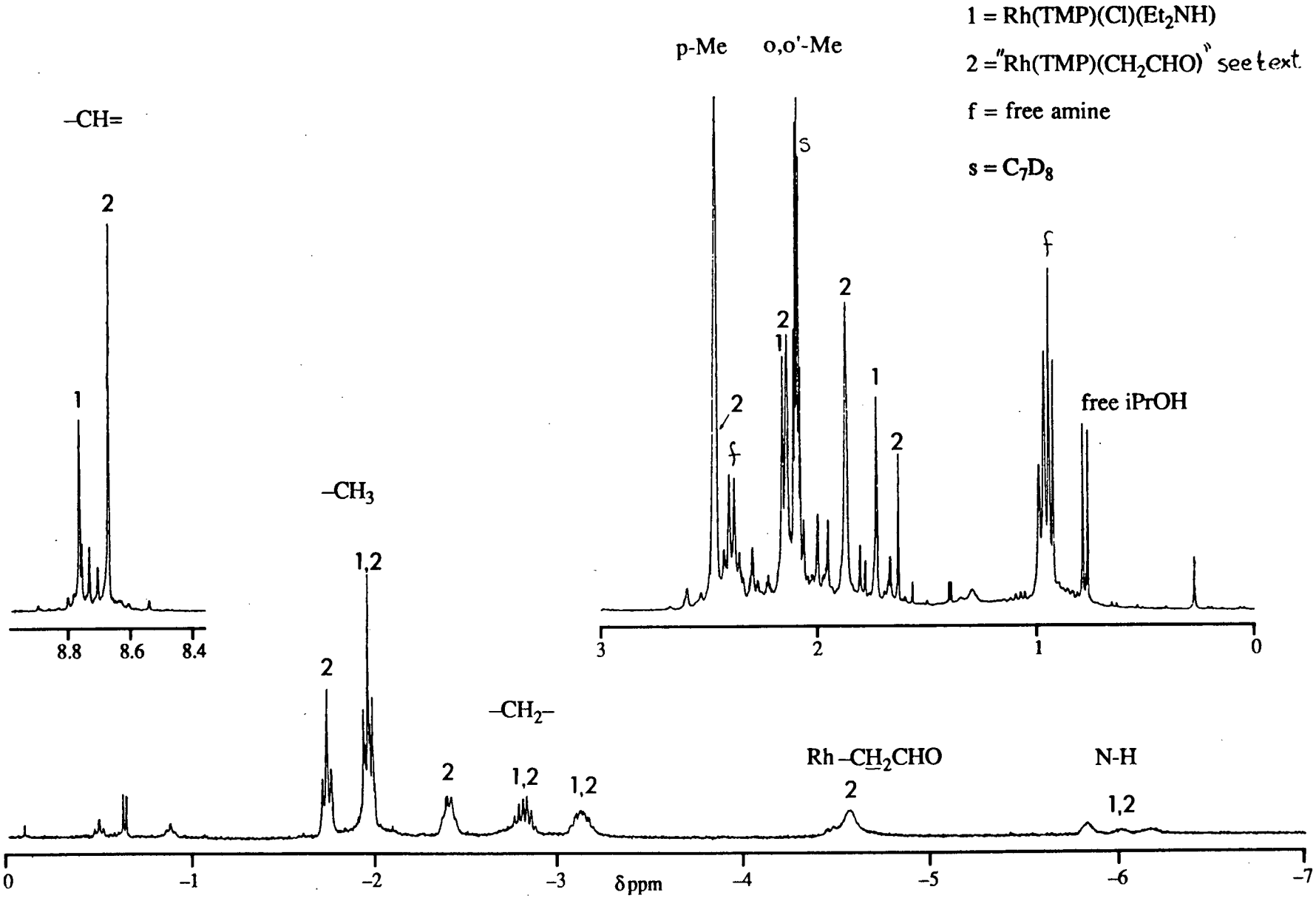

Figure. 4.11. The 300 MHz ^1H nmr spectrum of a C_7D_8 solution of Rh(TMP)(Cl)(iPrOH) with Et_3N, after addition of O_2. [Rh] ≈ 3×10^{-3} M, [Et_3N] ≈ 1×10^{-2} M, at 18 °C.

In summary, the reaction of Et_3N with Rh(TMP)(Cl)(iPrOH) or Rh(OEP)(Cl)(H_2O) leads to the same products (ignoring the minor species for the present) with the notable exception of a dimeric Rh(II) species being found only in the reaction with the OEP system. Also, the initial Et_3N redox reaction with Rh(TMP)(Cl)(iPrOH) is slower than with the OEP analogue at similar stoichiometries and concentrations, but the difference is not due to rate-limiting dissociation of iPrOH because Rh(TMP)(Cl)(Et_3N) rapidly forms and both the TMP and OEP complexes rapidly form Rh(por)(Cl)(Et_2NH). The redox reaction of Rh(OEP)(Cl)(H_2O) with Et_3N is rapid but is inhibited by CH_3CN, the implication being that coordination of Et_3N is required for the reduction to occur. These observations support the TMP ligand inhibition of the formation of a Rh-Rh metal-bonded species and also lead to the idea that under anærobic conditions the reduction of Rh(III) to Rh(II) involves equilibrium processes that lie to the Rh(II) side in the OEP case because of the formation of $[Rh(OEP)]_2$. A possible reaction sequence is shown by reactions (4.1–4.4).

$$Rh^{III}(por)(Cl)(L) + Et_3N \rightleftharpoons Rh^{III}(por)(Cl)(Et_3N) + L \qquad (4.1)$$

$$Rh^{III}(por)(Cl)(Et_3N) \rightleftharpoons Rh^{II}(por) + Et_2N\dot{C}HCH_3 + HCl \qquad (4.2)$$

$$Rh^{III}(por)(Cl)(L) + Et_2N\dot{C}HCH_3 \rightleftharpoons Rh^{II}(por) + Et_2NCH{=}CH_2 + HCl \qquad (4.3)$$

$$2\ Rh^{II}(OEP) \rightleftharpoons [Rh(OEP)]_2 \qquad (4.4)$$

The HCl produced by reactions 4.2 and 4.3 is mopped up by the amines present.

There is only weak evidence for the presence of a small amount of a Rh^{II}(TMP) species. The enamine produced in reaction 4.3 can be cleaved by HCl or H_2O to produce Et_2NH (152). By implication, the formation of Rh(por)(CH(Me)NEt_2) is via an initial H-atom abstraction from Et_3N by monomeric Rh^{II}(por) species, which are in low concentration in both the TMP and OEP systems (reaction 4.5 and 4.6). The hydride species has not been detected, even during the low-temperature nmr experiments and so is presumed to react with amine via Rh^{II}(por). Indeed, the reaction of Et_3N with Rh(OEP)(H) in CD_2Cl_2 is observed by ^1H nmr to give rapidly a product whose nmr spectrum is similar to that of Rh(OEP)(CD_2Cl) which is formed by reaction of Rh(II) species with CD_2Cl_2 (sect. 4.2.3).

$$Rh^{II}(por) + Et_3N \longrightarrow Et_2N\dot{C}HCH_3 + [Rh(por)(H)] \quad (4.5)$$

$$Rh^{II}(por) + Et_2N\dot{C}HCH_3 \longrightarrow Rh(por)(CH(Me)NEt_2) \quad (4.6)$$

4.2.3. Amine reaction with Rh(OEP)(Cl)(H_2O) in CH_2Cl_2

The reaction of Et_3N with the Rh(OEP)(Cl)(H_2O) species in CH_2Cl_2 is of interest for several reasons. The solvent is more polar than benzene or toluene and it is known to react with Rh(II) porphyrin species (sect. 1.4.1) to form $Rh^{III}(por)(CH_2Cl)$. Just such a side-reaction with CH_2Cl_2 is presented in this section and the following one (sect. 4.2.4). This reactivity has also been discussed in Chapter 3, but that work actually followed on the observations described in this chapter. All the experiments using CH_2Cl_2 as solvent are under anærobic conditions, except where noted.

Reaction under anærobic conditions, and in the dark, of 1 to 2 equivalents of Et_3N with Rh(OEP)(Cl)(H_2O) can be followed by ^1H nmr in CD_2Cl_2, and Rh(OEP)(Cl)(H_2O) is seen to be completely consumed within minutes, yielding a mixture of products which underwent slower reactions, over longer periods of hours and days. The "immediate" products of a typical sample examined by ^1H nmr (Fig. 4.12) include Rh(OEP)(Cl)($CH_2CH{=}NEt_2$) in 40% yield. The nmr resonances of Rh(OEP)(Cl)($CH_2CH{=}NEt_2$) are assigned by integration, selective decoupling and by comparison to the data for the TMP analogue (sect. 4.2.4) whose ligand ethyl proton resonances are better resolved. The porphyrin ethyl side-chain resonances are overlapped by those of other species, but the meso proton resonance at 10.12 ppm (s, 4H) is typical of a diamagnetic Rh(III) species. The ligand resonances are listed in Table 4.5 and the assignments are illustrated by the diagram following the Table. The ligand is considered to be an neutral η^1-ylidic enamine such as in $RhCl_3(dmso)_2(\eta^1\text{-}CH_2CH{=}NEt_2)$ (153), and the trans-ligand is assumed to be Cl^- to balance the charge, and to be consistent with a subsequent reaction product (see below).

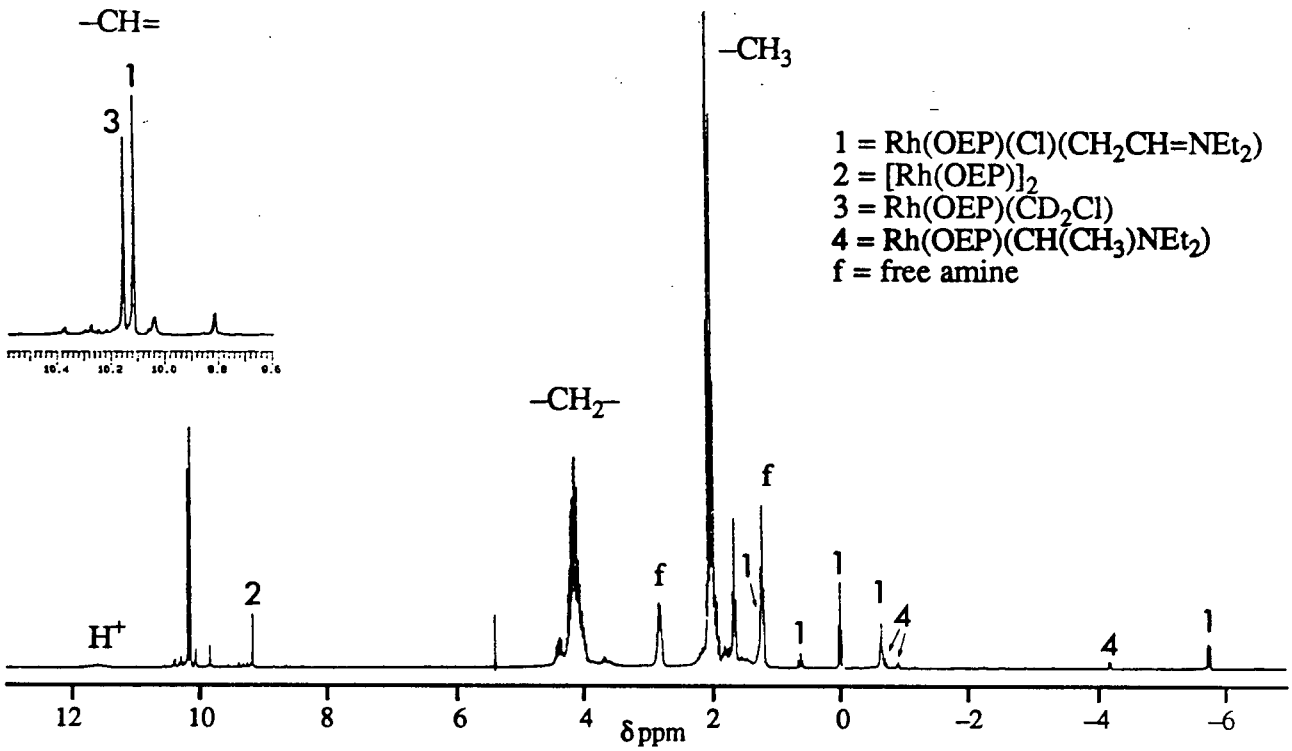

Figure 4.12. The 300 MHz ^1H nmr spectrum of a CD_2Cl_2 solution of Rh(OEP)(Cl)(H_2O) and Et_3N, 2 h after addition of Et_3N. [Rh] ≈ 8×10^{-3} M, [Et_3N] ≈ 1×10^{-2} M, at 18 °C, sealed in vacuo.

Table 4.5. Ligand ^1H nmr spectral data for Rh(OEP)(Cl)($CH_2CH{=}NEt_2$).[a]

proton	δ(ppm)	integral
$H_{3'(3)}$	1.18 t	2H
H_2	0.58 t	1H
$H_{4'(4)}$	-0.04 t	3H
$H_{3,4(3',4')}$	-0.70 m	5H
H_1	-5.81 dd	2H

a. 300 MHz; measured in CD_2Cl_2 solution at ca. 20°C.

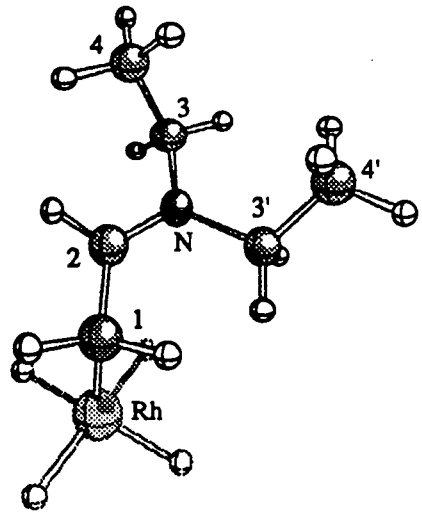

The two other initially formed major species are $[Rh(OEP)]_2$ (~5%, based on the meso proton resonance at 9.20 ppm) and another new species with a meso proton resonance at 10.15 ppm (~35%). The species associated with this resonance has no discernable ligand resonances and is believed to be $Rh(OEP)(CD_2Cl)$ by analogy to data for the TMP system (sect. 4.2.4). A very small amount of $Rh(OEP)(CH(Me)NEt_2)$ is also present, as judged by a doublet resonance at -4.2 ppm, and two triplets at ~-0.8 ppm.

Over the next few hours, the Rh^{II} dimer and the enamine complex are consumed with a concomitant increase in the relative amount of $Rh(OEP)(CD_2Cl)$ and $Rh(OEP)(Cl)(Et_2NH)$ (Table 4.1). In addition, a new meso-proton resonance (initially at 10.18 ppm) grew in as the resonances of the dimer and enamine complexes decrease. This resonance, and that of $Rh(OEP)(CD_2Cl)$ (initially at 10.15 ppm), shifted down-field over a few days to ~10.16 and ~10.12 ppm, respectively (Fig. 4.13). The new species associated with this resonance also has no discernable ligand resonances and is proposed to to be "Rh(OEP)(R)(amine)", where R is unknown, derived from the solvent because it apparently contains no protons (i.e., is probably deuterated) and the amine (Et_2NH or Et_3N) is in rapid exchange with free amine. The "free" amine resonances in the "three-day old" sample spectrum (Fig. 4.13) are at 2.36 ppm (q) and 0.75 ppm (t), the negative shift from the position of the free amine suggesting that the free amine is in rapid exchange with a Rh(por) species. Generally, Rh(OEP)(R)(L) species have labile ligands (sects. 1.4.1, 1.5.1 and 4.2.4) due to the trans effect of the alkyl group.

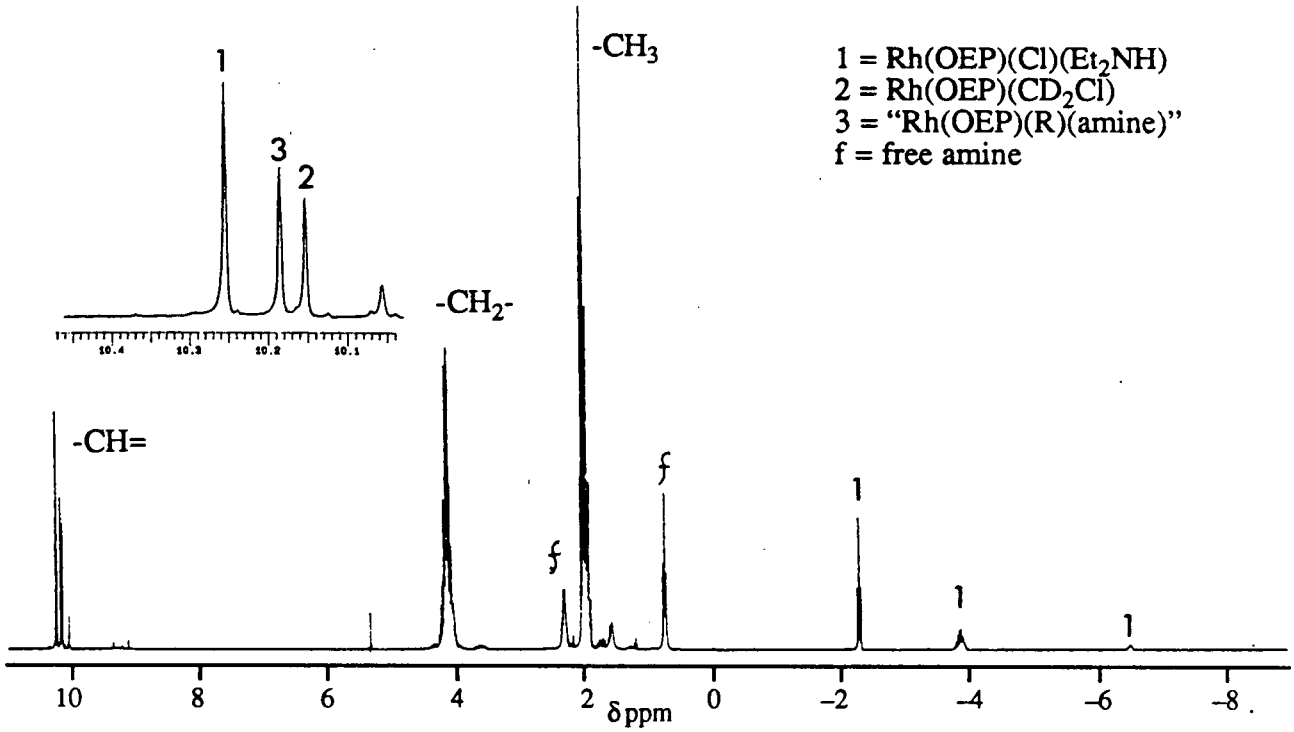

Figure 4.13. The 300 MHz ^1H nmr spectrum of a CD_2Cl_2 solution of Rh(OEP)(Cl)(H_2O) and Et_3N, 3 days after addition of Et_3N. [Rh] ≈ 8×10^{-3} M, [Et_3N] ≈ 1×10^{-2} M, at 18 °C, sealed in vacuo.

During the course of the reaction, the amine resonances shift from positions more positive than the those of free amines (Et_3N and Et_2NH) through the positions of the free amines and then to more negative values (Fig. 4.14). At the same time a broad peak moves from ~11.6 ppm to ~8.4 ppm and is probably H^+, as amine-HCl. The down-field shift of Et_3N upon protonation is documented (154). Rapid exchange of amine between the amine-HCl species and "Rh(por)(R)(amine)" in changing proportions during the course of the reaction would account for the variation of the free amine resonances and the apparent lack of amine ligand resonances for "Rh(por)(R)(amine)".

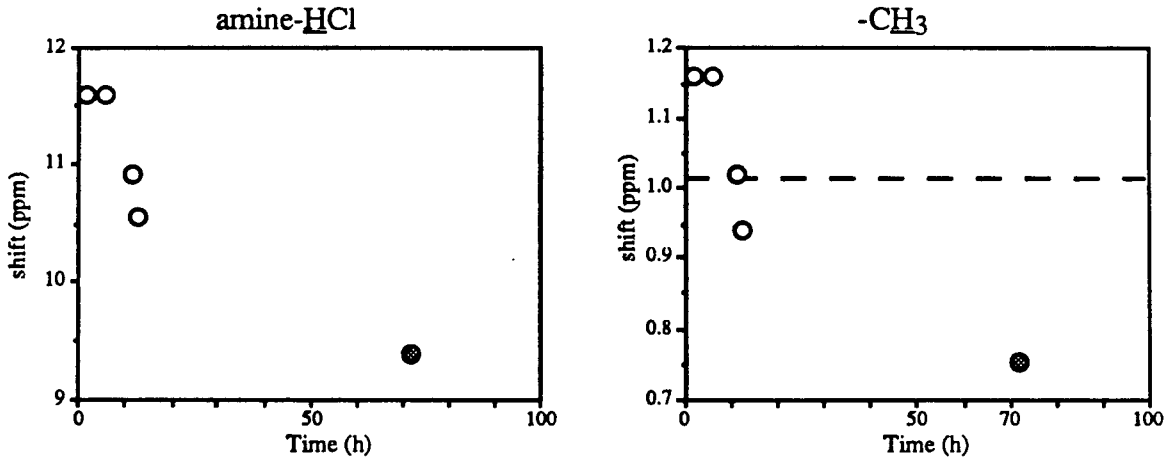

Figure 4.14. Plot of the ^1H nmr shifts of selected amine resonances: (O) run 1, (●) run 2, (- - -) average position of methyl proton resonances of Et_2NH and Et_3N. [Rh] ≈ 8×10^{-3} M, [Et_3N] ≈ 1×10^{-2} M, at 18 °C, sealed in vacuo.

4.2.4. Amine reaction with Rh(TMP)(Cl)(L) in CH_2Cl_2

In contrast to the system in aromatic solvents, Rh(TMP)(Cl)(Et_3N) is not the initial product of the reaction of Et_3N with Rh(TMP)(Cl)(iPrOH) in CD_2Cl_2 or CH_2Cl_2. The major products observed by ^1H nmr immediately after addition of ~3 equivalents of Et_3N to a CD_2Cl_2 solution of Rh(TMP)(Cl)(iPrOH), under anærobic conditions, are (e.g., Fig. 4.15): Rh(TMP)(CD_2Cl) (or Rh(TMP)(CH_2Cl)) in 30 to 50 % yield, Rh(TMP)(Cl)($CH_2CH{=}NEt_2$) in 20 to 30% yield, and that of Rh(TMP)(CH(Me)NEt_2) in 8 to 20%, based on nmr integration of the pyrrole resonances. Other products included Rh(TMP)(Cl)($CH_2CH{=}N(H)Et$) and [Rh(TMP)(Et_3N)(Et_2NH)]$^+$ (see below). The porphyrin ligand assignments are in Table 4.6 and are based on correlations from many different experiments and extents of reaction. The nmr based yields were variable from sample to sample but the ratios of the complexes to each other were always similar. The variability was traced to the presence of other pyrrole resonances overlapping the major peaks at ca 8.5 ppm. These could total as much as 36% yield. Realistically the major product yields are considered to be at the low end of the reported ranges.

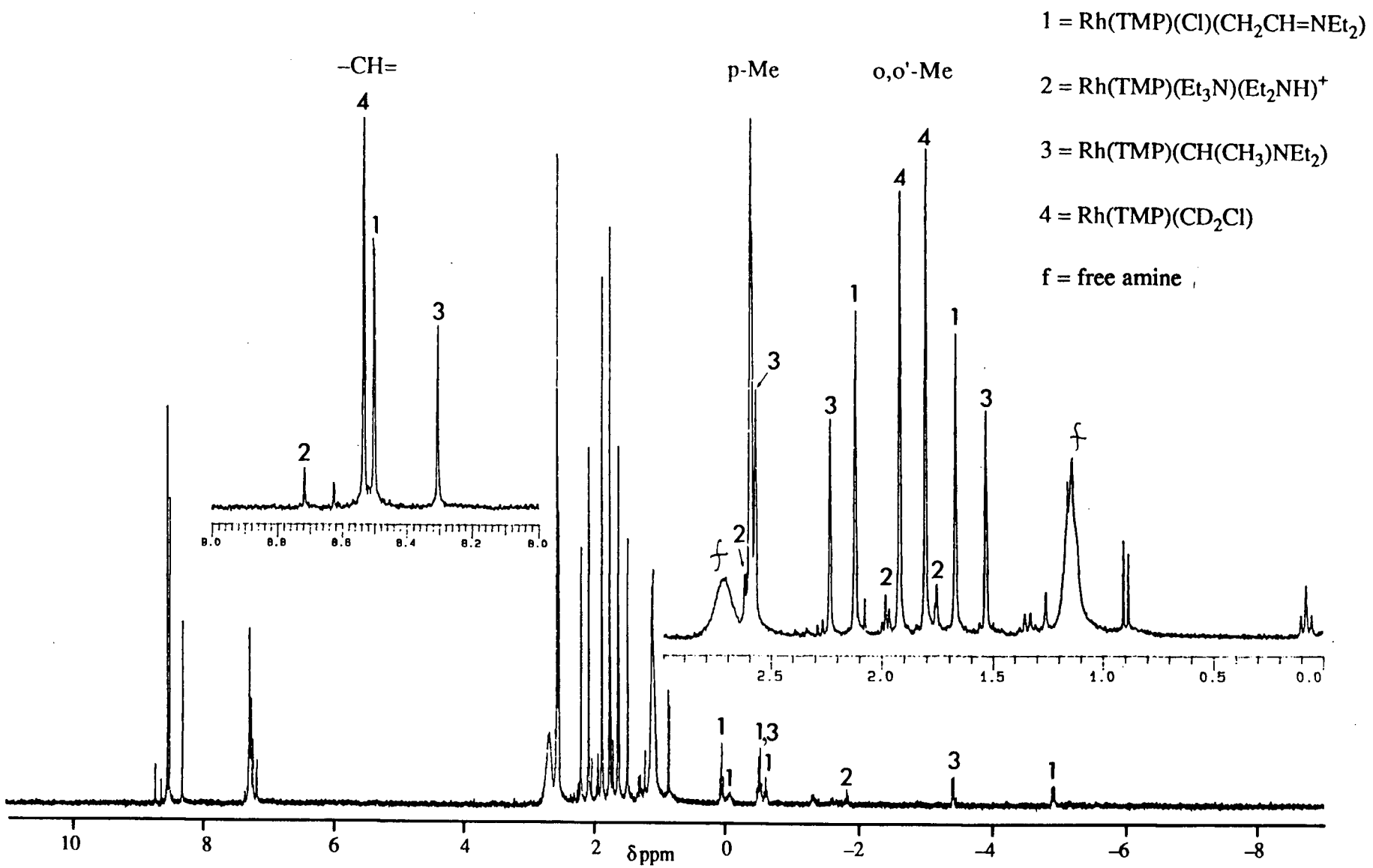

Figure 4.15. The 300 MHz ^{1}H nmr spectrum of a CD_2Cl_2 solution of Rh(TMP)(Cl)(iPrOH) and Et_3N, 10 min after thawing a sample frozen in liquid nitrogen. [Rh] ≈ 3.8×10^{-3} M, [Et_3N] ≈ 1×10^{-2} M, at 18 °C, sealed in vacuo.

Table 4.6. The ^1H NMR spectral data for various Rh(TMP) complexes in the ^1H nmr spectrum ilustrated in Fig. 4.15.[a]

complex	–CH=	m,m'-H[b]	p-CH_3	o,o'-CH_3	other
Rh(TMP)(CD_2Cl)	8.53	-	2.60[c]	1.92, 1.81	
Rh(TMP)(Cl)($CH_2CH{=}NEt_2$)	8.50	-	2.60[c]	2.12, 1.67	[d]
Rh(TMP)($CH(Me)NEt_2$)[e]	8.31	-	2.57	2.23, 1.53	-3.39 d (H_β), -1.30 m (H_α), -0.60 t (H_3), ~-0.5 t ($H_{3'}$)[c]
Rh(TMP)(Cl)($CH_2CH{=}N(H)Et$)[f]	8.63	-	-		-5.17 dd (Rh–CH_2–)
[Rh(TMP)(Et_3N)(Et_2NH)]$^+$	8.73	-	2.62	2.00, 1.77	Et_3N: -1.66 t (–CH_3), -2.33 q (–CH_2–) Et_2NH: -1.82 t (–CH_3), -2.91/-3.15 m (-CH_2), -6.31 s (NH)

a. In situ at 300 MHz; all singlets unless noted otherwise; integrations match assignments.
b. The resonances of all the complexes overlap at ~7.3 ppm.
c. Resonances overlapped by those of other species.
d. Ligand assignments listed in Table 4.7.
e. See Table 4.4 for labelling.
f. Partial assignment only.

The assignment of the Rh(TMP)(CD_2Cl) and Rh(TMP)(CH_2Cl) resonances is based on comparison of their nmr spectra in CD_2Cl_2 and CH_2Cl_2 . A resonance at -2.72 ppm is observed in the nmr specturm of the sample in CH_2Cl_2 but is absent in that of the deuterated sample; this -2.72 resonance is assigned as the "-CH_2Cl" ligand fragment (cf., sect. 3.2.2.1.1.). The same ligand resonance of Rh(TPP)(CH_2Cl)(py-d_5) is reported to be at -2.82 ppm (100). The $^2J_{Rh\text{-}H}$ coupling is not observed because the ligand site trans to -CH_2Cl in Rh(TMP)(CH_2Cl) is occupied by Et_3N, or Et_2NH, which is in exchange with free amine. This was apparent from low temperature nmr spectra obtained at longer reaction times but not always apparent at short reaction times (see later discussion). The porphyrin ligand assignments are given in Table 4.6.

The assignments of the ligand resonances for Rh(TMP)(Cl)($CH_2CH{=}NEt_2$) are based on integration and selective decoupling and are listed in Table 4.7, using the same labelling as shown in the diagram attached to Table 4.5. The porphyrin assignments are given in Table 4.6.

During the course of the decoupling experiments on the enamine ligand, a nearly identical but less intense set of resonances is found underlying the enamine ligand resonances. This set appears more clearly at later points in the reaction. Resonances at -5.17 ppm (dd) and the pyrrole at 8.63 ppm are believed to be part of the same complex. The former resonances are consistent with a Rh-CH_2-CH= fragment as in the enamine complex, and on the basis of integration the complex is proposed to be a mixture of cis- and trans-Rh(TMP)(Cl)($CH_2CH{=}N(H)Et$).

The resonances of the cationic Rh(TMP)(Et_3N)(Et_2NH)$^+$ complex grow in as those of Rh(TMP)(CH(Me)NEt_2) decrease over the first 10 to 30 min of reaction (Fig. 4.16). The pyrrole resonance is at 8.73 ppm and the resonances at 2.00 and 1.77 ppm are assigned to the inequivalent ortho-methyls. The assignments for the ligands are in Table 4.6.

Table 4.7. Ligand ^1H nmr spectral data for Rh(TMP)(Cl)($CH_2CH{=}NEt_2$).[a]

proton	δ	integral
H_2	1.53 t	1H
$H_{3'(3)}$	1.34 q	2H
$H_{4'(4)}$	0.08 t	3H
$H_{3(3')}$	-0.02 m	2H
$H_{4(4')}$	-0.52 t	3H
H_1	-4.92 dd	2H

a. 300 MHz; measured in CD_2Cl_2 solution at ca. 20°C.

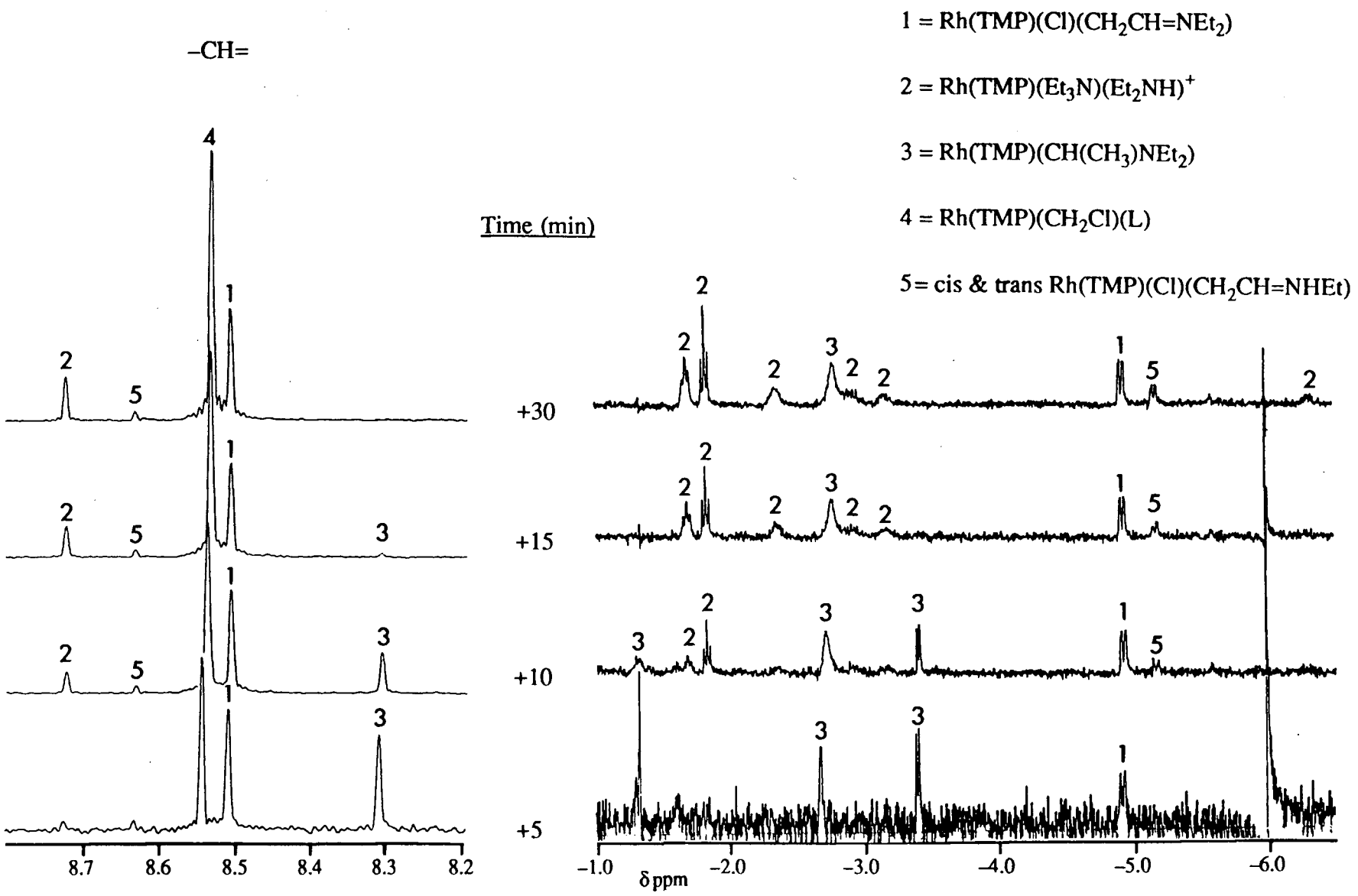

Figure 4.16. The 300 MHz ^1H nmr spectrum of a CH_2Cl_2 solution of Rh(TMP)(Cl)(iPrOH) and Et_3N, at various times after thawing a sample frozen in liquid nitrogen. [Rh] ≈ 3.0×10^{-3} M, [Et_3N] ≈ 1×10^{-2} M, at 18 °C, sealed in vacuo.

The resonances of Rh(TMP)(CH(Me)NEt_2) are partially obscured but still distinguishable and are listed in Table 4.6. The separation of the ortho-methyl resonances was 0.70 ppm which is comparable to the 0.72 ppm separation observed in C_7D_8 solution.

Like its OEP analogue, Rh(TMP)(Cl)($CH_2CH{=}NEt_2$) is not stable and further reaction occurs but at a much slower rate than for the decomposition of Rh(TMP)($CH(CH_3)NEt_2$) (Fig. 4.17). As the Rh(TMP)(Cl)($CH_2CH{=}NEt_2$) resonances decrease, those of Rh(TMP)(Cl)(Et_2NH) increase; this is seen, for example, by examining the respective pyrrole resonances (8.53 and 8.62 ppm) and the respective axial ligand resonances: Et_2NH (-1.83, -2.90, -3.32 and -5.96 ppm) and $:\bar{C}H_2CH{=}\overset{+}{N}Et_2$ (-4.92 ppm). The $[Rh(TMP)(Et_3N)(Et_2NH)]^+$ spectra remain roughly constant. The pyrrole resonance of Rh(TMP)(CD_2Cl) shifts slightly to 8.52 ppm and increases in intensity somewhat as well.

Spectra taken of sealed samples at longer times (2 days to several weeks) show only two pyrrole resonances (8.62 and 8.51 ppm) in about a 1:1.7 ratio (trace for 23 °C in Fig. 4.18). The pyrrole proton resonance at 8.62 ppm is that of Rh(TMP)(Cl)(Et_2NH) (vide supra). The other pyrrole resonance is temperature dependent and splits into two resonances (8.55 and 8.48 ppm) at -53 °C; there is a coalescence temperature at about -20°C (Fig. 4.18). Only resonances due to coordinated Et_2NH and Et_3N are present in the ligand region. At -53 °C, the integrations relative to the pyrrole region are consistent with one Et_2NH coordinated as Rh(TMP)(Cl)(Et_2NH) and the remaining Et_2NH being associated with the larger resonance at 8.48 ppm. The coordinated Et_3N resonances match the smaller 8.55 ppm resonance. When a sample in CH_2Cl_2, showing a similar composition by ambient temperature nmr, is then taken to -53 °C, the spectrum had two peaks at -2.85 and -3.44 ppm in the region expected for the -CH_2Cl ligand (Fig. 4.19). The smaller peak, at -2.85 ppm, roughly integrates to 2 protons relative to the integration of the ethyl groups of the coordinated Et_3N and is therefore assigned to Rh(TMP)(CH_2Cl)(Et_2NH), while the integration of the -3.44 ppm resonance integrates as 2 protons relative to the coordinated Et_2NH remaining after accounting for the Rh(TMP)(Cl)(Et_2NH) present. Thus the room temperature pyrrole resonance at 8.51 ppm (Fig. 4.18) is the fast exchange average of the pyrrole resonances for Rh(TMP)(CD_2Cl)(Et_3N) and Rh(TMP)(CD_2Cl)(Et_2NH).

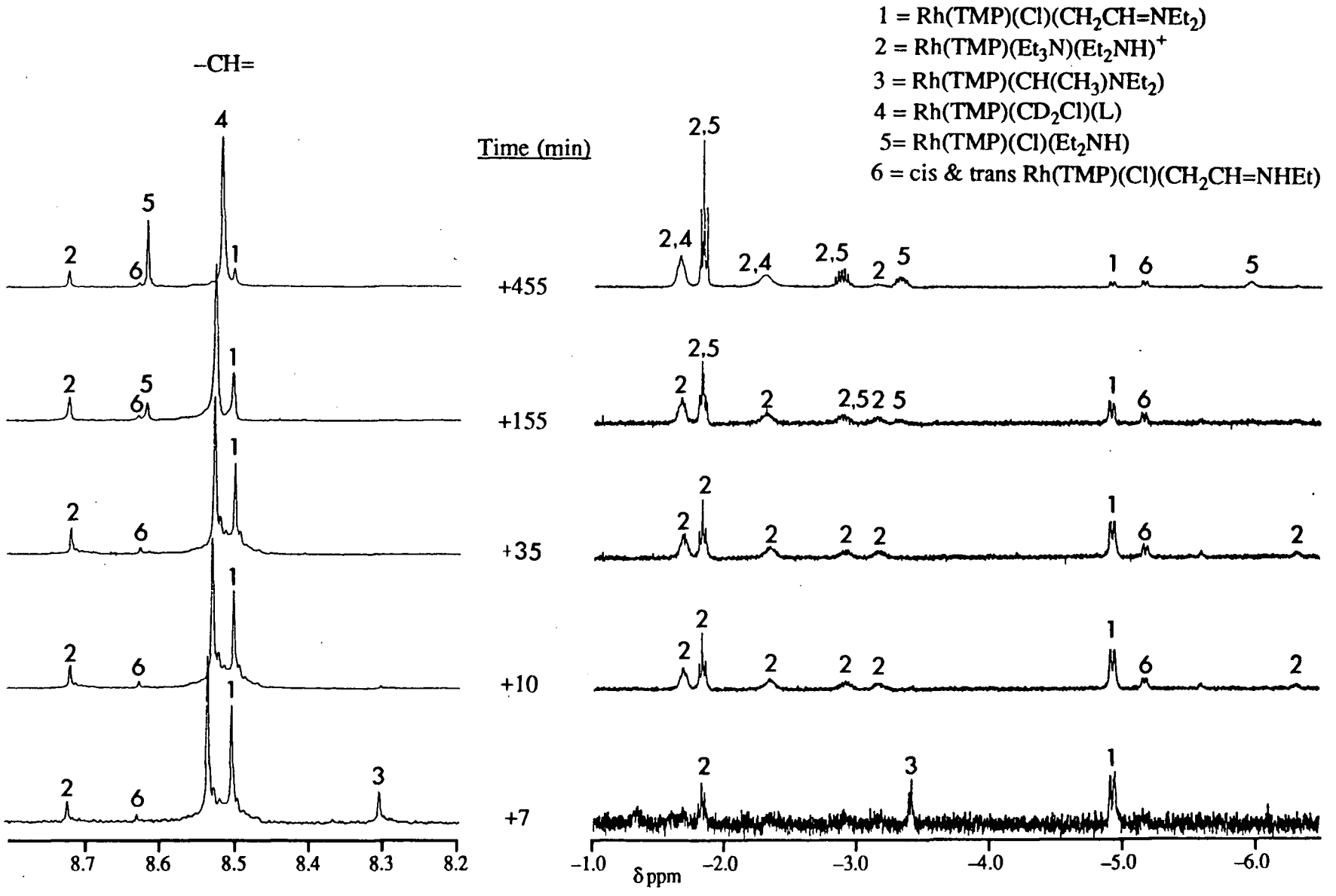

Figure 4.17. The 300 MHz ^1H nmr spectrum of a CD_2Cl_2 solution of Rh(TMP)(Cl)(iPrOH) and Et_3N, at various times after thawing a sample frozen in liquid nitrogen. [Rh] ≈ 3.0×10^{-3} M, [Et_3N] ≈ 1×10^{-2} M, at 19 °C, sealed in vacuo.

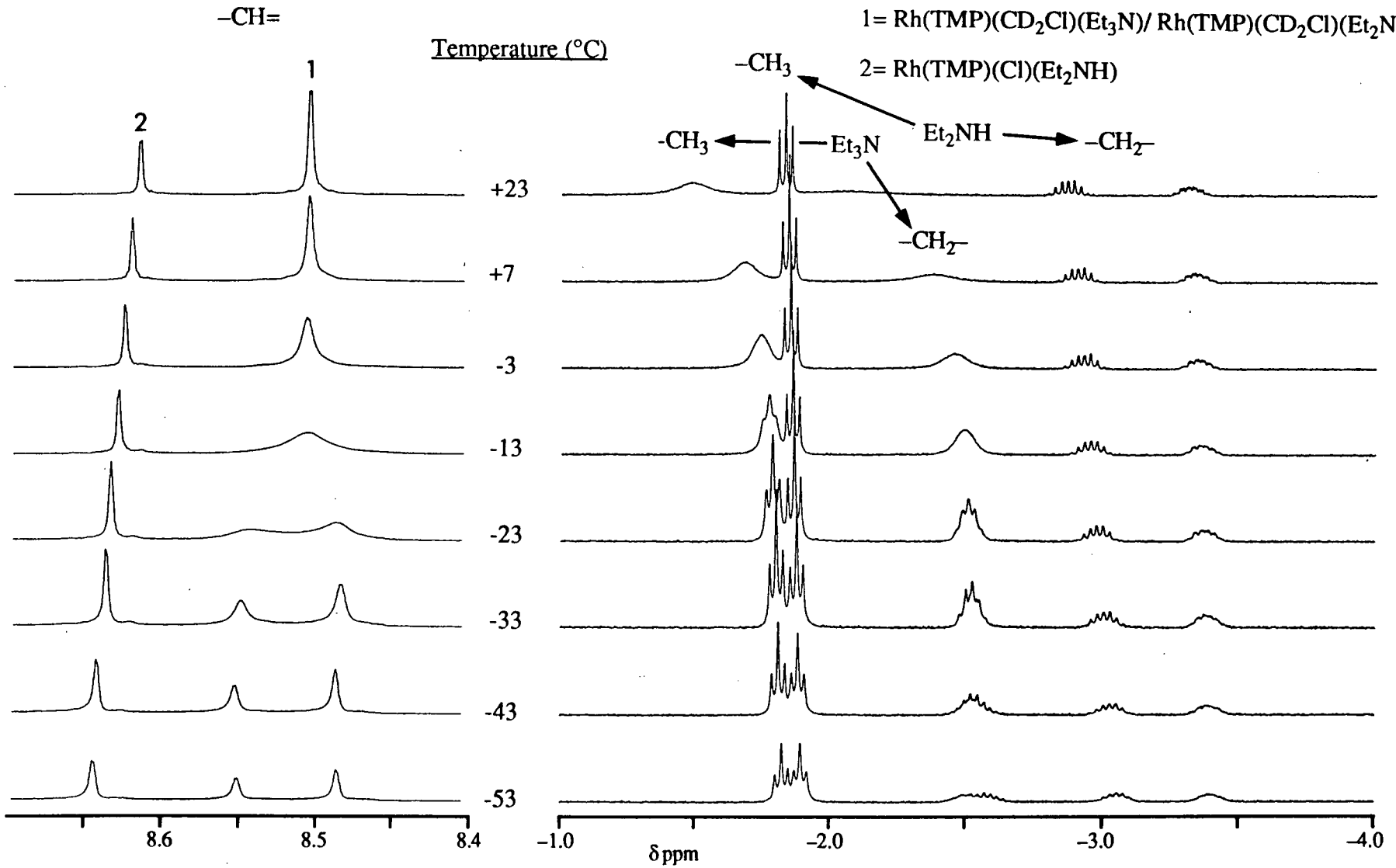

Figure 4.18. The 300 MHz ^{1}H nmr spectrum of a CD_2Cl_2 solution of Rh(TMP)(Cl)(iPrOH) and Et_3N, 14 days after after thawing a sample frozen in liquid nitrogen, at various temperatures. [Rh] ≈ 3.8×10^{-3} M, [Et_3N] ≈ 1×10^{-2} M, at 19 °C, sealed in vacuo.

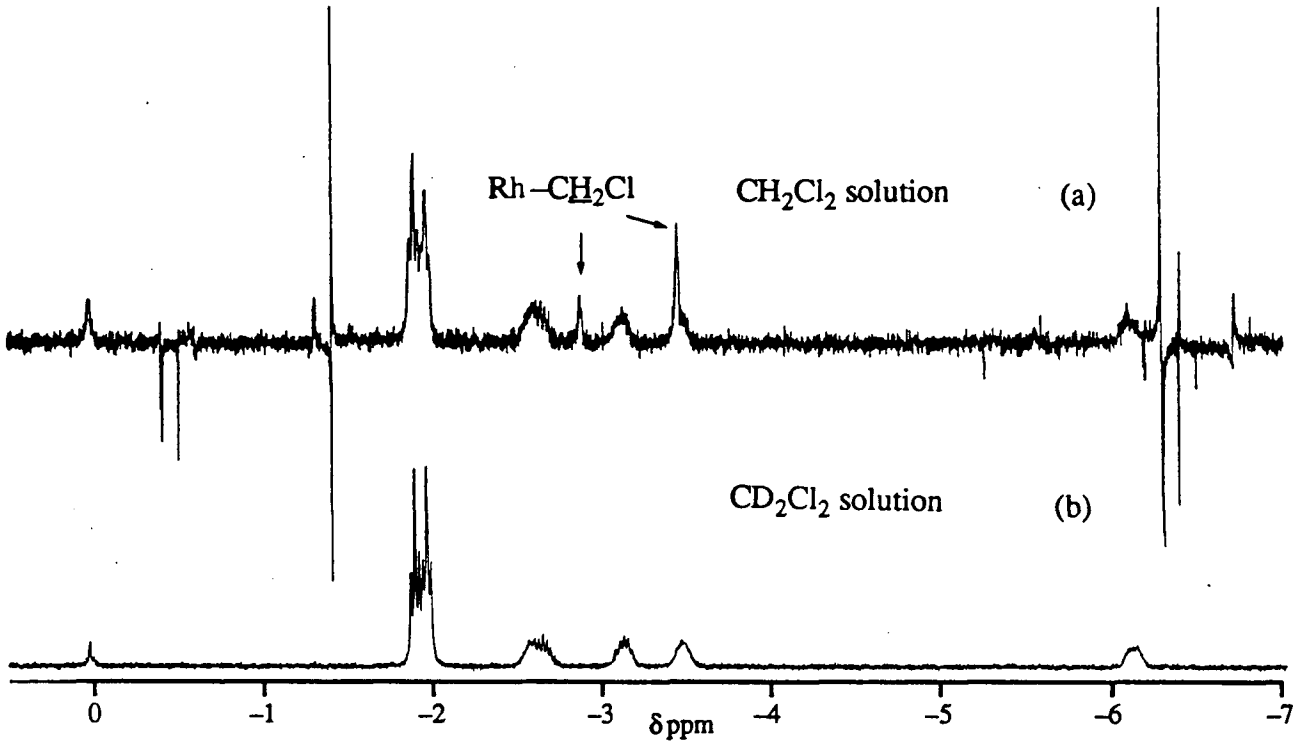

Figure 4.19. The comparison of 300 MHz ^1H nmr spectra of solutions of Rh(TMP)(Cl)(iPrOH) with added Et_3N in (a) CH_2Cl_2 at -53 °C and (b) CD_2Cl_2 (the -53 °C trace from Fig. 4.18).

For the most part, the reaction of Et_3N with Rh(TMP)(Cl)(L) in CH_2Cl_2 parallels that with the OEP analogue, the absence of $[Rh(TMP)]_2$ species being expected for the more hindered TMP complex. Reaction with CH_2Cl_2 occurs and Rh(por)(Cl)($CH_2CH{=}NEt_2$) is the other initial major product. The similar reactivity for both types of Rh(por)(Cl) complexes in CH_2Cl_2 contrasts with the slowness of reaction found for the TMP complex in aromatic solvents. The increased stabilisation of polar or ionic species such as might occur in reactions 4.2 and 4.3 (i.e., loss of HCl, see p. 131) presumably will promote the formation of Rh^{II}(por), the amine adduct of which reacts with CH_2Cl_2 to give Rh(por)(CH_2Cl)(amine) and Rh(por)(Cl)(amine) (by analogy to the PPh_3 complex reactions (3.80 and (3.9)), and the enamine; the imine isomer of this then coordinates to Rh(por)(Cl) to form Rh(por)(Cl)($CH_2CH{=}NEt_2$). The lack of Rh(por)(Cl)($CH_2CH{=}NEt_2$) found in benzene is due to the low proportion, relative to that in CH_2Cl_2, of the polar imine isomer in the aromatic solvent (equilibrium 4.7).

$$CH_2{=}CH\text{-}NEt_2 \rightleftharpoons :\bar{C}H_2CH{=}\overset{+}{N}Et_2 \qquad (4.7)$$

The enamine complex Rh(por)(Cl)($CH_2CH{=}NEt_2$) decomposes and Rh(por)(Cl)(Et_2NH) concentration concomitantly increases. The decomposition of Rh(por)(Cl)($CH_2CH{=}NEt_2$) probably occurs via dissociation of the enamine because retention of an alkyl fragment (i.e. Rh(por)(CH_2CHO)) was not observed. Dissociation of the enamine and its hydrolysis to CH_3CHO and Et_2NH (152) followed by complexation of Et_2NH would explain the findings; however, CH_3CHO has not been detected. In the OEP system, another uncharacterized complex also forms, and is formulated as Rh(OEP)(R)(Et_3N). The origin of the Rh(OEP)(R) fragment of the new complex is unclear because the R ligand is silent in the ^1H nmr. Because the formation of Rh(OEP)(Cl)(Et_2NH) appears to be stoichiometric with the decrease of the enamine complex, other uncharacterized species in solution (~25% initial products) and solvent are possibly involved.

4.3. Results and discussion of kinetic studies

The results of the ^1H nmr studies suggest that the first and critical step in the reaction of Et_3N with Rh(por)(Cl) is probably the coordination of Et_3N. In toluene and benzene solution, a labile Rh(TMP)(Cl)(Et_3N) complex is observed but the OEP analogue has not been detected. The aim of the kinetic studies was to investigate the system back to the point where the Rh(OEP)(Cl)(Et_3N) complex could be detected. (Visible spectroscopy was used because of convenience and the accessibility of a stopped-flow apparatus.) The reactions were followed in CH_2Cl_2 rather than toluene or benzene because the both the TMP and OEP complexes react at similar rates in CH_2Cl_2 and give similar products and thus the systems could be usefully compared. In addition to the H_2O complex, the Rh(por)(Cl)(CH_3CN) complexes were used.

Spectra covering the initial reaction in CH_2Cl_2 under anærobic conditions were obtained by "scanning" with a Durrum single beam, stopped-flow instrument (sect. 2.2.8). The Rh(por)(Cl)(CH_3CN) concentrations, after mixing, were ~2×10^{-5} M and about 150 equivalents of Et_3N were used. An initial period of rapid exponential change, complete in 2 to 10 s, was observed, followed by a very much slower change (Fig. 4.20). First, the whole spectra will be

considered, and then rates obtained from these stopped-flow data and data obtained at other concentrations will be discussed.

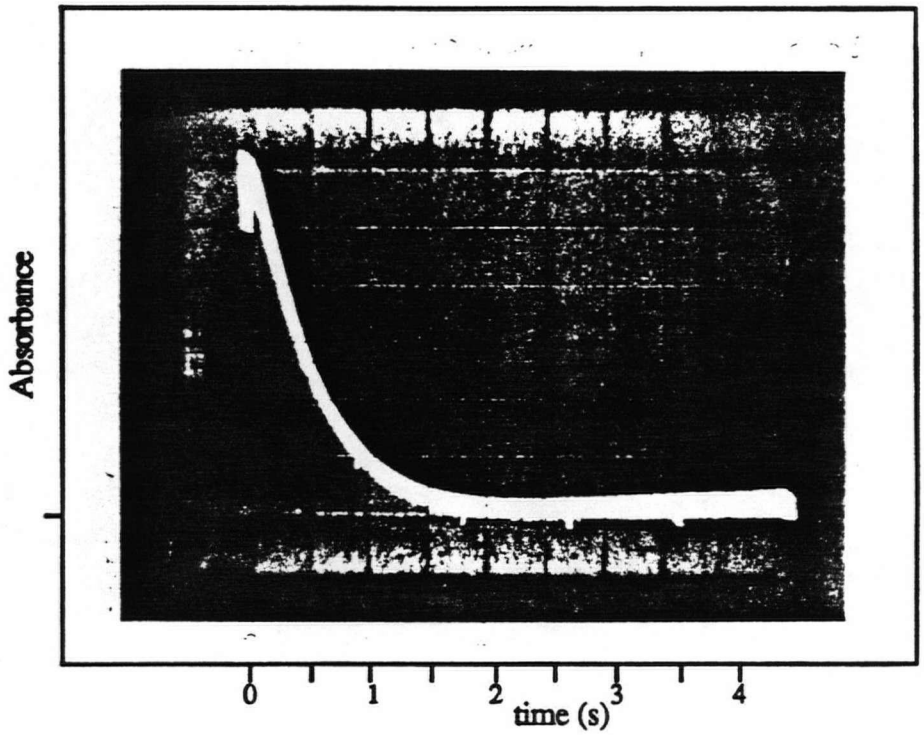

Figure 4.20. Typical stopped-flow traces (2 sets of 3 superimposed runs) of the change of absorbance at 552 nm of Rh(OEP)(Cl)(CH_3CN) during the reaction with Et_3N in CH_2Cl_2. [Rh] = 2.41×10^{-5} M, [Et_3N] = 3.33×10^{-3} M, at 25°C, under Ar.

The absorbances measured during the reaction of Et_3N with Rh(OEP)(Cl)(CH_3CN) or Rh(TMP)(Cl)(CH_3CN) in CH_2Cl_2 are summarized in Figures 4.21 and 4.22, respectively. The stopped flow data at two times, 4 and 10 s for the reaction with Rh(TMP)(Cl)(CH_3CN) and at 0.5 and 2 s for that of Rh(OEP)(Cl)(CH_3CN) are overlaid on the data graphically extrapolated back to t = 0 ("t_o", see below); spectra of the initial Rh(por)(Cl)(CH_3CN) complexes are also shown. The wavelength resolution of these stopped-flow spectra is low and variable (2 to 10 nm between points) and subject to interpolation errors as the lines were sketched in by hand. The accuracy of the absorbance scale is discussed in section 2.2.8 and for these spectra is considered to be ± 0.03 units; that of the wavelength scale is ±1 nm. The "final" spectra are similar to those obtained using the same solutions and a PE 552A scanning spectrophotometer (~2.5 min to scan to mid-point of

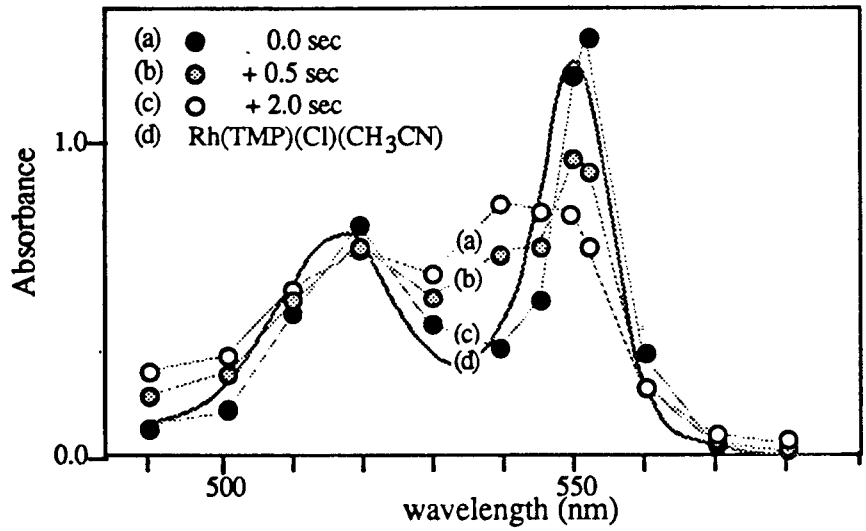

Figure 4.21. Changes of the visible spectrum during the first 2 seconds of the reaction of Et_3N with Rh(OEP)(Cl)(CH_3CN) in CH_2Cl_2: (a) the spectrum at "t_0", (b) after 0.5 s, (c) after 2.0 s and (d) Rh(OEP)(Cl)(CH_3CN). [Rh] = 2.41×10^{-5} M, [Et_3N] = 3.33×10^{-3} M, at 25°C, under Ar.

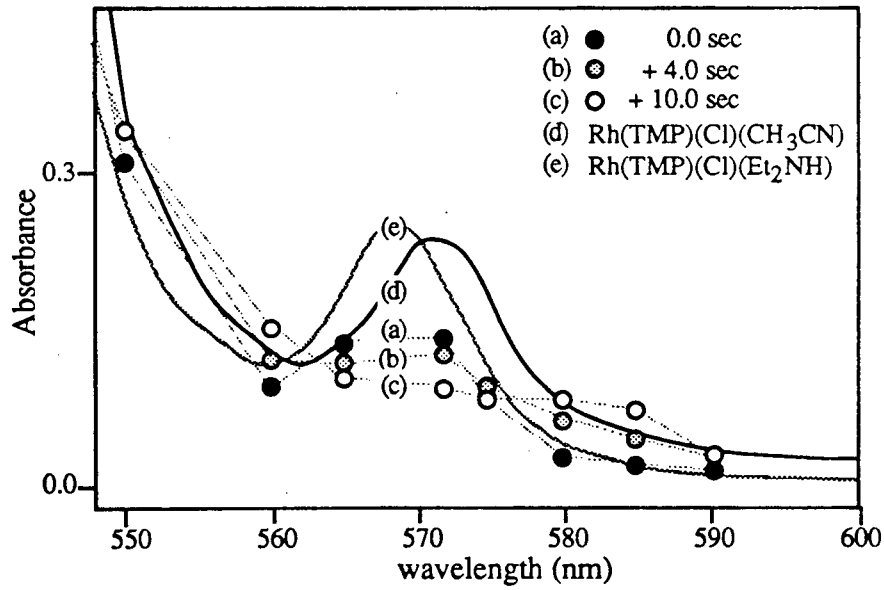

Figure 4.22. Changes of the visible spectrum during the first 10 seconds of the reaction of Et_3N with Rh(TMP)(Cl)(CH_3CN) in CH_2Cl_2: (a) the spectrum at "t_0", (b) after 4.0 s, (c) after 10.0 s, (d) Rh(TMP)(Cl)(Et_2NH), and (e) Rh(TMP)(Cl)(CH_3CN). [Rh] = 2.17×10^{-5} M, [Et_3N] = 3.33×10^{-3} M, at 25°C, under Ar.

500–600 nm region after mixing) and a HP 8452A diode array spectrometer (~18 s; 1 s for a scan and ~17 s for mixing) and are believed to be of the mixture of initial products observed by ^{1}H nmr (i.e., Rh(por)(CH_2Cl), Rh(por)(Cl)($CH_2CH{=}NEt_2$), Rh(por)(CH(Me)(NEt_2), etc.). Of more interest is the spectrum obtained by extrapolation to "t_o".

The extrapolation to t_o is done by linear extension of the smooth curve showing the absorbance change on the photographs of the oscilloscope traces (Fig. 4.20). These "t_o" spectra are similar to the spectra of the initial Rh(por)(Cl)(CH_3CN) complexes, but the differences are believed to be real. In particular, there are differences between the α bands (~570 nm) of the Rh(TMP)(Cl)(CH_3CN) and of the "t_o" spectrum of the TMP system, and between the β bands (~520 nm) of the Rh(OEP)(Cl)(CH_3CN) and of the "t_o" spectrum of the OEP system. The spectra of the Et_3N complexes are obviously not available for comparison but the changes indicate that the Rh(por)(Cl)(CH_3CN) complexes undergoes a very fast initial reaction to give the "t_o" spectrum. This is likely the formation of Rh(por)(Cl)(Et_3N). The relative rate of replacement of the CH_3CN from Rh(por)(Cl)(CH_3CN) is critical because of the extrapolation on which the "t_o" spectra are based.

At the 2.67 s/cm time-scale used for the photographs, any change in the first 200 to 300 ms is effectively ignored by the extrapolation to "t_o". The $t_{1/2}$ for substitution of CH_3CN in Rh(OEP)(Cl)(CH_3CN) or Rh(TMP)(Cl)(CH_3CN) by CO or PPh_3 is found to be ~80 ms (see below), with CH_3CN loss probably being the rate determining step. On the basis of the dynamics, and the data described above, the "t_o" spectra are ascribed to Rh(por)(Cl)(Et_3N).

The data for the change at or near the maximum absorbance of Rh(por)(Cl)(Et_3N) was examined more closely. For Rh(OEP)(Cl)(Et_3N) this was at the α band and for Rh(TMP)(Cl)(Et_3N) at the β band. The data could be treated as 1st order, the rate being obtained from plots of $\ln(A-A_\infty)$ vs. time using an apparent A_∞ estimated from the absorbances at the end of the period of rapid change (Fig. 4.20). Table 4.8 summarises the results for the reaction with Et_3N, and there are several salient features.

Table 4.8. Pseudo first order rate constants for the disappearance of Rh(por)(Cl)(Et_3N) in CH_2Cl_2.[a]

run	$[Rh]_o$ x10^5M	$[Et_3N]_o$ x10^5M	k_{obs} s^{-1}	$t_{1/2}$ s
Rh(TMP)(Cl)(Et_3N) data at 540 or 536 nm:				
1	2.10	86.0	0.19	3.63
2	"	173	0.19	3.71
3	"	345	0.20	3.40
4	2.10	345	0.25	2.74
5	1.00	345	0.52	1.33
6	2.17	333	0.23[b]	3.00
			0.18[b, c]	3.80
Rh(OEP)(Cl)(Et_3N) data at 552 nm:				
7	2.53	345	0.404	1.72
8	2.41	345	1.87[b]	0.372
			1.97[b, d]	0.352

a. The R values for the $\ln(A-A_\infty)$ vs. time plots were 0.990–0.999; runs 1-3 at 20 °C; runs 4-8 at 25 °C.

b Under argon.

c Measured from absorbance increase at 520 nm.

d Measured from absorbance increase at 540 nm.

Isosbestics subsequent to formation of Rh(OEP)(Cl)(Et_3N) are suggested in Figure 4.21 and comparison of the data for the absorbance decrease at 552 nm with those for the increase at 540 nm supports this (run 8). The support (from the stopped-flow data) for the apparent isosbestics in Figure 4.22 for the TMP case is weaker (run 6). Air apparently inhibits the OEP system (runs 7 vs. 8) but no such effect is observed for the TMP system (runs 4 vs. 6). Only the TMP system was tested for $[Et_3N]_o$ dependence, because it was difficult and cumbersome to minimize air leakage while using the Durrum stopped-flow apparatus; the data (runs 1-3) show k_{obs} is independent of $[Et_3N]$. The dependence of k_{obs} on $[Rh]_o$ (run 5 vs. 4,6) is inverse for the TMP system.

For the back-extrapolation to the "t_o" spectra to be meaningful, the $t_{1/2}$ of the postulated substitution of CH_3CN in Rh(por)(Cl)(CH_3CN) by Et_3N to form Rh(por)(Cl)(Et_3N) must be small in relation to the $t_{1/2}$ of the disappearance of Rh(por)(Cl)(Et_3N). To test the rates of simple substitution of CH_3CN at the Rh(III) center, the reactions of Rh(por)(Cl)(CH_3CN) with PPh_3 and CO were briefly examined. In the presence of excess ligand L, Rh(por)(Cl)(L) species form (Chapter 5); and Table 4.9 summarises some kinetic data. The experimental stopped-flow data all give good pseudo-first order plots. The PPh_3 data from the TMP system in particular gave practically superimposable absorbance values. The k_{obs} values are higher (by a factor of ~50) than those for the disappearance of Rh(por)(Cl)(Et_3N) (Table 4.8). As mentioned above, this observation is consistent with coordination of Et_3N as the process preceding the disappearance of the Et_3N complex. The k_{obs} values (Table 4.9) are also essentially the same, being independent of porphyrin type and, at least in the TMP system, of [PPh_3]. Although the lack of dependence on porphyrin type is probably fortuitous, loss of CH_3CN as the rate determining step of the substitution reaction seems highly likely.

The studies described in this kinetic section show that the OEP and TMP systems follow very similar reaction paths with Et_3N. The first step seems to be the very fast substitution of CH_3CN in Rh(por)(Cl)(CH_3CN) by Et_3N, forming Rh(por)(Cl)(Et_3N), probably in a S_N1 process, judged by the data on the reaction of Rh(por)(Cl)(CH_3CN) with CO and PPh_3. The amine complex then undergoes further transformations that give the products observed by ^1H nmr (i.e., reduction of Rh(III) to Rh(II), etc.). However, the stopped-flow data indicate that air inhibits the transformation of Rh(OEP)(Cl)(Et_3N) to the subsequent products. This observation raises an interesting point that, whereas the products of the reaction of Et_3N with Rh(por)(Cl)(L) under anærobic conditions are a mixture of Rh(por)(Cl)(Et_2NH) and significant amounts of relatively stable organometallic complexes, the same reaction in air gives relatively insignificant amounts of these organometallic species. This suggests that the manifold of reactions under ærobic conditions differs from that under anærobic conditions.

Table 4.9 Pseudo first order rate constants for the reaction of Rh(por)(Cl)(CH_3CN) with PPh_3 and CO in CH_2Cl_2.[a]

run	$[Rh]_o$ x10^5M	$[L]_o$ x10^5M	k_{obs} s^{-1}	$t_{1/2}$ s
Rh(TMP)(Cl)(CH_3CN) data at 536 nm:				
9	2.10	135[b]	9.23	0.075
10	"	540[b]	"	"
11	"	1080[b]	"	"
12	1.00	135[b]	8.94	0.078
13	2.10	~360[b]	9.79	0.071
Rh(OEP)(Cl)(CH_3CN) data at 552 nm:				
14	2.53	135[a]	9.09	0.076
15	"	~360[b]	9.73	0.071

a. The R values for the $\ln(A-A_\infty)$ vs. time plots were 0.999; at 25 °C.

b. L = PPh_3.

c. L = CO; reagent solution saturated with CO at 1 atm and 25 °C (sect. 2.2.8).

4.4. General Discussion

Under anærobic conditions, Et_3N readily replaces L in Rh^{III}(por)(Cl)(L) species to form the Rh^{III}(por)(Cl)(Et_3N) complex. Reduction of Rh^{III} to Rh^{II} follows, although the exact nature of the electron transfer mechanism has not been elucidated. Certainly an enamine is formed in CH_2Cl_2 indicating that dehydrogenation of the Et_3N has occurred, and, at least in CH_2Cl_2, probably via a net two-electron oxidation of the Et_3N with concomitant loss of protons (observed by ^1H nmr spectroscopy). The Et_3N would weaken the binding of the trans Cl^- ligand and create an incipient electrophilic centre at Rh. The $[Rh^{III}(OEP)]^+$ cation is a potent electrophile (21), and so a concerted Cl^- loss and electron transfer from Et_3N to $[Rh^{III}(por)]^+$ forming Rh^{II}(por), aminyl radical and presumably ejecting HCl (reactions 4.1–4.3, p. 131) is reasonable. In aromatic solvents, the same mechanism is believed to lead to $[Rh(OEP)]_2$ in the OEP system but, in the case of the TMP system, formation of Rh(II) is not favoured because of the low polarity of the solvent

and because dimerization of Rh^{II}(TMP) is not possible. The formation of $[Rh(OEP)]_2$ is believed to stabilize the Rh(II) product relative to the initial Rh(III) complex in aromatic solvents and so drive the reduction of the Rh(III). The Rh(por)(CH(Me)NEt_2) product subsequently forms slowly by reaction of Et_3N with Rh^{II}(por) (reactions 4.5–4.6, p. 131), and these slower reactions drive the reduction of Rh(III) in the TMP system in aromatic solvent.

A major driving force for both TMP and OEP systems through the reduction step in CH_2Cl_2 is believed to be the formation of Rh-C bonds (i.e., Rh(por)(CH_2Cl)), because both the TMP and OEP systems show comparable reactivity in this solvent, in contrast to the situation in aromatic solvents. Formation of a strong Rh-C bond is believed to be a large part of the driving force for other systems involving Rh^{II}(por) reactants (sect. 1.5.2 and 1.5.4).

The dealkylation of Et_3N to give Et_2NH is inferred to occur principally by acid hydrolysis of the free enamine (152) formed by the net oxidative dehydrogenation of Et_2N during the reduction of Rh(III) to Rh(II), rather than via a metal-centered process observed in non-porphyrin systems (148,155, 156). The dealkylation appears to be stoichiometric and not catalytic under the conditions used, due to the preferential coordination of Et_2NH to Rh(por)(Cl) relative to coordination of Et_3N; thus, further reduction cycles are inhibited. In aromatic solvents, a secondary source of Et_2NH is the oxidation of Rh(por)(CH(Me)NEt_2) but the Rh(por)(CH_2CHO) co-product is stable, and this source evidently is not important when Et_3N and Rh(OEP)(Cl)(H_2O) are reacted together in the presence of air in benzene, this forming principally Rh(OEP)(Cl)(Et_2NH). The low yield of Rh(por)(CH_2CHO) in this ærobic reaction, and the inhibition by air of the decomposition of Rh(OEP)(Cl)(Et_3N) indicated by the stopped-flow data, suggest that the Rh-centered reactions studied under anærobic conditions do not directly relate to the mechanism of the ærobic reaction.

In the absence of O_2, Rh(por)(CH(Me)NEt_2) is stable in aromatic solvents. Admission of O_2, or air, causes its rapid removal and formation of Rh(por)(CH_2CHO) (reaction 4.8). The mechanism is not obvious, and [O] is used to represent the unknown oxidant species.

$$Rh^{III}(por)(CH(CH_3)NEt_2) + [O] \longrightarrow Rh^{III}(por)(CH_2CHO) + HNEt_2 \qquad (4.8)$$

The ultimate source of aldehydic oxygen must be O_2, and a Rh^{II}(por) species is probably involved as the "carrier". The $[Rh^{II}(OEP)]_2$ dimer, and a probable Rh^{II} complex in the TMP system, were present before reaction with O_2. The $[Rh^{II}(TPP)]_2$ dimer is known to react with dry O_2 in toluene to form Rh(TPP)(O_2) (42,151) and similar species may be involved here; however, in the presence of excess H_2O the total amount of $[Rh^{II}(OEP)]_2$ present was unchanged while the oxidation still proceeded. This latter observation is consistent with the synthetic route to $[Rh(OEP)]_2$, which involves reacting a refluxing toluene solution of Rh(OEP)(H) with air (78), and appears to depend upon the presence of H_2O (sect. 3.3).

This investigation of the reaction of amines with Rh(por)(Cl)(L) has revealed several novel organometallic products as well as information on mechanistic aspects. At the same time it is clear that many components of the mechanism are not known. The trialkylamines, triethylamine and tributylamine, are capable of rapidly reducing Rh(OEP)(Cl)(H_2O) to $[Rh(OEP)]_2$, and the investigation has focused on the triethylamine reaction, but dimethylamine (Chapter 2), diethylamine, aniline, N-methyl-diphenylamine and N-ethyl piperidine all form complexes of the type Rh(OEP)(Cl)(amine) (Table 4.1). The secondary amines and aryl substituted amine complexes do not rapidly undergo intramolecular redox processes, although Proton Sponge™, an arylamine, does reduce the Rh(III) to Rh(II); this reaction might be driven by formation of the cyclised oxidized amine product, the trimethyldihydroperimidinium cation (155), although this possibility was not investigated. The range of complexes studied is too narrow to detect meaningful trends, although it is evident that, except for Proton Sponge, only tertiary amines with a N-CH_2– moiety, which is required for formation of the imine/enamine product, were effective reductants (157). As judged by oxidation potentials (157a) and photoelectron ionization potentials (157b) the aliphatic tertiary amines should be more easily oxidised in reversible one-electron systems than the corresponding secondary amines. This is in contrast to an Fe(por)(Cl) system where the presence of a secondary amine functional group is required for the oxidation (158).

Chapter 5
Characterization and chemistry of Rh^{III}(por) phosphine complexes

5.1. Introduction

In Chapter 3 of this thesis, PPh_3 was used as a ligand and substrate to probe the reaction of Rh(OEP)(H) with O_2. In addition, the investigation and development of metalloporphyrin chemistry (often utilising tertiary phosphine ligands) as it relates to catalysis involving small molecules such as O_2, CO and H_2, are of particular interest to our group, although much of our focus involving mono- and bidentate phosphines has been on ruthenium porphyrin chemistry (138,139,159-164). At the inception of the work described in this chapter, coordination of tertiary phosphine to a Rh(III) porphyrin superoxide complex at low temperature (76), and the reaction of $P(OMe)_3$ with $[Rh(OEP)]_2$ had been reported (42). During the course of the present work, electrochemical and ligand substitution studies of the superoxide complex (44) and some $Rh^{III}(TPP)(R)(PR_3)$ complexes have appeared (77), as well as the syntheses of some cationic Rh(III) bis-phosphine and phosphite complexes (32).

In this chapter, the characterization of $Rh(OEP)(Cl)(PPh_3)$ and its solution molecular structure are presented, as well as preliminary solution data on the bis-phosphine cations $[Rh(OEP)(L)_2]^+$, where L is PPh_3 or $P(^nBu)_3$. The latter complexes are of interest because isoelectronic ruthenium(II) porphyrin complexes containing tertiary phosphines as axial ligands have a key role in catalytic decarbonylation of aldehydes (162), and oxidation of phosphines by molecular oxygen (139).

The in situ formation of Rh(OEP) complexes of some diphosphines (dppm, dppe, dppp and dppb) is also discussed, while some data on corresponding complexes of Ru(II) porphyrins (161,165) are reinterpreted.

Some of the data on the $Rh(OEP)(Cl)(PPh_3)$ and $[Rh(OEP)(L)_2]^+$ (L = PPh_3 or $P(^nBu)_3$) systems have been published (75). The chloride complex was isolated by Dr. T. Leung of our group and limited ^1H and $^{31}P\{^1H\}$ nmr and visible spectral data collected by he and K. Menon.

The chloride complex was characterized by S. Ariel using X-ray crystallography. An alternative preparation (see sect. 2.1.5.3., method A in ref. 75) and the solution studies were performed by myself.

5.2. Results and Discussion

5.2.1. Reaction of Rh(OEP)(Cl)(PPh_3) with monophosphines

The non-ionic chlorotriphenylphosphine complex Rh(OEP)(Cl)(PPh_3) remains 6-coordinate in solution. Beer's Law was obeyed over the range (0.9–8.0) $\times 10^{-4}$ M in benzene solution, in the dark. The ^1H nmr spectra of solutions at 10^{-3} - 10^{-2} M (Table 5.1) are consistent with the presence of a diamagnetic Rh^{III}(OEP) species, that is asymmetrically substituted with regard to the porphyrin plane, i.e., two different axial ligands are present causing the $-CH_2-$ resonances to appear as an ABX_3 multiplet (138-141). There is no evidence for free phosphine in solutions of Rh(OEP)(Cl)(PPh_3), and the visible spectrum (Table 5.2) is unaffected by addition of Cl^-. Coordination of a single PPh_3 is shown by integration of the o-, m- and p-protons which are shifted upfield from their normal positions by the strong ring-current of the porphyrin (164,166). Further, the solid-state visible spectrum (Nujol, Table 5.2) shows absorption maxima that correspond closely to those measured in solution.

Addition of PPh_3 or P^nBu_3 to the complex in polar solvents (CH_3CN, CH_2Cl_2, diethyl ether, DMA) resulted in formation of cationic bis-phosphine complexes, reactions (5.1) and (5.2).

$$Rh(OEP)(Cl)(PPh_3) + PPh_3 \overset{K}{\rightleftharpoons} [Rh(OEP)(PPh_3)_2]^+ + Cl^- \qquad (5.1)$$

$$Rh(OEP)(Cl)(PPh_3) + 2P^nBu_3 \longrightarrow [Rh(OEP)(P^nBu_3)_2]^+ + Cl^- + PPh_3 \qquad (5.2)$$

The nmr spectroscopic evidence was cleanest for the reaction with P^nBu_3. Upon addition of two equivalents of phosphine to CD_3CN or CD_2Cl_2 solutions of Rh(OEP)(Cl)(PPh_3), the ^1H nmr spectrum of Rh(OEP)(Cl)(PPh_3) was replaced by a new set of signals due to $[Rh(OEP)(P^nBu_3)_2]^+$ (Table 5.1). The methylene protons of the ethyl side chains appear as the expected quartet, due to coupling with the adjacent $-CH_3$ group, while the upfield resonances due to coordinated P^nBu_3 were in a 2:1 equivalent ratio relative to the porphyrin.

Table 5.1. NMR spectral data for Rh(OEP) complexes of monodentate phosphines and other axial ligands.[a]

complex	^{1}H	meso-H	-CH_2-	-CH_3	o-	m-	p-	
Rh(OEP)(Cl)(PPh_3)		9.96 s[b]	4.10 m, 3.97 m	1.91 t	3.58 m	6.42 m	6.84 m	
		9.93 s[b]	4.09 m, 3.95 m	1.94 t	3.62 m	6.39 m	6.82 m	
		10.06 s[b]	3.93 m	1.90 t	~3.9 m[e]	6.28 m		
[Rh(OEP)(PPh_3)$_2$]$^+$		9.74 s[b]	3.96 q	1.88 t	3.45 m	6.38 m	6.85 m	
					-CH_2-	-CH_2-	-CH_2-	-CH_3
[Rh(OEP)(P^nBu_3)$_2$]$^+$		10.31 s[b]	4.17 q	1.92 t	-3.51 m	-1.93 m	0.06 m	0.18 t
		10.24 s[c]	4.15 q	1.94 t	-3.55 m	-1.92 m	0.07 m	0.2 m
Rh(OEP)(Cl)(CO)		10.36 s[f]	4.22 m	2.00 t				
Rh(OEP)(Cl)(THF)		10.31 s[f,g]	4.20 m	1.94 t				

$^{31}P\{^1H\}$	$\delta(^1J_{Rh-P})$
Rh(OEP)(Cl)(PPh_3)	9.56 d (124)[b]
	9.61 d (124)[c]
	9.05 d (116)[h]
[Rh(OEP)(PPh_3)$_2$]$^+$	-2.32 d (86)[c]
	-2.1 d (83)[i]
[Rh(OEP)(P^nBu_3)$_2$]$^+$	3.76 d (81)[b]

a. 300 MHz for ^{1}H; 121.421 MHz for $^{31}P\{^1H\}$ and at 20 °C unless otherwise noted.
b. In CD_3CN.
c. In CD_2Cl_2.
d. In C_6D_6; 80 MHz for ^{1}H, at 30 °C.
e. Overlaps with –CH_2- proton shifts.
f. Formed in situ (see text) in THF-d_8.
g. Formed in situ by dissolving Rh(OEP)(Cl)(H_2O) in THF-d_8.
h. In C_7H_8; 32.21 MHz for $^{31}P\{^1H\}$, at 30 °C.
i. In DMA; 32.21 MHz for $^{31}P\{^1H\}$, at 30 °C.

Table 5.2. Visible spectral data at 25 °C for Rh^{III}(OEP) complexes.

complex	solvent	Soret (nm)	(ε)[a] ($M^{-1}cm^{-1}$)	beta (nm)	(ε)[a] ($M^{-1}cm^{-1}$)	alpha (nm)	(ε)[a] ($M^{-1}cm^{-1}$)
Rh(OEP)(Cl)(PPh_3)	C_6H_6	422	158 000	533	21 000	563	24 000
	CH_2Cl_2	417	135 000	529	19 000	560	23 400
	Nujol	418		535		564	
	THF	[b]		529	20 000	562	22 000
	DMA	[b]		530		561	
	CH_3CN	[b]		528	17 800	560	22 500
[Rh(OEP)(PPh_3)$_2$]$^{+}$[c]	CH_2Cl_2	430	10 600	537	18 500	568	13 000
Rh(OEP)(Cl)(CO)[d]	C_6H_6	409		526		557	
	CH_2Cl_2	411	158 000	525	16 500	557	27 400
	THF	[b]		526		557	
Rh(OEP)(Cl)(CH_3CN)	CH_3CN[d]	[b]		521		552	
	CH_2Cl_2	400		518	14 800	550	26 300
Rh(OEP)(Cl)(THF)[d]	THF	[b]		517		549	

a. ± 5%.

b. Soret region not examined.

c. In situ formation, in the presence of added 6.75×10^{-4} M [Rh] and 1.96×10^{-2} M [$^{n}Bu_4N$][ClO_4].

d. In situ formation from Rh(OEP)(Cl)(H_2O).

Reaction (5.2) was also monitored by $^{31}P\{^{1}H\}$ nmr spectroscopy, free PPh_3 being clearly observed. An excess of PPh_3 (to ~10^{-1}M) was required for in situ formation of [Rh(OEP)(PPh_3)$_2$]$^{+}$, which was observable by ^{1}H and $^{31}P\{^{1}H\}$ nmr spectroscopy of CD_2Cl_2 solutions (Table 5.1). The conductance of a CH_3CN solution of Rh(OEP)(Cl)(PPh_3) after addition of PPh_3 rose to a limiting value of 125 Ω^{-1} cm^2 mol^{-1}, consistent with formation of a 1:1 electrolyte (167). Stronger binding of $P^{n}Bu_3$ relative to triarylphosphines has been reported for

Ru^{II}(OEP) and Ru^{II}(TPP) complexes (166) and was accounted for by the higher basicity of the trialkylphosphines (169).

Formation of mixed PPh_3 /P^nBu_3 or Rh(OEP)(Cl)(P^nBu_3) complexes was not evident by nmr. Also, the ionic bis-phosphine complexes were not formed at all in toluene or benzene solution. The more polar CH_2Cl_2 ($\varepsilon \approx 9$) or CH_3CN ($\varepsilon \approx 36$) were required to promote reactions (5.1) or (5.2).

Reactions (5.1) and (5.2) could also be monitored by visible spectroscopy. Addition of phosphine resulted in a red shift of the Soret and visible bands (Table 5.2) with a marked diminution of the α band (Fig. 5.1). On the basis of the results in this chapter, these findings are to be consistent with replacement of chloride by an additional phosphine ligand. A corresponding reverse blue shift of the spectrum of Ru(OEP)(P^nBu_3)(S) (S = DMSO or CH_3CN) compared with that of Ru(OEP)(P^nBu_3)$_2$ has been noted previously (166).

5.2.2. Solution equilibrium measurements

Equilibrium (5.1) was studied quantitatively using visible spectroscopy, following qualitative observations on the inhibition of the forward reaction in the presence of added chloride. The same isosbestic points (Fig. 5.1) were observed during a spectrophotometric titration with PPh_3 at a given temperature, or during variation of temperature over the range 10–30 °C at any chosen [PPh_3]. Indeed the latter type of experiment allows for a rapid estimation of K_{obs} as a function of temperature using just a single solution; such values were used to calculate K_{obs}.

Ambient light was excluded during sample manipulations by using dimmed room lighting and by covering all exposed surfaces with black plastic tape. Aliquots (μL) of 10^{-1} M PPh_3 in CH_2Cl_2 (alternatively solid PPh_3) were added to dilute solutions (~5×10^{-4} M) of Rh(OEP)(Cl)(PPh_3) in CH_2Cl_2. Formation of [Rh(OEP)(PPh_3)$_2$]$^+$ within seconds was evidenced by a red shift of the Soret from 419 nm to 429 nm, and the β and α bands from 529 nm to 537 nm and 560 nm to 568 nm, respectively, with a concomitant decrease in the intensity of the α band relative to the β band (Fig. 5.1). Measurements were also performed on solutions containing various amounts of [Ph_4As]Cl, [$^nBu_4N$]Cl or [$^nBu_4N$][ClO_4] to examine the effect of ionic

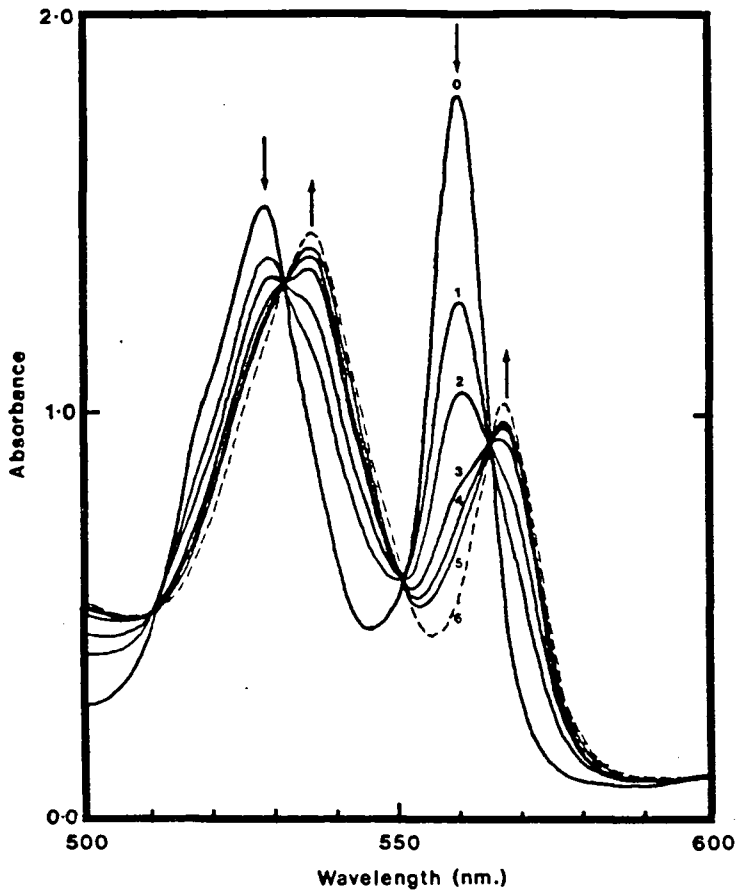

Figure 5.1. Spectroscopic titration of $Rh(OEP)(Cl)(PPh_3)$ with added PPh_3 in CH_2Cl_2 at 25 °C, [Rh] = 8×10^{-4} M; curves **0**–**5** result from added [PPh_3] of 0.0, 0.38, 1.09, 2.69, 5.01 and 7.18×10^{-2} M, respectively. **6** shows the spectrum of $[Rh(OEP)(PPh_3)_2]^+$ (formed at [PPh_3] $\approx 5 \times 10^{-2}$ M and $\mu \approx 0.02$ M).

strength and [Cl^-]. No change from the initial spectrum of the complex was noted on addition of the chloride salts to $Rh(OEP)(Cl)(PPh_3)$.

The value of K was found using visible data (at 560 nm) obtained using different combinations of initial concentrations of $Rh(OEP)(Cl)(PPh_3)$ (C_0), and added Cl^- (Cl_0) and PPh_3 (P_0). By defining A and A_0 as the absorbances measured at 560 nm with and without added PPh_3, and ε_0 and ε_∞ as the extinction coefficients of $Rh(OEP)(Cl)(PPh_3)$ and $[Rh(OEP)(PPh_3)_2]^+$, equation 5.3 may be derived (see Appendix C for derivation, l = pathlength):

$$K_{obs} = \frac{\left\{C_0 - \left[\frac{A - A_\infty}{(\varepsilon_0 - \varepsilon_\infty)l}\right]\right\}\left\{Cl_0 + C_0 - \left[\frac{A - A_\infty}{(\varepsilon_0 - \varepsilon_\infty)l}\right]\right\}}{\left\{\frac{A - A_\infty}{(\varepsilon_0 - \varepsilon_\infty)l}\right\}\left\{P_0 - C_0 - \left[\frac{A - A_\infty}{(\varepsilon_0 - \varepsilon_\infty)l}\right]\right\}} \qquad (5.3)$$

The ε_0 (23 400 M^{-1} cm^{-1}) and ε_∞ (6 500 M^{-1} cm^{-1}) values were available experimentally because the limiting spectra of $Rh(OEP)(Cl)(PPh_3)$ and $[Rh(OEP)(PPh_3)_2]^+$ for the equilibrium could be measured under readily attainable conditions (high [Cl^-] with no added phosphine, and high [PPh_3] and ionic strength with no added Cl^-, respectively). Because ionic species are involved, the thermodynamic equilibrium constant (K) will be a function of the mean ionic activity coefficient ($\gamma_\pm$) and the experimental equilibrium constant (K_{obs}, see Appendix D for raw data)

$$K = \gamma_\pm^2 \times \left\{\frac{[[Rh(OEP)(PPh_3)_2]^+][Cl^-]}{[Rh(OEP)(Cl)(PPh_3)][PPh_3]}\right\} = \gamma_\pm^2 K_{obs} \qquad (5.4)$$

where $\gamma_\pm$ is defined by the Debye-Hückel limiting law

$$\log_{10} \gamma_\pm = A z_+ z_- \mu^{1/2} \qquad (5.5)$$

The value of K was determined from the intercept of $\log_{10} K_{obs}$ plotted vs. $\mu^{1/2}$ at a particular temperature. Figure 5.2 shows such a plot for the data at 25 °C (Table 5.3), and, for the data at $\mu^{1/2} < 0.07$ $M^{1/2}$, the line drawn gives an intercept corresponding to $\log_{10} K = -1.75$ ($K = 1.74 \times 10^{-2}$). The slope of the least squares line drawn (of slope $-2Az_+z_-$ or $+2A$ for this

particular equilibrium) is 26.88. The calculated value for the slope using the standard expression (eq'n (5.6)) for A is 26.7, showing remarkably good agreement.

$$A = \frac{(2\pi N)^{1/2}}{2.303}\left(\frac{e^2}{10\varepsilon kT}\right)^{3/2} \qquad (5.6)$$

where N = Avogadro's number, e = electronic charge, ε = dielectric constant (8.90 for CH_2Cl_2 at 25 °C), k = the Boltzmann constant, and T = absolute temperature.

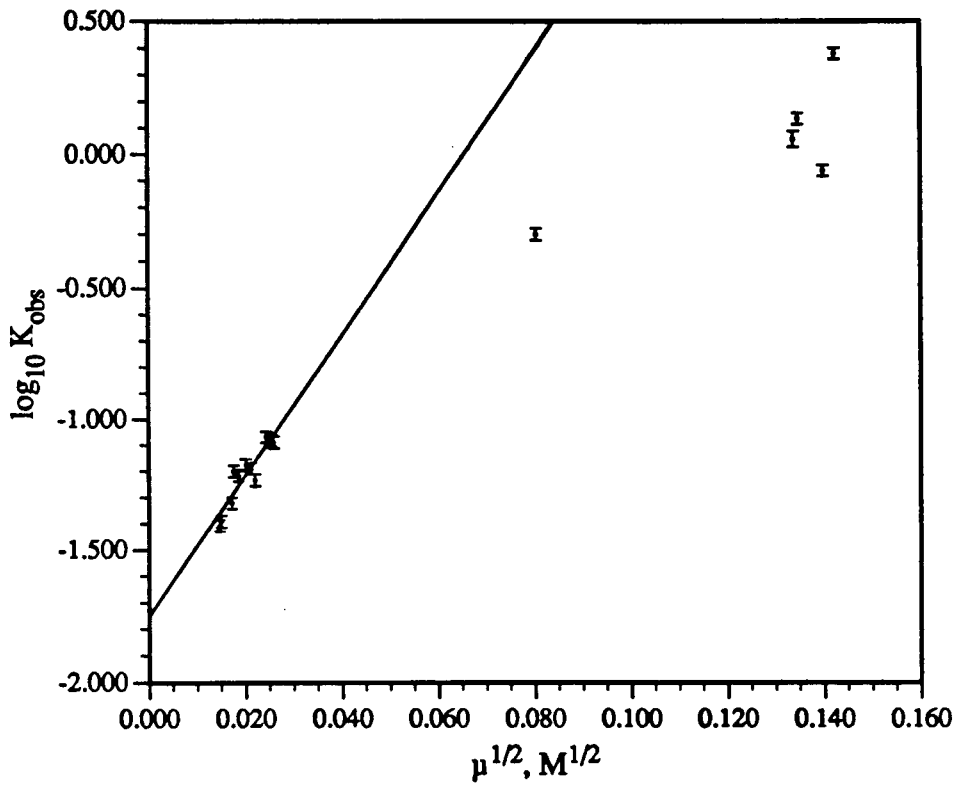

Figure 5.2. Plot of $\log_{10} K_{obs}$ vs. (ionic strength)$^{1/2}$ for data in Table 5.3.

Thermodynamic parameters for equilibrium (5.1) were obtained repeating the equilibrium measurements ($\log_{10} K_{obs}$ vs. $\mu^{1/2}$) at four other temperatures over the range of 10-20 °C. Values of K (temp) are 3.27×10^{-2} (10 °C), 2.62×10^{-2} (15 °C), 2.02×10^{-2} (20 °C), and 1.28×10^{-2} (30 °C) (see Appendix D for raw data). The data give a good van't Hoff plot from which values of ΔH^o (-33 ± 2 kJ mol^{-1}) and ΔS^o (-146 ± 8 J K^{-1}mol^{-1}) were estimated.

Table 5.3. Variation of K_{obs} for reaction 5.1 in CH_2Cl_2 at 25 °C.[a]

$\mu \times 10^4$ M	$K_{obs} \times 10^2$
2.16	3.91
2.26	4.06
2.97	4.77
3.11	6.29
3.45	6.06
4.05	6.65
4.50	6.44
4.88	5.83
5.94	8.53
6.49	8.28
6.74	8.13
64.8	49.9[b]
179.1	114[c]
181.5	136[d]
195.9	86.2[e]
202.6	239[f]

a. Up to $\mu = 6.74 \times 10^{-4}$ M, the ionic strength results solely from the ions generated by reaction 5.1, i.e., no salt has been added. Initial [Rh(OEP)(Cl)(PPh_3)] between $(4.0\text{-}8.0) \times 10^{-4}$ M. The estimated uncertainity in K_{obs} is ± 5% or better and in μ is ± 2.5% or better unless otherwise noted.

b. Added 6.48×10^{-3} M $[Ph_4As]Cl \cdot H_2O$.

c. Added 1.79×10^{-2} M $[Ph_4As]Cl \cdot H_2O$; K_{obs} ± 7%.

d. Added 1.82×10^{-2} M $[Ph_4As]Cl \cdot H_2O$; addition of H_2O to 2×10^{-2} M had no measurable effect on the equilibrium reaction.

e. Added 1.96×10^{-2} M $[^nBu_4N][ClO_4]$.

f. Added 2.03×10^{-2} M $[Ph_4As]Cl \cdot H_2O$.

The net rapid substitution reaction (5.1) almost certainly occurs via a dissociative process and a 5-coordinate intermediate, reactions (5.7), (5.8). The overall K value (= K_1K_2) shows that a

The net rapid substitution reaction (5.1) almost certainly occurs via a dissociative process and a 5-coordinate intermediate, reactions (5.7), (5.8). The overall K value (= K_1K_2) shows that a [PPh_3] of ~0.2 M is required to convert 90% of Rh(OEP)(Cl)(PPh_3) (initially at ~5×10^{-4} M) into $[Rh(OEP)(PPh_3)_2]^+$ at 25 °C.

$$Rh(OEP)(Cl)(PPh_3) \overset{K_1}{\rightleftharpoons} [Rh(OEP)(PPh_3)]^+ + Cl^- \qquad (5.7)$$

$$[Rh(OEP)(PPh_3)]^+ + PPh_3 \overset{K_2}{\rightleftharpoons} [Rh(OEP)(PPh_3)_2]^+ \qquad (5.8)$$

The stoichiometric conversion with P^nBu_3 implies that the equilibrium constant for (5.2) is > 10^3 at corresponding conditions. The large negative ΔS^o value (–146 J mol^{-1} K^{-1}) for reaction (5.1) is reasonable for transformation of neutral species into solvated charged ones. Chloride is expected to form a stronger bond than PPh_3 to Rh(III), and thus the overall exothermicity (–33 kJ mol^{-1}) of the forward reaction presumably results from contributions of the solvation enthalpies of the product ions.

5.2.3. Reactions of Rh(OEP)(Cl)(PPh_3) with CO

Under dark (thermal) conditions (see below), CH_2Cl_2 solutions of Rh(OEP)(Cl)(PPh_3) do not react with 1 atm CO (~5×10^{-3} M), implying that CO at this concentration cannot compete for $[Rh(OEP)(PPh_3)]^+$ with the back reaction of equilibrium (5.7), even though the [Cl^-] must be very low since K_1 is immeasurably small. At an added [PPh_3] of about 5×10^{-3} M, reaction (5.1) with Rh(OEP)(Cl)(PPh_3) (~5×10^{-4} M) would generate ~35% of the bis-phosphine cation. This implies that K_2 (reaction (5.8)) is much smaller for CO addition than for PPh_3. Isoelectronic with $[Rh(OEP)(PPh_3)]^+$, the neutral isolated Ru(OEP)(PPh_3) species reacts more readily with CO (139,162,164,166), presumably because the better π-acceptor properties of CO (vs. PPh_3) (170) are more compatible with the lower oxidation state of Ru(II). The lack of reaction with CO also indicates negligible dissociation of PPh_3 under these conditions to form Rh(OEP)(Cl), which is known to react with CO to form Rh(OEP)(Cl)(CO) (82) (see below), reactions (5.9) and (5.10):

$$Rh(OEP)(Cl)(PPh_3) \rightleftharpoons Rh(OEP)(Cl) + PPh_3 \qquad (5.9)$$

$$Rh(OEP)(Cl) + CO \rightleftharpoons Rh(OEP)(Cl)(CO) \qquad (5.10)$$

The $Rh(OEP)(Cl)(PPh_3)$ complex in benzene, THF or CH_3CN, however, is photochromic in the presence of 1 atm CO, and reacts according to reactions (5.9) and (5.10). Exposure to light or sunlight yields within minutes an in situ carbonyl (ν_{CO} = 2087 cm^{-1} in THF) with concomitant release of PPh_3, and the nmr data (Table 5.1) are consistent with the presence of Rh(OEP)(Cl)(CO). Quantitative re-formation of $Rh(OEP)(Cl)(PPh_3)$ occurs in the dark (under CO) over a few hours via the intermediate Rh(OEP)(Cl)(solvent) species (as judged by comparison with the visible spectrum of Rh(OEP)(Cl) dissolved in the appropriate solvent). Solutions of $Rh(OEP)(Cl)(PPh_3)$ in THF or CH_3CN on exposure to light in the absence of CO also yield the Rh(OEP)(Cl)(solvent) species. The visible spectral data are given in Table 5.2.

The noted reversible carbonylation-decarbonylation reaction, in the daylight and dark, respectively (somewhat atypical in that the decarbonylation process is often photo-assisted), is of potential interest as a further model for solar energy storage in biological systems (171).

The ^1H and $^{31}P\{^1H\}$ nmr data for all the species (Table 5.1) show shifts that are typical for diamagnetic, octahedral, metallo-porphyrin complexes (161,165,166), and the magnitudes of the $^1J_{Rh\text{-}P}$ coupling constants are appropriate for octahedral Rh(III) products (172).

5.2.4. Reactions of $Rh(OEP)(Cl)(H_2O)$ with diphosphines

Diphosphines (PP) are known to bind to Ru(II) porphyrins in (i) a monodentate dangling fashion, (ii) a bridging mode between two metal centers, or, (iii) more speculatively, in a bidentate mode on one metal center to form a "seven-coordinate" species (161,165). The data presented below for similar Rh(III) species are obtained on in situ samples usually formed by titration of a solution of $Rh(OEP)(Cl)(H_2O)$ with aliquots typically containing ~0.2 equivalents of dppm, dppe, dppp or dppb, or by preparation of solutions containing various ratios of diphosphine to $Rh(OEP)(Cl)(H_2O)$. The solubility of the systems decreased with increasing diphosphine carbon chain length and as the ratio of [diphosphine] to [Rh] increased; presumably oligomeric and polymeric $[(\text{-PP–}[Rh(OEP)]^+\text{–PP-})_n]Cl_n$ complexes are formed and some data on such species are presented below.

The diphosphines acting as monodentate ligands readily form Rh(OEP)(Cl)(PP) and $[Rh(OEP)(PP)_2]^+$ complexes, analogous to those formed by PPh_3. The ^1H nmr spectra of

solutions of Rh(OEP)(Cl)(PP) at 10^{-3} - 10^{-2} M (Table 5.4) are consistent with the presence of a diamagnetic metallo-octaethylporphyrin complex, that is asymmetrically substituted with regard to the porphyrin plane. The $-CH_2-$ ^1H nmr resonances of the free diphosphine ligands on coordination are shifted up-field by the porphyrin ring current (Table 5.4), as are the resonances of phenyl protons (Table 5.5), the phenyl protons of the free end of the dangling PP being less affected as the carbon chain lengthens. The $^{31}P\{^1H\}$ nmr resonances (Table 5.4) of the free end of the dangling phosphine are found at higher fields than the free ligand. However, the influence of the ring-current is perhaps obscured by superposition of a variation of δ values that may be related to the carbon backbone chain length (Fig. 5.3). The $^{31}P\{^1H\}$ nmr spectra of the dppm and dppe ligands show AMX patterns for the Rh bound end but the $^4J_{Rh\text{-}P}$ coupling for the dangling end of dppe was too small to observe, resulting in an AX pattern although that of dppm was AMX. Phosphorus-phosphorus coupling is not observed for dppp or dppb, and thus only an AX pattern is observed for the Rh bound ends. The $^1J_{Rh\text{-}P}$ couplings of all four PP complexes are close to that of $Rh(OEP)(Cl)(PPh_3)$.

The methylene protons of the ethyl side chains of the symmetrically substituted $[Rh(OEP)(dppm)_2]^+$ complex appear as the expected quartet and the dppm ^1H nmr ligand resonances are in a 2:1 ratio relative to the porphyrin (Tables 5.4 and 5.5). The ^1H nmr spectral resonances of the dangling diphosphine ligands are similar to those of the Rh(OEP)(Cl)(PP) complexes but the $^{31}P\{^1H\}$ nmr spectrum shows more complex AA'MM'X splittings (Fig. 5.4). This pattern is believed to arise because of virtual coupling between the Rh bound phosphorus on one side of the metal center and the dangling phosphorus on the opposite side (i.e., A with M'), making the chemically equivalent Rh bound phosphorus nuclei magnetically inequivalent. The neutral, isoelectronic, $Ru^{II}(TPP)(dppm)_2$ complex displays a related AA'XX' pattern of two triplets at 11 ppm (Ru-P) and -29 ppm (-P) in $CDCl_3$ (161), and thus the Rh-P inequivalence of the Rh(III) complex is not believed to be due to ion-pairing. The cationic $[Rh(OEP)(dppm)_2]^+$ complex can be observed by nmr in C_6D_6 (Table 5.4 and Fig. 5.5) where it must exist as a tight ion-pair and this, in principle, could introduce asymmetry into the complex, but the $^{31}P\{^1H\}$ spectra in C_6D_6 and $CDCl_3$ are nearly identical and thus effects due to ion-pairing are not obvious.

Table 5.4. Various ^1H and $^{31}P\{^1H\}$ nmr spectral data for Rh(OEP) complexes of monodentate diphosphines.[a]

complex	^1H meso-H	$-CH_2-$	$-CH_3$	$P-CH_2-$[b]	$-CH_2-$	$-CH_2-$	$-CH_2-$
Rh(OEP)(Cl)(dppm)	10.00 s	3.92 m, 3.73 m	1.81 t	-2.22 d			
Rh(OEP)(Cl)(dppe)	9.99 s	3.94 m, 3.82 m	1.86 t	-2.75 m	-0.75 m		
Rh(OEP)(Cl)(dppp)	10.05 s	3.97 m, 3.83 m	1.88 t	~-2.7 m	~-1.3 m	~0.6 m	
Rh(OEP)(Cl)(dppb)	10.01 s	3.93 m, 3.77 m	1.84 t	-3.00 m	-1.44 m	0.01 m	0.68 m
$[Rh(OEP)(dppm)_2]^{+}$[c]	9.70 s	3.88 q	1.75 t	-2.87 t[e]			
$[Rh(OEP)(dppm)_2]^{+}$[d]	10.05 s	f	f	-2.48 t[e]			

$^{31}P\{^1H\}$ δ(J):	Rh-P	dangling–P
Rh(OEP)(Cl)(dppm)	16.00 dd ($^1J_{Rh-P}$ = 117; $^2J_{P-P}$ = 35)	-31.50 dd ($^3J_{Rh-P} \approx 3$; $^2J_{P-P}$ = 35)
Rh(OEP)(Cl)(dppe)	18.64 dd ($^1J_{Rh-P}$ = 118; $^3J_{P-P}$ = 33.3)	-14.22 d ($^3J_{P-P}$ = 33.3)
Rh(OEP)(Cl)(dppp)	14.62 d ($^1J_{Rh-P}$ = 116)	-22.54 s
Rh(OEP)(Cl)(dppb)	15.03 d ($^1J_{Rh-P}$ = 117)	-18.18 s
$[Rh(OEP)(dppm)_2]^{+}$[c]	6.05 dt[g]	-31.69 t[g]
$[Rh(OEP)(dppm)_2]^{+}$[d]	6.68 dt	-30.55 t

a. The Rh(OEP)(Cl)(PP) complexes were made in situ by mixing 1:1 ratio of PP to Rh in C_6D_6 (see text); 300 MHz for ^1H; 121.421 MHz for $^{31}P\{^1H\}$ at 20 °C.

b. Only the diphosphine methylene resonances are listed; see Table 5.5 for phenyl proton resonances.

c. In $CDCl_3$.

d. Prepared in situ by mixing 3:1 ratio of PP to Rh.

e. Triplet is barely resolved as shoulders on central signal.

f. Overlapped by other resonances (see text).

g. Estimated coupling constants: (P_M-C-P_A-Rh-$P_{A'}$-C-$P_{M'}$) $^1J_{Rh-P_A} \sim 120$ Hz, $^3J_{Rh-P_M} \sim -2$ Hz, $^2J_{P_A-P_M} \sim 34$ Hz, $^2J_{P_A-P_{A'}} \sim 100$ Hz, $^4J_{P_A-P_{M'}} \sim 20$ Hz.

Table 5.5. Various ^1H nmr spectral data for the phenyl protons of monodentate diphosphine ligands in Rh(OEP) complexes.[a]

complex	Rh-P(Ph)$_2$-			dangling-P(Ph)$_2$		
	p-	m-	o-	p-	m-	o-
Rh(OEP)(Cl)(dppm)	6.34	6.01	3.65[b]	6.70		6.20
Rh(OEP)(Cl)(dppe)	6.48	6.14	3.68	6.84	6.74	6.48
Rh(OEP)(Cl)(dppp)	6.47	6.15	3.7[b]	~6.8		c
Rh(OEP)(Cl)(dppb)	6.50	6.22	c	d	d	d
[Rh(OEP)(dppm)$_2$]$^{+}$[e]	6.68	5.88	3.23	6.96	6.81	6.13

a. In C_6D_6, unless otherwise stated; 300 MHz at 20 °C; all resonances are multiplets.
b. Overlapped by $-CH_2-$ resonances of ethyl side chains, assigned using COSY.
c. Overlapped by other resonances.
d. Overlapped by free dppb.
e. In $CDCl_3$.

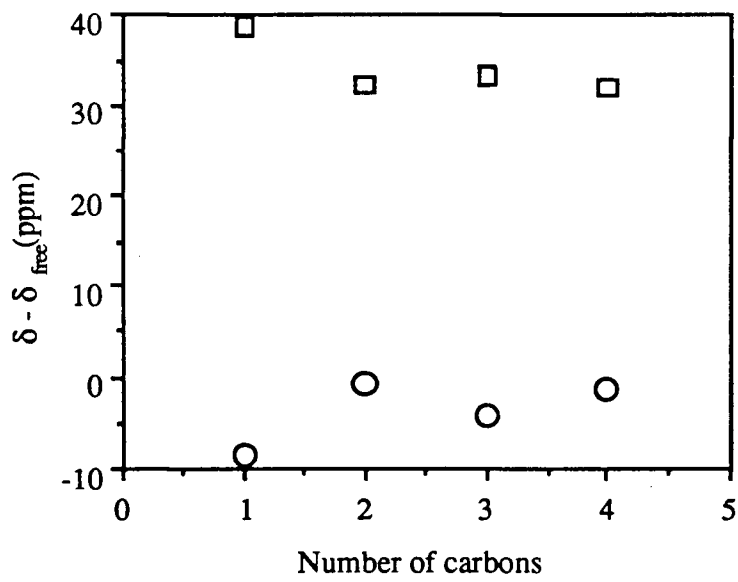

Figure 5.3. Variation of $^{31}P\{^1H\}$ nmr δ–δ_{free} shifts for the PP ligand of Rh(OEP)(Cl)(PP) with the chain length of the diphosphine backbone. Data for Rh bound P(□) and dangling P (○) are shown.

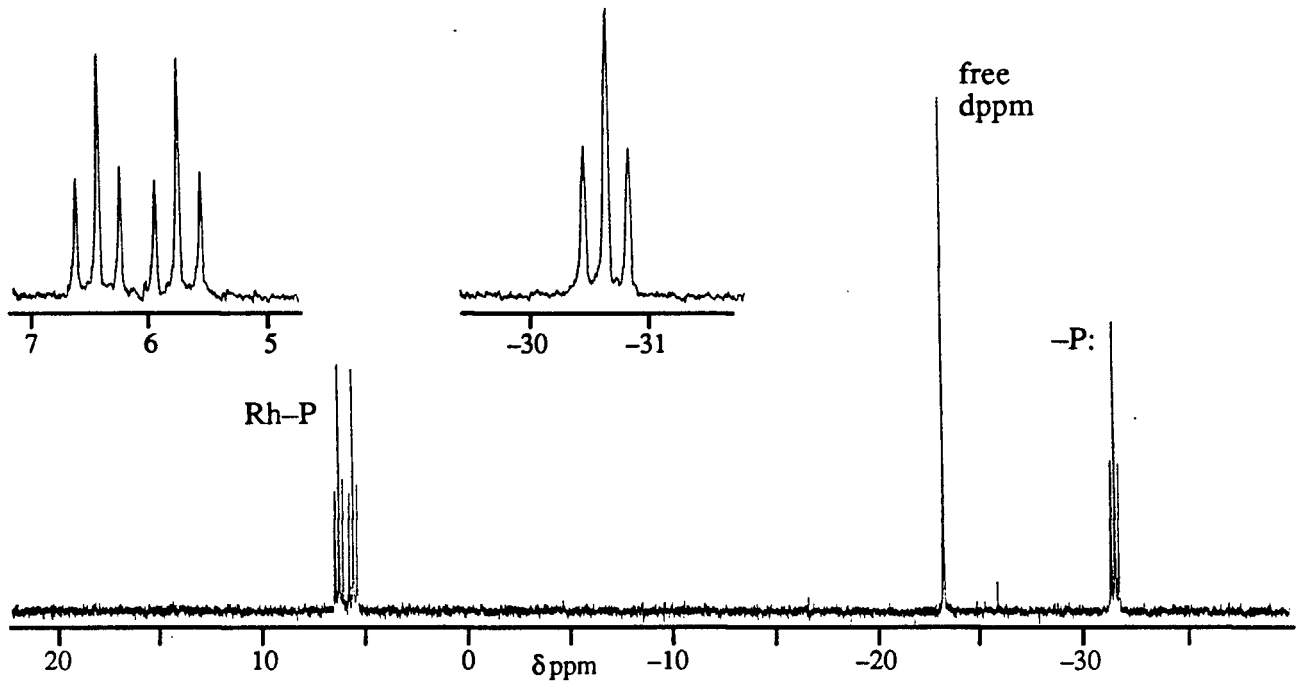

Figure 5.4. The $^{31}P\{^{1}H\}$ nmr spectrum of $[Rh(OEP)(dppm)_2]^+$ in $CDCl_3$ at 20 °C. Prepared in situ under Ar, [Rh] ≈ 10^{-2} M, [dppm] ≈ 3×10^{-2} M.

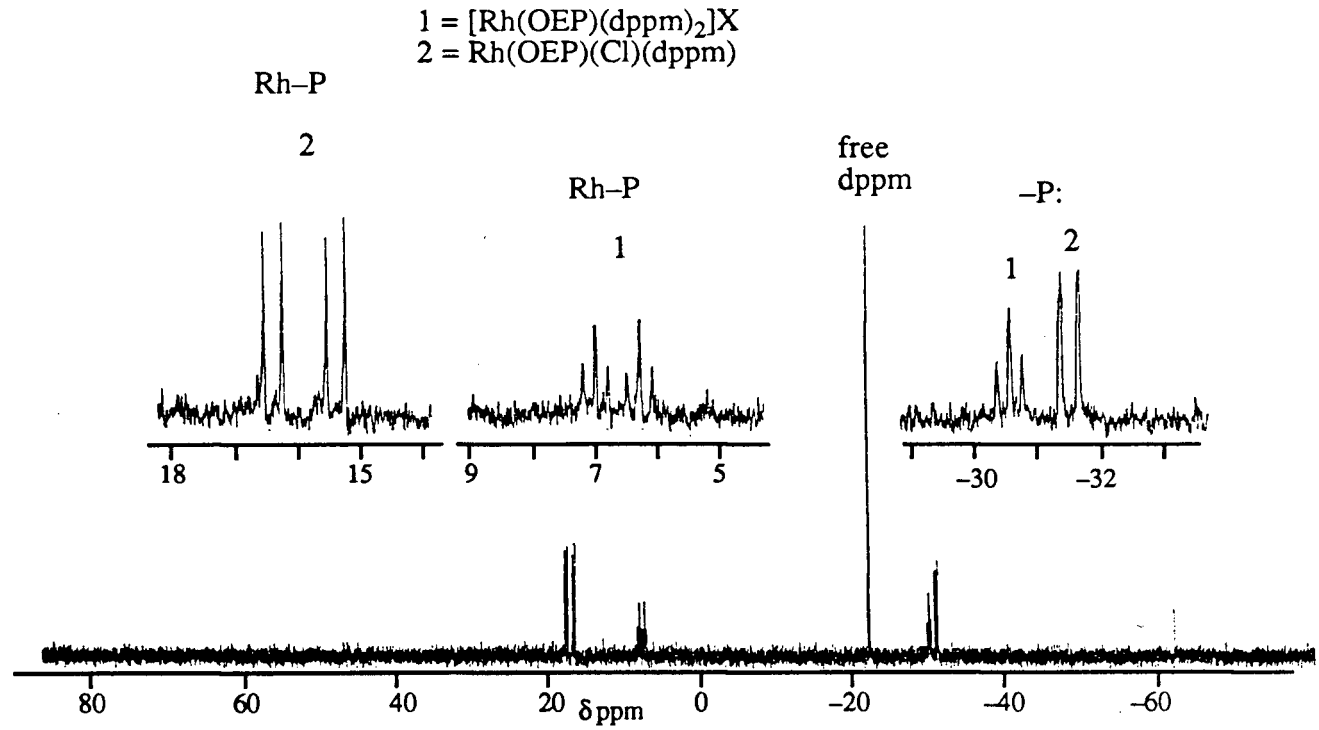

Figure 5.5. The $^{31}P\{^{1}H\}$ nmr spectrum of a C_6D_6 solution of Rh(OEP)(Cl) in the presence of ~2.4 equivalents of dppm at 20 °C. Prepared under Ar.

Clear identification of cationic bis-phosphine complexes with dppe, dppp or dppb in C_6D_6 is obscured by the increasing complexity of the nmr spectra during the titrations in this solvent, and only for dppm is simple formation of mono- and bis-phosphine complexes observed as [PP] is increased. In some of these solutions (e.g., with ~1 equivalent dppb), $^{31}P\{^1H\}$ nmr resonances indicative of Rh-bound phosphine similar to the bis-phosphine cations were found in conjunction with other $^{31}P\{^1H\}$ and ^1H nmr resonances corresponding to those of the bridging species discussed below, but without evidence for the corresponding dangling phosphine. This is suggestive of ion-paired species such as "[Cl-Rh(OEP)-μdppb-Rh(OEP)-μdppb-Rh(OEP)(Cl)]Cl".

Addition of 0.5 equivalents of diphosphine to solutions of Rh(OEP)(Cl) usually leads to formation of $[Rh(OEP)(Cl)]_2$-μPP complexes as the major species. The ^1H and $^{31}P\{^1H\}$ nmr data on the complexes are summarized in Table 5.6. The $^{31}P\{^1H\}$ nmr spectra are characterized by a lack of resonances for a dangling phosphine. The spectra of the dppm and dppe systems show similar 6-line AA'XX' patterns, because of magnetic inequivalence of the phosphorus nuclei due to coupling across the bridging phosphine and so an AX pattern is observed. The chain length of the dppp is too long for P-P or Rh-P coupling across the backbone. The cumulative effect of the ring currents of two porphyrins causes the $-CH_2-$ ^1H nmr resonances of the diphosphines to be shifted further up-field than those observed for the dangling phosphine complexes. The meso resonances are also slightly shifted from the values for the dangling species, and the methylene resonances of the ethyl side-chains (at least within the μdppm species) are well separated as expected for a species with cofacial porphyrins (e.g. like $[Rh(OEP)]_2$) (78). The dppm phenyl proton resonances are particularly affected by steric crowding enforced by the close proximity of the porphyrins. At -10 °C, a number of small broad ^1H nmr resonances in the 7 to 0 ppm range are shown by a COSY experiment to be two sets of five interrelated resonances (Fig. 5.6). These are assigned as μ-dppm phenyl protons, each multiplet being 2H based on integration of the 1D spectrum, and are in a 1:2 ratio with the set of shifted porphyrin resonances just mentioned. The ligand ^1H nmr resonances are broad above room temperature but the $^{31}P\{^1H\}$ nmr AAXX' pattern remains at temperatures up to 44 °C and the respective $^1J_{Rh\text{-}P}$ couplings in mixtures of Rh(OEP)(Cl)(dppm) and

Table 5.6. Various ^1H and $^{31}P\{^1H\}$ nmr spectral data for Rh(OEP) complexes containing bridging diphosphines.[a]

complex	^1H meso-H	$-CH_2-$	$-CH_3$	$P-CH_2-$[b]	$-CH_2-$	$-CH_2-$	$-CH_2-$
$[Rh(OEP)(Cl)]_2$-μdppm	9.73 s	4.07 m, 3.88 m	1.76 t	-5.37 t			
$[Rh(OEP)(Cl)]_2$-μdppe	9.29 s	3.44 m	1.55 t	-5.60 s			
$[Rh(OEP)(Cl)]_2$-μdppp	9.77 s	3.81 m	1.76 t	-4.26 m [c]			
$[Rh(OEP)(Cl)]_2$-μdppb	9.64 s	3.66 m, 3.49 m	1.46 t	-4.27 m	-2.85 m		

$^{31}P\{^1H\}$	δ(J): Rh-P
$[Rh(OEP)(Cl)]_2$-μdppm	11.41 m[d]
$[Rh(OEP)(Cl)]_2$-μdppe	17.56 m[d]
$[Rh(OEP)(Cl)]_2$-μdppp	16.67 d (J_{Rh-P} = 117)

a. C_6D_6; 300 MHz for ^1H; 121.421 MHz for $^{31}P\{^1H\}$ at 20 °C.
b. Only the diphosphine methylene resonances are listed.
c. Overlapped by $P-CH_2-$.
d. 6 lines. Estimated coupling constants: $(Rh-P_A-C-P_{A'}-Rh)$ $^1J_{Rh-P_A} \sim 120$ Hz, $^3J_{Rh-P_{A'}} \sim -2$ Hz, $^2J_{P_A-P_{A'}} \sim 34$ Hz.

$[Rh(OEP)(Cl)]_2$-μdppm remain at 84 °C; thus dppm is only slowly exchanged between the two species. However, the ratio of their respective meso proton integrations varies reversibly with temperature, consistent with an equilibrium involving the two species. A possible conformation that satisfies two sets of pair-wise equivalences of phenyl protons is shown in Figure 5.7, where the porphyrins are nearly parallel. The **A** ring protons show shifts to more higher field than the corresponding dangling phosphine complex (Table 5.5) due to the effect of two porphyrin ring-currents, and the **B** ring protons show both up- and down-field relative shifts due to their additional mutual ring-current effects. The porphyrin $-CH_2-$ proton resonances of the μdppm species appear as two multiplets. The lower field multiplet broadens more than the higher field multiplet as temperature increases and probably represents the "inside" environment between the porphyrins.

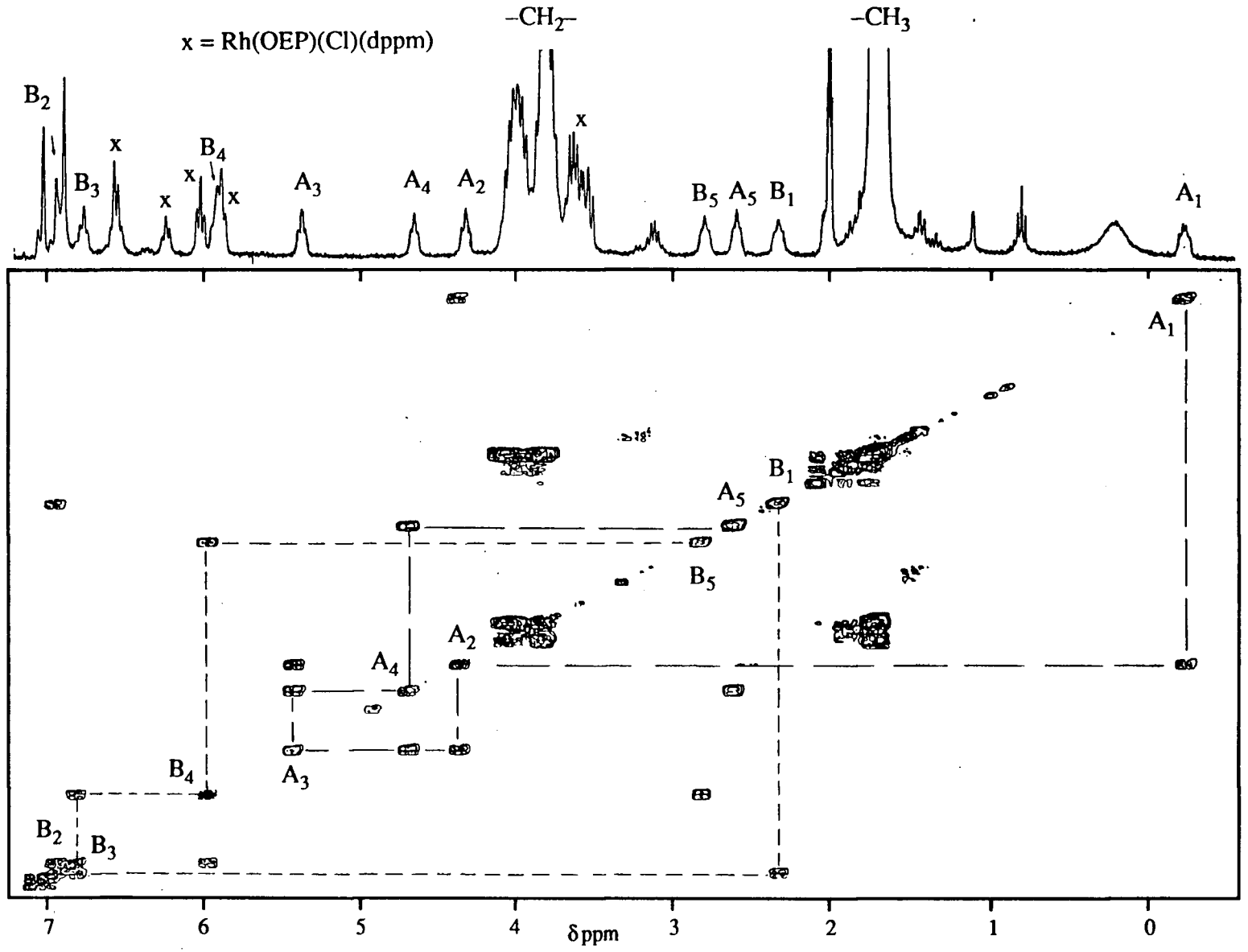

Figure 5.6. The COSY spectrum of a C_7D_8 solution of $[Rh(OEP)]_2$-μdppm at –10 °C. The long and short dashed lines connect the two sets of μdppm phenyl protons (i.e: 2 sets of 5 multiplets of 2H per multiplet labelled as in Fig. 5.7).

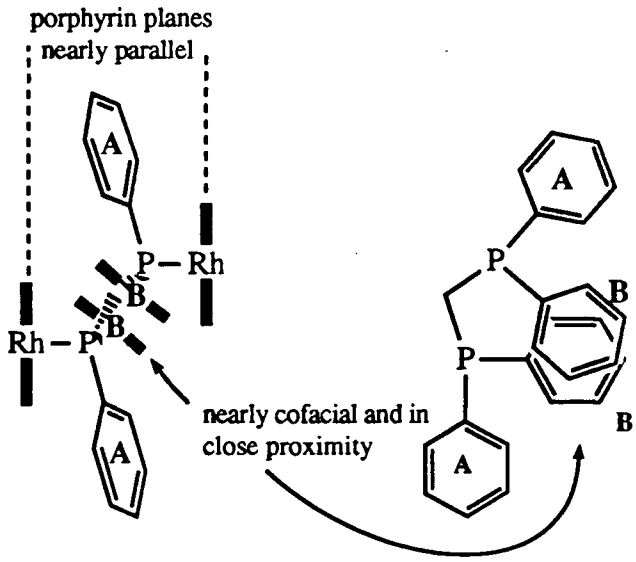

Figure 5.7. Sketch of a possible conformation for dppm in [Rh(OEP)]$_2$-μdppm.

The titrations of Rh(OEP)(Cl)(H_2O) with the diphosphines could be monitored also by visible spectroscopy, at [Rh] ≈ 5×10^{-4} M. Figure 5.8 illustrates the changes of the β and α bands after addition of 0.54, 0.9 and 2.0 equivalents of dppm to Rh(OEP)(Cl) in CH_2Cl_2. The spectra of CH_2Cl_2 solutions after addition of 0.9 and 2.0 equivalents are very similar to those of Rh(OEP)(Cl)(PPh_3) and [Rh(OEP)(PPh_3)$_2$]$^+$, respectively, and are most probably those corresponding to the respective diphosphine analogues. The spectrum of the Rh(OEP)(Cl)(H_2O) complex is completely removed by addition of ~0.5 equivalents of dppm, and the resulting spectrum is different from those of the mono- and bis-diphosphine complexes, being therefore attributable to the [Rh(OEP)]$_2$-μdppm complex. A similar progression is observed in C_6H_6 but only to the mono-bisphosphine. The relatively clean step-wise progression through the μdppm, mono- and bis-dppm species is in accord with the nmr data.

Isosbestics at 530, 548 and 563 nm are observed in the 500–600 nm region during the addition of the first to second equivalent of dppm, but varying the temperature of an intermediate spectrum (i.e., 1.4 equivalents; presumably giving a mixture of Rh(OEP)(Cl)(dppm) and [Rh(OEP)(Cl)(dppm)$_2$]$^+$) gave a different set of isosbestics at 559, 562, 569 and 578 nm, the α band intensities of the equilibrated species diminishing together as the temperature increases.

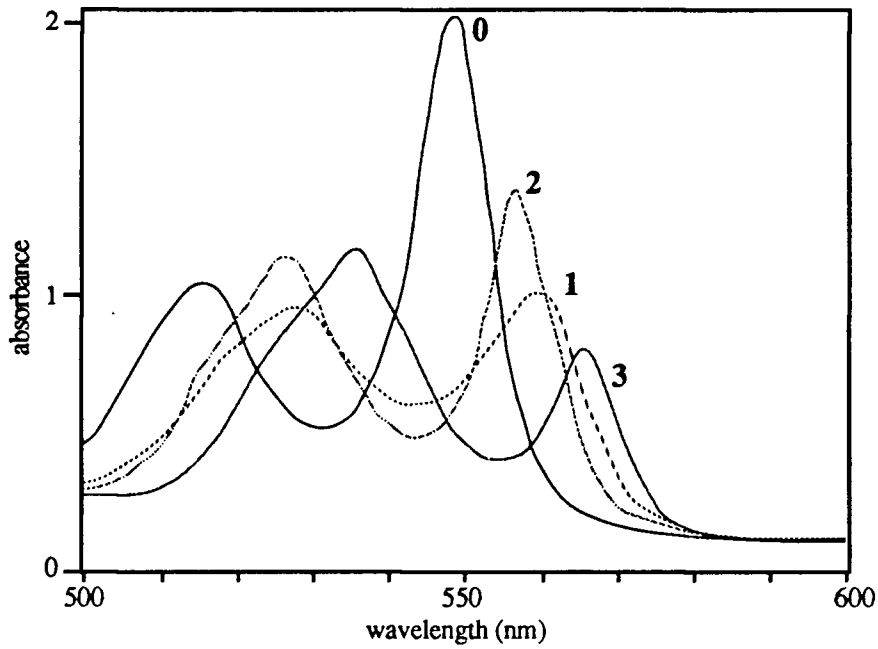

Figure 5.8. Spectroscopic titration of Rh(OEP)(Cl)(H_2O) with added dppm in CH_2Cl_2 at 25 °C, [Rh] = 7.25×10^{-4} M; curves **0**–**3** result from added [dppm] of 0.0, 0.5, 0.9, 2.0 equivalents, respectively.

The α band of the [Rh(OEP)(Cl)]$_2$-μdppm complex is at 560 nm and thus the changes observed are probably due to a equilibrium between the μdppm, mono- and bis-dppm complexes (reactions (5.11) and (5.13)).

$$[Rh(OEP)(Cl)(dppm)_2]^+ + Cl^- \rightleftharpoons Rh(OEP)(Cl)(dppm) + dppm \quad (5.11)$$

$$Rh(OEP)(Cl)(dppm) \rightleftharpoons Rh(OEP)(Cl) + dppm \quad (5.12)$$

$$Rh(OEP)(Cl)(dppm) + Rh(OEP)(Cl) \rightleftharpoons [Rh(OEP)(Cl)]_2\text{-}\mu dppm \quad (5.13)$$

The observation of nmr coupling across the dppm and dppe bridges, but not dppp, provides a useful probe of communication between the porphyrins of the bridged species. A related question is whether the length of the bridge also affects the electronic spectrum of the chromophore, i.e., the porphyrin, in comparison to the spectrum of the mono-PP species, and indeed the visible spectrum of the μdppm and mono-dppm complexes differ (vide infra).

Data in the 500–600 nm region taken during titrations of Rh(OEP)(Cl)(H_2O) with dppe or dppp reveal that the visible spectra of the solutions after addition of 1 equivalent of PP are very

similar for both systems and are similar to that of the Rh(OEP)(Cl)(dppm) species; all are probably Rh(OEP)(Cl)(PP) species, the 3 species having β bands at ~530 nm and the α bands ~560 nm in C_6H_6. However, although the nmr data show fairly clean step-wise addition of dppe to Rh(OEP)(Cl)(H_2O) to form the μdppe species with addition of up to 0.5 equivalents of dppe, and then the mono-dppe species at ~1 equivalent added dppe, the visible data show only the superposition of the spectra of Rh(OEP)(Cl)(H_2O) and Rh(OEP)(Cl)(dppe) over the whole range of added dppe. In the dppp system, the visible spectrum of Rh(OEP)(Cl)(H_2O) is completely removed by the addition of 0.5 equivalents of dppp, being replaced by a spectrum similar to that of the Rh(OEP)(Cl)(dppp) species (531 nm β band, 561 nm α band). Addition of a further 0.5 equivalents resulted in little change to the spectrum. This suggests that the spectrum of [Rh(OEP)(Cl)]$_2$-μdppp is the same as that of Rh(OEP)(Cl)(dppp) and that there is no effect on the chromophore at that chain length. The visible data for the dppe system do not reveal the spectrum of the μdppe species because it appears that such a species is not detectably formed at the concentration used for the visible titration ([Rh] = 2.38×10^{-4} M) which is ~10 times more dilute than that used for the nmr titration experiments.

Attempts were made to isolate the μ-dppm complex, as its spectroscopic data suggested that it was the most stable and cleanly formed in the series. Unfortunately, attempts to precipitate the complex from its solutions gave mixtures of free diphosphine (as colourless crystals), starting material and the bridged complex. Isolation by freeze-drying a benzene solution of the μ-dppm complex prepared by careful titration gave an impure material.

5.3. General Discussion

The findings on reactivity of the PPh_3 complexes can be summarized as shown in Scheme 5.1. Phosphine ligation of Rh(OEP)(Cl)(PPh_3) with loss of Cl^- in a thermal reaction is thermodynamically favoured relative to corresponding CO ligation. However, reactivity toward CO with loss of PPh_3 (even in the presence of excess PPh_3) is enhanced by "forcing" the system through an unsaturated intermediate generated photochemically. These equilibria are of particular relevance to the reactions of M(por)L_2 complexes (M = Fe, Ru; L = phosphine, CH_3CN, THF

etc.) with gas molecules such as CO and O_2, that also go via a dissociative mechanism (159, 160, 162,173-182).

$$M(por)(L)_2 \underset{+L}{\overset{-L}{\rightleftharpoons}} M(por)L \underset{-gas}{\overset{+gas}{\rightleftharpoons}} M(por)(gas)(L) \qquad (5.14)$$

Enhancement of the concentration of the 16-electron, 5-coordinate complexes is probably important in a catalytic context, such as decarbonylation of aldehydes which might proceed via the M(por)(CO)L species (159,160,178-180). In this regard, preliminary data indicate that phenyl-acetaldehyde can be used as a carbonyl source, instead of CO gas, to form Rh(OEP)(Cl)(CO) from Rh(OEP)(Cl)(PPh_3). For example, a THF solution containing 7×10^{-4} M Rh(OEP)(Cl)(PPh_3) and excess aldehyde (~0.2 M) slowly generates at 20 °C a solution of Rh(OEP)(Cl)(CO) as judged by visible spectroscopy data, although organic co-products were not tested for.

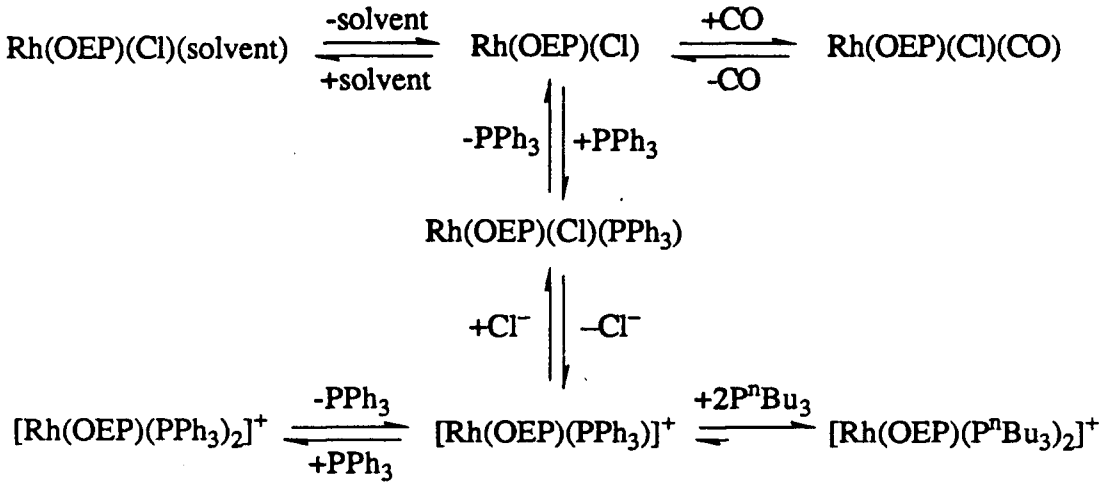

Scheme 5.1. Reactivity scheme for solutions of Rh(OEP)(Cl)(PPh_3).

The use of diphosphines introduces novel possibilities besides the formation of monodentate complexes analogous to the PPh_3 and P^nBu_3 species. Scheme 5.2 summarizes the transformations observed during the titration experiments. In particular, the formation of μ-diphosphine metallo-porphyrin complexes is established, although this finding is not unprecedented, a singlet at 3.7 ppm in the $^{31}P\{^1H\}$ nmr spectrum of a $CDCl_3$ solution of a 1:1

Ru(OEP)(CO)(EtOH)/dppe mixture at -20 °C being ascribed to a μ-dppe species (165). The corresponding ^1H nmr spectrum contained a peak at -5.76 ppm which was tentatively ascribed to the $-CH_2-$ group of the dppe ligand of a seven-coordinate species; this ^1H resonance is probably better assigned to the μdppe ligand by comparison to data for the Rh analogues (Table 5.6).

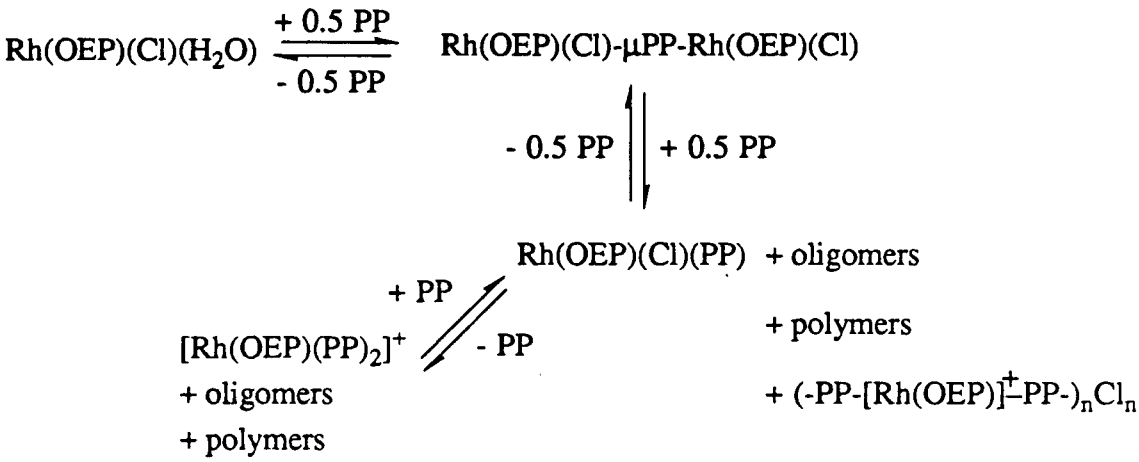

Scheme 5.2. Formation of various rhodium diphosphine complexes.

The propensity of the longer chain diphosphines to form oligomers and polymers has been noted before with Ru(II) porphyrins (161). The benzene solubility of some of the cationic Rh(III) species is surprising. The solubilizing ability of the diphosphines perhaps lies in stabilization of ion-pairs because the dangling diphosphines, or porphyrin oligomer, contain a suitably dimensioned pocket, for the Cl^- anion, containing the positively charged Rh center. Additionally, dangling phosphines may simply enhance the solubility of the porphyrin species sufficiently to compensate for the unfavourable solvation energetics. Tertiary phosphines with long chain alkyl substituents are used to enhance the solubility of Rh, Pd or Pt organometallic species in organic solvents (119).

Chapter 6

General conclusions and suggestions for further work

The work in this thesis comprised research into the reactions of some small molecules with various Rh(por) species. The original motivation was to probe the formation of MOOH from the reaction of a metal hydride with O_2, the metal in this instance being Rh. Some comments as to the direction of future work are also presented.

The reaction of Rh(OEP)(H) with O_2 in organic solvents was examined by visible, ^1H and $^{31}P\{^1H\}$ nmr spectroscopy as a candidate system for the net insertion of O_2 into the metal-hydride bond. The products of the room temperature reaction in dry benzene were $[Rh(OEP)]_2$ and H_2O, but nmr data for a thermally unstable $Rh^{III}(OEP)(OOH)(H_2O)$ intermediate were obtained at -40 °C in CD_2Cl_2. Under other conditions, uncharacterised species were observed along with some Rh(OEP)(OH). The system was clearly too sensitive to impurities under the conditions used. The more hindered TMP may be a better possibility, principally because formation of Rh-Rh bonded dimers is prevented. Because of synthetic difficulties only small quantities of Rh(TMP)(H) were prepared, and preliminary studies of the reaction of O_2 with the hydride gave contradictory results.

The addition of PPh_3 to CH_2Cl_2 solutions of Rh(OEP)(H) promoted a rapid minor reaction involving the solvent giving $Rh(OEP)(Cl)(PPh_3)$, $Rh(OEP)(CH_2Cl)(PPh_3)$ and $[Rh(OEP)(PPh_3)_2]^+$ in ~20% yield, the other major reaction product being the hydride $Rh(OEP)(H)(PPh_3)$. Addition of O_2 to these solutions appeared to promote further the solvent reaction to the extent that the $Rh(OEP)(Cl)(PPh_3)$ and $Rh(OEP)(CH_2Cl)(PPh_3)$ became the major species (in equimolar amounts) in solution, without concomittant formation of $OPPh_3$. The formation of $Rh(OEP)(CH_2Cl)$ by reaction with the solvent appears to involve a $Rh^{II}(OEP)(PPh_3)$ species because $[Rh(OEP)]_2$ and, by implication, $Rh^{II}(OEP)$ do not react with CH_2Cl_2 at comparable rates. In benzene solution there was evidence that attack by the Rh center on the phenyl ring of the PPh_3 occurred.

The sensitivity of the reaction of Rh(OEP)(H) with O_2 to initial conditions, and the observation of products containing Rh(II) and Rh-CH_2Cl, suggest a radical mechanism, which is consistent with known Rh-H chemistry.

Initiation/termination:

$$2Rh(OEP)(H) \rightleftharpoons [Rh(OEP)]_2 + H_2 \quad (6.1)$$

$$[Rh(OEP)]_2 \rightleftharpoons 2Rh(OEP)\cdot \quad (6.2)$$

and in the presence of PPh_3

$$[Rh(OEP)]_2 + PPh_3 \rightleftharpoons \cdot Rh(OEP)(PPh_3) + Rh(OEP)\cdot \quad (6.3)$$

Propagation:

$$Rh(OEP)\cdot + O_2 \rightleftharpoons Rh(OEP)(O_2) \quad (6.4)$$

$$Rh(OEP)(O_2) + Rh(OEP)(H) \longrightarrow Rh(OEP)(OOH) + Rh(OEP)\cdot \quad (6.5)$$

Termination:

$$Rh(OEP)(OOH) + Rh(OEP)(H) \longrightarrow [Rh(OEP)]_2 + H_2O + \tfrac{1}{2}O_2 \quad (6.6)$$

and in the presence of PPh_3

$$\cdot Rh(OEP)(PPh_3) + CH_2Cl_2 \rightleftharpoons Rh(OEP)(Cl)(PPh_3) + \cdot CH_2Cl \quad (6.7)$$

$$Rh(OEP)\cdot + \cdot CH_2Cl \rightleftharpoons Rh(OEP)(CH_2Cl) \quad (6.8)$$

Of interest was the effect of H_2O on the reaction of Rh-H with O_2 and the formation of $[Rh(OEP)]_2$ as a product. A stabilising effect on $[Rh(OEP)]_2$ by excess H_2O when O_2 was present was also observed during the investigation of the reaction of Et_3N with Rh(por)(Cl). The presence of PPh_3, a Lewis base, did not promote formation of the dimer under similar conditions. Clearly the preliminary mechanism presented does not adequately address the effect of Lewis bases and H_2O on the mechanism. The equilibrium behaviour of Rh(II) species (monomeric and dimeric) is central to the chemistry of rhodium porphyrins, and investigation of the effects of steric hindrance (i.e., using TMP to prevent dimerisation), Lewis bases and protic reagents (i.e., H_2O) is of interest.

The mechanisms of the reactions of some tertiary alkylamines (principally Et_3N) with Rh^{III}(por)(Cl)(L) (por = OEP or TMP, L = H_2O or iPrOH) were explored. The formation of $[Rh^{II}(OEP)]_2$ species under mild conditions was observed with some amines, and several novel organometallic derivatives of Et_3N have been found. A portion of the tertiary amine was oxidatively dealkylated to the dialkylamine. Detailed spectroscopic examination of the interaction of Rh(por)(Cl)(L) with Et_3N revealed a complex manifold of reactions. The interaction gave products, identified by visible spectroscopy (scanning and stopped-flow) and ^1H nmr spectroscopy to be Rh(por)(CH(Me)NEt_2), Et_2NH as Rh(por)(Cl)(Et_2NH), and Rh(por)(CH_2CHO). This indicated amine C-H and C-N bond cleavages and net 1-electron reduction of Rh(III) to Rh(II) species ($[Rh(OEP)]_2$). Of other amines examined, aniline, N-methyl-diphenylamine and N-ethyl piperidine all formed complexes of the type Rh(OEP)(Cl)(amine), although the N-ethyl piperidine complex decomposed within 24 h. Proton Sponge and tributylamine gave $[Rh(OEP)]_2$ as a major product under anærobic conditions and, with the latter amine, the Rh(OEP)(Cl)($^nBu_2NH$) complex was also observed.

Stopped-flow data showed that Et_3N initially replaced L of the Rh^{III}(por)(Cl)(L) species to form a Rh^{III}(por)(Cl)(Et_3N) complex. An equilibrium involving reduction of Rh^{III} to Rh^{II} resulted and in aromatic solvents, under anærobic conditions, slow reaction of Rh^{II}(por) with Et_3N proceeded to give Rh(por)(CH(Me)NEt_3). The formation of Rh(II) was inhibited in the presence of the competing donor ligand CH_3CN, and also when the porphyrin was TMP. Thus it appears that formation of $[Rh(OEP)]_2$ provids the driving force in the OEP systems, while there is no comparable driving force in the TMP system because steric hindrance prevented dimer formation. In CH_2Cl_2, reaction of Et_3N with Rh(por)(Cl)(L) was fast, giving a mixture principally of Rh(por)(CH_2Cl)(amine) and the η^1-ylidic enamine complex, Rh(por)(Cl)($CH_2CH{=}NEt_2$) with minor mounts of Rh(por)(CH(Me)NEt_3) being formed, irrespective of the porphyrin used. The formation of Rh(por)(CH_2Cl) species for both TMP and OEP could provide a similar driving force for both systems unlike for the chemistry of aromatic solvents. The solutions containing Rh(por)(Cl)($CH_2CH{=}NEt_2$) or Rh(por)(CH(Me)NEt_3) complexes, ultimately form Rh^{III}(por)(Cl)(Et_2NH). The bulk of the Et_2NH formed was probably from the acid hydrolysis of

the free enamine, itself formed from the net 2-electron oxidation of Et_3N via an aminyl radical. The data also show that there was a requirement for an oxidant (i.e., air or O_2) to produce at least some of the C-N cleavage products (Et_2NH and Rh(por)(CH_2CHO)), while oxidation *after* formation of Rh(OEP)(CH(Me)NEt_2) led to more Rh(OEP)(CH_2CHO) than when air was present initially, when Et_3N reacted with Rh(OEP)(Cl)(H_2O). Thus the reaction sequence suggested from the investigation of the anærobic systems is believed not to be the same as that of the purely ærobic system. The O atom in the stable Rh(OEP)(CH_2CHO) species appeared to be from the added O_2. Coordination of the Et_2NH product to Rh^{III}(por)(Cl) to form Rh(OEP)(Cl)(Et_2NH) probably prevented catalytic dealkylation under the conditions used.

Enough mechanistic information about the alkylamine reaction has been extracted to provide a useful framework from which more definitive studies can be undertaken in the future. The non-metal containing products need defining, as well as the less well characterised Rh-R and Rh(II) species, before kinetic analysis. There is potential for a number of interesting VT nmr spectral studies of the conformations (and associated thermodynamics) of ligands bound to Rh^{III}(TMP). The ^1H nmr spectra of Rh(TMP)(Cl)(Et_2NH), Rh(TMP)(Cl)(CH_2Cl_2) and Rh(TMP)(CH(Me)NEt_2) were particularly temperature dependent, and the activation parameters for the associated processes need determining. The solution behaviour of Rh(TMP)(Cl)(L) and Rh(TMP)(Cl)(solvent) versus the less hindered corresponding OEP complexes is interesting from the point of view of possible local modification of solvent structure by formation of a "solvent-free cavity" if two five-coordinate Rh^{III}(TMP)(L) species associate in solution. In addition, the effects of size and/or Lewis acid/base behaviour may be distinguishable (Table 2.8, p. 66). The solvation data will be particularily important in the context of the direct reaction of H_2 with Rh(por)(Cl) species to give Rh(por)(H), possibly via a dihydrogen complex precursor; reaction in both solution and solid state has been observed and it will be interesting to see if the hydride formation occurs via an intermolecular or intramolecular (i.e., H-atom tunnelling) process.

The synthesis, along with characterisation by visible, ^1H and $^{31}P\{^1H\}$ nmr spectroscopy, of the mono-phosphine complex Rh(OEP)(Cl)(PPh_3) are presented. Additionally, spectroscopic evidence is presented for solution equilibria of Rh(OEP)(Cl)(PPh_3) involving

formation of $Rh(OEP)(L)_2^+$ (L = PPh_3, P^nBu_3) via thermal reactions, and Rh(OEP)(Cl)(L') (L' = CO, THF, CH_3CN) via photochemical processes. Thermodynamic data ($\Delta H^o = -33 \pm 2$ kJ mol^{-1} and $\Delta S^o = -146 \pm 8$ J $K^{-1}mol^{-1}$) have been estimated for the formation of the bis(triphenylphosphine) species in CH_2Cl_2 (reaction (6.9)).

$$Rh(OEP)(Cl)(PPh_3) + PPh_3 \overset{K}{\rightleftharpoons} [Rh(OEP)(PPh_3)_2]^+ + Cl^- \qquad (6.9)$$

Some complexes of $Rh^{III}(OEP)$ containing dppb, dppe, dppm and dppp have been characterised in situ using visible, ^1H and $^{31}P\{^1H\}$ nmr spectroscopy. The diphosphines bind to Rh(III) porphyrins in a monodentate dangling fashion ($Rh^{III}(OEP)(Cl)(PP)$ and $[Rh^{III}(OEP)(PP)_2]^+$), or in a bridging mode between two metal centers ($[Rh^{III}(OEP)(Cl)]$-μPP-$[Rh^{III}(OEP)(Cl)]$). The solubility of the systems decreases with increasing diphosphine carbon chain length and as the ratio of the [diphosphine] to [Rh] increased, because of formation of polymeric material. Some nmr data on cationic oligomeric species such as $(\text{-PP–}[Rh(OEP)]^+\text{–PP-})_nCl_n$ complexes in benzene are presented.

The solubility of the cations in non-polar solvent is interesting and needs further investigation. The stability in low-polarity solvents of ionic intermediates containing long chain phosphines may be greater than normally thought. The electronic interactions across the PP bridges are also interesting as are the factors stabilising the apparently quite distorted dppm bridged complex, whose temperature-dependent nmr spectra deserve further investigation.

References

1. In "Activation of Dioxygen Species and Homogeneous Catalytic Oxidation". Ed. T.J. Collins. NATO workshop report. Galzignano. 1984. p.4.
2. H. Mimoun. Angew Chem. Int. Ed. Engl. **21**, 734 (1982).
3. T. Mashiko and D. Dolphin. In "Comprehensive Coordination Chemistry". Vol 2. Eds. G. Wilkinson, R.D. Gillard and J.A. McCleverty. Pergamon Press. Oxford. 1987. pp. 813-897.
4. D. Dolphin (ed.). "The Porphyrins". Academic Press. New York. 1978–1979. Vol. 1 p. 415*ff*, and Vol. VII Chap. 1.
5. D.H. Karweik and N. Winograd. Inorg. Chem. **15**, 2336 (1976).
6. J.H. Dawson and M. Sono. Chem. Rev. **87**, 1255 (1987).
7. J. Setsune and D. Dolphin. Can. J. Chem. **65**, 459 (1987).
8. L. Randaccio, N.B. Pahor, E. Zangrando and L.E. Marzilli. Chem. Rev. **18**, 225 (1989).

8a. B.B. Wayland, S.L. Van Voorhees and K.J. Del Rossi. J. Am. Chem. Soc. **109**, 6513 (1987).

8b. Y. Wang and R.G. Finke. Inorg. Chem. **28**, 986 (1989).

9. M.K. Geno and J. Halpern. J. Am. Chem. Soc. **109**, 1238 (1987).
10. J. Deisenhofer and M. Michel. Angew. Chem. Int. Ed. Engl. **28**, 829 (1989).

10a. R. Huber. Angew. Chem. Int. Ed. Engl. **28**, 848 (1989).

10b. D.R. Doiron and C.J. Gomer. Prog. Clinical. Biol. Res. **170** (1984).

11. Y. Aoyama, K. Aoyagi, H. Toi and H. Ogoshi. Inorg. Chem. **22**, 3046 (1983).
12. R. Guilard, C. Lecomte and K.M. Kadish. Stucture and Bonding, **64**, 205 (1987).
13. R. Guilard and K.M. Kadish. Chem. Rev. **88**, 1121 (1988).
14. P.J. Brothers and J.P. Collman. Acc. Chem. Res. **19**, 209 (1986).
15. R.P. Hughes. In "Comprehensive Organometallic Chemistry". Vol. 5. Eds. G. Wilkinson, F.G.A. Stone and E.W. Abel. Pergamon Press. Oxford. 1982. Chap. 35. p. 388ff.

16. G.A. Taylor and M. Tsutui. J. Chem. Educ. **52**, 715 (1975).

17. H. Ogoshi, J. Setsune, T. Omura and Z. Yoshida. J. Am. Chem. Soc. **97**, 6461 (1975).

18. Z. Yoshida, H. Ogoshi, T. Omura, E. Watanabe and T. Kurosaki. Tetrahedron Lett. **11**, 1077 (1972).

19. A. Takenaka, Y. Sasada, T. Omura, H. Ogoshi and Z. Yoshida. J. Chem. Soc. Chem. Commun. 792 (1973).

20. A. Takenaka, Y. Sasada, H. Ogoshi, T. Omura and Z. Yoshida. Acta. Cryst. **B31**, 1 (1975).

21. Y. Aoyama, T. Yoshida, K. Sakurai and H. Ogoshi. Organometallics, **5**, 168 (1986).

22. S. Yamamoto, M. Hoshino, K. Yasufuku and M. Imamura. Inorg. Chem. **23**, 195 (1984).

23. M. Hoshino and K. Yasufuku. Inorg. Chem. **24**, 4408 (1985).

24. C.L. Yao, J.E. Anderson and K.M. Kadish. Inorg. Chem. **26**, 2725 (1987).

25. R. Grigg, J. Trocha-Grimshaw and V. Viswanatha. Tetrahedron Lett. **4**, 289 (1976).

26. A.M. Abeysekera, R. Grigg, J. Trocha-Grimshaw and V. Viswanatha. Tetrahedron Lett. **36**, 3189 (1976).

27. A.M. Abeysekera, R. Grigg, J. Trocha-Grimshaw and V. Viswanatha. J. Chem. Soc. Chem. Commun. 227 (1976).

28. A.M. Abeysekera, R. Grigg, J. Trocha-Grimshaw and V. Viswanatha. J. Chem. Soc. Perkin Trans. 1, 36 (1977).

29. A.M. Abeysekera, R. Grigg, J. Trocha-Grimshaw and V. Viswanatha. J. Chem. Soc. Perkin Trans. 1, 1395 (1977).

30. H.J. Callot, F. Metz and C. Piechoki. Tetrahedron, **38**, (1982).

31. E. Cetinkaya, A.W. Johnson, M.F. Lappert, G.M. McLaughlin and K.W. Muir. J. Chem. Soc. Dalton, 1236 (1974).

32. T. Boschi, S. Licoccia and P. Tagliatesta. Inorg. Chim. Acta, **126**, 157 (1987).

33. E.B. Fleischer and D. Lavallee. J. Am. Chem. Soc. **89**, 7132 (1967).

34. E.B. Fleischer, R. Thorp and D. Venerable. J. Chem. Soc. Chem. Commun. 479 (1969).

35. Y. Aoyama, A. Yamagishi, Y. Tanaka, H. Toi and H. Ogoshi. J. Am. Chem. Soc. **109**, 4735 (1987) and references therein.

36. A.M. Abeysekera, R. Grigg, J. Trocha-Grimshaw, V. Viswanatha and T.K. King. Tetrahedron Lett. **36**, 3192 (1976).

37. H. Ogoshi, T. Omura and Z. Yoshida. J. Am. Chem. Soc. **95**, 1666 (1973).

38. N. Sadasivan and E.B. Fleischer. J. Inorg. Nucl. Chem. **30**, 591 (1968).

39. E.B. Fleischer and N. Sadasivan. J. Chem. Soc. Chem. Commun. 159 (1967).

40. N. Sadasivan and E.B. Fleischer. J. Inorg. Nucl. Chem. **30**, 591 (1968).

41. B.R. James and D.V. Stynes. J. Am. Chem. Soc. **94**, 6225 (1972).

42. B.B. Wayland and A.R. Newmann. J. Am. Chem. Soc. **101**, 6472 (1979).

43. B.B. Wayland and A.R. Newmann. Inorg. Chem. **20**, 3093 (1981).

44. J.E. Anderson, C.L. Yao and K.M. Kadish. Inorg. Chem. **25**, 3224 (1986).

45. H.J. Callot and E. Schaeffer. Nouv. J. Chim. **4**, 311 (1980).

46. M.D. Farnos, B.A. Woods and B.B. Wayland. J. Am. Chem. Soc. **108**, 3659 (1986).

47. A.D. Adler, F.R. Longo, F. Kampas and J. Kim. J. Inorg. Nucl. Chem. **32**, 2443 (1970).

48. E.B. Fleischer, F.L. Dixon and R. Florian. Inorg. Nucl. Chem. Lett. **9**, 1303 (1973).

49. L.K Hanson, M. Gouterman and J.C. Hanson. J. Am. Chem. Soc. **95**, 4822 (1973).

50. K. Kalyanasundaram. Chem. Phys. Lett. **104**, 357 (1984).

51. T. Boschi, S. Licoccia and P. Tagliatesta. Inorg. Chim. Acta, **119**, 191 (1986).

52. K.M. Kadish, C.L. Yao, J.E. Anderson and P. Cocolios. Inorg. Chem. **24**, 4515 (1985).

53. T. Boschi, S. Licoccia and P. Tagliatesta. Inorg. Chim. Acta, **143**, 235 (1988).

54. M. Krishnamurthy. Inorg. Chim. Acta, **25**, 215 (1977).

55. K.R. Ashley, S.B. Shyu and J.G. Leipoldt. Inorg. Chem. **19**, 1613 (1980).

56. K.J. Del Rossi and B.B. Wayland. J. Am. Chem. Soc. **107**, 7941 (1985).

57. B.B. Wayland, S.L. Van Voorhees and C. Wilker. Inorg. Chem. **25**, 4039 (1986).

58. M. Hoshino, K. Yasufuku, S. Konishi and M. Imamura. Inorg. Chem. **23**, 1982 (1984).

59. K.M. Kadish, J.E. Anderson and R. Guilard. Inorg. Chem. **25**, 1277 (1986).

60. Y. Aoyama, T. Kamohara, A. Yamagishi, H. Toi and H. Ogoshi. Tetrahedron Lett. **28**, 2146 (1987).

61. J.P. Collman, C.E. Barnes and L.K. Woo. Proc. Natl. Acad. Sci. USA, **80**, 7684 (1983).

62. B.B. Wayland and K.J. Del Rossi. J. Organomet. Chem. **276**, C27 (1984).

63. B.B. Wayland, V.L. Coffin and M.D. Farnos. Inorg. Chem. **27**, 2745 (1988).

64. J. Setsune, Z. Yoshida and H. Ogoshi. J. Chem. Soc. Perkin Trans. 1, 982 (1982).

65. H. Ogoshi, J. Setsune and Z. Yoshida. J. Am. Chem. Soc. **99**, 3869 (1977).

66. N.L. Jones, P.J. Carroll and B.B. Wayland. Organometallics, **5**, 33 (1986).

67. T. Boschi, S. Licoccia, R. Paolesse and P. Tagliatesta. Inorg. Chim. Acta, **145**, 19 (1988).

68. R. Zanoni, T. Boschi, S. Licoccia, R. Paolesse and P. Tagliatesta. Inorg. Chim. Acta, **145**, 175 (1988).

69. J.W. Buchler, W. Kokisch and P.D. Smith. Stucture and Bonding, **34**, 79 (1978).

70. B.B. Wayland, S.L. Van Voorhees and K.J. Del Rossi. J. Am. Chem. Soc. **109**, 6513 (1987).

71. B.R. James and D.V. Stynes. J. Chem. Soc. Chem. Commun. 1261 (1972).

72. H. Sakurai, H. Uchikubo, K. Ishizu, K. Tajima, Y. Aoyama and H. Ogoshi. Inorg. Chem. **27**, 2691 (1988).

73. Y. Aoyama, A. Yamagishi, M. Asagawa, H. Toi and H. Ogoshi. J. Am. Chem. Soc. **110**, 4076 (1988).

74. A. Antipas and M. Gouterman. J. Am. Chem. Soc. **105**, 4896 (1983).

75. D.C. Thackray, S. Ariel, T.W. Leung, K. Menon, B.R. James and J. Trotter. Can. J. Chem. **64**, 2440 (1986).

76. B.B. Wayland and B.A. Woods. J. Chem. Soc. Chem. Commun. 475 (1981).

77. K.M. Kadish, C. Araullo and C. Yao. Organometallics, **7**, 1583 (1988).

78. J. Setsune, Z. Yoshida and H. Ogoshi. J. Chem. Soc. Perkin Trans. 1, 983 (1982).

79. Z. Yoshida and H. Ogoshi. Japan. Kokai **77** 59,199 (1977).

80. H. Ogoshi, J. Setsune and Z. Yoshida. J. Organomet. Chem. **159**, 317 (1978).

81. B.B. Wayland, A. Duttaahmed and B. A. Woods. J. Chem. Soc. Chem. Commun. 142 (1983).

82. I.A. Cohen and B.C. Chow. Inorg. Chem. **13**, 488 (1974) and references therein.

83. R.S. Paonessa, N.C. Thomas and J. Halpern. J. Am. Chem. Soc. **107**, 4333 (1985).

84. B.B. Wayland, B.A. Woods and V. Coffin. Organometallics, **5**, 1059 (9186).

85. V. Coffin, W. Brennen and B.B. Wayland. J. Am. Chem. Soc. **110**, 6063 (1988).

85a. B.B. Wayland, A.E. Sherry and V.L. Coffin. J. Chem. Soc. Chem. Commun. 662 (1989).

85b. A.E. Sherry and B.B. Wayland. J. Am. Chem. Soc. **111**, 5010 (1989).

86. J.L. Roberts and D.T. Sawyer. J. Am. Chem. Soc. **103**, 712 (1981).

87. D.T. Sawyer, E.J. Nanni and J.L. Roberts. Adv. Chem. Ser. **201**, 585 (1982).

88. A. Takenaka, S.K. Syal, Y. Sasada, T. Omura, H. Ogoshi and Z. Yoshida. Acta Cryst. Sect. B, **B32**, 62 (1976).

89. J.E. Anderson, C. Yao and K.M. Kadish. J. Am. Chem. Soc. **109**, 1106 (1987).

90. J.E. Anderson, Y.H. Liu and K.M. Kadish. Inorg. Chem. **26**, 4174 (1987).

91. J.E. Anderson, C. Yao and K. M. Kadish. Organometallics, **6**, 706 (1987).

92. C.E. Johnson and F.A. Bovey. J. Chem. Phys. 29, 1012 (1958).

93. J. Setsune, T. Yazawa, H. Ogoshi and Z. Yoshida. J. Chem. Soc. Perkin Trans. 1, 1641 (1980).

94. H. Ogoshi, J. Setsune, Y. Nambo and Z. Yoshida. J. Organomet. Chem. **159**, 329 (1978).

95. H.J. Callot and E. Schaeffer. J. Chem. Soc. Chem. Commun. 937 (1978).

95a. A.E. Sherry and B.B. Wayland. J. Am. Chem. Soc. **112**, 1259 (1990).

96. Y. Aoyama, T. Yoshida and H. Ogoshi. Tetrahedron Lett. **26**, 6107 (1985).

97. B.B. Wayland and B.A. Woods. J. Chem. Soc. Chem. Commun. 700 (1981).

98. B.B. Wayland, B.A. Woods and R. Pierce. J. Am. Chem. Soc. **104**, 302 (1982).

99. H. Ogoshi, J. Setsune and Z. Yoshida. J. Organomet. Chem. **185**, 95 (1980).

100. J.E. Anderson, C. Yao and K.M. Kadish. Inorg. Chem. **25**, 718 (1986).

101. J.H. Callot and F. Metz. Nouv. Chim. **9**, 167 (1985).

102. H.J. Callot and C. Piechocki. Tetrahedron Lett. **21**, 3489 (1980).

103. T. Boschi, S. Licoccia, R. Paolesse, P. Tagliatesta, G. Pelizzi and F. Vitali. Organometallics, **8**, 330 (1989).

104. R.H. Crabtree. "The Organometallic Chemistry of the Transition Elements" John Wiley & Sons Inc. New York. 1988.

105. Footnote 14 in ref 100.

106. S.L. Van Voorhees and B.B. Wayland. Organometallics, **4**, 1887 (1985).

107. Y. Aoyama, T. Yoshida, K. Sakurai and H. Ogoshi. J. Chem. Soc. Chem. Commun. 478 (1983).

108. B.B. Wayland, B.A. Wood and V.M. Minda. J. Chem. Soc. Chem. Commun. 634 (1982).

109. I. Artaud, N. Gregoire, J.P. Battoni, D. Dupre and D. Mansuy. J. Am. Chem. Soc. **110**, 8714 (1988).

110. D.R. Paulson, R. Ullman, R.B. Sloane and G.L. Closs. J. Chem. Soc. Chem. Comm. 186 (1974).

111. X. Li, S. Shinoda and Y. Saito. J. Mol. Cat. **49**, 113 (1989).

112. R. Irie, X. Li and Y. Saito. J. Mol. Cat. **23**, 17 (1984).

113. R. Irie, X. Li and Y. Saito. J. Mol. Cat. **23**, 23 (1984).

114. R. Irie, X. Li and Y. Saito. J. Mol. Cat. **18**, 263 (1983).

115. Y. Aoyama, K. Midorikawa, H. Toi and H. Ogoshi. Chem. Lett. 1651 (1987).

116. Y. Aoyama, T. Fujisawa, T. Watanabe, H. Toi and H. Ogoshi. J. Am. Chem. Soc. **108**, 943 (1986).

117. Y. Aoyama, Y. Tanaka, T. Fujisawa, T. Watanabe, H. Toi and H. Ogoshi. J. Org. Chem **52**, 2555 (1987).

118. Y. Aoyama, Y. Tanaka, T. Yoshida, H. Toi and H. Ogoshi. J. Organomet. Chem. **329**, 251 (1987).

119. J.T. Groves and T.E. Nemo. J. Am. Chem. Soc. **105**, 6243 (1983).

120. The procedure for synthesis the Ir analogue was followed. J.L. Herde, J.C. Lambert and C.V. Senoff. Inorg. Synth. **15**, 19 (1974).

121a. From $[RhCl(cyclooctene)_2]_2$. R. Cramer. Inorg. Synth. **15**, 14 (1974).

121b. From $RhCl_3 \cdot xH_2O$ and CO. J.A. McCleverty and G. Wilkinson. Inorg. Synth. **8**, 211 (1966).

121c. λ_{max}/nm (log ε) in $CHCl_3$: 403 (5.12), 520 (4.12), 554 (4.40); in ref. 17.

122. As in Method A in ref 75.

123. J.W. Buchler, L. Puppe, K. Rohbock and H.H. Schneehage. Chem. Ber. **106**, 2710 (1973).

123a. Data on the synthesis of Rh(TMP)(H) was published during the editing of this thesis: δ Rh-H at -39.99 ppm (d, J_{Rh-H} = 43.9 Hz). A.E. Sherry and B.B. Wayland. J. Am. Chem. Soc. **112**, 1259 (1990).

124. Deuterated NMR Solvents - Handy Reference Data, Merck & Co., Inc.

125. Data recorded by Dr. C.L. Lee of our group.

126. J.K.M. Sanders and B.K. Hunter. "Modern NMR Spectroscopy". Oxford Univ. Press (1987). Oxford. p. 167.

127. Based on the solubility of CO in toluene:
$[CO]_{saturated} = 7.078 \times 10^{-3} + \{1.579 \times 10^{-5}(T(°C))\{(T(K)/300\ K)(P_{CO}^{Torr}/760\ Torr/atm)\}\}$.
J. Horiuchi. Sci. Pap. Inst. Phys. Chem. Res. (Jpn). **17**, 125 (1931); J. Gjaldbaek. Acta Chem. Scand. **6**, 623 (1952).

128. D. Mansuy. Pure Applied Chem. **59**, 759 (1987).

129. D. Mansuy. "Catalytic Systems for Biomimetic Oxidation of Hydrocarbons" Proc. 6th Intern. Symp. on Homog. Catal., Vancouver, 1988, Abstract PL-1.

130. J.T. Groves, S. Krishnan, G.E. Avaria and T. Nemo. Adv. Chem. Ser. **191**, 277 (1980).

131. I. Tabushi. Coord. Chem. Rev. **86**, 1 (1988).

131a. Z. Tyeklár and K.D. Karlin. Acc. Chem. Res. **22**, 241 (1989).

132. B.R. James, R.H. Morris and P. Kvintovics. Can. J. Chem. **64**, 897 (1986), and references therein.

133. H.L. Roberts and W.R. Symes. J. Chem. Soc. (A), 1450 (1968).

134. L.E. Johnston and J.A. Page. Can. J. Chem. **47**, 4241 (1969).

135. J.F. Endicott, C.L. Wong, T. Inoue and P. Natarajan. Inorg. Chem. **18**, 450 (1979).

136. M.T. Atlay, M. Preece, G. Strukul and B.R. James. Can. J. Chem. **61**, 1332 (1983).

137. J.P. Collman and K. Kim. J. Am. Chem. Soc. **108**, 7847 (1986).

138. B.R. James, D. Dolphin, T. W. Leung, F. W. B. Einstein and A. C. Willis. Can. J. Chem. **62**, 1238 (1984) and references therein.

139. B.R. James, S. R. Mikkelsen, T. W. Leung, G. M. Williams and R. Wong. Inorg. Chim. Acta, **85**, 209 (1984).

140. C. Sishta, M. Ke, B.R. James and D. Dolphin. J. Chem. Soc. Chem. Commun. 787 (1986) and references therein.

141. M.J. Camenzind, B.R. James and D. Dolphin. J. Chem. Soc. Chem. Commun. 1137 (1986).

142. C. A. Busby and D. Dolphin. J. Magn. Reson. **23**, 211 (1976).

143. Chem3D™ version 1.0. Cambridge Scientific Computing, Inc. 1987.

144. p. 215 in ref 126.

145. S.L. Van Voorhees and B.B. Wayland. Organometallics, **6**, 204 (1987).

146. H. Suzuki, S. Matsuura, Y. Moro-Oka and T. Ikawa. Chem. Lett. 1011 (1982).

147. A set of weak resonances at 10.2, 6.72, 5.78 and 3.4 ppm can also be found in the ^1H nmr spectra of CD_2Cl_2 solutions of Rh(OEP)(H)/PPh_3 after addition of O_2.

148. For example, see refs in S.I. Murahashi, and T. Watanabe. J. Am. Chem. Soc. **101**, 7429 (1979).

149. In 56% yield; in ref. 78.

150. In $CHCl_3$, nm (M^{-1} cm^{-1}): 386(194 980), 512(17 783), 544(44 668); in ref. 78.

151. J.E. Anderson, C.-L. Yao, and K.M. Kadish. Inorg. Chem. **26**, 3224 (1986).

152. K.P.C. Vollhardt. "Organic Chemistry" W.H. Freeman & Co. New York. 1987. p. 677.

153. S.N. Gamage, R.H. Morris, S. Rettig, B.R. James. J. Organomet. Chem. **309**, C59 (1986).

154. S. Gamage. Ph.D Thesis. University of British Columbia. (1985).

155. S.N. Gamage, R.H. Morris, S.J. Rettig, D.C. Thackray, I.S. Thorburn and B.R. James. J. Chem. Soc. Chem. Commun. 894 (1987).

156. R. McCrindle, G. Ferguson, G.J. Arsenault and A.J. McAlees. J. Chem. Soc. Chem. Commun. 571 (1983).

157. J.R. Lindsay Smith and D.N. Mortimer. J. Chem. Soc. Chem. Commun. 64 (1985).

157a. C.K. Mann and K.K. Barnes. "Electrochemical Reactions in Non-aqueous Systems". Marcel Dekker, New York. 1970.

157b. K. Watanabe and J.R. Mottl. J. Chem. Phys. **26**, 1773 (1957).

158. C.E. Castro, M. Jamin, W. Yokoyama and R. Wade. J. Am. Chem. Soc. **108**, 4179 (1986).

159. B.R. James, A. W. Addison, M. Cairns, D. Dolphin, N. P. Farrell, D. R. Paulson and S. Walker. In "Fundamental Research in Homogeneous Catalysis." Vol 3. ed. M. Tsutui. Plenum Press, New York. 1979. p.751.

160. B.R. James. In "Fundamental Research in Homogeneous Catalysis." Vol 5. ed. A.E. Shilov. Gordon and Beach, New York. 1986. p.309.

161. R. G. Ball, G. Domazetis, D. Dolphin, B. R. James and J. Trotter. Inorg. Chem. **20**, 1556 (1981).

162. G. Domazetis, B. R. James, B. Tarpley and D. Dolphin. Am. Chem. Soc. Symp. Ser. No. 152, 243 (1981).

163. M. Barley, J. Y. Becker, G. Domazetis, D. Dolphin and B. R. James. Can. J. Chem. **61**, 2389 (1983).

164. C. Sishta, M.J. Camenzind, B.R. James and D. Dolphin. Inorg. Chem. **26**, 1181 (1987) and references therein.

165. G. Domazetis, B.R. James and D. Dolphin. Inorg. Chim. Acta, **54**, L47 (1981).

166. S. Ariel, D. Dolphin, G. Domazetis, B. R. James, T. W. Leung, S. J. Rettig, J. Trotter and G. M. Williams. Can. J. Chem. **62**, 755 (1984).

167. J. T. Mague and J. P. Mitchener. Inorg. Chem. **8**, 119 (1969).

168. A. Davidson, D. V. Howe and E. T. Shawl. Inorg. Chem. **6**, 458 (1967).

169. T. Allman and R. G. Goel. Can. J. Chem. **60**, 716 (1982).

170. M.N. Golovin, M.M. Rahman, J.E. Belmonte and W.P. Giering. Organometallics, **4**, 1981 (1985).

171. D.V. Stynes. J. Am. Chem. Soc. **96**, 5942 (1974).

172. E.B. Boyar, D.S. Moore, S.D. Robinson, B.R. James, M. Preece and I. Thorburn. J. Chem. Soc. Dalton Trans. 617 (1985) and references therein.

173. D.V. Stynes and X. Chen. Inorg. Chem. **26**, 3145 (1987).

174. D.V. Stynes, D. Fletcher and X. Chen. Inorg. Chem. **25**, 3483 (1986).

175. X. Chen and D.V. Stynes. Inorg. Chem. **25**, 1173 (1986).

176. N. P. Farrell, D. Dolphin and B. R. James. J. Am. Chem. Soc. **100**, 324 (1978).

177. B. R. James. In "The Porphyrins". Vol. V. Edited by D. Dolphin. Academic Press, New York. 1978. p.205.

178. S. G. Walker. M.Sc. Thesis, University of British Columbia. (1980).

179. B. Tarpey. M.Sc. Thesis, University of British Columbia (1981).

180. R. Belani. M.Sc. Thesis, University of British Columbia. (1985).

181. J. Martinson, M. Miller, D. Trojan and D. A. Sweigart. Inorg. Chem. **19**, 2162 (1980).

182. L.F. Baringer, D.P. Rillema and J.H. Ham. J. Inorg. Chem. Biochem. **21**, 195 (1984).

183. J.R. Chipperfield, S. Franks and F.R. Hartley. Am. Chem. Soc. Symp. Ser. No. 196. 1982. Ch. 16.

Appendix A

Rhodium porphyrin organometallics literature data summary

Table A.1. Rh^{III}(por)(R) species (R = hydrocarbyl), and methods of their synthesis.[a]

-R	precursor[b]	alkylating reagent	product[c]	ref
$C{\equiv}CC_6H_5$	Rh(III)	$LiC{\equiv}CC_6H_5$	y,F	1
C_6H_5	Rh(III)	C_6H_5Li	y,F	1
"	$Rh(II)^+$	C_6H_6	y,S	2
p-$C_6H_4CH_3$	Rh(III)	p-$CH_3C_6H_4Li$	y,F	1
"	$Rh(II)^+$	$C_6H_5CH_3$	y,S	2
$CH{=}CH_2$	Rh(I)	$HC{\equiv}CH$	y,F	1
μ-(-CH=CH-)	Rh(II)	"	y,F	3
cis-$CH{=}CHC_6H_5$	Rh(I)	$HC{\equiv}CC_6H_5$	y,F	1
trans-$CH{=}CHC_6H_5$	Rh(I)	trans-$BrHC{=}CHC_6H_5$	y,S	1
μ-(-CH=C(C_6H_5)-)	Rh(II)	"	y,F	3
CH_3	Rh(?)[d]	?	y,S	4
"	Rh(I)[e]	CH_3I	y,F	5
"	Rh(III)[f]	CH_3Li	y,F	1
"	Rh(I)[f]	CH_3I	y,F	1
C_2H_5	Rh(III)	C_2H_5Li	y,F	1
"	Rh(?)[d]	?	y,S	4
μ-(-CH_2CH_2-)	Rh(I)[d]	$BrCH_2CH_2Br$	y,S	4
n-C_3H_7	Rh(III)	n-C_3H_7Li	y,F	1
n-C_4H_9	Rh(III)	n-C_4H_9Li	y,F	1
n-C_5H_{11}	Rh(III)	n-$C_5H_{11}Li$	y,F	1
n-C_6H_{13}	Rh(III)	n-$C_6H_{13}Li$	y,F	1
n-C_9H_{19}	Rh(III)	n-$C_9H_{19}Li$	y,F	1
$CH_2CH{=}CHC_6H_5$	Rh(II)	$CH_2{=}CHCH_2C_6H_5$	y,F	3
$CH_2CH{=}CHC_3H_7$	Rh(II)	$CH_2{=}CHC_4H_9$	y,F	3, 6
$CH_2C_6H_5$	Rh(II)	$BrCH_2C_6H_5$	y,F	3
"	Rh(I)	$ClCH_2C_6H_5$	y,S	7
"	Rh(II)	$C_6H_5CH_3$	i,S	7
p-$CH_2C_6H_4CH_3$	Rh(II)	p-$CH_3C_6H_4CH_3$	i,S	7
m-$CH_2C_6H_4CH_3$	Rh(II)	m-$CH_3C_6H_4CH_3$	i,S	7
$CH_2CH(CH_3)C_6H_5$	Rh(II)	$CH_3CH_2(CH_3)C_6H_5$	i,S	7
"	Rh(H)	$CH_2{=}C(CH_3)C_6H_5$	i,S	7
$CH_2CH_2C_6H_5$	Rh(II)	$CH_3CH_2C_6H_5$	i,S	7
"	Rh(I)	$CH_2BrCH_2C_6H_5$	y,S	7
$CH_2CH_2CH_2C_6H_5$	Rh(II)	$CH_3CH_2CH_2C_6H_5$	i,S	7
"	Rh(I)	$CH_2BrCH_2CH_2C_6H_5$	y,S	7
$CH(C_6H_5)CH_3$	Rh(II)	$CH_3CH_2C_6H_5$	i,S	7
"	Rh(I)	$CH_3CHBrC_6H_5$	y,S	7
$CH(C_6H_5)CH_2CH_3$	Rh(II)	$CH_3CH_2CH_2C_6H_5$	i,S	7
"	Rh(I)	$CH_3CH_2CHBrC_6H_5$	y,S	7
$CH(CH_3)CH_2C_6H_5$	Rh(II)	$CH_3CH_2CH_2C_6H_5$	i,S	7
"	Rh(I)	$CH_3CHBrCH_2C_6H_5$	y,S	7
"	Rh(H)	$CH_3CH{=}CHC_6H_5$	i,S	7
C_7H_9	Rh(I)	quadricyclane	y,F	8
C_7H_{11}	Rh(I)	[4.1.0.$0^{2,7}$]tricycloheptane	y,F	8

a. OEP, unless stated otherwise.

b. Rh(I) = $[Rh^{I}(por)]^{-}$; Rh(II) = $[Rh^{II}(por)]_2$; Rh(III) = $Rh^{III}(por)(X)$, Rh(III)$^+$ = $[Rh^{III}(por)]^{+}$; Rh(H) = Rh(por)(H).

c. y = isolated; i = prepared in situ; F = fully characterised (spectroscopy and elemental analysis); S = spectroscopically characterised.

d. TPP.

e. MeDME.

f. Also isolated as $Rh^{III}(OEP)(CH_3)(B)$, B = 4-CH_3-py, py, 4-CN-py (ref. 1).

1. H. Ogoshi, J. Setsune, T. Omura and Z. Yoshida. J. Am. Chem. Soc. **97**, 6461 (1975).
2. Y. Aoyama, T. Yoshida, K. Sakurai and H. Ogoshi. Organometallics, **5**, 168 (1986).
3. H. Ogoshi, J. Setsune and Z. Yoshida. J. Am. Chem. Soc. **99**, 3869 (1977).
4. B.B. Wayland, S.L. Van Voorhees and C. Wilker. Inorg. Chem. **25**, 4039 (1986).
5. Y. Aoyama, K. Aoyagi, H. Toi and H. Ogoshi. Inorg. Chem. **22**, 3046 (1983).
6. Z. Yoshida and H. Ogoshi. Japan. Kokai **77** 59,199 (1977).
7. K.J. Del Rossi and B.B. Wayland. J. Am. Chem. Soc. **107**, 7941 (1985).
8. H. Ogoshi, J. Setsune and Z. Yoshida. J. Organomet. Chem. **185**, 95 (1980).

Table A.2. $Rh^{III}(por)(R)$ species containing heteroatoms, and methods of their synthesis.[a]

-R	precursor[b]	alkylating reagent	product[c]	ref
$CH_2CH_2NH_2 \cdot HCl$	Rh(I)	$(CH_2CH_2)NH$	y,F	1
$CH_2CH{=}CHCN$	Rh(II)	$CH_2{=}CHCH_2CN$	y,F	2, 3
CH_2CH_2CN	Rh(I)	$CH_2{=}CHCN$	y,F	4
CH=NBu	Rh(H)	BuNC	y,S	5
"	Rh(II)	BuNC, H_2O	y,S	5
CH_2OH	Rh(H)[d]	CH_2O	y,S	6
"	Rh(H)	"	y,S	7, 8
CH_2OCH_3	Rh(III)[d]	CH_2N_2; MeOH	y,F	9
$CH(OCH_3)CO_2C_2H_5$	Rh(III)	$N_2CHCO_2C_2H_5$; MeOH	y,F	9
"	Rh(III)[d]	"	y,F	9
$CH(OCH_2C_6H_5)CO_2C_2H_5$	Rh(III)[d]	$N_2CHCO_2C_2H_5$; bzOH	y,F	9
$CH(OAc)CO_2C_2H_5$	Rh(III)[d]	$N_2CHCO_2C_2H_5$; AcOH	y,F	9
$C(CO_2C_2H_5){=}CH_2$	Rh(III)[d]	$N_2C(CO_2C_2H_5)CH_3$	y,F	9
$CO_2C_2H_5$	Rh(III)[d]	$N_2C(CO_2C_2H_5)CH_3$[e]	y,F	9
$C(CO_2CH_3){=}CH_2$	Rh(III)	$N_2C(CO_2CH_3)CH_3$	y,F	9
"	Rh(III)[d]	$N_2C(CO_2CH_3)CH_3$	y,F	9
CO_2CH_3	Rh(III)[d]	$N_2C(CO_2CH_3)CH_3$[e]	y,F	9
$C(CO_2CH_3){=}CHCO_2CH_3$	Rh(III)[d]	$N_2C(CO_2CH_3)CH_2CO_2CH_3$	y,F	9
CH_2CH_2OH	Rh(I)	$(CH_2CH_2)O$	y,F	1
$CH(CH_3)OH$	Rh(H)	CH_3CHO	y,S	10
$CH(C_2H_5)OH$	Rh(H)	CH_3CH_2CHO	i,S	10
$CH(C_6H_5)OH$	Rh(H)	C_6H_5CHO	i,S	10

A.2 (cont'd) -R	precursor[b]	alkylating reagent	product[c]	ref
$CH_2CH(OC_2H_5)_2$	Rh(I)	$ClCH_2CH(OC_2H_5)_2$	y,S	11
"	Rh(III)	$CH_2{=}CHOC_2H_5$, NEt_3	y,F	11
CH_2CHO[f]	Rh(II)	$CH_2{=}CHOC_2H_5$	y,F	11, 12
"	Rh(III)	$CH_2{=}CHOC_2H_5$, NEt_3; H^+	y,F	11
"	Rh(I)	$ClCH_2CH(OC_2H_5)_2$; H^+	y,F	11
"	Rh(H)	$HOCH_2CHO$; H^+	i,S	13
$CH_2C(O)CH_3$	Rh(III)$^+$	$CH_3C(O)CH_3$	y,S	14
"	Rh(III)[g]	$CH_3C(O)CH_3$	y,S	15
$CH(C(O)CH_3)_2$	Rh(III)$^+$	$CH_2(C(O)CH_3)_2$	y,S	14
$CH(C(O)CH_3)C(O)C_2H_5$	Rh(III)$^+$	$CH_2(C(O)CH_3)C(O)C_2H_5$	y,S	14
$CH_2CH_2CH_2C(O)CH_3$	Rh(I)	$C_3H_5C(O)CH_3$	y,F	1
C_7H_9O-exo	Rh(I)	nortricyclanone	y,F	1
$C_7H_{10}CO_2CH_3$	Rh(I)	h	y,F	1
$CH_2CH_2CH_2CO_2CH_2CH_3$	Rh(I)	$C_3H_5CO_2CH_2CH_3$	y,F	1
m-$C_6H_4CO_2CH_3$	Rh(III)$^+$	$C_6H_5CO_2CH_3$	y,F	16
p-$C_6H_4CO_2CH_3$	"	"	y,F	16
p-$C_6H_4OCH_3$	Rh(III)$^+$	$C_6H_5OCH_3$	y,F	16
"	Rh(III)	$LiC_6H_5OCH_3$	y,F	17
CH_2I	Rh(I or II?)[d]	CH_2I_2	y,S	6
"	Rh(III)[d]	CH_2N_2	y,F	9
p-C_6H_4Cl	Rh(III)$^+$	C_6H_5Cl	y,F	16
CH=CHCl	Rh(III)	HC≡CH	y,F	11
CH=C(C_6H_5)Cl	Rh(III)	HC≡CC_6H_5	y,F	11
C(O)$CH_2C_6H_5$	"	" ; H_2O	y,F	11
C(O)C_5H_{11}	Rh(III)	HC≡CC_4H_9; H_2O	y,F	11
C(O)$CH_2CH_2CH_2OH$	Rh(III)	HC≡CCH_2CH_2OH; H_2O	y,F	11
CHO	Rh(III)	CO, KOH	i,S	18
"	Rh(III)[d]	"	i,S	18
"	Rh(II)	CO, H_2O	y,S[i]	5
"	"	CO, H_2	y,S	5
"	Rh(H)	CO	y,S	19
"	Rh(H)[d]	CO, H_2	i,S	20
"	Rh(H)[d]	CO, H_2	i,S	20

a-d. As in Table A.2.

e. Excess reagent.

f. Also isolated as Rh^{III}(OEP)(CH_2CHO)(B) (B = py, PPh_3); ref. 13.

g. por = cis- and trans-5,15-bis(2-hydroxy-1-naphthyl)-octaethylporphyrin, tetrakis(2-hydroxyphenyl)porphyrin, trans-5,15-di(8-quinolyl)octaethylporphyrin.

h. 1-methoxycarbonyl[4.1.0.$0^{2,7}$]tricycloheptane.

i. Including single-crystal X-ray diffraction.

1. H. Ogoshi, J. Setsune and Z. Yoshida. J. Organomet. Chem. **185**, 95 (1980).

2. H. Ogoshi, J. Setsune and Z. Yoshida. J. Am. Chem. Soc. **99**, 3869 (1977).

3. Z. Yoshida and H. Ogoshi. Japan. Kokai **77** 59,199 (1977).
4. H. Ogoshi, J. Setsune, T. Omura and Z. Yoshida. J. Am. Chem. Soc. **97** 6461 (1975).
5. B.B. Wayland, B.A. Woods and R. Pierce. J. Chem. Soc. **104**, 302 (1982).
6. B.B. Wayland, S.L. Van Voorhees and C. Wilker. Inorg. Chem. **25**, 4039 (1986).
8. S.L. Van Voorhees and B.B. Wayland. Organometallics, **4**, 1887 (1985).
9. H.J. Callot and E. Schaeffer. Nouv. J. Chim. **4**, 311 (1980), H.J. Callot and E. Schaeffer. J. Chem. Soc. Chem. Commun. 937 (1978).
10. B.B. Wayland, B.A. Woods and V.M. Minda. J. Chem. Soc. Chem. Commun. 634 (1982).
11. H. Ogoshi, J. Setsune, Y. Nambo and Z. Yoshida. J. Organomet. Chem. **159**, 329 (1978).
12. Z. Yoshida and H. Ogoshi. Japan. Kokai **77** 59,200 (1977).
13. B.B. Wayland, S.L. Van Voorhees and K.J. Del Rossi. J. Am. Chem. Soc. **109**, 6513 (1987).
14. Y. Aoyama, T. Yoshida and H. Ogoshi. Tet. Lett. **26**, 6107 (1985).
15. Y. Aoyama, A. Yamagishi, Y. Tanaka, H. Toi and H. Ogoshi. J. Am. Chem. Soc. **109**, 4735 (1987).
16. Y. Aoyama, T. Yoshida, K. Sakurai and H. Ogoshi. Organometallics, **5**, 168 (1986).
17. J. Setsune, T. Yazawa, H. Ogoshi and Z. Yoshida. J. Chem. Soc. Perkin I, 1641 (1980).
18. B.B. Wayland, A. Duttaahmed and B.A. Wood. J. Chem. Soc. Chem. Commun. 142 (1983).
19. B.B. Wayland and B.A. Woods. J. Chem. Soc. Chem. Commun. 700 (1981).
20. B.B. Wayland, S.L. Van Voorhees and C. Wilker. Inorg. Chem. **25**, 4039 (1986).

Table A.3. $Rh^{III}(EP)(R)$ species prepared from the "out-of-plane" Rh(I) complexes.

-R	alkylating reagent	product[a]	ref
CH_3	CH_3I	y,F	1, 2
"	CH_3SO_2F	y,F	1
CH_2CH_3	CH_3CH_2I	y,F	1
"	$CH_3CH_2SO_2F$	y,F	1
$CH_2CH_2CH_2CH_3$	$CH_3CH_2CH_2CHCHO$	y,F	3, 4
C_6H_5	C_6H_5CHO	y,F	3, 4
"	$(C_6H_5C(O))_2O$	y,F	5, 1
"	C_6H_5Br	y,S	4
"	C_6H_5I	y,S	3
p-C_6H_4CN	p-BrC_6H_4CN	y,F	3
p-C_6H_4F	p-BrC_6H_4F	y,F	3
$CH(CH_3)C(O)C_6H_5$	$CH_3CH_2C(O)C_6H_5$	y,F	3, 5
$CH_2C(O)C_3H_5$	$CH_3C(O)C_3H_5$	y,F	3, 5
$CH_2CH_2CH_2C(O)$-p-C_6H_4F	p-$FC_6H_4C(O)C_3H_5$	y,F	3, 5
$CH_2C(O)C_6H_5$	$CH_3C(O)C_6H_5$	y,F	3, 5
$CH_2C(O)$-2-furyl	$CH_3C(O)$-2-furyl	y,F	3

A.3 (cont'd) -R	alkylating reagent	product[a]	ref
$C(O)CH_3$	CH_3I	y,F	1, 2
"	CH_3SO_2F	y,F	1
"	CH_3CO_2H	y,S	1
"	$(CH_3CO)_2O$	y,F	5, 1
$C(O)CH_2CH_3$	CH_3CH_2I	y,F	1
"	$CH_3CH_2SO_2F$	y,F	1
"	$(CH_3CH_2CO)_2O$	y,F	5, 1
$C(O)CH_2CH_2CH_3$	$(CH_3CH_2CH_2CO)_2O$	y,F	5, 1
$C(O)C_6H_5$	C_6H_5CHO	y,F	3, 2
"	C_6H_5CHO	y,F	3
"	$C_6H_5C(O)Cl$	y,F	5, 1
"	$(C_6H_5C(O))_2O$	y,F	5, 1
"	C_6H_5Br	y,S	4
"	C_6H_5I	y,S	3
$C(O)$-p-C_6H_4F	p-BrC_6H_4F	y,F	3
$CO_2CH_2CH_3$	$CH_3CO_2CH_2CH_3$	y,F	3
"	$BrCH_2CO_2CH_2CH_3$	y,F	3
$CO_2CH_2CH_2CH_2CH_3$	$HCO_2CH_2CH_2CH_2CH_3$	y,F	3
$CO_2C_6H_5$	$HCO_2C_6H_5$	y,F	3
"	$CH_3CO_2C_6H_5$	y,F	3

a. y = isolated; i = prepared in situ; F = fully characterised (spectroscopy and elemental analysis); S = spectroscopically characterised.

1. A.M. Abeysekera, R. Grigg, J. Trocha Grimshaw and V. Viswanatha. J. Chem. Soc. Perkin I, 36 (1977).
2. R. Grigg, J. Trocha Grimshaw and V. Viswanatha. Tetrahedron Lett. **4**, 289 (1976).
3. A.M. Abeysekera, R. Grigg, J. Trocha Grimshaw and V. Viswanatha. J. Chem. Soc., Perkin I, 1395 (1977).
4. A.M. Abeysekera, R. Grigg, J. Trocha Grimshaw and V. Viswanatha. Tetrahedron Lett. **36**, 3189 (1976).
5. A.M. Abeysekera, R. Grigg, J. Trocha Grimshaw and V. Viswanatha. J. Chem. Soc. Chem. Commun. 227 (1976).

Table A.4. $Rh^{III}(TTP)(R)$ species electrochemically prepared from $Rh^{II}(TPP)$.[a]

-R	n	alkylating reagent	ref
C_nH_{2n+1}	1	CH_3I	1
"	2	$C_nH_{2n+1}X$ (X=Br, I)	1
"	3	"	1
"	"	$H_2C{=}CHC_3H_7$	2
"	"	$HC{\equiv}CC_3H_7$	2
"	4	$C_nH_{2n+1}X$ (X=Cl, Br, I)	1
"	"	$H_2C{=}CHC_4H_9$	2
"	"	$HC{\equiv}CC_4H_9$	2
"	5	$C_nH_{2n+1}X$ (X=F, Cl, Br, I)	1
"	"	$H_2C{=}CHC_5H_{11}$	2
"	"	$HC{\equiv}CC_5H_{11}$	2
"	6	$C_nH_{2n+1}X$ (X=?)	3
"	"	$HC{\equiv}CC_6H_{13}$	2
$CH(CH_3)CH_2CH_3$		$CH_3CH_2CH(CH_3)Cl$	1
$C(CH_3)_3$		$(CH_3)_3CCl$	1
$C_nH_{2n}X$ (X=Cl, Br, I)	1	$C_nH_{2n}X_2$ (X=Cl, Br, I)	1
"	3	"	3
"	4	"	3
"	5	"	3
$C_nH_{2n}I$	6	$C_nH_{2n}I_2$	3
CHX_2 (X=Cl, I)		CHX_3 (X=Cl, I)	1
CX_3 (X=Cl, I)		CX_4 (X=Cl, I)	1

a. $Rh^{II}(TPP)$ prepared in situ from $1e^-$ reduction at -1.20 V (vs. SCE) of $[Rh^{III}(TPP)(NHMe_2)_2]Cl$ in THF, 0.2 M TBAP; products isolated from bulk electrolysis and characterized by ^1H nmr in C_6D_6.

1. J.E. Anderson, C. Yao and K.M. Kadish. J. Am. Chem. Soc. **109** 1106 (1987).
2. J.E. Anderson, C. Yao and K.M. Kadish. Organometallics, **6**, 706 (1987).
3. J.E. Anderson, Y.H. Liu and K.M. Kadish. Inorg. Chem. **26**, 4174 (1987).

Appendix B

Spectral data for Rh(TMP)(Cl)(phosphine) complexes

Table B.1. The ^1H NMR spectral data for Rh(TMP)(Cl)(phosphine) complexes in C_6D_6.[a]

phosphine	–CH=	m,m'-H	p-CH_3	o,o'-CH_3	coordinated phosphine
PPh_3	8.756	7.241,6.879	2.391	2.193,1.279	6.377, 6.186, 4.371
					-CH_2- -CH_2- -CH_2- -CH_3
P^nBu_3	8.804	7.273,6.929	2.424	2.637,1.448	-2.440, -1.164, (0.264), 0.814

$^{31}P\{^1H\}$	$\delta(^1J_{Rh-P})$
PPh_3	3.2 d (115)
P^nBu_3	17.8 d (117)

a. Prepared in situ from Rh(TMP)(Cl)(iPrOH) plus excess phosphine; all singlets and at 19°C except where noted otherwise, integrations matching assignments, at 300 MHz.

Appendix C
The derivation of equation 5.3

In addition to the existing variables defined for equation (5.3), the following are used in this derivation: $C^+ = [[Rh(OEP)(PPh_3)_2]^+]$, $Cl = [Cl^-]$, $C = [Rh(OEP)(Cl)(PPh_3)]$ and $P = [PPh_3]$

The expression for K_{obs} based on equilibrium (5.1) is

$$K_{obs} = \frac{C^+ \cdot Cl}{C \cdot P}, \qquad (C.1)$$

which can be written in terms of initial concentrations and C,

$$K_{obs} = \frac{(C_0 - C)\cdot(Cl_0 + C_0 - C)}{C\cdot(P_0 - C_0 - C)} \qquad (C.2)$$

The property actually measured is the absorbance at 560 nm,

$$A = \varepsilon_0 lC + \varepsilon_\infty lC^+, \qquad (C.3)$$

which again can be written in terms of initial concentrations and C,

$$A = \varepsilon_0 lC + \varepsilon_\infty l(C_0 - C), \qquad (C.4)$$

and rearranging to obtain the equation

$$C^+ = \frac{(A - A_\infty)}{(\varepsilon_0 - \varepsilon_\infty)l} \qquad (C.5)$$

Substitution of equation (C.5) into (C.2) gives the equation used to calculate the values of K_{obs},

$$K_{obs} = \frac{\left\{C_0 - \left[\frac{A - A_\infty}{(\varepsilon_0 - \varepsilon_\infty)l}\right]\right\}\left\{Cl_0 + C_0 - \left[\frac{A - A_\infty}{(\varepsilon_0 - \varepsilon_\infty)l}\right]\right\}}{\left\{\frac{A - A_\infty}{(\varepsilon_0 - \varepsilon_\infty)l}\right\}\left\{P_0 - C_0 - \left[\frac{A - A_\infty}{(\varepsilon_0 - \varepsilon_\infty)l}\right]\right\}} \qquad (C.6)$$

Appendix D

Tables of K_{obs} for reaction 5.1 at various ionic strengths and temperatures

Table D.1. Variation of K_{obs} for reaction 5.1 in CH_2Cl_2 at 10 °C.[a]

$\mu \times 10^4$ M	$K_{obs} \times 10^2$	Absorbance 560 nm / baseline		$[Rh]_o \times 10^4$	$[PPh_3]_o \times 10^4$	$[Cl^-]_o$[b] $\times 10^4$	$[salt]_o$[c] $\times 10^4$
2.76	8.86	0.661	0.092	4.43	54.5	—	—
3.20	10.9	1.038	0.109	6.29	33.5	—	—
3.57	11.6	0.513	0.079	4.43	130	—	—
3.89	14.0	0.463	0.083	4.43	203	—	—
4.93	16.5	0.745	0.108	6.29	114	—	—
5.49	13.0	0.653	0.109	6.29	295	—	—
64.8	107	0.704	0.083	4.66	90.4	64.8	—
64.8	107	0.565	0.090	4.66	220	64.8	—
64.8	107	0.507	0.083	4.66	337	64.8	—
avg	107						
179.1	211	1.404	0.044	8.05	56.8	179.1	—
179.1	232	0.975	0.043	7.67	162.6	179.1	—
179.1	258	0.756	0.055	7.17	303.7	179.1	—
179.1	232	0.625	0.053	6.47	502.1	179.1	—
avg	233						
181.5	312	0.674	0.031	5.37	127.2	181.5[e]	—
181.5	280	0.550	0.032	5.37	277.3	181.5[e]	—
181.5	236	0.481	0.035	5.37	666.7	181.5[e]	—
avg	282[d]						
195.9	157	0.473	0.045	5.15	30.0	—	195.9
202.6	473	0.914	0.053	5.15	30.0	202.6	—
202.6	513	0.684	0.041	5.15	76.3	202.6	—
202.6	516	0.518	0.053	5.15	232.8	202.6	—
avg	501						

a. Up to $\mu = 6.74 \times 10^{-4}$ M, the ionic strength results solely from the ions generated by reaction 5.1, i.e., no salt has been added. Initial [Rh(OEP)(Cl)(PPh_3)] between (4.0-8.0) $\times 10^{-4}$ M. Pathlength of cell = 0.1 cm. The estimated uncertainity in K_{obs} is ± 5% or better and in μ is ± 2.5% or better unless otherwise noted.

b. Added $[Ph_4As]Cl \cdot H_2O$.

c. Added $[^nBu_4N][ClO_4]$.

d. K_{obs} ± 9%.

e. Addition of H_2O to 2×10^{-2} M had no measurable effect on the equilibrium reaction.

Table D.2. Variation of K_{obs} for reaction 5.1 in CH_2Cl_2 at 15 °C.[a]

$\mu \times 10^4$ M	$K_{obs} \times 10^2$	Absorbance 560 nm / baseline		$[Rh]_o \times 10^4$	$[PPh_3]_o \times 10^4$	$[Cl^-]_o$[b] $\times 10^4$	$[salt]_o$[c] $\times 10^4$
2.59	6.98	0.689	0.091	4.43	54.5	—	—
2.84	7.65	1.099	0.110	6.29	33.5	—	—
3.38	8.62	0.544	0.079	4.43	130	—	—
3.77	10.8	0.482	0.083	4.43	203	—	—
4.65	12.1	0.792	0.107	6.29	114	—	—
5.31	10.0	0.680	0.107	6.29	295	—	—
64.8	81.6	0.754	0.082	4.66	90.4	64.8	—
64.8	84.6	0.593	0.085	4.66	220	64.8	—
64.8	83.1	0.535	0.083	4.66	337	64.8	—
avg	83.1						
179.1	128	1.542	0.040	8.05	56.8	179.1	—
179.1	180	1.045	0.039	7.67	162.6	179.1	—
179.1	202	0.796	0.046	7.17	303.7	179.1	—
179.1	188	0.641	0.040	6.47	502.1	179.1	—
avg	175[d]						
181.5	238	0.729	0.031	5.37	127.2	181.5[f]	—
181.5	230	0.588	0.032	5.37	277.3	181.5[f]	—
181.5	195	0.499	0.035	5.37	666.7	181.5[f]	—
avg	221 [e]						
195.9	128	0.485	0.037	5.15	30.0	—	195.9
202.6	372	0.958	0.050	5.15	30.0	202.6	—
202.6	388	0.739	0.040	5.15	76.3	202.6	—
202.6	401	0.538	0.043	5.15	232.8	202.6	—
avg	387						

a. Up to $\mu = 6.74 \times 10^{-4}$ M, the ionic strength results solely from the ions generated by reaction 5.1, i.e., no salt has been added. Initial [Rh(OEP)(Cl)(PPh_3)] between $(4.0\text{-}8.0) \times 10^{-4}$ M. Pathlength of cell = 0.1 cm. The estimated uncertainity in K_{obs} is ± 5% or better and in μ is ± 2.5% or better unless otherwise noted.

b. Added $[Ph_4As]Cl \cdot H_2O$.

c. Added $[^nBu_4N][ClO_4]$.

d. K_{obs} ± 13%.

e. K_{obs} ± 7%.

f. Addition of H_2O to 2×10^{-2} M had no measurable effect on the equilibrium reaction.

Table D.3. Variation of K_{obs} for reaction 5.1 in CH_2Cl_2 at 20 °C.[a]

$\mu \times 10^4$ M	$K_{obs} \times 10^2$	Absorbance 560 nm / baseline		$[Rh]_o \times 10^4$	$[PPh_3]_o \times 10^4$	$[Cl^-]_o$[b] $\times 10^4$	$[salt]_o$[c] $\times 10^4$
2.37	5.24	0.724	0.089	4.43	54.5	—	—
2.54	5.55	1.149	0.109	6.29	33.5	—	—
3.19	6.43	0.577	0.079	4.43	130	—	—
3.61	9.02	0.508	0.082	4.43	203	—	—
4.36	7.62	0.841	0.108	6.29	114	—	—
5.11	8.02	0.722	0.107	6.29	295	—	—
64.8	62.4	0.805	0.083	4.66	90.4	64.8	—
64.8	65.3	0.635	0.086	4.66	220	64.8	—
64.8	64.5	0.568	0.083	4.66	337	64.8	—
avg	64.1						
179.1	111	1.577	0.038	8.05	56.8	179.1	—
179.1	142	1.117	0.037	7.67	162.6	179.1	—
179.1	158	0.842	0.036	7.17	303.7	179.1	—
179.1	149	0.674	0.036	6.47	502.1	179.1	—
avg	140[d]						
181.5	182	0.787	0.031	5.37	127.2	181.5[f]	—
181.5	178	0.631	0.032	5.37	277.3	181.5[f]	—
181.5	156	0.523	0.035	5.37	666.7	181.5[f]	—
avg	172[e]						
195.9	104	0.507	0.038	5.15	30.0	—	195.9
202.6	296	0.994	0.044	5.15	30.0	202.6	—
202.6	300	0.793	0.040	5.15	76.3	202.6	—
202.6	310	0.574	0.043	5.15	232.8	202.6	—
avg	302						

a. Up to $\mu = 6.74 \times 10^{-4}$ M, the ionic strength results solely from the ions generated by reaction 5.1, i.e., no salt has been added. Initial [Rh(OEP)(Cl)(PPh_3)] between (4.0-8.0) $\times 10^{-4}$ M. Pathlength of cell = 0.1 cm. The estimated uncertainity in K_{obs} is ± 5% or better and in μ is ± 2.5% or better unless otherwise noted.

b. Added $[Ph_4As]Cl \cdot H_2O$.

c. Added $[^nBu_4N][ClO_4]$.

d. K_{obs} ± 10%.

e. K_{obs} ± 6%.

f. Addition of H_2O to 2×10^{-2} M had no measurable effect on the equilibrium reaction.

Table D.4. Variation of K_{obs} for reaction 5.1 in CH_2Cl_2 at 25 °C.[a]

$\mu \times 10^4$ M	$K_{obs} \times 10^2$	Absorbance 560 nm / baseline		$[Rh]_o \times 10^4$	$[PPh_3]_o \times 10^4$	$[Cl^-]_o$[b] $\times 10^4$	$[salt]_o$[c] $\times 10^4$
2.16	3.91	0.724	0.089	4.43	54.5	—	—
2.26	4.06	1.149	0.109	6.29	33.5	—	—
2.97	4.77	0.577	0.079	4.43	130	—	—
3.11	6.29	1.269	0.037	7.52	38.0	—	—
3.45	6.06	0.508	0.082	4.43	203	—	—
4.05	6.65	0.841	0.108	6.29	114	—	—
4.50	6.44	1.035	0.037	7.52	109	—	—
4.88	5.83	0.722	0.107	6.29	295	—	—
5.94	8.53	0.792	0.037	7.52	269	—	—
6.49	8.28	0.700	0.037	7.52	501	—	—
6.74	8.13	0.659	0.037	7.52	718	—	—
64.8	48.8	0.850	0.083	4.66	90.4	64.8	—
64.8	50.6	0.678	0.085	4.66	220	64.8	—
64.8	50.2	0.605	0.083	4.66	337	64.8	—
avg	49.9						
179.1	99.0	1.604	0.038	8.05	56.8	179.1	—
179.1	114	1.186	0.037	7.67	162.6	179.1	—
179.1	125	0.902	0.036	7.17	303.7	179.1	—
179.1	119	0.716	0.036	6.47	502.1	179.1	—
avg	114[d]						
181.5	142	0.843	0.032	5.37	127.2	181.5[e]	—
181.5	139	0.678	0.033	5.37	277.3	181.5[e]	—
181.5	126	0.550	0.035	5.37	666.7	181.5[e]	—
avg	136						
195.9	86.2	0.530	0.041	5.15	30.0	—	195.9
202.6	237	1.031	0.046	5.15	30.0	202.6	—
202.6	236	0.844	0.040	5.15	76.3	202.6	—
202.6	243	0.613	0.043	5.15	232.8	202.6	—
avg	239						

a. Up to $\mu = 6.74 \times 10^{-4}$ M, the ionic strength results solely from the ions generated by reaction 5.1, i.e., no salt has been added. Initial [Rh(OEP)(Cl)(PPh_3) between (4.0-8.0) $\times 10^{-4}$ M. Pathlength of cell = 0.1 cm. The estimated uncertainity in K_{obs} is ± 5% or better and in μ is ± 2.5% or better unless otherwise noted.

b. Added $[Ph_4As]Cl \cdot H_2O$.

c. Added $[^nBu_4N][ClO_4]$.

d. K_{obs} ± 7%

e. Addition of H_2O to 2×10^{-2} M had no measurable effect on the equilibrium reaction.

Table D.5. Variation of K_{obs} for reaction 5.1 in CH_2Cl_2 at 30 °C.[a]

$\mu \times 10^4$ M	$K_{obs} \times 10^2$	Absorbance 560 nm / baseline		$[Rh]_o \times 10^4$	$[PPh_3]_o \times 10^4$	$[Cl^-]_o$[b] $\times 10^4$	$[salt]_o$[c] $\times 10^4$
1.98	3.04	0.786	0.085	4.43	54.5	—	—
2.06	3.18	1.228	0.107	6.29	33.5	—	—
2.77	3.63	0.646	0.078	4.43	130	—	—
3.28	4.69	0.561	0.079	4.43	203	—	—
3.74	5.00	0.943	0.106	6.29	114	—	—
4.65	4.54	0.791	0.106	6.29	295	—	—
64.8	40.0	0.884	0.082	4.66	90.4	64.8	—
64.8	40.4	0.718	0.084	4.66	220	64.8	—
64.8	39.5	0.644	0.083	4.66	337	64.8	—
avg	40.0						
179.1	93.2	1.617	0.037	8.05	56.8	179.1	—
179.1	93.7	1.246	0.036	7.67	162.6	179.1	—
179.1	99.2	0.964	0.036	7.17	303.7	179.1	—
179.1	94.3	0.762	0.036	6.47	502.1	179.1	—
avg	95.1						
181.5	112	0.895	0.032	5.37	127.2	181.5[d]	—
181.5	107	0.732	0.033	5.37	277.3	181.5[d]	—
181.5	100	0.583	0.036	5.37	666.7	181.5[d]	—
avg	107						
195.9	71.2	0.543	0.033	5.15	30.0	—	195.9
202.6	204	1.048	0.040	5.15	30.0	202.6	—
202.6	188	0.891	0.040	5.15	76.3	202.6	—
202.6	191	0.655	0.042	5.15	232.8	202.6	—
avg	194						

a. Up to $\mu = 6.74 \times 10^{-4}$ M, the ionic strength results solely from the ions generated by reaction 5.1, i.e., no salt has been added. Initial [Rh(OEP)(Cl)(PPh_3)] between (4.0-8.0) $\times 10^{-4}$ M. Pathlength of cell = 0.1 cm. The estimated uncertainity in K_{obs} is ± 5% or better and in μ is ± 2.5% or better unless otherwise noted.

b. Added $[Ph_4As]Cl \cdot H_2O$.

c. Added $[^nBu_4N][ClO_4]$.

d. Addition of H_2O to 2×10^{-2} M had no measurable effect on the equilibrium reaction.

Appendix E

Assignment of the ligand ^1H nmr resonances of Rh(OEP)(CH(Me)NEt_2)

The data shown in Table E.1 (and Table 4.2) were determined from selective decoupling and COSY ^1H nmr experiments performed on various nmr samples containing Rh(OEP)(CH(Me)NEt_2). The spectra illustrated in Figures E.1 and E.2 are representative examples. These spectra were obtained on the same sample as illustrated in Figure 4.4b (page 116).

The selective decoupling experiments linking $H_{2'}$ with $H_{3'}$, and H_α with H_β were done but are not illustrated. The H_α with H_β linkage is also shown by COSY data (Fig. E.2). In addition, off-resonance effects on H_β due to irradiation of the $H_{1'}$ resonance can be seen in Fig. E.1d.

Table E.1. Ligand ^{1}H nmr spectral data for Rh(OEP)(CH(Me)NEt$_2$).[a]

proton	δ	integral
$H_{2'}$	-0.61 m	1H
H_3	-0.81 t	3H
$H_{3'}$	-0.95 t	3H
$H_{2(1)}$	-1.60 m	1H
$H_{1(2)}$	-1.87 m	1H
$H_{1'}$	-2.28 m	1H
H_α	-2.30 m	1H
H_β	-3.96 d	3H

a. 300 MHz; measured in C_7D_8 solution at ~20°C.

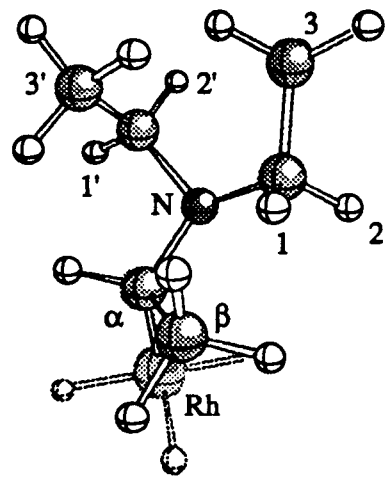

Figure E.2. Atom labelling scheme for the -(CH(Me)NEt$_2$) ligand of Rh(OEP)(CH(Me)NEt$_2$).

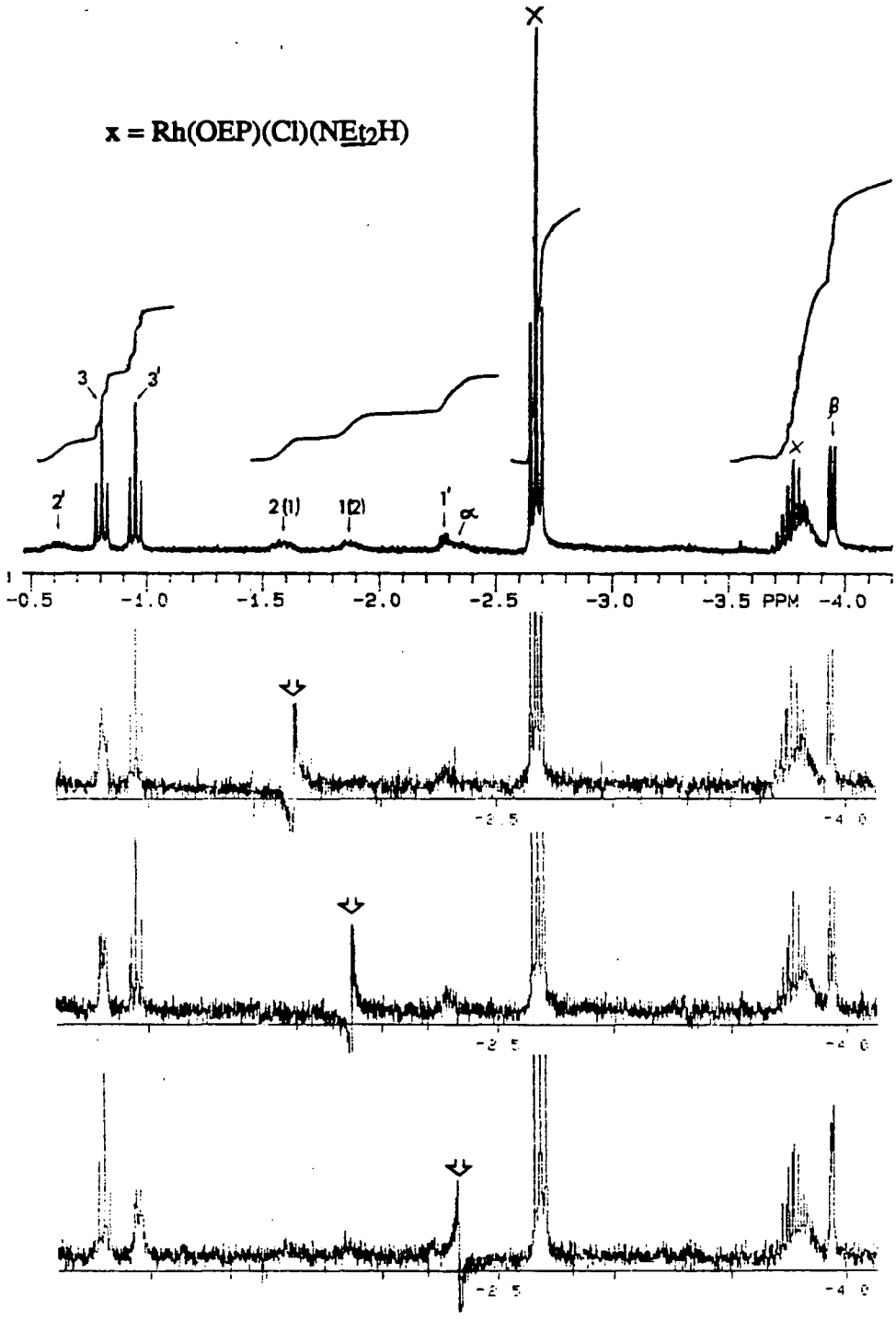

Figure E.2. The 300 MHz partially decoupled ^1H nmr spectra of the -(CH(Me)NEt_2) ligand of Rh(OEP)(CH(Me)NEt_2), prepared in situ in C_7D_8 solution at 20°C, in vacuo in a sealed nmr tube. Labelling as shown in Figure E.1. (a) undecoupled, (b-d) location of irradiation shown by the appropriate arrow.

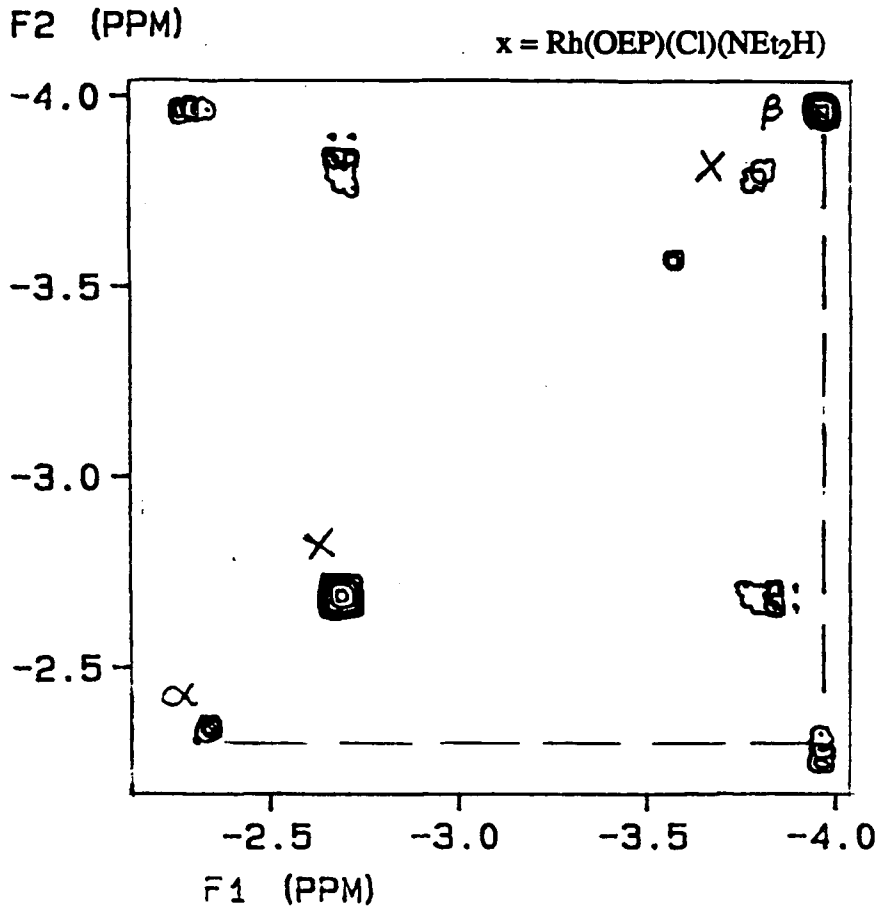

Figure E.3. The 300 MHz ^1H COSY spectrum of part of the -CH(Me)NEt_2) ligand of Rh(OEP)(CH(Me)NEt_2), prepared in situ in C_7D_8 solution at 20°C, in vacuo in a sealed nmr tube. Labelling as shown in Figure E.1.